



**HAL**  
open science

# Numerical Study of Davey- Stewartson I systems

Umar Dauda Muhammad

► **To cite this version:**

Umar Dauda Muhammad. Numerical Study of Davey- Stewartson I systems. Commutative Algebra [math.AC]. Université Bourgogne Franche-Comté, 2021. English. NNT : 2021UBFCK047 . tel-04354438

**HAL Id: tel-04354438**

**<https://theses.hal.science/tel-04354438>**

Submitted on 19 Dec 2023

**HAL** is a multi-disciplinary open access archive for the deposit and dissemination of scientific research documents, whether they are published or not. The documents may come from teaching and research institutions in France or abroad, or from public or private research centers.

L'archive ouverte pluridisciplinaire **HAL**, est destinée au dépôt et à la diffusion de documents scientifiques de niveau recherche, publiés ou non, émanant des établissements d'enseignement et de recherche français ou étrangers, des laboratoires publics ou privés.



Université de Bourgogne, U.F.R. Sciences et Techniques  
Institut de Mathématiques de Bourgogne  
Ecole doctorale Carnot-Pasteur

# THÈSE

pour l'obtention du grade de

## Docteur de l'Université de Bourgogne en Mathématiques

*présentée et soutenue publiquement par*

**Umar Dauda, MUHAMMAD**

le 13 décembre 2021

---

### **Numerical Study of Davey-Stewartson I Systems**

---

Directeur de thèse : **Christian Klein**

---

#### **Jury composé de**

---

Jean-Claude Saut	Université Paris-Sud 11	Président de Jury
Mariana Haragus	Université de Franche-Comté	Examinatrice
Nikola Stoilov	Université de Bourgogne	Examineur
Katharina Schratz	Sorbonne Université	Rapporteuse
Christof Sparber	University of Illinois at Chicago	Rapporteur
Christian Klein	Université de Bourgogne	Directeur

---

---

# Acknowledgement

First of all, special thanks go to my thesis supervisor Professor Christian Klein, who stood by my side in making sure the text is clear and readable. I remain grateful for the motivations, supports and recommendations that permitted me to meet several international collaborators. It was indeed magnificent having him as a thesis advisor.

I must acknowledge Professor Jörg Frauendiener, for the incredible collaborations during my two times visits to New Zealand despite the Covid-19 outbreak on the second visit. It was with his help, most parts of the thesis are successfully written. I strongly appreciate his indefatigable efforts in keeping me busy with many tasks remotely and physically where possible during the collaborations.

My sincere thanks go directly to Professor Georgi Grahovski (University of Essex, England), Professor Peter Miller (University of Michigan, USA), Professor Svetlana Roudenko (George Washington University), Dr. Marco Fasoldini (University of Kent, Canterbury, England), for the fruitful discussions during their special visits to the department de Mathématiques, Université de Bourgogne at several occasions.

I must thank Professor Jean-Claude Saut and Professor Mariana Haragus for accepting the proposed topic of the thesis and being part of the comité de suivi de thèse. My profound gratitudes to Professor Katharina Schratz and Professor Christof Sparber as the integral part of the comité de suivi de thèse.

I am solemnly grateful to Dr. Nikola Stoilov for being supportive, helpful and patient throughout the period of the study and of course for providing useful suggestions during the write-up. To him, I am infinitely grateful.

My sincere thanks also go to the director of the École doctorale Professor Hans-Rudolf Jauslin, the entire administrators of the Institute de Mathématique de Bourgogne (IMB, Dijon) and l'École Doctorale (Carnot-Pasteur ): Anissa Bellaassali, Magali Crochot, Nadia Bader, Francis Léger and Emeline Iltis. With their supports, it had been possible to attend courses at Levi-Civita Institute in Lizzano in Belvedere, Bologna (BO) Italy (2018) and the visits to University of Otago New-Zealand (2019 and 2020-2021).

A massive thanks to the entire staff of the Institute de Mathématique de Bourgogne (IMB, Dijon) to mention few: Professor Giuseppe Dito, Professor Peter Schauenburg, Professor Hose-Luis Jaramillo and Professor Nikola Kitanine. Warmest thanks to all PhD students of the time. It was a privilege to be part of this wonderful team. Thanks to Lamis Al-Sheik for being an incredible colleague and friend.

Moreover, I profoundly thank the PhD students I came across during my stay at university of Otago, New-Zealand, especially in the science III building. It was in fact great meeting people like Pedro Henrique, Josh Ritchie, Lydia Turley, Ben Wilks and Yiming Ma, for creating a friendly atmosphere that allowed room for scientific discussions.

I would like to extend my profound gratitudes to the entire staff and members of the former postgraduate college of University of Otago (UO) New-Zealand, Abbey college, for being friendly and organizing useful and memorable events. It was truly amazing having these incredible people around: Amir Amini, Hannah Gunther, Katrina Dey, Hisham Abdulhakem, Michael Skilbeck, Pradeesh Parameswaran (Pradoodle), Harry Davies, Sherry Hsueh-Yu Tseng, Parth Juneja, Ronny Rowe, Kirill Misiuk, and Stepan Belousov.

A wholehearted gratitude goes to my alma-matter, the Kano University of Science & Technology (KUST) Wudil, Kano-Nigeria. Their tremendous supports, gestures and approvals made it possible studying under a favourable condition. Moreover, I am equally thankful to the Kano State Government for the supports, motivations and of course the sponsorships. In fact, the interwoven cordial relations and ties between these two institutions had made an overwhelming contributions towards making our studies successful.

Finally, I would like to thank my family for being concerned, supportive and, upon all, patient throughout the period of the study.

*Dedicated to my mother and  
to the loving memories of my father  
and his brother ( the most caring uncle).*

---

# Résumé

Dans cette thèse, nous discutons, numériquement, les problèmes d'explosions, une perte de régularité d'une solution de certaines EDP par rapport à la donnée initiale, pour des équations dispersives non linéaires. L'explosion est un phénomène qui peut apparaître dans le contexte d'équations non linéaires d'évolution telles que l'équation de Burgers sans viscosité, indiquant une existence finie en temps de leurs solutions ou un collapse catastrophique du système dynamique sous-jacent dans la modélisation de situations réalistes. C'est-à-dire qu'il existe un  $t_* < \infty$  tel que pour  $t \rightarrow t_*$  certaines normes de la solution, comme les normes  $\|\cdot\|_q$  for  $1 \leq q \leq \infty$  divergent. Comme des explosions peuvent apparaître pour un grand nombre d'équations d'évolution, elles sont intéressantes d'un point de vue mathématique et physique, de savoir pourquoi, de quelle manière et avec quel profile l'explosion se produit. Quelques équations dispersives non linéaires avec une non-linéarité polynomiale, telle que les familles d'équations de Schrödinger non-linéaires (NLS), de Davey-Stewartson (DS), peuvent avoir des solutions avec une explosion en temps fini.

Les équations NLS font partie des EDP dispersives non linéaires importantes dans des applications telles que l'optique non linéaire, les ondes d'eau e.t.c. Cependant, une explosion pour NLS peut apparaître en fonction de la puissance de la non-linéarité pour des données initiales particulières. Il s'avère que l'étude du type de l'explosion pour des équations NLS est difficile sans méthodes numériques robustes avec une amélioration dynamique de la résolution proche de l'explosion. Par un changement dynamique d'échelles des équations NLS, on étudie les propriétés d'explosion de solutions avec des simulations numériques. La méthode de changement d'échelles dynamique nous permet de faire des simulations numériques près d'une singularité aussi précises que possibles. L'idée de base de ce changement d'échelles consiste à exploiter une symétrie exacte de NLS avec un changement simultané de l'espace, du temps et de la solution, mais avec un facteur dépendant du temps. Cela permet d'étudier une explosion auto-similaire avec un schéma allouant automatiquement la résolution numérique si nécessaire. Pour les équations NLS, nous présentons des résultats numériques concernant la structure de l'explosion dans dimension deux et plus dans une situation avec symétrie radiale.

Parce que le système DS est une généralisation en deux dimensions de l'équation NLS, des études d'explosion similaires peuvent être effectuées. Notre intérêt principal est le soi-disant système DS I qui peut être vu comme une équation NLS non locale. Nous présentons une approche de haute précision pour traiter numériquement les anti-dérivé

---

es de cette équation. Cette approche est hybride et utilise une régularisation analytique du symbole de Fourier singulier pour ces anti-dérivés pour des solutions de la classe de Schwartz. Une méthode spectrale de Fourier est appliquée au résiduel menant à une *précision spectrale*, c'est-à-dire une diminution exponentielle d'erreurs. Avec ce code, nous étudions la structure d'explosion des solutions pour Davey-Stewartson (DS) I intégrable pour des conditions aux limites triviales à l'infini avec les données initiales de la classe de Schwartz. Les solutions stationnaires localisées sont construites et montrées d'être instables par rapport à la dispersion et l'explosion. Une explosion en temps fini des données initiales de la classe de Schwartz est discutée.

---

# Abstract

In this thesis, we discuss, numerically, the issues of blow-up, a loss of regularity of a solution to some PDE with respect to the initial data, for non-linear dispersive equations. Blow-up is a phenomenon that can exist in the context of non-linear evolution equations such as the inviscid Burgers equation, indicating a finite time existence of their solutions or a catastrophic break down of the underlying dynamical system in modeling realistic situations. That is to say, there exists some  $T_* < \infty$  such that for  $t \rightarrow T_*$  certain norms of the solution, like the norms  $\|\cdot\|_q$  for  $1 \leq q \leq \infty$ , diverge. Due to its potential to appear in various evolution equations, it becomes an interesting phenomenon from a mathematical and physical point of view to know why, at which rate and with which profile the blow-up occurs. Some non-linear dispersive equations, having a power nonlinearity, such as families of non-linear Schrödinger equations e.g. NLS equations, Davey-Stewartson systems e.t.c., can have solutions with a finite time blow-up.

NLS equations are among the important non-linear dispersive equations in applications such as non-linear optics, water-waves e.t.c., however, blow-up (also referred to as *wave-collapse* in the NLS context) may or can appear depending on the power of the nonlinearity, particular initial data e.t.c. It turns out that exploring the blow-up structure for the NLS equations seems difficult without a robust numerical method that provides an improved refinement of the resolution near blow-up. By a dynamical rescaling approach to the NLS equations, one studies the blow-up properties of solutions near collapse with numerical simulations. The method of dynamic rescaling allows us to do numerical simulations near a singularity as accurate as possible. The basic idea of the dynamic rescaling is to exploit an exact symmetry of the NLS equations under a simultaneous rescaling of space, time and the solution, but with a time-dependent factor. This allows to study a self-similar blow-up with a scheme automatically allocating numerical resolution where needed. For the NLS equations, we present numerical results regarding the structure of blow-up in dimension two and higher in a radially symmetric setting.

Because the DS system is a generalisation of the two dimensional NLS equation, similar blow-up studies can be carried out. Our principal interest is the so-called DS I system which can be seen as a nonlocal NLS equation. We present a high-accuracy approach to numerically treat the anti-derivatives in this equation. This approach is hybrid and uses an analytic regularization of the singular Fourier symbol for these anti-derivatives for Schwartz class solutions. A Fourier spectral method is applied to the residual leading to *spectral accuracy*, i.e. an exponential decrease of errors. We generate a code and investigate

---

the blow-up (singularity) structure of solutions to the integrable Davey-stewartson (DS) I system for trivial boundary conditions at infinity with Schwartz class initial data. Localized stationary solutions are constructed and shown to be unstable against dispersion and blow-up. A finite-time blow-up of initial data in the Schwartz class of smooth rapidly decreasing functions is discussed.

# Contents

<b>I</b>	<b>Basic Introduction</b>	<b>xvii</b>
<b>1</b>	<b>Introduction</b>	<b>1</b>
1.1	Motivation & Mathematical Background . . . . .	1
1.2	Overview of the Thesis . . . . .	16
<b>2</b>	<b>Concept of Dispersive Equations, Blow-up, Hamiltonian System and Integrability</b>	<b>17</b>
2.1	Dispersive PDEs . . . . .	18
2.2	Linear Dispersive PDEs . . . . .	19
2.3	Nonlinear Dispersive PDEs . . . . .	19
2.3.1	The NLS equation . . . . .	21
2.3.2	The Davey-Stewartson (DS I) . . . . .	22
2.4	Blow-up: Power Nonlinearity . . . . .	22
2.4.1	Dissipative type . . . . .	23
2.4.2	Dispersive type: gKdV . . . . .	25
2.4.3	Blow-up scenario . . . . .	26
2.5	Hamiltonian systems and Integrability . . . . .	27
<b>II</b>	<b>Numerical Aspects</b>	<b>33</b>
<b>3</b>	<b>Numerical Approaches</b>	<b>34</b>
3.1	Introduction . . . . .	34
3.2	Interpolating polynomials . . . . .	35
3.3	Numerical Differentiation Matrices . . . . .	39
3.3.1	Chebyshev Differentiation Matrices . . . . .	42
3.3.2	Numerical differentiation for pseudo-spectral series . . . . .	44

3.3.3	Discussion . . . . .	49
3.4	Numerical Time Integration Approaches . . . . .	50
3.4.1	Stiff equations . . . . .	50
3.4.2	Numerical Techniques for Stiff PDEs . . . . .	51
3.4.3	Runge-Kutta Method . . . . .	52
3.5	Driscoll's Composite Runge-Kutta Method . . . . .	52
3.5.1	Split-Stepping Approach . . . . .	54
<b>III</b>	<b>Review on NLS equations</b>	<b>57</b>
<b>4</b>	<b>The NLS equations: Existence Properties and Numerical Observations of Blow-ups</b>	<b>58</b>
4.1	Local and Global Existence Properties . . . . .	60
4.1.1	Conservation Properties of NLS . . . . .	60
4.2	Blow-up Alternative . . . . .	64
4.2.1	Critical NLS: Sufficient condition for global existence . . . . .	65
4.3	Ground state . . . . .	66
4.3.1	Pohozaev Identities . . . . .	67
4.3.2	Critical NLS: Variational Characterization . . . . .	68
4.4	Virial theorem (Variance Identity) . . . . .	68
4.4.1	Critical NLS: sufficient conditions for blow-up . . . . .	69
4.5	Numerical observations of blow-up . . . . .	71
4.5.1	NLS: Self-Similarity . . . . .	72
4.6	Critical NLS: Asymptotic Self-similar blow-up solution . . . . .	73
4.6.1	NLS: Dynamic rescaling . . . . .	74
4.6.2	Blow-up rate . . . . .	78
4.6.3	Blow-up profile . . . . .	80
4.7	Convergence of Asymptotic Profile near Blow-up Regime . . . . .	83
4.7.1	Critical and supercritical collapse . . . . .	83
4.8	The 2D NLS and DS I . . . . .	85

<b>IV</b>	<b>Numerical Study: Blow-up in Davey-Stewartson I systems</b>	<b>87</b>
<b>5</b>	<b>The DS I: Numerical Study of blow-up</b>	<b>88</b>
5.1	Davey-Stewartson System: The general setting . . . . .	88
5.2	Numerical Study of Davey-Stewartson I System . . . . .	89
5.2.1	Main Results: Conjectures . . . . .	91
5.2.2	DSI: Basic Facts . . . . .	92
5.2.3	Numerical approach for DS I . . . . .	94
5.2.4	Localized stationary DS I solutions . . . . .	97
5.2.5	Time evolution . . . . .	99
5.2.6	Time evolution of the dromion . . . . .	101
5.2.7	Gaussian initial data . . . . .	105
5.3	Conclusion and Further studies . . . . .	106
<b>A</b>	<b>Notations and blow-up</b>	<b>108</b>
A.1	Function spaces: $L^p$ , $W^{k,p}$ and $H^k$ . . . . .	108
A.2	The Laplacian . . . . .	109
A.3	Blow-up in Hopf equation . . . . .	110
<b>B</b>	<b>Taylor coefficients of analytic functions: Numerical Computation</b>	<b>111</b>
B.1	Cauchy Integral via fast Fourier transform (FFT) . . . . .	112
B.1.1	Taylor series of analytic functions . . . . .	112
B.1.2	Fornberg algorithm . . . . .	113
B.1.3	Fornberg error estimates . . . . .	116
B.1.4	Implementing the Fornberg algorithm . . . . .	117
B.1.5	Interpolation and the Fornberg Algorithm . . . . .	117
B.1.6	More Examples . . . . .	121
B.1.7	Conditioning of the Cauchy Integral for Interpolants . . . . .	124
B.1.8	Discussion . . . . .	127

<b>C The NLS equation</b>	<b>128</b>
C.0.1 Virial identity . . . . .	130
C.0.2 Proof of Pohozaev Identities . . . . .	133
C.1 Asymptotic profile of the ground state $Q$ for NLS . . . . .	134
<b>D Algorithms</b>	<b>142</b>
D.1 Function evaluation and differentiation algorithms . . . . .	142
D.2 Numerical stability of algorithm . . . . .	142
<b>Bibliography</b>	<b>144</b>

# List of Figures

1.1	An example of two dimensional dispersive waves, [115][130]. . . . .	1
1.2	Solutions to the $u_{tt} = u_{xx}$ for $u_0(x) = \exp(-x^2)$ and $u_t(0, x) = 0$ . Cf. [76, 96].	2
1.3	Solutions to the Airy equation for $u_0(x) = \exp(-x^2)$ . Cf. [96, 224]. . . . .	3
1.4	Left: solutions to the Hopf equation for $u_0(x) = \exp(-x^2)$ . Right: the characteristics showing the multi-valuedness as the shock-time is reached. Cf. [96]. . . . .	4
1.5	Solutions to the Burgers equation (1.1.6) for $u_0(x) = \exp(-x^2)$ with ( $\varepsilon = 10^{-2}$ ) on the left and numerically computed energy $E(t) = \int u^2 dx$ on the right, Cf. [96]. . . . .	5
1.6	For $u_0(x) = \exp(-x^2)$ and $\varepsilon = 10^{-1}$ , left: solution to the equation (1.1.7). Right: description of rapidly modulated oscillations in the solution (left figure) at $t = 0.82489$ . . . . .	5
1.7	An elastic collision: 2-soliton solution of the KdV equation, [86] [240] [208].	6
1.8	Dispersive wave-packet $\psi$ of NLS at some time $t_0$ and dimension $d = 1$ . . . . .	8
1.9	Peregrine breather. Cf. [172] . . . . .	10
2.1	The dispersion relation $\omega(k)$ in dimension $d = 1$ . . . . .	20
2.2	Solution to (2.4.3) with $q = 2$ near blow-up for $u_0(x) = 10.1 \exp(-x^2)$ . . . . .	24
2.3	For $u_0(x) = A \exp(-x^2)$ , on the left: maximum $\max_{x \in [-10\pi, 10\pi]} u(t, x)$ starts to blow up for any amplitude in the range $6 - 10$ , and on the right: the blow-up rate traced by fitting $\log_{10} \ u(t)\ _{\infty}$ according to $\log_{10} \ u(t)\ _{\infty} = \alpha \log_{10}  t_* - t  + \beta$ . . . . .	25
2.4	Solution to the gKdV, $p = 4$ , for $u_0 = 1.01u_{\text{sol}}$ , perturbed soliton. See [96]. . . . .	26
3.1	Comparison of Lagrange polynomial interpolations using 61 equispaced-points and 61 Chebyshev-points on $[-1, 1]$ . Left: the functions $u, v, w$ are interpolated on equispaced with effect of error oscillations at the boundaries. Right: the effect of oscillations is damped out by interpolating $u, v, w$ on Chebyshev nodes. Cf. [209] . . . . .	39
3.2	Comparison of Lebesgue functions for $N+1$ equispaced-points (top) and $N+1$ Chebyshev-points (bottom) on $[-1, 1]$ , with $N = 60$ used. Cf. Trefethen [208].	40

3.3	Convergence of the 2nd-order finite differences for an entire function $\sin(\pi x)$ (shown $\bullet$ ) and analytic functions $2/(3+x)$ and $1/(1+x^2)$ (shown in $\circ$ and $*$ respectively) defined on $[-1,1]$ . (Cf. Trefethen [209]). . . . .	42
3.4	The Chebyshev spectral differentiations of functions defined on $[-1,1]$ . At the top, absolute errors in the 1st and 2nd Chebyshev spectral derivatives of $1/(1+x^2)$ and at the bottom for $2/(3+x)$ , (cf. Trefethen[209]). . . . .	43
3.5	Epsilon commutative diagram. . . . .	44
3.6	The maximum absolute error of the $s$ th numerical derivative of the function $u(x) = \sin(\pi x)$ on Chebyshev nodes in $[-1, 1]$ for various degrees $N$ of the polynomial interpolant using (left) Clenshaw's algorithm and (right) chebfft algorithm. . . . .	49
3.7	Logarithmic plots of the numerical (-o-) and exact (---) solutions of the problem (3.4.1), for $y_0 = 10$ , by explicit (Euler) and implicit (RK2) schemes at time-steps $h$ . . . . .	50
4.1	Blow-up solution to the focusing NLS equation (4.1.1) at the critical dimension $d = 1$ with $\sigma = 2$ for initial data $\exp(-x^4/4) \in H^1(\mathbb{R})$ . . . . .	63
4.2	Asymptotic profile of the blow-up solution at the critical dimension, where $d = 2$ and $\sigma = 1$ on the domain $[0, 100]$ for an initial data $u(0, \rho) = 5e^{-\rho^2/d}$ . . . . .	78
4.3	The behaviour of $\alpha(\tau)$ (top panel) and $\lambda(\tau)$ (lower panel) for $ u(\tau, \rho) $ as $\tau$ approaches $\tau_{max} = \infty$ , in the critical case with $d = 2$ and $\sigma = 1$ on $[0, \infty]$ . . . . .	78
4.4	Blow-up rate in the critical dimension, where $d = 2$ and $\sigma = 1$ . The bold dashed line represents the equation of the line $y = 0.5198x - 0.04623$ while the bold-line represents the $\log \lambda(t)$ . This is equivalent to $\log \lambda(t) \sim 0.5198 * \log(T_* - t)$ . . . . .	79
4.5	Chebyshev coefficients of $ u(1000, \rho) $ on the domain $[0, 100]$ in the critical dimension, $d = 2$ and $\sigma = 1$ . . . . .	80
4.6	An admissible solution to the profile equation (4.6.17) at the supercritical dimension, where $d = 1$ and $\sigma = 3$ . . . . .	82
4.7	Convergence of the blow-up solution, at $\tau = 1$ , to the focusing NLS equation to the self-similar blow-up profile $Q$ with $u_0(\rho) = 2.2e^{-\rho^2/d}$ at dimensions $d = 2$ and $\sigma = 1$ . . . . .	82

5.1	The Fourier coefficients of the function (5.2.20) on the left, and the difference of the numerically computed action of the operator $\partial_\xi^{-1}\partial_\eta + \partial_\eta^{-1}\partial_\xi$ on (5.2.20) and the exact expression on the right. . . . .	97
5.2	Localized stationary solution to DS I (5.2.9) for $\omega = 1$ on the left, dromion solution (5.2.10) for radiating boundary conditions on the right. . . . .	98
5.3	Contour plot of the solution in Fig. 5.2 on the left, and its Fourier coefficients on the right. . . . .	98
5.4	The solution $\tilde{Q}$ of Fig. 5.2 on the right on the $\xi$ -axis (red) together with the $Q$ of Fig. 5.2 (blue) on the left, and a logarithmic plot of the solution of Fig. 5.2 on the $\xi$ -axis on the right. . . . .	99
5.5	Difference of the DS I solution for the initial data $\Psi(\xi, \eta, 0) = Q(\xi, \eta)$ and $Qe^{it}$ , on the left the $L^\infty$ norm of the difference in dependence of time where $\text{err} = \ \Psi(t, \xi, \eta) - e^{it}Q(\xi, \eta)\ _\infty$ , on the right is just the difference for $t = 1$ . . . . .	101
5.6	Solution to DS I for the initial data $\Psi(\xi, \eta, 0) = 0.9Q$ , on the left for $t = 5$ , on the right the $L^\infty$ norm in dependence of time. . . . .	102
5.7	Solution to DS I for the initial data $\Psi(\xi, \eta, 0) = Q - 0.1 \exp(-\xi^2 - \eta^2)$ , on the left for $t = 5$ , on the right the $L^\infty$ norm in dependence of time. . . . .	102
5.8	DSI solution close to blow-up for initial data $\Psi(\xi, \eta, 0) = 1.1Q$ . On the left the evolution of the $L^\infty$ norm of the solution, on the right the conservation of mass $\Delta = \log_{10}(1 - m(t)/m(0))$ , which stays below $-14$ until we get close to the critical time. The fitted blow-up time is $t^* = 5.332$ . . . . .	103
5.9	Left: DSI solution close to blow-up for initial data for $\Psi(\xi, \eta, 0) = 1.1Q$ . Right: Difference of the DS I solution close to blow-up and a scaled dromion. . . . .	104
5.10	Blow-up rate for initial data $\Psi(\xi, \eta, 0) = 1.1Q$ . On the left $\ \Psi\ _\infty$ , the red lines have the form $a \log_{10}(t^* - t) + b$ , with values obtained by fitting the last several thousand points before we lose precision, $a_\infty = 1.13$ , $a_{\Psi_x} = 2.18$ and $b_\infty = 1.2$ , $b_{\Psi_x} = 10.0$ and $t^* = 0.5394$ . . . . .	104
5.11	Solution to DS I for the initial data $\Psi(\xi, \eta, 0) = 3 \exp(-\xi^2 - \eta^2)$ , on the left for $t = 1$ , on the right the $L^\infty$ norm in dependence of time. . . . .	105
5.12	Left: DS I solution close to blow-up for Gaussian initial data $\Psi(\xi, \eta, 0) = 4.5e^{-\xi^2 - \eta^2}$ . Right: difference of the DS I solution and a rescaled dromion close to blow-up for Gaussian initial data. . . . .	106

5.13 DS I solution close to blow-up for Gaussian initial data $\Psi(\xi, \eta, 0) = 4.5e^{-\xi^2 - \eta^2}$ . Blow up time at $t = 0.1583$ . . . . .	106
5.14 Blow-up rate for initial data $\Psi = 4.5e^{-\xi^2 - \eta^2}$ . Left: $\ \Psi\ _\infty$ , the red lines have the form $a \log_{10}(t^* - t) + b$ , with values obtained by fitting the last several thousand points before we lose precision, $a_\infty = 1.28$ , $a_{\Psi_x} = 2.45$ and $b_\infty = 0.65$ , $b_{\Psi_x} = 9.08$ and $t^* = 0.1583$ . . . . .	107
B.1 Close up plots of the errors $E_k = a_k - \tilde{a}_k$ in the first 10 Taylor coefficients of analytic function $u(x) = 2/(3 + x)$ on $[-1, 1]$ obtained from Fornberg algorithm on $u(x)$ having $m = 32$ points on a circle and its $N$ degree Chebyshev interpolant $p_N^C(x)$ . Left: Errors in the Fornberg-Taylor coefficients of the $u(x)$ (shown in blue starred-dotted lines -*-) and Taylor-coefficients of the interpolant with $N = 26$ (in green triangles $\triangle$ ) and that of the exact interpolant (in blue dotted-broken lines -•-). Right: Same as in the left with $m = 32$ but $N = 36$ is used. . . . .	119
B.2 Close-up view of the absolute error $ a_n - \tilde{a}_n^B $ in the Taylor coefficients of an $N$ degree barycentric polynomial interpolant with $m$ points on the circle. For $m = 16, N = 26, 32$ (the blue starred-solid line -*- and the red starred-broken-line -*-) while $m = 32$ then $N = 64, 72$ are used (broken lines with blue dots • and solid line with dots (black) • resp.). . . . .	120
B.3 Absolute errors $ a_k - \tilde{a}_k^C $ in the Taylor coefficients of an $N$ degree Chebyshev polynomial interpolant of $1/(1 + x^2)$ with 32 points on the circle. . . . .	122
B.4 Absolute errors $ a_k - \tilde{a}_k^C $ in the Fornberg Taylor coefficients of degree $N$ Chebyshev polynomial interpolants of $\sin(\pi x)$ and $e^{-1/(x-2)}$ with 32 points on the circle around $x_0 = 0$ . <b>Top:</b> the errors in computing the Fornberg-Taylor coefficients of the function $\sin(\pi x)$ (blue starred-broken lines -*- and that of its Chebyshev interpolant (in green circled-broken lines -o-) are shown. <b>Bottom:</b> same for the function $\exp(-1/(x - 2))$ . . . . .	122
B.5 Absolute errors $ a_k - \tilde{a}_k^C $ in the Fornberg Taylor coefficients of degree $N$ Chebyshev polynomial interpolants of $e^{-1/(x^2+1)}$ with 32 points on the circle around $x_0 = 0$ . Same description as in the Figure B.4. . . . .	123



# I

---

## Basic Introduction

---



---

# Chapter 1

## Introduction

### 1.1 Motivation & Mathematical Background

It is evident that we are all surrounded by wave phenomena since one can easily notice some of them when a pebble is dropped onto a water surface such as a pond, a lake, the ocean, some sort of disturbances in a form of circular ripples are formed. The created waves evolve with time, broaden and *disperse* away after a while, because as the waves travel they start losing their shapes due to the fact that different frequencies of the individual waves have different group speeds, as obviously shown in the Figure 1.1. The medium in which such waves travel is referred to as *dispersive*.

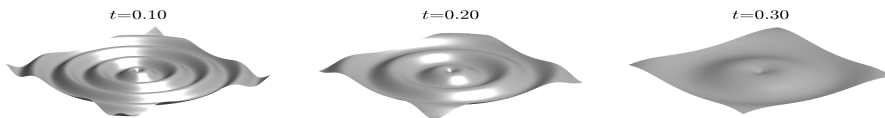


Figure 1.1: An example of two dimensional dispersive waves, [115][130].

Even though, in principle, *dissipation* can cause damping of the wave phenomena, we put more emphasis on the dispersive waves since most of the waves existing in real media are strongly dispersive in nature as stressed by V.E. Zakharov (see [96]). Therefore, we focus on the study of dispersive equations, particularly in the presence of non-linearity.

Nonlinear dispersive equations (NDEs), in a situation where dissipation is dominated by dispersion, are important due to their ubiquity in applications. Examples include the prominent equations of mathematical physics: Korteweg-de-Vries (KdV) and nonlinear Schrödinger (NLS) equations present in hydrodynamics, plasma physics, nonlinear optics, Bose-Einstein condensates, quantum mechanics, general relativity, ... It is important to stress that dispersive equations, as those mentioned are mostly derived as asymptotic models, i.e. obtained in certain limiting situations.

In the field of mathematical physics, electromagnetic waves are mostly governed by partial differential equations (PDEs) and the nonlinear dispersive equations receive special considerations in the theory of PDEs. Even though in the last three decades, the theory of dispersive PDEs has seen remarkable progress, still several questions arise due to some mathematical difficulties related to the possible existence of rapidly oscillating regimes in their solutions. The solutions describing the relevant dynamics could exhibit different

properties of parabolic and hyperbolic equations such as blow-ups (a loss of regularity), stable or solitonic structure, shocks, dispersion, symmetries, . . . , for instance see [130, 49] .

This work is devoted to the study of weakly nonlinear evolutionary systems. Our interests are families of NLS equations. We focus on the weakly nonlinear wave evolution equations in a semi-linear form, containing the linear  $\mathbf{L}u$  and non-linear  $\mathbf{N}[\cdot]$  terms:

$$\partial_t u = \mathbf{L}u + \mathbf{N}[u] \quad (1.1.1)$$

where  $\partial_t = \frac{\partial}{\partial t}$  and  $\mathbf{L}$  are respectively the time and linear spatial derivative operators.

Let us first consider the classical wave equation in one-dimension

$$u_{tt} - c^2 u_{xx} = 0, \quad c > 0. \quad (1.1.2)$$

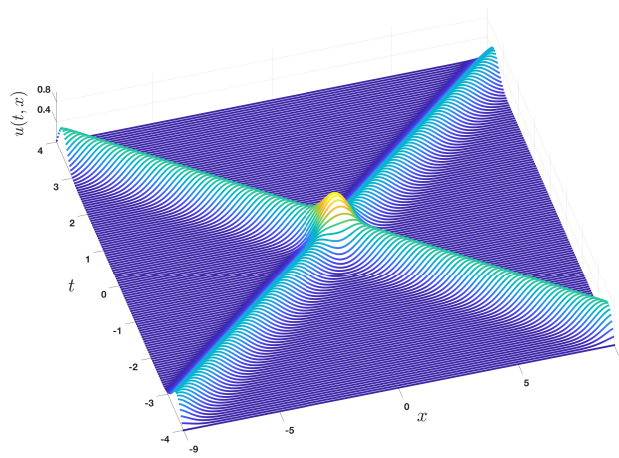


Figure 1.2: Solutions to the  $u_{tt} = u_{xx}$  for  $u_0(x) = \exp(-x^2)$  and  $u_t(0, x) = 0$ . Cf. [76, 96].

The dispersive property for linear PDEs is best analysed via Fourier transform. That is, when the transform  $\mathcal{F}[u](k, \omega) = \int_{\mathbb{R}^2} u(t, x) e^{i(kx - \omega t)} dx dt$  is applied one gets the so-called dispersion relation  $\omega(k) = \pm ck$ , describing the behaviour in which a plane-wave  $e^{i(kx - \omega t)}$  travels in the space. An important quantity associated with the wave-frequency  $\omega$  is the group velocity  $v_g := d\omega/dk$ , which for the wave equation (1.1.2) the  $v_g = \pm ck = \text{const.}$ ; and this implies that a localized initial data (say  $\exp(-x^2)$ ) travels with-out losing its shape for all time. Therefore, the wave equation (1.1.2) is not dispersive. A general solution to the equation (1.1.2) as given by d'Alembert formula (in terms of characteristics  $x \pm ct$ ) is

$$u(t, x) = f(x - ct) + g(x + ct). \quad (1.1.3)$$

The arbitrary functions  $f$  and  $g$  describe travelling waves along the characteristics and can be considered as the boundary values that are fixed for an initial value problem as shown

in Figure 1.7. Consequently, since the solutions are localized in space  $x$ , they are solitary waves. Due to linearity, superposition principle holds; when two solutions are superposed they appear as a sum (see the hump in the Figure 1.1), Cf. [96] and for details [24, 50, 110].

If instead the Airy-equation (linearized KdV)

$$u_t + u_{xxx} = 0, \quad (1.1.4)$$

is considered, it is apparent from the dispersion relation  $\omega(k) = -k^3$  that the group velocity  $v_g$  is a non-constant real function, i.e.  $\nabla\omega(k) \neq \text{const.}$  As shown in the Figure 1.1, the solution propagates at varying speeds and will disperse, unlike for the classical wave-equation (1.1.2) where solutions in future look the same in the past. The effect of dispersion can be seen in the figure 1.1 for Gaussian initial data. This is to say that a localized initial data propagated by the Airy equation will eventually be dispersed to infinity in the form of ripples 1.1. The dispersive properties are clear from the fundamental solution  $F(x, t)$  of the Airy equation in terms of Airy function  $F(x, t) = \frac{1}{t^{1/3}} Ai(x/t^{1/3})$  because as  $Ai(x)$  decreases exponentially on the right it oscillates rapidly on the left (see the dispersive estimates of the  $Ai(x)$  in [96] and the references there in).

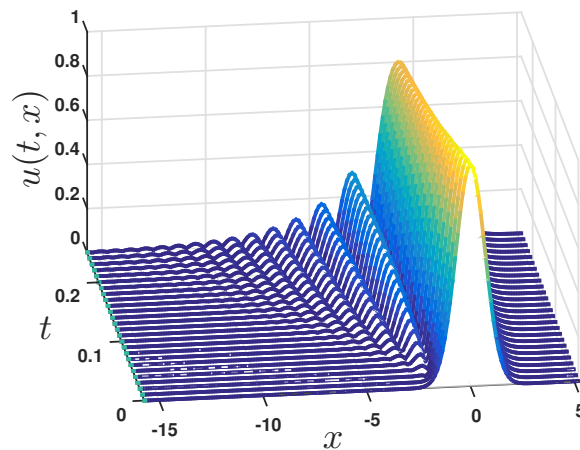


Figure 1.3: Solutions to the Airy equation for  $u_0(x) = \exp(-x^2)$ . Cf. [96, 224].

There can be a situation where dispersion is negligible but nonlinearity is not as may be observed from the solution behaviour of the Hopf equation

$$u_t + 6uu_x = 0. \quad (1.1.5)$$

Solution to this equation is obtainable via the method of characteristics and will assume the form of d'Alembert formula  $u(t, x) = u_0(x - u_0 t)$  except that the  $u$  plays the role of speed. This would mean that the greater the amplitude  $u$  the faster the solution propagates.

As a result of this, the propagated localized initial data develops a behaviour of *gradient catastrophe* in finite time. More precisely, the gradient of the solution  $u_x$  becomes infinite as  $t \rightarrow t_c := -1/\min_{\xi \in \mathbb{R}} u'_0(\xi)$  where  $\xi := x - u_0 t$ . Consequently, solutions for  $t > t_c$  become multi-valued and thus called shock solutions. This situation is possible, especially, in the context of water waves, where nonlinearity plays vital role over dispersion.<sup>1</sup>

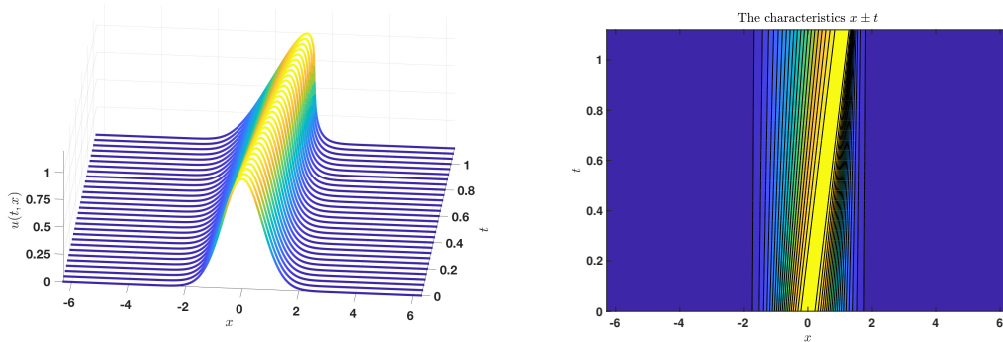


Figure 1.4: Left: solutions to the Hopf equation for  $u_0(x) = \exp(-x^2)$ . Right: the characteristics showing the multi-valuedness as the shock-time is reached. Cf. [96].

One may intend to obtain regular solutions to the Hopf equation (1.1.5), it turns out that is possible provided it is regularized by adding dissipative or dispersive terms. A term proportional to  $u_{xxx}$  is introduced for the latter, and  $u_{xx}$  for the former using a constant  $\varepsilon \ll 1$ . Dissipative regularisation leads to smooth solutions decaying slowly (since energy is not conserved) with a gradient of the order  $1/\varepsilon$ , whereas for the dispersive regularisation solutions tend to develop rapidly amplifying oscillations, see Fig. 1.6 .

In general, the regularisation terms are introduced in the semi-classical limit of a closely related equations thereby making solutions less singular, in the sense that regular data do not evolve into singular quantities. The introduced dissipation term corresponds to addition of viscosity to the system in a sense that, in certain limit, the solution behaviour of the equation (1.1.5) near point of gradient-catastrophe can be determined. In the absence of the dissipation (damping) term, steepening leads to shock waves and infinite steep solution whereas the presence of dissipation would cause to have a solution of finite width. The Hopf equation (1.1.5) is seen as dissipationless limit of the Burgers equation  $u_t + 6uu_x = u_{xx}$ . If we consider slow-variable transformations  $t \rightarrow \varepsilon t$ ,  $x \rightarrow \varepsilon x$  and  $u(t, x) \rightarrow u(\varepsilon t, \varepsilon x)/\varepsilon$  of the

<sup>1</sup>It is apparent from the relevant figures that the effect of nonlinearity in the equation (1.1.5) causes solutions beyond some  $t_c$  finite, for generic initial data, become discontinuous, therefore *shock waves* are formed. More precisely,  $u(t, x)$  approaches a point of *gradient catastrophe*, where  $u$  itself or its derivatives may be discontinuous or unbounded as  $t \rightarrow t_c$ .

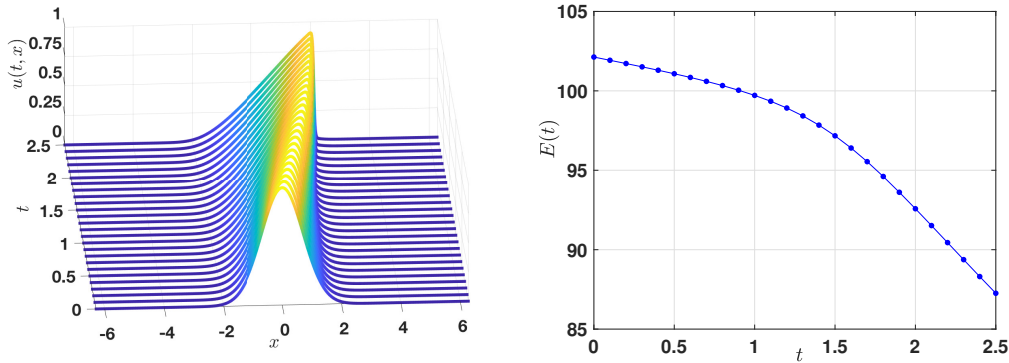


Figure 1.5: Solutions to the Burgers equation (1.1.6) for  $u_0(x) = \exp(-x^2)$  with ( $\varepsilon = 10^{-2}$ ) on the left and numerically computed energy  $E(t) = \int u^2 dx$  on the right, Cf. [96].

Burgers equation  $u_t + 6uu_x = u_{xx}$  we obtain

$$u_t + 6uu_x = \varepsilon u_{xx}. \quad (1.1.6)$$

Then, taking the formal limit  $\varepsilon$  to zero brings us back to the equation (1.1.5). Taking the inverse view, the equation (1.1.6) can be seen as a dissipative regularisation of the Hopf equation (1.1.5), a regularisation for which the point of gradient catastrophe is moved to  $t = \infty$ . On the other hand, applying the same slow-variables transformation on the KdV equation  $u_t + 6uu_x + u_{xxx} = 0$  one gets

$$u_t + 6uu_x + \varepsilon^2 u_{xxx} = 0, \quad \varepsilon \ll 1. \quad (1.1.7)$$

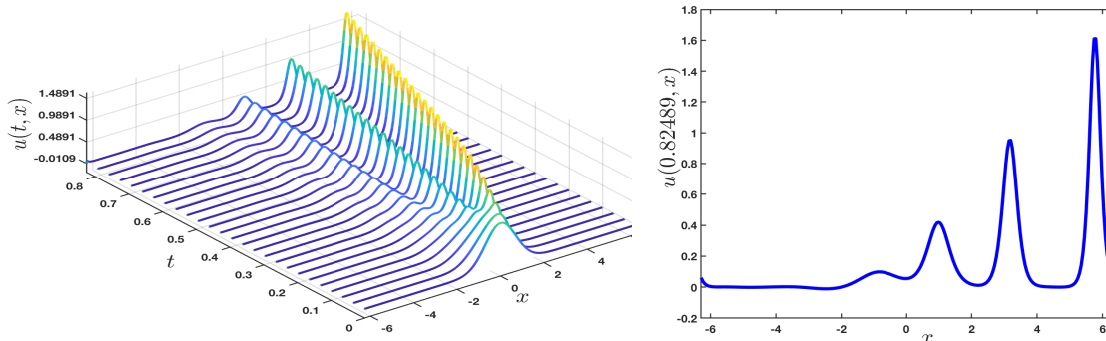


Figure 1.6: For  $u_0(x) = \exp(-x^2)$  and  $\varepsilon = 10^{-1}$ , left: solution to the equation (1.1.7). Right: description of rapidly modulated oscillations in the solution (left figure) at  $t = 0.82489$ .

Then, as  $\varepsilon \rightarrow 0$ , the inviscid equation (1.1.5) is recovered. In turn, the equation (1.1.7) serves as the dispersive regularizer of the Hopf equation (1.1.5). The dispersive regularisation, as  $\varepsilon \rightarrow 0$ , shows solutions are rapidly modulated and oscillate in the

dispersive-shock regions (Fig 1.6). Moreover, shock-wave solutions can be observed in higher dimensional version of Hopf equation. Singularity formation is also present in the solutions of many equations of fluid dynamics; like the 3D incompressible Navier-Stokes equation, the 2D incompressible Euler's equation, the Einstein equation of general relativity (GR). Loosely speaking, a singularity can be formed whenever the non-linearity overpowers the dispersive or dissipative behaviour of the equation at hand.

We have noticed that nonlinearity tends to steepen the localized initial data while the dispersion intends to flatten it. The situation where the steepening due to nonlinearity gets compensated by the spreading due to dispersion we will have the so-called *solitons*, the famous solitary wave solutions. This special type of solution is firstly observed in the solutions of the celebrated Korteweg-de Vries (KdV) equation which appears in the study of shallow-water waves:

$$u_t + 6uu_x + u_{xxx} = 0; \quad u : (0, \infty) \times \mathbb{R} \rightarrow \mathbb{R}, \quad t \in \mathbb{R}^*. \quad (1.1.8)$$

The dispersive equation (1.1.8) admits a solitary wave (1-soliton) solution for fixed speed  $c > 0$ :

$$u(t, x) = f(\tilde{x} - ct) = \frac{c}{2} \operatorname{sech}^2 \left[ \frac{\sqrt{c}}{2} (\tilde{x} - ct) \right], \quad \tilde{x} = x - x_0 \quad (1.1.9)$$

with the maximum at its vanishing argument  $x - ct - x_0 = 0$ . The soliton is produced as a result of the balance between the nonlinearity and the dispersion effects. Solitons, as can be observed in the Figure 1.7, retain their shapes after collision.

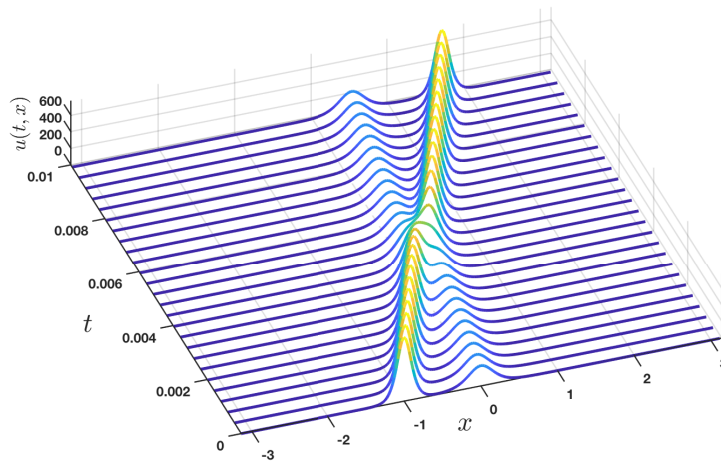


Figure 1.7: An elastic collision: 2-soliton solution of the KdV equation, [86] [240] [208]. They were firstly observed by a naval architect, John Scott Russell in 1834 and their mathematical model was firstly introduced by Boussinesq (1877) and reformulated in

1895 by D. Korteweg and G. de Vries [193]. The equation that extends KdV to 2D is Kadomtsev-Petviashvili (KP) one

$$(u_t + 6uu_x + u_{xxx})_x + \beta u_{yy} = 0, \quad \beta = \pm 1. \quad (1.1.10)$$

In general, the central issues in the study of nonlinear dispersive PDEs theory is that the solution to a system describing the nonlinear wave propagation phenomena has the tendency to cease to exist or break in a finite time. This is the effect of nonlinearity being dominant, a behaviour known in mathematics and physics as “*blow-up*” or “*wave-collapse*”. In other words, we say the mathematical model develops a singularity, however it is possible that it may or may not be a good model of physical reality. Some of the consequences of blow-up are that solutions or other quantities associated to the system, such as mass or energy, may become unbounded. The strong influence or effect of nonlinearity is mostly responsible for blow-up. To put things into perspectives, it is well-known that, typically, in a physical system nothing becomes infinite. If it happens to be the case, for instance energy goes beyond a limit, is an indication that the underlying model is either invalid, or breaks down, or, as in the asymptotic models, more terms are need in the asymptotic expansion in its derivation. A typical case of blow-up for asymptotic models is the NLS equation.

Another dispersive equation that is present in several physical applications is the complex-valued nonlinear Schrödinger (NLS) equation that reads:

$$\begin{cases} i\psi_t + \Delta\psi = f(|\psi|^2)\psi, & \psi : \mathbb{R}^+ \times \mathbb{R}^d \rightarrow \mathbb{C} \\ \psi(0, \mathbf{x}) = \psi_0(\mathbf{x}) \in H^s(\mathbb{R}^d) & \psi_0 : \mathbb{R}^d \rightarrow \mathbb{C} \end{cases} \quad (1.1.11)$$

where  $i = \sqrt{-1}$  and  $\Delta = \sum_{1 \leq j \leq d} \partial_{x_j}^2$  is a Laplacian in  $\mathbb{R}^d$ . The NLS equation is a nonlinear variant of the Schrödinger equation (SE) in quantum mechanics<sup>2</sup>

$$i\hbar\psi_t + \frac{\hbar^2}{2m}\Delta\psi = V\psi, \quad \psi : \mathbb{R} \times \mathbb{R}^d \rightarrow \mathbb{C}, \quad \hbar > 0 \quad (1.1.12)$$

where, the function  $\psi$  describes the propagation of particle-wave like objects, such as photons, electrons, protons e.t.c, at the microscopic level,  $V = V(\mathbf{x}, t)$  is a potential function in  $L^2(\mathbb{R}^d, d\mathbf{x})$  and  $\hbar$  is a Planck constant. The SE (1.1.12) is of the form of the equation  $i\varepsilon\psi_t + \varepsilon^2\Delta\psi = f(|\psi|^2)\psi$  (where  $\varepsilon$  plays the role of  $\hbar$ ), the NLS equation (1.1.11) in its semiclassical limit with  $\varepsilon \rightarrow 0$  corresponding to the transition from quantum to classical mechanics in the case of the SE.

---

<sup>2</sup>The Schrödinger equation is a quantum counterpart of Newton’s 2nd law of motion in classical mechanics where  $\psi(t, \mathbf{x})$  is a wave function assigning to every point  $(t, \mathbf{x})$  a complex number and  $V(t, \mathbf{x})$  is the potential that signifies the environment of the existing particle.

Furthermore, using the general power non-linearity  $f(|\psi|^2) = \gamma|\psi|^{2\sigma}$  with non-linearity exponent  $\sigma > 0$ , the focusing ( $\gamma = 1$ ) resp. defocusing ( $\gamma = -1$ ) NLS equation is

$$i\psi_t + \Delta\psi + \gamma|\psi|^{2\sigma}\psi = 0, \quad \gamma = \pm 1. \quad (1.1.13)$$

It is highlighted in [11] [163] that, slowly varying wave-packet (envelope) dynamics of a wave moving through a weakly nonlinear dispersive medium have a standard description in terms of the quasi-monochromatic (plane) waves (in form of carrier waves),  $u = \varepsilon\psi e^{i(\mathbf{k}\cdot\mathbf{x} - \omega t)}$  with amplitude  $\varepsilon\psi$  and  $\varepsilon \ll 1$ . In the modulational regime in a situation where dissipation is insignificant, the NLS equation can heuristically be derived by considering an expansion of generalized weakly-nonlinear dispersion relation at the least non-trivial order of the wave-train of the weakly-nonlinear carrier wave given in the asymptotic expansion of

$$u(t, \mathbf{x}) = \varepsilon\psi(\varepsilon\mathbf{x} - \varepsilon^2\mathbf{v}_g t) e^{i(\mathbf{k}\cdot\mathbf{x} - \omega t)} + c.c., \quad \varepsilon \ll 1, \quad \mathbf{v}_g = \nabla_{\mathbf{k}}\omega \quad (1.1.14)$$

where  $\psi$  solves cubic NLS where  $\sigma = 1$  and  $c.c.$  = complex conjugate (see [235],[89],[90] and [39], [202]). Higher order terms in  $\varepsilon$  in the expansion will lead to higher nonlinearity exponents. Moreover, an alternative informal derivation of the NLS equation for instance in dimension 2 can be obtained from the Maxwell's equations using paraxial approximation, see Chapter 1 of [51].

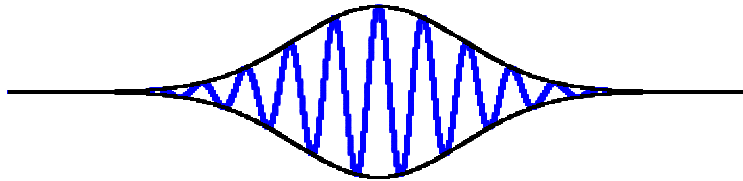


Figure 1.8: Dispersive wave-packet  $\psi$  of NLS at some time  $t_0$  and dimension  $d = 1$ .

The NLS equation is a universal one, in applications, that appears to describe the propagation of nonlinear waves [222] including a laser beam in a medium with sensitive refractive index (growing proportionately) to the amplitude of the complex-valued wave field  $\psi$  such as optical fibers [137], gravity waves on the free surface of inviscid (ideal) fluid (water-waves) [222] [172], plasma waves and Bose-Einstein condensates. It is viewed as a good model for rogue-waves formations [180] [46] with solutions such as the Peregrine breather, the Akhmediev breather, and Kuznetsov-Ma breather [172].

A special case is when  $d = 2$ ,  $\sigma = 1$ ,  $\gamma = 1$  that appears in nonlinear optics. There, the time parameter  $t$  is taken as the distance variable across the beam whereas the beams transverse through the coordinates  $\mathbf{x} = (x_1, x_2)$ , see [33], [47],[207], [6], [113]. In dimension

$d = 3$ , using a similar setting as in dimension 2, in the context of plasmas the NLS equation (1.1.11) is considered as the limit of Zakharov system for Langmuir waves [232], [113], [233], and [74], and the variable  $t$  is the usual time coordinate. Blow-up in these contexts has physical consequences due to self-focusing where  $\gamma = 1$ . In the case of electromagnetic waves in dimension  $d = 2$ , singularity corresponds to the focusing of the beam and increase in the amplitude of the wave function  $\psi$ . For Langmuir waves, the singularity or the blow-up is explained there to represent collapse or filamentation (self-focusing) of the wave.

The focusing NLS equation ( $\gamma = 1$ ) in dimension  $d = 2$  can have a global solution whenever  $\sigma < 1$  and blow-up in finite time for  $\sigma \geq 1$ . In the case  $\sigma = 1$ , the NLS equation is cubic and  $L^2$ -critical (i.e. the mass is invariant under scaling, where the solution becomes narrower and taller). With regards to the local existence in  $t$ , the lifespan of  $\psi(t, \cdot)$  (on small neighbourhood of  $t$ ), for  $\psi_0 \in H^1(\mathbb{R}^2)$ , depends on the initial profile [27], [28]; this dependence is reflected in the asymptotic profile, near blow-up, too [187]. Thus, blow-up behaviour becomes interesting to not only the non-integrable 2D cubic NLS equation but also to its integrable versions, the Davey-Stewartson systems (DS I and DS II).

In the lower dimension  $d = 1$ , the complex field  $\psi(t, x)$  in the cubic NLS equation

$$i\psi_t + \psi_{xx} + |\psi|^2\psi = 0, \tag{1.1.15}$$

with the decaying boundary condition  $\lim_{x \rightarrow \pm\infty} \psi = 0$  has a solution

$$\psi(x, t) = \sqrt{(2\gamma)} e^{i(\frac{c}{2}x + (\gamma - \frac{c^2}{4})t + \varphi_0)} \operatorname{sech}[\sqrt{\gamma}(x - x_0 - ct)], \tag{1.1.16}$$

a localized solitary wave solution travelling with a speed  $c$ , where  $\gamma \in \mathbb{R}^+$ . Moreover, Zakharov and Shabat [239] solved (1.1.15) for initial data  $\psi_0(x)$  decaying sufficiently fast as  $|x|$  grows to infinity via the *inverse scattering transform* (IST)<sup>3</sup>, and moreover showed that NLS is an integrable equation, which means it possesses infinitely many conservation laws, a hierarchy of commuting flows, a Lax pair definition etc. Furthermore it is an infinite dimensional Hamiltonian systems in which IST serves as a canonical transformation to action-angle variables (see Section 1.6 of [4] and [5]). There are numerous examples of 1+1 dimensional PDEs, but in higher dimensions they are much rarer and with more complicated structure. Nevertheless, with the alternate derivation of a physical model by Davey & Stewartson (1974) on the surface evolution of packet water waves, closely equivalent to the NLS in dimension 2 is derived.

---

<sup>3</sup>Inverse scattering is a nonlinear analogue of the linear Fourier Transform.

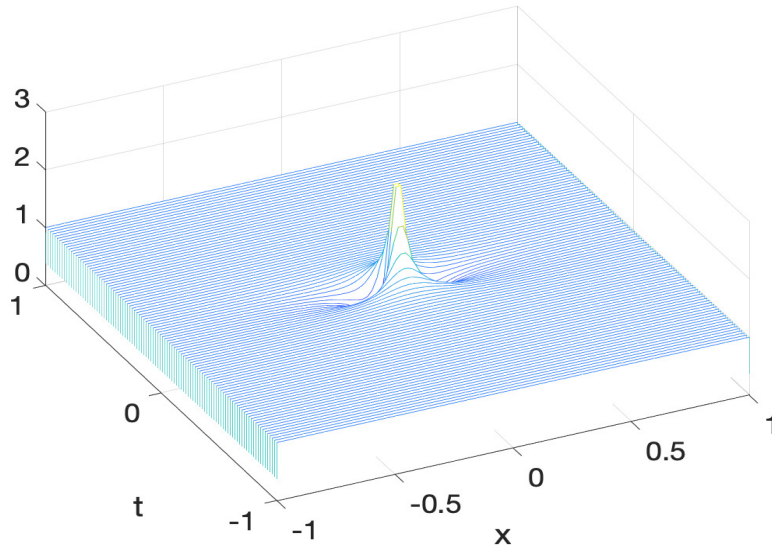


Figure 1.9: Peregrine breather. Cf. [172]

It is noteworthy to mention that the NLS equation is local, meaning that only partial derivatives are involved in contrast to the case of non-local equations like the Davey-Stewartson (DS) system, a non-local critical cubic NLS equation, where anti-derivatives appears.

Numerical studies carried out on the semi-classical limit for one dimensional focusing and defocusing NLS shows instability in their semi-classical asymptotics, see [60], [40] and [92]. It is mentioned there that, solution behaviour for the latter is much like that of the KdV equation.

The family of the dispersive DS systems, defined in  $\mathbb{R}^2$  for  $\mathbf{x} = (x, y) \in \mathbb{R}^2$ , is

$$i\psi_t + \alpha\partial_x^2\psi + \beta\partial_y^2\psi = (\gamma|\psi|^2 + \partial_x\phi)\psi; \quad \psi : \mathbb{R} \times \mathbb{R}^2 \rightarrow \mathbb{C} \quad (1.1.17)$$

$$\partial_x^2\phi + \beta\partial_y^2\phi = -\rho(|\psi|^2)_x; \quad \phi : \mathbb{R}^2 \rightarrow \mathbb{R} \quad (1.1.18)$$

where the coefficients  $\alpha, \beta, \gamma, \rho$  are real numbers. The complex-valued function  $\psi$  is referred to as the *main field*, while the real field  $\phi$  is a *mean velocity potential* like in e.g. Navier-Stokes. The boundary conditions associated to the system on the main field  $\psi$  is usually of Dirichlet type,  $\psi(t, x, y) \rightarrow 0$  as  $x^2 + y^2 \rightarrow \infty$ , while on the mean-field  $\phi$  it depends on the sign of  $\beta$  (see Ablowitz et al. [2], Ablowitz and Clarkson [5]). There are different cases, depending on the choice of  $\alpha$  and  $\beta$  where  $(\alpha, \beta) = (\pm 1, \pm 1)$ , leading to  $(+, +)$  elliptic-elliptic,  $(+, -)$  elliptic-hyperbolic systems,  $(-, +)$  elliptic-hyperbolic and  $(-, -)$  hyperbolic-hyperbolic, see [41] and [71]. The DS system is integrable [56] by means

of IST method in the cases  $(+, -)$  and  $(-, +)$  for certain values of the parameters. The former appeared in a work by Davey and Stewartson [41] studying the evolution of surface water-waves packet. Like the NLS equation, "the DS system provides a canonical description of the amplitude dynamics of a weakly nonlinear two-dimensional wave packet when a mean field is driven by modulation" [202]. We note here that there are no known examples of local integrable systems in dimensions higher than 1+1 (except for those that are linearisable by a direct change of variables).

The DS systems are derived from the "*universal*" models that provide the descriptions of interacting long and short waves, as the singular limit of the Zakharov-Rubenchik or Benney-Roskes systems [12, 236]. The rigorous derivation is given in [41, 10, 122] in the context of water waves as in ([202], Ch. 11). The full description of the inverse scattering theory for the DS systems are discussed in greater details as found in [5] (sect. 5.5) and [96] (sect. 4.8). Several numerical studies on the DS systems were carried out, see [41], [14],[87] for details.

The DS systems, as the 2d generalization of the integrable cubic NLS equation, particularly the DS I and DS II, plays important role in applications [17],[124]. The two integrable equations (DS I and DS II) describe the evolution of weakly nonlinear waves propagating in one of the directions whose amplitude is slowly varying from the two sides [41]. They also appear in modelling the evolution of plasma under the effect of magnetic field [165]. In nonlinear optics, the potential  $\varphi$  is used as a rectified field [124], [56]. In [221], DS is used to model 2D nonlinear excitations in Bose-Einstein Condensates (BEC).

Classical theory of PDEs [202] points at a mechanism for loss of regularity in 2d NLS equation. This equation undergoes self similar blow-up, as a rescaling transformation preserves the  $L^2$  norm. As DS has the same nonlinearity it is plausible that a similar mechanism exists there. The DS II case is well studied [105], and there is even an exact solution which blows up at one point in space and time given by Ozawa [173]. Extensive numerical studies [97], [99] show that, blow-up indeed exists and [105] studies the mechanism in detail showing that the Ozawa type blow up is generic, and the critical profile is a rescaled lump. In several cases one can continue after the blow-up [88].

Our main goal is to study critical problems that still remain obscure for DS I. Recent studies on the DS I suggests that blow-up exists for small Gaussian initial data but due to the demand for high numerical resolution, the blow-up mechanism remained unknown [14]. The blow-up mechanism for its counterpart, DS II, is recently established in [105].

Due to existence of singularities in these equations it is reasonable to look for suitable function space of solutions. In this regards, the appropriate function spaces are the *Schwartz*

space  $\mathcal{S}(\mathbb{R}^2)$  and Sobolev spaces  $H^s(\mathbb{R}^d)$ . The latter in particular, capture not only the analytic behaviour of the function but also that of its (weaker or classical) derivatives up to some order  $s$ . The correct  $s$  is known for a solution  $u$  if one considers symmetries of the NLS equation such as scaling and translation.

Important desirable features describing what it means to solve a dynamical system (or PDE) are well-posedness conditions of the (physical) problem. Roughly speaking, wellposedness implies existence, uniqueness and continuous dependence of the solution on the given initial data of the problem. Depending on the function space of the initial data, there are numerous wellposedness results for the DS system. Global solutions  $(\psi, \varphi)$  to the DS II for sufficiently small initial data  $\psi_0 \in L^2(\mathbb{R}^2)$  and unique maximal solutions for any initial data in  $L^2(\mathbb{R}^2)$  for a finite time  $T_* > 0$  [71]. Some regular results on  $\psi$  for  $\psi_0 \in H^1(\mathbb{R}^2)$  are established too, see Sec. 12.3 of [202]. Fokas and Sung [59] proved the existence of unique DS I solution  $C(\mathbb{R}, \mathcal{S}(\mathbb{R}^2))$  for  $\psi_0$  in the Schwartz  $\mathcal{S}(\mathbb{R}^2)$  and  $\varphi_1, \varphi_2 \in C(\mathbb{R}, \mathcal{S}(\mathbb{R}^2))$ .

It can easily be observed that the NLS equation (1.1.11) under the scaling

$$\mathbf{x} \rightarrow \tilde{\mathbf{x}} = \lambda^{-1}\mathbf{x}, \quad t \rightarrow \tilde{t} = \lambda^{-2}t, \quad \psi(\mathbf{x}, t) \rightarrow \tilde{\psi}(\tilde{t}, \tilde{\mathbf{x}}) = \lambda^{\frac{1}{\sigma}}\psi(\lambda^{-1}\mathbf{x}, \lambda^{-2}t)$$

stays invariant whereas the mass  $M(\psi) := \int_{\mathbb{R}^2} |\psi|^2$  scales like  $\lambda^{\frac{2d-\sigma}{\sigma d}} M[\psi]$ . Thus, NLS equation is  $L^2$ -critical when  $\sigma d = 2$  and blow-up may occur [202]. A special tool for detecting blow-up is dynamic rescaling, sometimes referred to as a 'litmus test':

$$\mathbf{x} \rightarrow \mathbf{x}' = \frac{\mathbf{x}}{\lambda(t)}, \quad t \rightarrow \tau = \int_0^t \frac{ds}{\lambda^2(s)} \quad \text{and} \quad \psi(\mathbf{x}, t) \rightarrow \psi'(\tau, \mathbf{x}') = \lambda^{\frac{1}{\sigma}}(t)\psi(\mathbf{x}', \tau) \quad (1.1.19)$$

The scaling factor  $\lambda(t)$  depends on  $t$  instead so that  $\lambda(t) \rightarrow 0, \tau \rightarrow \infty$  as  $t \rightarrow T_*$  (the blow-up time  $T_*$ ). It plays a significant role in capturing the self-similarity behaviour of the blow-up dynamics for the underlying dynamical equations.

Blow-up solutions, obtained from dynamic rescaling (1.1.19), are usually characterized by the *blow-up rate* and *blow-up profile*. The former is a law, given by  $\lambda(t)$ , obeyed by  $\psi$  as blow-up time  $T_*$  is approached while the latter gives the profile of  $\psi$  near  $T_*$  and, in general, is completely described by the ground state of the solution  $\psi$ . The blow-up profile near blow-up time  $T_*$  stays put and thus one keeps certain norm constant and studies the behaviours of the scaling parameter. These two properties can signal instability of the blow-up solution if presence of discontinuous change in any one of them occur under a continuous perturbation (see [52]). For instance, the  $L^2$ -critical focusing NLS equation in dimension  $d = 2$ , near the blow-up time we have  $\|\psi(t)\|_\infty \sim \frac{1}{\lambda(t)} = (t - t_*)^{-1/2}$  by keeping the norm of the infinity norm of the blow-up constant (see details in chapter 3 on

dynamic rescaling of the NLS). Similarly, with  $L^2$ -norm of the blow-up profile constant, the  $\|\nabla\psi(t, \cdot)\|_2 \sim (t - t_*)^{-1}$ . These signify the blow-up rates of the blow-up solutions to the critical cubic NLS in dimension  $d = 2$ .

There are quite a number of analytic results for blow-up in both NLS equation and DS systems involving dynamic rescaling (1.1.19). These include the work of Merle [152] on the focusing NLS with self-similar blow-up solution (in  $H^1$ ). The  $L^2$ -critical case is found for  $(1 + 1)$ -dimensions in the quintic NLS equation (blow up is possible), whereas for  $(2 + 1)$ -dimensions it is in cubic NLS equation. Hence, the DS system is  $L^2$  critical in this sense. However, the  $2 + 1$  hyperbolic type NLS equation admits no blow-up, see [213]. The DS II type does blow up, see [41]. An Ozawa type of solution (pseudo-conformal):

$$\psi_c(x, y, t) = e^{i\frac{b(x^2 - y^2)}{a + bt}} \frac{\psi_0(x', y')}{(a + bt)}; \quad \psi_0(x', y') = \frac{2}{1 + x'^2 + y'^2}, \quad x' = \frac{x}{a + bt}, \quad y' = \frac{y}{a + bt}$$

used there shows the existence of blow-up at time  $T_* = -\frac{a}{b}$ ,  $ab < 1$ . As a result,  $\psi_c$  is a blow-up solution to the DS II preserving  $\|\psi_c\|_{L^2} = \|\psi_0\| = 2\sqrt{\pi}$ . Moreover, as  $t \rightarrow T_*$ , the  $\|\psi_c\|^2 \rightarrow 4\pi\delta$  in  $S'(\mathbb{R}^2)$  (tempered distribution) where  $\delta$  is a Dirac measure. In addition,  $\|\nabla\psi_c(t, \cdot)\|_2 \sim (t - t^*)^{-2}$  and  $\|\psi_c(t, \cdot)\|_\infty \sim (t - t^*)^{-1}$  are observed.

Questions arising in the DS systems, particularly DSI and DSII, are: the existence of a blow-up mechanism other than Ozawa (probably the Merle-Raphael type) and the blow-up profile or any other types. These are what we are to explore. In a situation, where analytical results are difficult to find we resort to numerical methods. It is shown in [97] that the DS Ozawa solution is unstable. The identification of the blow-up mechanism for DS II studied in [105] is conclusive due to the use of sufficiently high resolutions. Also for sufficient mass of particular Gaussian initial data, the DS II solution possesses a generic blow-up of Ozawa type. It is unknown for the DS I whether the blow-up is of the type described for DS II.

The ubiquitous nature of the dispersive PDEs in application makes them interesting, however, exact solutions are rare. Therefore, reliable and well-capacitated numerical techniques are needed. In this regards, spectral methods are some of the suitable candidates; they approximate the studied function in terms of a series of globally defined smooth functions and then provide a rule for differentiation. For the purpose of finite truncation of spectral series involved, in practice, we work with functions represented on the computational domain as a finite sum of functions defined globally on the same domain. The differentiation rule then can be represented as the action of the *differentiation matrix* on the coefficients space. For example, a smooth function  $u(x)$  in one dimension can be approximated by an  $N$ -degree interpolating polynomial  $u_N(x)$  in terms of  $N$  global "basis"

functions  $\phi_n$ , for  $n = 0, \dots, N - 1$

$$u(x) \approx u_N(x) = c_0\phi_0(x) + c_1\phi_1(x) + \dots + c_{N-1}\phi_{N-1}(x)$$

and the approximation to the first derivative of  $u_N$ , at collocation points  $x_m$ , is represented in terms of matrix elements  $D_{mn}$  with  $m, n = 1, \dots, N - 1$  and  $c_m \equiv u(x_m)$

$$u'_N(x_m) = \sum_{n=0}^N b_n \phi_n \equiv \sum_{n=0}^N D_{mn} u_n, \quad m = 0, \dots, N - 1 \quad (1.1.20)$$

where  $b_n = D_{mn}c_m$  for  $m, n = 0, \dots, N - 1$ . In general case,  $c_n = J_{mn}u_m$ , where matrix  $J$  generates  $c_n$  from the collocation points so that  $u'_N(x_m) = \tilde{D}u_N(x_m)$  where  $\tilde{D} = J^{-1}DJ$ . Spectral methods (SMs) differ from the finite element methods (FEMs), even though they are built based on the same notion. SMs use a global approach with a set of nonzero basis functions over the whole domain while the basis functions for FEMs are only nonzero on small domains (i.e. FMEs approximate functions locally). As a result, SMs are important for their accuracy. Smooth functions are approximated with an error converging "exponentially", as fast as possible. Solution to time dependent equations preferably need global methods like SMs especially when higher resolution in space and longer time integration are in demand. Nevertheless, implementing FEMs can be more expensive computationally than SMs except in a case when SMs is used in the approximation of problems having discontinuous  $c_n$  or complicated underlying domains. Errors can grow due to Gibbs phenomenon, see [208] and [20] and the Chapter on Numerical approaches.

The spectral methods are useful in approximating solutions to ODEs and PDEs. When solving the time dependent PDEs, solutions are assumed to take the form (1.1) which generates a system of ODEs in the coefficients  $c_n$  that can be solved numerically, thus NLS equations and DS systems fall into the class of equations that SMs is applicable. In discrete settings, polynomial interpolant at optimal collocation points are important, for instance Chebyshev points  $x_n = \cos(n \arccos(x))$  are useful in minimizing Runge's phenomenon effect that might occur when equally spaced nodes are used [208],[209],[190][192]. In relation to the higher resolution requirements, unlike the DSII where the lump (vacuum, asymptotic profile) and also Ozawa are slowly decaying, fast Fourier Transform (FFT) for computing spatial derivatives, requires a total resolution of the order of  $2^{30}$  to get sufficient resolution [94], the dromion/vacuum solution of the DSI is exponentially decaying. Therefore, for DSI higher resolutions are not necessarily needed to gain the desired accuracy [14].

Issues associated with the numerical studies of evolutionary dispersive PDEs apart from computational accuracy and efficiency is *stiffness* for numerical time integrations. Even though, spectral methods are popular for how accurate and efficient they can solve

a problem where applicable, the ODEs obtained from the PDE after spatial discretisation are stiff thereby making them numerically challenging. Loosely speaking a system is *stiff* if explicit integration schemes are inefficient due to stability requirements. Although, there is no precise definition of stiffness we will give some description in a situation where it occurs. Perhaps, the easiest way to describe stiffness is as follows. Consider the linear evolution system of equations in  $\mathbb{R}^2$ :

$$u_t = \mathbf{M}u \quad \text{with} \quad u = u(t) = \begin{pmatrix} u_1(t) \\ u_2(t) \end{pmatrix}, \quad \mathbf{M} = \begin{pmatrix} \mu & 0 \\ 0 & \nu \end{pmatrix}, \quad \mu, \nu \in \mathbb{C} \quad (1.1.21)$$

whose solution is given by  $u(t) = (u_1(0)e^{\mu t}, u_2(0)e^{\nu t})$ . Assume  $\Re(\mu) = -\alpha < 0$  and  $\Re(\nu) = -\beta < 0$  for positive real numbers  $\alpha, \beta$ . If either  $\alpha$  or  $\beta$  is much smaller than the other, then one of the components of  $u(t)$  would decay to zero much faster than the other. Thus, we must deal with two different time scales, and this characterizes stiffness of the system.

The demand for suitable and powerful techniques in solving nonlinear dispersive equations like NLS and DS cannot be underestimated. In tradition, one uses spectral techniques for spectral differentiation in space ( for fast error convergence) and apply time integration schemes such as the Euler, the leap-frog, the Adams, the Runge-Kutta schemes... Nevertheless, stiffness may compromise the spectral accuracy in principle. Stiff equation is one containing terms that could potentially incur significant variations leading to instability of the time integration technique. Stiffness in an equation is an efficiency issue; it is an indication of small time-step (stability) requirement for explicit numerical schemes. In practice, one uses small time steps for they only increase the computational time not the storage unlike when used on the space discretization. Runge-Kutta schemes (implicit for stiff part and explicit for nonstiff terms) turn out to be a suitable candidate for the time integration. Of course, there are several other methods for studying systems of such kind which include: Integrating factor and deferred-correction-schemes, time-splitting schemes, exponential time-differencing-schemes, RK sliders ...

For dispersive PDEs, stiffness comes from the dispersive terms, mostly the linear part. The linear part associated to the DS system generating the linear stiffness, can be dealt with using an implicit-explicit methods (IMEX-method). The idea is that, the stiffness part (linear terms) is solved using stably-implicit scheme while the non-stiff part ( usually the nonlinear terms) by an explicit method as proposed by Driscoll [44].

## 1.2 Overview of the Thesis

The thesis is organized into five parts: the introduction, the numerical aspects, review of the NLS equations, numerical study of blow-up in Davey-Stewartson system I and appendices. Chapter 2 is devoted to the introduction of dispersive linear and non-linear equations, blow-up, Hamiltonian and integrable systems. A particular case of blow-up solutions to dissipative and dispersive PDEs with power non-linearity is discussed. In chapter 3, the aspects of interpolations, differentiation matrices, errors and some time-integration schemes for dispersive PDEs are explained. Chapter 4 provides a thorough review to the focusing and defocusing Nonlinear Schrödinger equations. Specific considerations are given to the NLS equation on the existence properties of solutions, blow-up solutions, blow-up rates and blow-up profiles. Some concluding remarks about the results of the 2D NLS and the DS I are revisited in the end section of the chapter. In Chapter 5, we provide a detailed numerical study of DS I and concluding remarks are made for further studies.

Finally, in the Appendix, useful notations, definitions and proofs of some auxiliary theorems and propositions used in the chapters of the thesis are provided in Appendix A. An attempt is made to compute the higher derivatives of analytic functions in Appendix B. This includes the numerical computation of Taylor's coefficients of functions via Fonberg's algorithm, useful for solving PDEs. It is explained, there, the problem of the numerical study of the DS II on a sphere; the logarithmic terms in the solution of the elliptic equation led to a badly approximated results. Furthermore, special attention is paid on the Taylor coefficients of the interpolation polynomials such as barycentric and Chebyshev ones. Some useful results for NLS equations are stated and proved in appendix C. Appendix D provides the main algorithms used in appendix B.

---

## Chapter 2

# Concept of Dispersive Equations, Blow-up, Hamiltonian System and Integrability

In this chapter, we give brief introduction to the concepts of dispersive PDEs with linear and non-linear examples; and provide a few details about the dispersive nature of the NLS equations and DS systems. We treat, with examples, few PDEs which the phenomena of blow-up may show up. Finally, we introduce Hamiltonian systems and show the importance of some dispersive PDEs that are Hamiltonian.

To begin, suppose we have  $\Omega \subset \mathbb{R}^d$ , an open subset of  $\mathbb{R}^d$ , for fixed  $d \in \mathbb{N}$  and a Hilbert space  $\mathcal{H}$ . Given an integer  $k \geq 1$ , a  $k$ th-order partial differential equation (PDE) in space is a  $k$ th degree polynomial  $\mathcal{P}$  of partial derivatives

$$\mathcal{P} : \mathbb{R}^{dk} \times \mathbb{R}^{d(k-1)} \times \cdots \times \mathbb{R}^d \times \mathbb{R} \times \Omega \rightarrow \mathcal{H}, \quad (2.0.1)$$

having  $u : \Omega \subset \mathbb{R}^d \rightarrow \mathcal{H}$  and  $f : \Omega \rightarrow \mathcal{H}$ , defined by

$$\mathcal{P}\left(D^k u, D^{k-1} u, \dots, Du, u, \mathbf{x}\right) = f(\mathbf{x}), \quad (2.0.2)$$

or equivalently, for smooth  $\alpha_\ell(D^{k-1} u, \dots, u, \mathbf{x}) \in C^\infty(\mathbb{R}^d)$  and  $|\ell| \leq k$ ,

$$\sum_{|\ell| \leq k} \alpha_\ell(D^{k-1} u, \dots, Du, u, \mathbf{x}, t) D^\ell u = f(\mathbf{x}) \quad (2.0.3)$$

The notations:  $D^\ell = \partial_{x_1}^{\ell_1} \cdots \partial_{x_d}^{\ell_d}$  for  $\partial_{x_j} = \partial/\partial x_j$ ,  $|\ell| = \sum_j \ell_j$  while  $\ell = (\ell_1, \dots, \ell_d)$ . The space variable  $\mathbf{x} = (x_1, \dots, x_d) \in \mathbb{R}^d$ . If we further redefine  $u$  and  $f$  each as the map  $\mathbb{R} \times \Omega \rightarrow \mathcal{H}$  for  $(t, \mathbf{x}) \mapsto \mathcal{H}$ , the general time evolution semi-linear equation (first order in time  $t$ ) is given by

$$\partial_t u + \sum_{|\ell|=k} \alpha_\ell(t, \mathbf{x}) D^\ell u + \alpha_0(D^{k-1} u, \dots, Du, u, \mathbf{x}, t) = f(t, \mathbf{x}) \quad (2.0.4)$$

The use of  $u \in \mathcal{H}$  implies that for any  $v \in \mathcal{H}$  then  $\langle u, v \rangle = \int_{\mathbb{R}^d} uv < \infty$  e.g.  $\mathcal{H} = (L^2, d\mathbf{x})$ . Solution of such equations depends on the specified conditions given on the boundary and initial data on the graph of  $u$ . The reason of being called *evolution* is with the anticipation that solution  $u(t, \mathbf{x})$  may evolve from a prescribed or supplied initial data which serves as

the initial state of the system. Moreover, we may have higher order time derivatives, but for the purpose of this work we restrict to the first order in time semi-linear equations.

Here, we are mainly concerned with the *semi-linear* equations with constant coefficients

$$\partial_t u = \mathbf{L}u + \mathbf{N}[u] \quad (2.0.5)$$

where  $\mathbf{L}$  is a linear differential operator (responsible for the dispersion) and  $\mathbf{N}[u]$  denotes the non-linear function in  $u$ .

## 2.1 Dispersive PDEs

Let us start with a linear evolution equation in a  $d$ -dimensional frame:

$$G(\partial_t, \nabla)u(t, \mathbf{x}) = 0, \quad (2.1.1)$$

with the operator  $G$  depending on the gradient  $\nabla$  and time derivative operators. We seek for the *plane-wave* solution given in terms of *wave-form*  $F_p(\mathbf{k} \cdot \mathbf{x} - \omega t)$

$$u(t, \mathbf{x}) := F_p(\mathbf{k} \cdot \mathbf{x} - \omega t) = F_0 e^{i(\mathbf{k} \cdot \mathbf{x} - \omega t)}, \quad i = \sqrt{-1} \quad (2.1.2)$$

with constants  $F_0, \omega$  respectively representing the amplitude and frequency. The notation  $\mathbf{k} = (k_1, \dots, k_d)$  is the *wave-vector* of the *wave-numbers*  $k_j$ , for  $j = 1, \dots, d$  with the corresponding directions at the position  $\mathbf{x} = (x_1, \dots, x_d)$ . If  $u$  solves (2.1.1), then

$$G(-i\omega, i\mathbf{k}) = 0 \quad (2.1.3)$$

defines the *dispersion relation* to the (2.1.1),<sup>1</sup> From (2.1.3), one derives an expression for the frequency  $\omega$ , as a function of  $\mathbf{k}$ , which may be complex-valued for dissipative equations. For dispersive equations  $\omega$  is a real-valued function

$$\omega = \omega(\mathbf{k}) \quad (2.1.4)$$

where the plane-wave solution (2.1.2) propagates with the phase and group velocities respectively, where with  $|\mathbf{k}|^2 = k_1^2 + \dots + k_d^2$  and  $\mathbf{n} := \mathbf{k}/|\mathbf{k}|$ ,

$$v_p(\mathbf{k}) = \frac{\omega(\mathbf{k})}{|\mathbf{k}|} \cdot \mathbf{n}, \quad v_g = \nabla_{\mathbf{k}} \omega(\mathbf{k}). \quad (2.1.5)$$

---

<sup>1</sup>The dispersion relation (2.1.3) describes the movement of the plane-wave. The number  $\omega$  is also known as the phase of wave having frequency  $\omega/2\pi = 1/T_f$ , the temporal frequency being  $T_f$ . The wave length of the wave is  $\lambda = 2\pi/|\mathbf{k}|$ .

If it happens that  $v_p \neq v_g$ , the evolution equation is considered to be *dispersive* with a *dispersive-wave solution*. In other words, the evolution equation is dispersive whenever  $v_p$  depends on  $\mathbf{k}$  as expressed in the form (2.1.4), i.e. if  $v_g$  is not constant or simply  $v'_g = \nabla^2 \omega \neq 0$ . This would mean, wave-solution  $u$  evolving in time, is dispersive if different wave-frequencies ( or equivalently wave-lengths) correspond to different phase-velocities,<sup>2</sup>. This does not happen to all evolution equations. For instance, let  $d = 1$  in the classical wave-equation:

$$\partial_t^2 u - c^{-1} \partial_x^2 u = 0 \quad (2.1.6)$$

is *non-dispersive*, since any solution  $u(x, t)$  of any wavelength propagates with the constant velocity, i.e.  $v_g = \pm 1/\sqrt{c} = v_p$  for the dispersion relation  $w(k) = \pm k/\sqrt{c}$ , where  $c$  is the speed of the wave solution  $u$ . Nevertheless, the wave equation (2.1.6) becomes weakly dispersive in higher dimensions  $d \geq 2$ . Again, the transport equation  $\partial_t u = \alpha \nabla u$  for  $\alpha \in \mathbb{R}^*$  is non-dispersive since  $\omega(\mathbf{k}) = -\alpha \mathbf{k}$  and or  $\omega''(\mathbf{k}) \neq 0$ . Mathematically, a PDE in  $\mathbb{R}^d$  is dispersive whenever the function

$$v_p : \mathbb{R}^d \rightarrow \mathbb{C} \text{ defined by } \mathbf{k} \mapsto \frac{\omega(\mathbf{k})}{|\mathbf{k}|} \cdot \mathbf{n}, \text{ for } \mathbf{n} := \mathbf{k}/|\mathbf{k}| \text{ a normal unit-vector,}$$

is *non-constant real-valued*.

## 2.2 Linear Dispersive PDEs

Some of the evolution equations among *linear dispersive* equations include, Airy (A), Klein Gordon (KG) and linear Schrödinger equations (LSE). For  $u : \mathbb{R} \times \mathbb{R}^d \rightarrow \mathbb{C}$

$$\mathbf{A} : \partial_t u = \partial_x^3 u; \quad \mathbf{KG} : \partial_t^2 u = \nu \Delta u - \mu^2 u, \quad \mu \in \mathbb{R}^+, \nu \in \mathbb{R}^*; \quad \mathbf{LSE} : \partial_t u = i\hbar \Delta u, \quad \hbar \in \mathbb{R}^+;$$

having respectively, the dispersion relations  $\omega_A(k) = -k^3$ ,  $\omega_K(\mathbf{k}) = \pm(\nu + \mu^2|\mathbf{k}|^2)^{1/2}$  and  $\omega_S(\mathbf{k}) = \hbar|\mathbf{k}|^2$ . One easily checks that  $\omega''_K(\mathbf{k}) \neq 0$  and  $\omega''_S(\mathbf{k}) \neq 0$ , where  $\mathbf{k} = (k_1, \dots, k_d)$ .

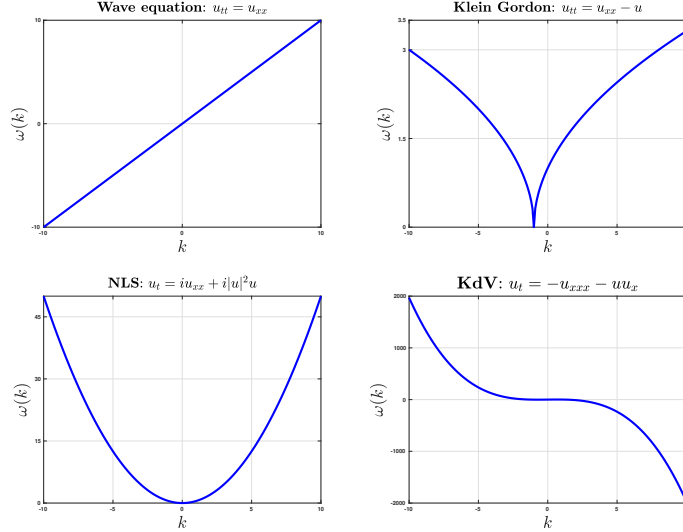
## 2.3 Nonlinear Dispersive PDEs

Among the *nonlinear dispersive* equations are the following respective equations of Sine-Gordon (SG) and Korteweg de Vries (KdV): with  $u : \mathbb{R} \times \mathbb{R} \rightarrow \mathbb{C}$ ,

$$\mathbf{SG} : \partial_t^2 u = \partial_x^2 u - \sin(u), \quad \mathbf{KdV} : \partial_t u = -\partial_x^3 u - \frac{1}{2} \partial_x(u^2). \quad (2.3.1)$$

---

<sup>2</sup>In the physical context, it implies as time evolves a single wave-packet decomposes into wave-trains (different waves) which as a result will disperse through the medium.


 Figure 2.1: The dispersion relation  $\omega(k)$  in dimension  $d = 1$ .

Their respective approximate dispersion relations are:  $\omega_{\text{SG}}(k) \approx \sqrt{k^2 + 1}$  and  $\omega_{\text{KdV}}(k) \approx \alpha k - \beta k^3$ . The  $\omega_{\text{KdV}}(k)$  is obtained via Taylor expansion about  $hk = 0$  up to the order  $O(k^5)$  as  $k \rightarrow 0$ . This comes from the general dispersion relation  $\omega^2 = gk \tanh(kh)$  of surface water waves evolution model where surface tension is negligible, with gravity  $g$  and  $h$  is the depth of the still water. The equations are dispersive according to their dispersion property.

Dispersive equations, of special interest, include the non-linear Schrödinger (NLS):

$$\partial_t u = i(\Delta u + f(|u|^2)) \quad (2.3.2)$$

with power non-linearity  $f(|u|^2) = \gamma|u|^{2\sigma}$  for  $u : \mathbb{R} \times \mathbb{R}^d \rightarrow \mathbb{C}$ ,  $0 < \sigma \leq \infty$  and  $\gamma = \pm 1$ , describing the evolution of weakly nonlinear waves and the Davey Stewartson (DS) systems

$$\begin{cases} i\psi_t + \alpha\partial_{xx}^2\psi + \partial_{yy}^2\psi = (\gamma|\psi|^2 + \partial_x\phi)\psi; & \psi : \mathbb{R} \times \mathbb{R}^2 \rightarrow \mathbb{C} \\ \partial_{xx}^2\phi + \beta\partial_{yy}^2\phi = \rho\partial_x(|\psi|^2), & \phi : \mathbb{R}^2 \rightarrow \mathbb{R}, \quad \mathbf{x} = (x, y) \in \mathbb{R}^2 \end{cases} \quad (2.3.3)$$

where  $\gamma = \pm 1$ ,  $\rho > 1$  and, at least, in the integrable case  $(\alpha, \beta) = (\pm 1, \pm 1)$ . They are clearly dispersive equations. For NLS equation, the dispersion relation would be

$$\omega(\mathbf{k}) = |\mathbf{k}|^2 + \gamma, \quad \mathbf{k} = (k_x, k_y) \in \mathbb{R}^2$$

whereas that of the DS system expressed in its nonlocal form

$$i\psi_t + \alpha\partial_{xx}^2\psi + \partial_{yy}^2\psi = \left( \gamma|\psi|^2 + \rho\partial_x [(\partial_{xx}^2\psi + \partial_{yy}^2\psi)^{-1}\partial_x(|\psi|^2)] \right)\psi$$

is  $\omega(\mathbf{k}) = \alpha k_x^2 + k_y^2$  with  $\mathbf{k} = (k_x, k_y)$ . The operator  $\partial_x^{-1}$  can be seen as an anti-derivative operator acting like the Fourier multiplier  $-i/k_x$ :

$$\partial_x^{-1}u(x) = \frac{1}{2} \left[ \int_{-\infty}^x - \int_x^{\infty} \right] u(x') dx' \quad (2.3.4)$$

where  $(\partial_{xx}^2 + \beta\partial_{yy}^2)^{1/2} \approx \partial_x + \frac{\beta}{2}\partial_x^{-1}\partial_{yy}^2$  because

$$(k_x^2 + \beta k_y^2)^{1/2} = k_x(1 + \beta k_y^2/k_x^2)^{1/2} \approx k_x + \frac{\beta}{2}k_x^{-1}k_y^2$$

for  $|k_y/k_x| \ll 1$ . In fact, if we take out the  $x$ -coordinate dependence of  $\psi$  in the DS system an NLS equation is recovered.

### 2.3.1 The NLS equation

The Cauchy problem

$$\psi_t = \mathbf{L}\psi + \mathbf{N}[\psi] := i\Delta\psi + i\gamma|\psi|^{2\sigma}\psi, \quad \psi : \mathbb{R} \times \mathbb{R}^d \rightarrow \mathbb{C}, \quad \psi(0, \mathbf{x}) \in H^s(\mathbb{R}^2) \quad (2.3.5)$$

defined on the whole  $\mathbb{R}^d$  with  $\psi \rightarrow 0$  as  $|\mathbf{x}| \rightarrow \pm\infty$  and  $\gamma = \pm 1$ . The non-linearity  $\mathbf{N} : \mathcal{F} \rightarrow \mathbb{C}$  defined via  $w \in \mathbb{C} \mapsto |w|^{2\sigma}w$  is smooth when  $\sigma \in \mathbb{N}^+$ , which are the algebraic cases. The non-linearity naturally comes from the Hamiltonian potential  $V(\psi) = \frac{\gamma}{2\sigma+2}|\psi|^{2\sigma+2}$ . The Cauchy problem (2.3.5) in the cases  $\sigma = 1, 2$  are mostly studied in the physical context, usually referred to as respectively *cubic* and *quintic* NLS equations. The  $\gamma = \pm 1$  characterizes respectively the *focusing* and *defocusing* NLS.

In order to understand the behaviour of the solution, it is worth understanding the dispersive nature of this equation. This can be achieved by seeking the solution of the plane-wave type  $\psi(t, \mathbf{x}) = u_0 e^{i(\mathbf{k}\cdot\mathbf{x} - \omega t)} = u(t) e^{i\mathbf{k}\cdot\mathbf{x}}$  so that  $u(t)$  solves

$$\partial_t u = i(-|\mathbf{k}|^2 + \gamma|u|^{2\sigma})u.$$

Provided  $|u(t)| = \lambda$  constant, this yields an explicit solution to the equation (2.3.5):

$$\psi(t, \mathbf{x}) = u_0 e^{i\mathbf{k}\cdot\mathbf{x}} \cdot e^{i(-|\mathbf{k}|^2 + \gamma|\lambda|^{2\sigma})t}, \quad (2.3.6)$$

where obviously  $\psi_0(\mathbf{x}) = u_0 e^{i\mathbf{k}\cdot\mathbf{x}} \in H^s(\mathbb{R}^d)$  for any finite  $u_0 \in \mathbb{C}$ . The term  $e^{i(-|\mathbf{k}|^2 + \gamma|\lambda|^{2\sigma})t}$  is responsible for the oscillations of  $\psi(t, \mathbf{x})$  in time. In the defocusing case,  $\gamma = -1$  allows the dispersive effect to take place, thereby the linearity dominates. Thus the solution dies out

to constant as  $t \rightarrow \infty$ . Whereas, the focusing case  $\gamma = 1$  could lead to the suppression of the contribution of the linearity term  $e^{-i|\mathbf{k}|^2 t}$  with  $t \rightarrow \infty$  thereby the non-linearity dominates, especially with the amplitude  $|u_0| = \lambda \gg |\mathbf{k}|$ , i.e. when  $|u_0| = \lambda$  is much greater than  $|\mathbf{k}|$ . Thus, the solution  $\psi(t, \mathbf{x})$  becomes *singular* or simply *blow-up*.

### 2.3.2 The Davey-Stewartson (DS I)

The Cauchy problem for the DS system (2.3.3) supplied with boundary conditions for  $\beta = -1 < 0$ ,  $\alpha = 1$  and initial data  $\psi_0 \in H^1(\mathbb{R}^2)$  defines the particular DS I system

$$\left\{ \begin{array}{l} i\psi_t + \partial_{xx}^2 \psi + \partial_{yy}^2 \psi = (\gamma|\psi|^2 + \partial_x \phi)\psi; \quad \psi : \mathbb{R} \times \mathbb{R}^2 \rightarrow \mathbb{C} \\ \partial_{xx}^2 \phi - \partial_{yy}^2 \phi = \rho \partial_x (|\psi|^2), \quad \phi : \mathbb{R}^2 \rightarrow \mathbb{R}, \\ \lim_{\eta \rightarrow -\infty} \phi(\xi, \eta) = \varphi_1(\xi, t), \quad \lim_{\xi \rightarrow -\infty} \phi(\xi, \eta) = \varphi_2(\eta, t), \quad \text{if } \alpha < 0 \\ \psi(0, x, y) = \psi_0 : \mathbb{R}^2 \rightarrow \mathbb{C}, (x, y) \mapsto \psi_0(x, y), \end{array} \right. \quad (2.3.7)$$

where  $\xi = \frac{1}{\sqrt{2}}(x - y)$ ,  $\eta = \frac{1}{\sqrt{2}}(x + y)$  and the  $\varphi_1$  and  $\varphi_2$  can be chosen at will (Sulem [202], Chapter 12). The case when  $\alpha > 0$  is used, the operator there behaves like elliptic one. The function  $\psi$  is identified as the *main-field* while the forcing term  $\phi$  is regarded as the *mean-field*. Thus, the first equation in the system is the generalized two dimensional cubic NLS with  $\phi$  as a forcing term.

The integrable DS system appears to model the evolution of weakly non-linear surface water-waves moving along one direction with the amplitude slowly varying in the direction of  $x$  and  $y$ , see [[41],[43]]. The systems are also applicable in plasma physics, modelling the evolution of plasma material with the influence of the magnetic field, for instance see [165],[166] and the references therein.

## 2.4 Blow-up: Power Nonlinearity

We have presented several potential mechanisms that suggest certain nonlinear PDEs possess solutions that become singular in finite time. The questions we are interested in are: how, when, with what profile and which nonlinearity does blow-up occur. The power nonlinearity plays role in the blow-up solutions for the semi-linear equations such as the generalised KdV equations, NLS and related equations, see [127] for details.

### 2.4.1 Dissipative type

A prototypical example of blow-up due to power nonlinearity can be observed in the  $1 + d$ -dimensional ordinary differential equation, the exponent  $\sigma \in \mathbb{R}^+$  with  $0 < \sigma < \infty$ :

$$u_t = |u|^{2\sigma}u; \quad u : \mathbb{R} \times \mathbb{R}^d \rightarrow \mathbb{C}, \quad u(0, \mathbf{x}) = u_0(\mathbf{x}). \quad (2.4.1)$$

If  $d = 1$ , the equilibrium (stationary) solution  $u = 0$  is unique but unstable, since for  $u_0 > 0$  and  $u_0 < 0$  cases considered respectively (i.e. assuming  $u_{\pm} = 0 \pm \delta$  for  $\delta > 0$  small) the solution

$$u(t) = \pm \left( \frac{1}{2(T_* - t)\sigma} \right)^{\frac{1}{2\sigma}}, \quad T_* = (2\sigma)^{-1}|u_0|^{-2\sigma} \quad (2.4.2)$$

diverges as  $\lim_{t \rightarrow T_*} u(t) = \pm\infty$  respectively and faraway from converging to 0. The  $T_*$  is the blow-up time. In other words, the solution  $u(t)$  exists locally in the finite time  $T_*$  and would not extend beyond  $T_*$ . The problem is locally well-posed and  $T_*$  has a lower bound depending on the  $\|u_0\|$  appropriately chosen.

Let us consider a semi-linear equation where the linear part tends to smooth out the nonlinearity. Consider a nonlinear equation of the type

$$u_t = \Delta u + f(u^q), \quad q > 1$$

where  $f(u^q)$  has the tendency to diverge with  $u \rightarrow \infty$ . A typical example of such in one-dimension is the heat-diffusion equation with non-linearity  $f(u^q) = u^q$  for  $q > 1$ ,

$$\begin{cases} u_t = u_{xx} + u^q & \text{on } \Omega \subset \mathbb{R}^1, \\ u(0, x) = u_0; \quad u(t, x) = 0 & \text{on } \partial\Omega \end{cases} \quad (2.4.3)$$

for finite closed domain  $\Omega$ . The solution to the nonlinear equation  $u_t = u^q$ , that,

$$u(t) = \frac{1}{(q-1)^{1/(q-1)} \left( \frac{1}{(q-1)u_0^{q-1}} - t \right)^{1/(q-1)}}$$

blows-up in finite time  $T_*(u_0) = (q-1)/|u_0|^{q-1}$  for  $u_0 > 0$ . Moreover, the linear equation  $u_t = u_{xx}$  in the dimension  $d = 1$  for  $\Omega = [0, L]$  has the well-known solution

$$u(t, x) = \sum_{j=1}^n c_n \sin\left(\frac{\pi j}{L}x\right) e^{-(\frac{\pi j}{L})^2 t}$$

where  $c_n$  are the Fourier sine series coefficients. Here,  $u(t, x) \rightarrow 0$  as  $t \rightarrow \infty$ . Whereas behaviour of  $u(t, x)$  in the equation (2.4.3) depends on whether the nonlinearity or the diffusion term  $\partial_x^2 u$  overtakes the other. In a situation where nonlinearity dominates, blow-up

is possible. With these information we may characterize blow-up to the equation (2.4.3).

If the given initial data  $u_0$  is sufficiently small in size, then the solution  $u(t)$  to the equation (2.4.3) exists globally. Consequently, the energy dissipates to zero and after a finite time  $T$  the  $u(t)$  will be as if controlled by the linear problem. However, for sufficiently large  $u_0(x)$  as will be clear later, the solution  $u(t, x_*) \rightarrow \infty$  in the sense that

$$\max_{x \in [0,1]} u(t, x_*) \rightarrow \infty \quad \text{as } t \rightarrow T_*.$$

That is,  $u(t, x)$  blows-up at a finite time  $T_*$  about a point  $x_*$ . Despite the fact that the blow-up time  $T_*$  and the position  $x_*$  depend on  $u_0$ , as can be seen in Figure 2.2, close to the blow-up point  $(T_*, x_*)$  the solution is nearly independent of the initial data  $u_0(x)$ . Apparently, close to  $T_*$  the solution  $u(t, x)$  becomes singular about  $x_*$  and grows narrowly and focusing but maintains its profile shape (see the figure on the right of Figure 2.2). Moreover,  $\|u(t, x)\|_\infty \rightarrow \infty$  as  $t \rightarrow T_*$  and the blow-up rate suggested by the Figure 2.3 on the right is roughly  $\|u\|_\infty^2 \sim (t_* - t)^{-1}$  for  $\alpha = -0.5012$  and  $\beta = 0.5$  and  $t_* = 0.4999$ .

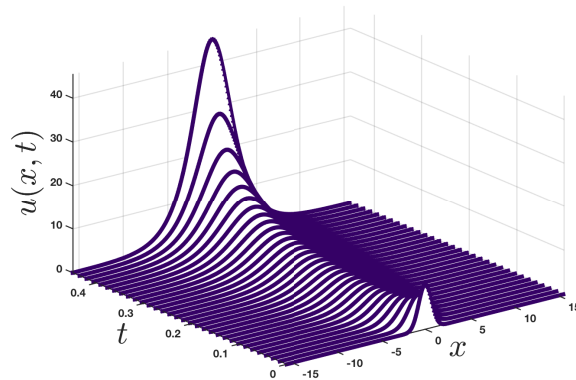


Figure 2.2: Solution to (2.4.3) with  $q = 2$  near blow-up for  $u_0(x) = 10.1 \exp(-x^2)$ .

If the domain  $\Omega$  in (2.4.3) is extended to the whole real line  $\mathbb{R}$ , the diffusion effect becomes stronger and  $u(t, x)$  will slowly diffuse away. This is the case even for a localized type of initial data, e.g.  $\exp(-x^2)$  Fig. 2.2. Moreover, extending the equation (2.4.3) to dimension  $d > 1$ , the behaviour of  $u(t, x)$  depends on the existing relation between the nonlinearity exponent  $q$  and the dimension  $d$ , see [66, 219, 106]. The equation (2.4.3) in higher dimension has a critical exponent  $q = q_c = 1 + 2/d$  as shown in [66]. If  $1 < q_c < 1 + 2/d$ , any small initial data  $u_0$  would lead to global bounded solution that would exist for all  $t$ . If, otherwise,  $q_c \geq 1 + 2/d$ , then arbitrary  $u_0 > 0$  could generate blow-up solution. In the case  $d = 1$  and  $q_c = 3$ , however, we detected the blow-up because  $\Omega$  is closed and finite otherwise we must have  $q = 3$  in order for us to see it.

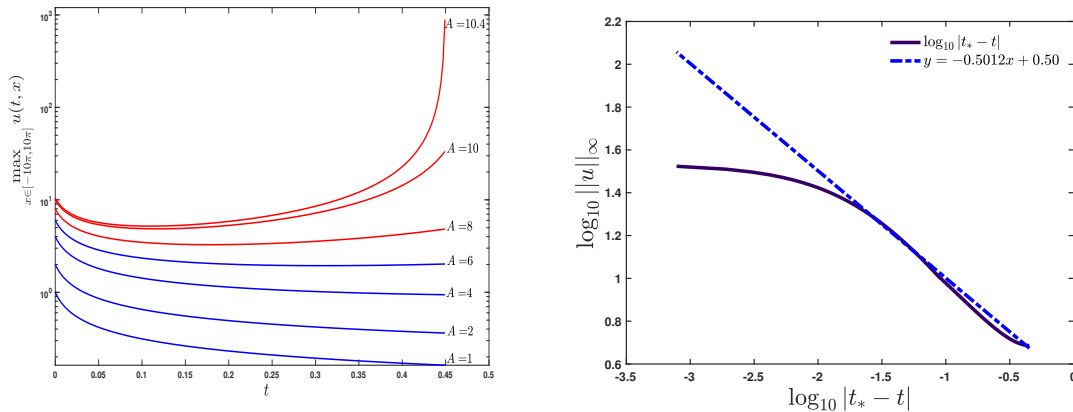


Figure 2.3: For  $u_0(x) = A \exp(-x^2)$ , on the left: maximum  $\max_{x \in [-10\pi, 10\pi]} u(t, x)$  starts to blow up for any amplitude in the range 6 – 10, and on the right: the blow-up rate traced by fitting  $\log_{10} \|u(t)\|_{\infty}$  according to  $\log_{10} \|u(t)\|_{\infty} = \alpha \log_{10} |t_* - t| + \beta$ .

## 2.4.2 Dispersive type: gKdV

We have seen soliton as a balance of dispersion and nonlinearity effects, we may be concerned about solution behaviour for general power nonlinearity. In this case, a typical dispersive equation to consider is the generalized Korteweg de-Vries (gKdV) equation

$$u_t + u^p u_x + u_{xxx} = 0, \quad p \in \mathbb{N} \quad (2.4.4)$$

It extends the classical KdV equation with general nonlinearity exponent  $p$ . The general power nonlinearity exponent  $p = 1$  corresponds to the KdV equation. If  $p < 4$ , solutions are known to be global in time. For  $p = 4$ , results by Y. Martel, F. Merle and P. Raphaël ([139, 140, 141, 146] and the references therein) show that smaller perturbation of the solitary wave solution of the KdV will lead to a dispersed solution, however, larger mass perturbation will yield to the so-called  $L^\infty$ -blow-up, i.e. the norm  $\|u(t)\|_{\infty}$  or  $\max(u(t))$  becomes unbounded in finite time. There, the blow-up rates for both  $\|u(t)\|_{\infty}$  and  $\|u_x(t)\|_2$  diverge at the rate  $\sim (t_* - t)^{-1/2}$  and are obtained by fitting, numerically, the norm  $\ln \|u(t)\|$  to  $\alpha \ln(t - t_*) + \beta$  by finding  $\alpha, \beta$  and  $t_*$ . The numerical experiment carried out in [100] shows agreement with the analytically predicted rate [139]. The profile at which blow-up occurs is given by the soliton solution, see [100].

It is observed in the Fig. 2.4 there is dispersive oscillations to the left of the soliton solution as blow-up time is approached. When the blow-up asymptotic profile, given by a soliton, becomes concentrated and narrower to a point for the  $L^2$ -critical gKdV, there are outgoing

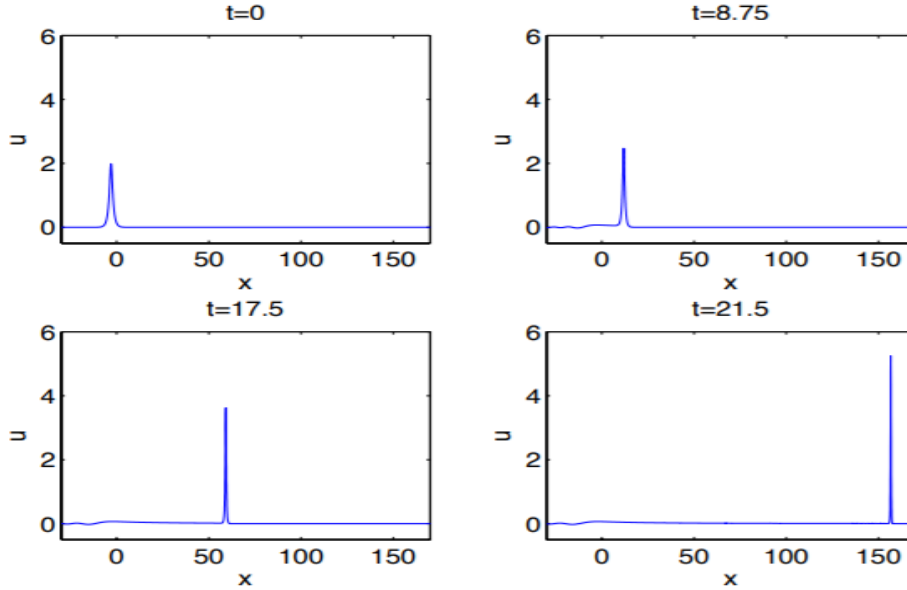


Figure 2.4: Solution to the gKdV,  $p = 4$ , for  $u_0 = 1.01u_{\text{sol}}$ , perturbed soliton. See [96].

wave train of circular waves whose total mass is that of the conserved mass of the soliton, [138, 140]. This is because, as the profile shrinks to a point, the support is zero.

### 2.4.3 Blow-up scenario

To sum up things, since it is not only divergence of  $u(x, t)$  signifies blow-up, but also, unboundedness of the derivative of  $u$  (i.e. the gradient catastrophe) could imply singularity as in Hopf equation with  $u_0(x)$  having  $u_0'(x)$  negative somewhere<sup>3</sup>. Thus, we will consider finite time blow-up of evolution equation to mean either  $u(t, x)$  or its gradients  $u_x(t, x)$  and  $u_t(t, x)$  becomes unbounded in a certain norm within a finite time. Below we give the blow-up structure of semilinear evolution equation.

In general, we will consider a Cauchy problem given in the form of a semi-linear equation in  $\mathbb{R}^d$  with  $\mathbf{x} \in \Omega \subset \mathbb{R}^d$ , a smooth bounded domain  $\Omega$ ,

$$\partial_t u = \mathbf{L}u + \mathbf{N}(u), \quad u(0, \mathbf{x}) = u_0(\mathbf{x}) \geq 0, \quad t > 0 \quad (2.4.5)$$

$u_0 \in H^s(\mathbb{R}^d)$ , having the boundary condition  $u(t, \mathbf{x}) = 0$  for  $\mathbf{x} \in \partial\Omega$ ,  $t \geq 0$ , and a unique solution  $u(t, x)$  defined on the maximal time interval  $[0, T_*)$ , for  $0 \leq T_* < \infty$ . If  $T_* = \infty$ ,

<sup>3</sup>The 1d inviscid Burgers equation  $u_t + (u^2)_x/2 = 0$ ,  $u_0(x) = \varphi(x)$ , for  $t > 0$  and  $\varphi$  bounded and continuously differentiable, has solution of the form  $u(t, x) = \varphi(x - tu(t, x))$  through which by implicit differentiation one proves  $u_t$  and  $u_x$  are unbounded in finite time. In fact,  $T_* = \min_{x \in \mathbb{R}} (-1/\partial_x \varphi(x))$ , the characteristics shock time.

then the solution is said to be global. It blows-up in finite time if  $T_* < \infty$  and certain norm

$$\lim_{t \rightarrow T_*} \|u(t, \cdot)\|_{W^{k,p}(\Omega)}, \quad 1 \leq p \leq \infty, \quad k \in \mathbb{N}^+$$

diverges, for a Sobolev space  $W^{k,p}(\Omega)$  e.g.  $\lim_{t \rightarrow T_*} \sup_{\mathbf{x} \in \Omega} |u(\mathbf{x}, t)| = \infty$ . We will use data from the Schwartz space  $\mathcal{S}(\mathbb{R}^d)$  since it is a dense subset of  $H^k(\mathbb{R}^d) = W^{k,2}(\mathbb{R}^d)$  for all  $k$ . Blow-up could mean that, for a regular initial data, say  $u_0(x) \in H^k(\mathbb{R}^d)$ , solution cease to be in  $H^k(\mathbb{R}^d)$  in finite time.

Furthermore, one proceeds to ask for the blow-up solution behaviour such as the blow-up rate, the blow-up profile, stability and instability, and self-similarity or generic type of blow-up<sup>4</sup>. Blow-up occurring in finite time  $t_*$  has a corresponding position in space, say  $x_*$ . Therefore, there is blow-up at the point  $(t_*, x_*)$ .

## 2.5 Hamiltonian systems and Integrability

A dynamical system<sup>5</sup>, with  $d$  degrees of freedom (generalizing Newton's equations) endowed with the canonical coordinates  $\mathbf{q} := (q_1, \dots, q_d)$  and  $\mathbf{p} := (p_1, \dots, p_d)$ , the position and momentum coordinates respectively, has its evolution completely described by the Hamilton's equations of motion

$$\frac{dq_j}{dt} = \frac{\partial H}{\partial p_j}, \quad \frac{dp_j}{dt} = -\frac{\partial H}{\partial q_j}, \quad j = 1, \dots, d \quad (2.5.1)$$

the initial state  $(q_0, p_0)$  and  $H = H(\mathbf{p}, \mathbf{q}, t)$ . The Hamilton's equation (2.5.1) is defined on a domain  $\Omega \subset \mathbb{R}^{2d}$  of the phase space  $(\mathbf{q}, \mathbf{p})$  and the smooth function  $H$ , usually referred to as *Hamiltonian*, represents the total amount of mechanical energy of our dynamical system. Let us define on the phase space, a Poisson bracket, for  $f, g \in C^\infty(\Omega)$ , in the local coordinates  $(x_1, \dots, x_d)$  on a manifold  $M$  takes the form [182]

$$\{f, g\} = \sum_{j,k=1}^d \omega_{jk}(x) \frac{\partial f}{\partial x_j} \frac{\partial g}{\partial x_k} = (\nabla f)^T \boldsymbol{\omega} \nabla g \quad (2.5.2)$$

where  $\nabla f = (\partial_{x_1}, \dots, \partial_{x_d})$  with a skew-symmetric square matrix  $\boldsymbol{\omega} = (\omega_{jk}(z))_{j,k=1}^d$  which satisfies the Jacobi-identity

$$\{f, \{g, h\}\} + \{g, \{h, f\}\} + \{h, \{f, g\}\} = 0, \quad (2.5.3)$$

<sup>4</sup>Generic blow-up here means whether it is of a type for a particular class of blow-ups, e.g. Pseudo-conformal transform type of blow-up, the loglog blow-up.

<sup>5</sup>Dynamical system can be described as a natural phenomenon that evolves in "time".

as well as linearity, skew-symmetry and Leibniz property respectively: for constants  $a, b$

$$\{af + bg, h\} = a\{f, h\} + b\{g, h\}, \quad \{f, g\} = -\{g, f\}, \quad \{f, gh\} = g\{f, h\} + \{f, g\}h \quad (2.5.4)$$

Among the set of the functions on  $M$ , a non-constant function commuting with all other functions on  $M$  with respect to the Poisson bracket is known as *Casimir*,  $C_\omega$ . In turn, for such function to be obtained  $\omega$  has to be singular with  $\nabla C_\omega$  contained in its null space. According to the Darboux'theorem, for  $n$ -independent Casimirs  $C_1, \dots, C_n$  (the corank of  $\omega$ ) we can generate canonical coordinates introduced earlier  $(q_1, \dots, q_d, p_1, \dots, p_d)$  together with  $(C_1, \dots, C_n)$  on  $M$  in a way that

$$\omega = \begin{pmatrix} \mathbf{0} & \mathbf{1} & \mathbf{0} \\ -\mathbf{1} & \mathbf{0} & \mathbf{0} \\ \mathbf{0} & \mathbf{0} & \mathbf{0} \end{pmatrix}$$

where  $\mathbf{1}$  and  $\mathbf{0}$  respectively identity and zero matrices in the appropriate dimensions. Thus, the Poisson bracket (2.5.2) in these canonical coordinates becomes

$$\{f, g\} = \sum_{k=1}^d \left[ \frac{\partial f}{\partial q_k} \frac{\partial g}{\partial p_k} - \frac{\partial f}{\partial p_k} \frac{\partial g}{\partial q_k} \right] \quad (2.5.5)$$

where the following relations hold  $\{q_j, p_k\} = \delta_{jk}$ ,  $\{q_j, q_k\} = \{p_j, p_k\} = 0$  for  $j, k = 1, \dots, d$ . With these, the equation (2.5.1) can equivalently be expressed in the form

$$\frac{dq_j}{dt} = \{q_j, H\}, \quad \frac{dp_j}{dt} = \{p_j, H\}, \quad j = 1, \dots, d \quad (2.5.6)$$

A smooth solution  $u = u(\mathbf{p}, \mathbf{q}, t)$  satisfying  $u_t = 0$  (equiv. to  $u_t = \{u, H\} = 0$ ) when the Hamilton's equations hold is called the *first integral of motion* or *conserved quantity* or *constant of motion* and therefore we say  $u$  is constant and sometimes referred to as the Hamiltonian. Consequently, the underlying dynamical system is known as *Hamiltonian* system if it is completely described by the Hamiltonian  $H(\mathbf{p}, \mathbf{q}, t)$  satisfying the Hamilton's equation defined on a  $2d$ -dimensional phase space. It becomes *completely integrable* if it has  $d$  independent integrals of motion in involution, i.e.  $\{u_j, u_k\} = 0$  for all  $j, k = 1, \dots, d$ .

Given a phase space  $M$ , let  $(M, u_1, \dots, u_d)$  be an integrable system with  $u_1 = H$  the Hamiltonian. Also, let  $\tilde{M} = \{(\mathbf{p}, \mathbf{q}) \in M, u_k(p, q) = c_k\}$  where  $c_k$  are constants,  $k = 1, \dots, d$  be an  $n$ -dimensional level surface in terms of the first integrals  $u_k$ . Then Arnold-Liouville theorem states that  $\tilde{M}$  is diffeomorphic to a torus  $\mathbf{T}^d = S^1 \times \dots \times S^1$  if  $\tilde{M}$  is compact and connected manifold, and action-angles coordinates

$$I_1, \dots, I_d, \theta_1, \dots, \theta_d, \quad 0 \leq \theta \leq 2\pi$$

can be introduced in a way that  $\theta_k$ 's are coordinates of  $\tilde{M}$  and  $I_k$ 's as actions  $I_k = I_k(u_1, \dots, u_d)$  are integrals of motion. This theorem guarantees the existence of a canonical transformation for integrable system in which the actions are preserved and the evolution of angles in the time parameters  $(t_1, \dots, t_d)$  is linear unlike in its original coordinates  $(\mathbf{p}, \mathbf{q})$ .

Our abstract description of Hamiltonian system shows it constitutes of finite number of dynamical systems given by the finite number of ODES  $u_t = \{u, H\}$ . However, PDEs describe class of dynamical systems that directly form infinite dimensional Hamiltonian system. The Poisson brackets in this case are extended to the infinite dimensional phase spaces to describe dynamics that governing the PDEs. The Poisson brackets are defined on the functional of functions  $F[u] = \int_{\mathbb{R}^d} f[u] d\mathbf{x}$  with the infinite dimensional phase space coordinates  $u(t, \mathbf{x})$  instead of on the function as given in (2.5.5) as

$$\{F, G\} = \int_{\mathbb{R}^d} \frac{\delta F}{\delta u} S \frac{\delta G}{\delta u} d\mathbf{x} \quad (2.5.7)$$

where  $S$  is a skew-adjoint differential operator chosen in a way that the Jacobi identity of the Poisson bracket also holds,  $f[u] = f(u, u_x, u_{xx}, \dots)$  and

$$\frac{\delta F}{\delta u} = \frac{\partial f}{\partial u} - \frac{\partial}{\partial x} \frac{\partial f}{\partial u_x} + \frac{\partial^2}{\partial x^2} \frac{\partial f}{\partial u_{xx}} - \dots \quad (2.5.8)$$

Therefore, for a given functional on the phase space, say  $H$ , we can construct a Hamiltonian dynamics on any other functional, say  $F$ , via the relations

$$F_t = \{F, H\} \iff u_t = \{u, H\} = S \frac{\delta H}{\delta u}. \quad (2.5.9)$$

The KdV equation  $u_t - uu_x - 6u_{xxx} = 0$  is Hamiltonian where  $S = \frac{\partial}{\partial x}$  and its Hamiltonian functional  $H[u] = \int_{-\infty}^{\infty} (u^3 - u_x^2/2) dx$  have the Poisson bracket  $\{F, G\} = \int_{-\infty}^{\infty} \frac{\delta F}{\delta u} \frac{\partial}{\partial x} \frac{\delta G}{\delta u} dx$  with only one Casimir<sup>6</sup>  $\int_{-\infty}^{\infty} u dx$  [69], [234].

Some of the conserved quantities associated to NLS are the mass  $M(\psi) = \int_{\mathbb{R}^d} |\psi|^2$  and Hamiltonian  $H(\psi) = \int_{\mathbb{R}^d} (|\nabla\psi|^2 - \frac{1}{\sigma+1} |\psi|^{2\sigma+2})$  (see appendix III for the proofs). We would verify this as follows. The focusing NLS equation and its conjugate:

$$\psi_t = i\Delta\psi + i|\psi|^{2\sigma}\psi, \quad \psi_t^* = -i\Delta\psi^* - i|\psi|^{2\sigma}\psi^* \quad (2.5.10)$$

can be written in terms of Hamilton's equations

$$i\psi_t = \frac{\delta H}{\delta \psi^*}, \quad i\psi_t^* = -\frac{\delta H}{\delta \psi} \quad (2.5.11)$$

---

<sup>6</sup>Recall that here the Casimir of the Poisson bracket (2.5.7) on the manifold  $M$  here is the nonconstant function that commutes with all other functions on  $M$ .

where  $\delta H/\delta\psi$  is the variational derivative of  $H := H(\psi, \psi^*)$  w.r.t.  $\psi$ . For suitably smooth  $\tilde{\psi} \rightarrow 0$  as  $|\mathbf{x}| \rightarrow 0$  one defines

$$\int_{\mathbb{R}^d} \frac{\delta H}{\delta\psi} \tilde{\psi} = \lim_{\varepsilon \rightarrow 0} \left[ \frac{H(\psi + \varepsilon\tilde{\psi}, \psi^*) - H(\psi, \psi^*)}{\varepsilon} \right].$$

The term in the right hand side simplifies to

$$\begin{aligned} \lim_{\varepsilon \rightarrow 0} \frac{H(\psi + \varepsilon\tilde{\psi}, \psi^*) - H(\psi, \psi^*)}{\varepsilon} &= \lim_{\varepsilon \rightarrow 0} \frac{1}{\varepsilon} \int_{\mathbb{R}^d} \left[ (\varepsilon \nabla \tilde{\psi}) \nabla \psi^* - \varepsilon \tilde{\psi} \psi^\sigma (\psi^*)^{\sigma+1} + o(\varepsilon^2) \right] \\ &= \lim_{\varepsilon \rightarrow 0} \int_{\mathbb{R}^d} \left[ -(\nabla^2 \psi^*) \tilde{\psi} - |\psi|^{2\sigma} \psi^* \tilde{\psi} + o(\varepsilon) \right] \\ &= - \int_{\mathbb{R}^d} (\Delta \psi^* + |\psi|^{2\sigma} \psi^*) \tilde{\psi} = \int_{\mathbb{R}^d} \frac{\delta H}{\delta\psi} \tilde{\psi}, \end{aligned}$$

where the second equality is obtained by applying integration by parts to the first term  $\varepsilon \nabla \tilde{\psi} \nabla \psi^*$  and dividing through with  $\varepsilon$ . One sees that

$$-\frac{\delta H}{\delta\psi} = \Delta \psi^* + |\psi|^{2\sigma} \psi^*$$

and will recover the second equation of (2.5.10). Similarly, replacing  $\psi^*$  by  $\psi$  and by using  $i\psi_t = \frac{\delta H}{\delta\psi^*}$  one gets the first equation in (2.5.10).

Given that DS system is non-local, the options we have at our disposal are either considering it as a constrained system (where no dynamical equation for  $\varphi$  involved), or local Hamiltonian operator with non-local density or non local Hamiltonian operator. DS I and DS II systems are described as Hamiltonian dynamical systems by means of inverse scattering in [5]. However, following [18] the DS I system can be shown to be Hamiltonian system as follows. In terms of characteristic coordinates, the DS I takes the form

$$i\psi_t + \psi_{\xi\xi} + \psi_{\eta\eta} = \varphi_\xi + \varphi_\eta - \rho|\psi|^2\psi \quad (2.5.12)$$

$$2\varphi_{\xi\eta} = \rho \left( (|\psi|^2)_\xi + (|\psi|^2)_\eta \right) \quad (2.5.13)$$

for (complex) envelope  $\psi(t, \xi, \eta)$  of a free surface of the water-wave and a (real)  $\varphi$  velocity potential of the mean motion generated by surface wave. Define new fields

$$A^{(1)} = -\varphi_\eta + \frac{\rho}{2}|\psi|^2, \quad A^{(2)} = \varphi_\xi - \frac{\rho}{2}|\psi|^2 \quad (2.5.14)$$

to rewrite DS I as 
$$i\psi_t + \psi_{\xi\xi} + \psi_{\eta\eta} + (A^{(1)} - A^{(2)})\psi = 0 \quad (2.5.15)$$

$$A^{(1)} = \varphi_1^{(0)}(t, \eta) - \frac{\rho}{2} \int_{-\infty}^{\xi} (|\psi|^2)_\eta d\xi', \quad A^{(2)} = \varphi_2^{(0)}(t, \xi) + \frac{\rho}{2} \int_{-\infty}^{\eta} (|\psi|^2)_\xi d\eta' \quad (2.5.16)$$

for arbitrary boundaries  $\varphi_1^{(0)}(t, \eta)$  and  $\varphi_2^{(0)}(t, \xi)$ . Another possible representation of (2.5.15) with the  $A^{(1)}$  and  $A^{(2)}$  replaced with

$$B^{(1)} = \varphi_1(t, \eta) - \frac{\rho}{4} \left( \int_{-\infty}^{\xi} - \int_{\xi}^{+\infty} \right) (|\psi|^2)_{\eta} d\xi', \quad B^{(2)} = \varphi_2(t, \xi) + \frac{\rho}{2} \left( \int_{-\infty}^{\eta} - \int_{\eta}^{+\infty} \right) (|\psi|^2)_{\xi} d\eta' \quad (2.5.17)$$

so that (2.5.15) becomes

$$i\psi_t + \psi_{\xi\xi} + \psi_{\eta\eta} + (B^{(1)} - B^{(2)})\psi = 0 \quad (2.5.18)$$

where the arbitrary boundaries here are  $\varphi_1(t, \eta)$  and  $\varphi_2(t, \xi)$ . The appropriate boundary conditions are selected from the specified multi-scale limit used in the derivation of DS I. For instance, the multi-scale limit of the Kadomtsev-Petviashvili (KP I) equation, whilst wellposedness in time is being kept, generates the form of the equation (2.5.15).

For the sake of convenience, the 2-component form of the DS I is best expressed as

$$iP_t + \sigma_3(P_{\xi\xi} + P_{\eta\eta}) + [\Phi, P] = 0 \quad (2.5.19)$$

where, with Pauli matrix  $\sigma_3 = \begin{pmatrix} 1 & 0 \\ 0 & -1 \end{pmatrix}$ ,

$$P = \begin{pmatrix} 0 & \psi \\ \tilde{\psi} & 0 \end{pmatrix}, \quad \Phi = \begin{pmatrix} A^{(1)} & 0 \\ 0 & A^{(2)} \end{pmatrix} \quad \text{or} \quad \Phi = \begin{pmatrix} B^{(1)} & 0 \\ 0 & B^{(2)} \end{pmatrix} \quad (2.5.20)$$

with corresponding 2-component fields for the different choices of the arbitrary boundaries

$$A^{(1)} = \varphi_1^0(t, \eta) - \frac{\rho}{2} \int_{-\infty}^{\xi} (P^2)_{\eta} d\xi', \quad A^{(2)} = \varphi_2^{(0)}(t, \xi) + \frac{\rho}{2} \int_{-\infty}^{\eta} (P^2)_{\xi} d\eta' \quad (2.5.21)$$

$$B^{(1)} = \varphi_1(t, \eta) - \frac{\rho}{4} \left( \int_{-\infty}^{\xi} - \int_{\xi}^{+\infty} \right) (P^2)_{\eta} d\xi',$$

$$B^{(2)} = \varphi_2(t, \xi) + \frac{\rho}{2} \left( \int_{-\infty}^{\eta} - \int_{\eta}^{+\infty} \right) (P^2)_{\xi} d\eta' \quad (2.5.22)$$

and  $[\cdot, \cdot]$  denotes a commutation relation for operators. These lead to the reduced DS I equation to the form  $\tilde{\psi} = \rho\psi^*$ . Moreover, the DS I appears to be the compatibility condition given as the representation of the Lax pair

$$[L_1, L_2] = 0 \quad (2.5.23)$$

where  $L_1$  and  $L_2$  are linear operators defined as, in terms of the coordinates  $u = (\xi + \eta)/2$

and  $v = (\xi - \eta)/2$ ,

$$L_1(P) = \partial_u + \sigma_3 \partial_v + P \quad (2.5.24)$$

$$L_2(P) = i\partial_t + \sigma_3 \partial_v^2 + P\partial_v - \frac{1}{2}\sigma_3 P_u + \frac{1}{2}P_v + \Phi. \quad (2.5.25)$$

The operators  $L_1$  and  $L_2$ , are known to be the Zakharov-Shabat hyperbolic spectral operators defined on the plane and are viewed as those defining a linear spectral problem where  $P$  serves as the data. With the boundaries given at all time in (2.5.21), one solves the Cauchy problem for DS I by suitably defining the Spectral Transform of  $P$ . See the details for this in section 3 of [18].

Now, utilizing the form of the boundary fields (2.5.22), let us introduce the functional

$$H[\psi] = \int_{\mathbb{R}^2} \left[ \tilde{\psi}(\partial_\xi^2 + \partial_\eta^2)\psi - \frac{1}{4}\psi\tilde{\psi}(\partial_\xi\partial_\eta^{-1} + \partial_\eta\partial_\xi^{-1})\psi\tilde{\psi} + (\varphi_1 - \varphi_2)\psi\tilde{\psi} \right] d\xi d\eta, \quad (2.5.26)$$

i.e. the Hamiltonian for DS I, and the canonically defined Poisson bracket

$$\{F, G\} = i \int_{\mathbb{R}^2} \left[ \frac{\delta F}{\delta\psi} \frac{\delta G}{\delta\tilde{\psi}} - \frac{\delta F}{\delta\tilde{\psi}} \frac{\delta G}{\delta\psi} \right] d\xi d\eta \quad (2.5.27)$$

where  $\tilde{\psi}$  is conjugate variable of  $\psi$  as defined earlier. Therefore, the equation governing the motion of the dynamics described by DS I are

$$\psi_t = \{\psi, H\}, \quad \tilde{\psi}_t = \{\tilde{\psi}, H\}. \quad (2.5.28)$$

These equations of motion would lead to the DS I system, and turns out the only Hamiltonian case is when  $\varphi_1 \equiv \varphi_2 \equiv 0$ . When this is satisfied, it guarantees the DS I to be a Hamiltonian system with an infinite number of independent continuous involutory integrals of motion, thereby making DS I a completely integrable Hamiltonian system.

## II

---

### Numerical Aspects

---

# Chapter 3

## Numerical Approaches

In this chapter, we consider the numerical aspects of spatial and temporal discretization of nonlinear dispersive problems on  $\mathbb{R} \times \mathbb{R}^d$  for  $d \in \mathbb{N}$ .

### 3.1 Introduction

The basic idea of approximation theory is to "seek for  $p(x)$ , a function from a certain class of functions, that approximates a given (continuous) function  $u(x)$  on a domain  $I \subset \mathbb{R}^d$ " such that the maximum error

$$\|u(x) - p(x)\| = \max_{x \in I} |u(x) - p(x)| \quad (3.1.1)$$

is minimized, i.e.  $p(x)$  is close enough to  $u(x)$ . If such  $p(x)$  exists then it is unique, referred to as *approximant* of  $u(x)$  and the best approximation of  $u(x)$  (Rivlin [192], pg. 2),<sup>1</sup>. Our gauge for the best approximant  $p(x) \in \mathcal{P}_N$  is the uniform-norm (3.1.1), where  $\mathcal{P}_N$  is a finite dimensional subspace of some normed linear space.

If instead, a discrete data set is given, the approximation process is known as *interpolation*, and the approximant is referred to as *interpolant*. Basically, one finds a simple approximant  $p(x)$ , e.g. polynomial, so that  $p(x_n)$  matches  $u(x_n)$  for each  $n$ , i.e. the deterministic relationship  $p(x_n) = u(x_n)$  holds for  $0 \leq n \leq N$ . In general, a finite discrete set  $\{u(x_n)\}_{n=0}^N$  is interpolated to a (continuous) function  $u(x)$  on a set of discrete points  $\{x_n\}_{n=0}^N$ . For continuous  $u(x)$ , the interpolant  $p(x)$  matches  $u(x_n)$  at every grid point  $x_n$  as in (3.2.10), this allows us to use the type of estimate (3.1.1) that is valid for all  $x$ .

An approximant plays a crucial role in understanding the behaviour of functions that may appear too complicated to deal with, i.e by representing them with simpler ones such as algebraic and trigonometric polynomials, which are more convenient for function representation. Thus, they are useful in determining, numerically, within a predetermined precision, an unknown solution to a differential equation and numerical evaluation of integrals that may be difficult to determine. We expect errors as one puts data into computers with finite precision. These errors, if too large, will pollute the approximation method making it unreliable and therefore accuracy cannot be guaranteed. Major works

---

<sup>1</sup>Roughly speaking, an approximant  $p^*(x) \in X$ , a finite dimensional normed linear subspace of  $Y$ , is best if for any  $p(x) \in Y$ , the distance  $\|p(x) - p^*(x)\|$  is least.

concerning approximation of functions include Szabados [205], Atkinson and Vertesi [9], Gautschi [70] and Trefethen [209, 208].

Another important application of approximation is how to interpolate the derivatives of the underlying function. Since differentiation is a linear operation, using the interpolation process of approximate derivatives we can derive differentiation matrices thereby making implementation easier on computational devices. See (Trefethen [209], Ch. 2) and (William et al. [185] pg. 1091).

In this chapter we discuss the problem of interpolations of a function  $u(x)$  defined on  $[-1, 1]$ . We consider an approximant on a set of *equally* and *unequally* distributed grid points. As approximation is involved, the errors associated to the interpolation of a function are discussed. Various numerical differentiation algorithms are used to investigate the errors involved in the higher derivatives such as recursive matrix differentiation, Clenshaw-differentiation, and Chebyshev-Fourier differentiation.

### 3.2 Interpolating polynomials

Given  $\{u(x_n)\}_{n=0}^N$  on a discrete data set  $\{x_n\}_0^N$ , an interpolation problem of a function  $u(x)$  on an interval  $[a, b]$  is the process of finding a function  $p(x)$  that fits  $u(x)$  at the finite set of discrete points  $\{x_n\}_0^N$ . The approximant  $p(x)$  is said to interpolate  $u(x)$  at the discrete points. Our concern is preferably to work with  $p(x)$  being an algebraic or trigonometric polynomial.

**Definition 3.2.1.** Let  $\{x_n\}_0^N$  be  $N + 1$  distinct (interpolating) points in the interval  $[a, b]$  with corresponding function values  $u := \{u(x_n)\}$  with  $u(x_n) = u_n$ . A polynomial interpolant  $p_N \in \mathcal{P}_N$  (a space of polynomials of degree  $\leq N$ ) of  $u(x)$ , if it exists, is a unique polynomial of degree at most  $N \geq 1$  satisfying

$$p_N(x_n) = u(x_n) \quad \text{for } 0 \leq n \leq N. \quad (3.2.1)$$

By the above definition, we interpolate discrete sets of data values  $\{u(x_n)\}_0^N$  to approximate a function  $u(x) \in C(I)$ .

**Definition 3.2.2.** An interpolation problem (3.2.1) is said to be well-posed if such  $p_N(x)$  exists and is unique, moreover depends continuously on the input (initial) data.

Let  $U := (U, \|\cdot\|_U)$  and  $V := (V, \|\cdot\|_V)$  be any two normed linear spaces with respect to their norms. Consider a problem described by the map

$$u : U \rightarrow V \quad \text{such that} \quad x \in U \mapsto u(x) \in V. \quad (3.2.2)$$

For any  $x, \tilde{x} \in U$ , define an *absolute condition number*  $\Lambda_{\text{abs}}$  and *relative condition number*  $\Lambda_{\text{rel}}$  respectively, associated to the problem, by

$$\begin{aligned}\Lambda_{\text{abs}} &:= \lim_{\epsilon \rightarrow 0^+} \sup_{\|\tilde{x}-x\|_U \leq \epsilon} \frac{\|u(\tilde{x}) - u(x)\|_V}{\|\tilde{x} - x\|_U}, \\ \Lambda_{\text{rel}} &:= \lim_{\epsilon \rightarrow 0^+} \sup_{\|\tilde{x}-x\|_U \leq \epsilon} \left[ \left( \frac{\|u(\tilde{x}) - u(x)\|_V}{\|u(x)\|_V} \right) / \left( \frac{\|\tilde{x} - x\|_U}{\|x\|_U} \right) \right].\end{aligned}\tag{3.2.3}$$

These condition numbers quantify the corresponding changes in the output space  $V$  as a result of small perturbations that may occur in the input space  $U$ . The  $\tilde{x} = x + \delta(x)$  above is the perturbation. We consider the problem to be "*well-conditioned*" if the condition number is sufficiently small close to zero and "*ill-conditioned*" when large.

**Definition 3.2.3.** An interpolation operator is the projection:  $\mathcal{P}_N : C([a, b]) \rightarrow \mathcal{P}_N$  such that  $\mathcal{P}_N(u(x)) = p_N(x) \in \mathcal{P}_N$

$$p_N(x) = \sum_{n=0}^N c_n \phi_n(x)\tag{3.2.4}$$

for some basis functions  $\phi_n(x) \in \mathcal{P}_N$  and unknown coefficients  $c_n \in \mathbb{R}$  for all  $n$ .

Let  $U = C([a, b])$  and  $V = \mathcal{P}_N$  with their respective norms, endow the operator with the induced norm (*operator norm*)

$$\Lambda_N := \|\mathcal{P}_N\|_{U,V} := \sup_{0 \neq u(x) \in U} \frac{\|\mathcal{P}_N(u(x))\|_V}{\|u(x)\|_U} = \sup_{\|u(x)\|_U=1} \|\mathcal{P}_N(u(x))\|_V < \infty.\tag{3.2.5}$$

The bounded operator (3.2.5) is referred to as "*Lebesgue constant*". If it is linear and  $\|\mathcal{P}_N(u)\|_V \leq \Lambda_N \|u\|_U \forall u \in U$ , it can be verified to satisfy

$$\|\mathcal{P}_N(u - \tilde{u})\|_V = \|\mathcal{P}_N(u) - \mathcal{P}_N(\tilde{u})\|_V \leq \Lambda_N \|u - \tilde{u}\|_U.$$

Here the norms are uniform norms and therefore  $\|u\|_U = \|u\|_\infty := \max_{a \leq x \leq b} |u(x)|$ .

**Definition 3.2.4.** An interpolation problem (3.2.1) is *well-conditioned* if the condition number  $\Lambda_N$  is relatively small close to zero, and *ill-conditioned* otherwise.

It is worth mentioning that  $\Lambda_N = \Lambda_{\text{abs}}$ ,<sup>2</sup>. Furthermore, the definition of well-posedness comes down to the conditioning that the Lebesgue constant  $\Lambda_N$  is very small. Moreover,  $\Lambda_N$  depends on the degree  $N$  of the polynomial and the choice of interpolation points as we can see later in the case of the Lagrange interpolant. Generally, we deal with two categories of conditioning: one for the values of interpolation points and the other for expansion coefficients  $c_n$ .

<sup>2</sup>It is preferable to use relative condition numbers since due to floating point operations the computational devices do not produce absolute errors but relative errors.

**Definition 3.2.5.** A method or algorithm that solves a given problem (3.2.1) is said to be stable if it is both forward and backward stable.

Consider solving a problem  $p(x) = u$  numerically. If the algorithm produces solution  $\tilde{u}$ , the forward (resp. backward) error is  $\delta(u) = \tilde{u} - u$  ( resp.  $\delta x = u - \tilde{x}$ ) for  $\tilde{x} - x$ .

**Definition 3.2.6.** An algorithm that solves  $p(x) = u$  is forward stable if the forward error  $\delta(u)$  is small, and backward stable if  $\delta x$  is small such that  $p(x + \delta x) = \tilde{u}$ .

The main sources of errors in an algorithm are due to truncation and round-off. The "smallness" for all  $x$  can imply that  $\delta x$  is either the same as or close enough or few orders of magnitude larger than the machine epsilon  $\epsilon_M$ . The  $\epsilon_M$  may also be referred to as *unit round-off*. In other words, an algorithm is stable if small perturbation  $\delta x$  corresponds to the small perturbation  $\delta u$ . This also means an algorithm will be stable if it is backward stable.

Suppose for simplicity that  $u(x)$  is approximated by an algebraic polynomial, where  $\phi_n(x) = x^n$

$$p_N(x) = \sum_{n=0}^N c_n x^n = c_0 + c_1 x + c_2 x^2 + \dots + c_N x^N. \quad (3.2.6)$$

Based on the interpolation condition (3.2.1), we are tasked to finding the vector  $\mathbf{c} := [c_0, \dots, c_N]$ . On evaluating (3.2.6) on the  $N + 1$  grid points, a set of  $N + 1$  linear equations having  $N + 1$  unknowns is generated which can be re-expressed in the matrix-vector form  $\mathbf{V}\mathbf{c} = \mathbf{u}$ . That is,

$$\begin{bmatrix} 1 & x_0 & x_0^2 & \dots & x_0^N \\ 1 & x_1 & x_1^2 & \dots & x_1^N \\ \vdots & \vdots & \vdots & \dots & \vdots \\ 1 & x_N & x_N^2 & \dots & x_N^N \end{bmatrix} \begin{bmatrix} c_0 \\ c_1 \\ \vdots \\ c_N \end{bmatrix} = \begin{bmatrix} u_0 \\ u_1 \\ \vdots \\ u_N \end{bmatrix} \quad (3.2.7)$$

The matrix  $\mathbf{V}$  is called *Vandermonde matrix*. It is not too difficult to verify that

$$\det(V) = \prod_{n < m} (x_n - x_m), \quad m, n = 0, \dots, N \quad (3.2.8)$$

is non-zero since  $x_n$  are distinct points for all  $n$ . This guarantees the existence of a unique solution to the system (3.2.7). Consequently, the existence and uniqueness of  $p_N(x)$  follow.

An alternative approach that produces such  $p_N(x)$  is the *Lagrange form*

$$L_N(x) = \sum_{n=0}^N \ell_n(x) u(x_n), \quad \ell_n(x) = \prod_{\substack{m=0 \\ m \neq n}}^N \frac{(x - x_m)}{(x_n - x_m)} \quad (3.2.9)$$

satisfying the interpolation problem (3.2.1). The polynomial representation (3.2.9) must produce the same polynomial (3.2.6) for uniqueness reason. i.e.,  $p_N(x) = L_N(x)$ . If  $u(x) \in$

$C^k(I)$  (a class of  $k$  times continuously differentiable functions in an interval  $I = [a, b]$ ), for  $d = N + 1$ , the theoretical *interpolation error* bounds of the interpolant  $p_N(x) \in \mathcal{P}_N$ , the Lagrange form (3.2.9), are given by

$$|u(x) - p_N(x)| \leq \frac{\max_{\zeta \in I} u^{(N+1)}(\zeta)}{(N+1)!} \cdot \max_{x \in I} \left| \prod_{n=0}^N (x - x_n) \right|, \quad \zeta \in I. \quad (3.2.10)$$

Assume we have equispaced-points:  $x_{n+1} - x_n = \delta = (b - a)/N$  and  $|\max_{\zeta \in I} u^{(N+1)}| \leq C$ , for some finite constant  $C$ . The factor  $\max_{x \in I} |\prod_n (x - x_n)|$  in (3.2.10), by calculating the maximum, has an upper bound  $\delta^{N+1} N! / 4$  resulting in the interpolation error bound  $C\delta^{N+1} / 4(N+1)$  of (3.2.9). Apparently, the error bound suggests that  $C\delta^{N+1} \ll 1$ , but this is not true in general to have  $\delta^{N+1}$  dominating  $C$ . For instance, the error grows as  $N$  gets bigger in the interpolation of  $1/(1+x^2)$  on  $[a, b]$ . However, if the points are asymptotically distributed, in  $N$ , unevenly having density of the form

$$\rho(x) \sim N[\pi^2(1-x^2)]^{-1/2}, \quad (3.2.11)$$

the intensity of the interpolation errors can be lessened as depicted in the Figure 3.1. Some of these points with property (3.2.11) are the well-known Chebyshev nodes in the interval  $[-1, 1]$ :

$$x_n = \cos(n\pi/N), \quad n = 0, 1, \dots, N. \quad (3.2.12)$$

In Figure 3.1 the Lagrangian polynomial (3.2.9) is used to interpolate the functions  $u(x) = \sin(\pi x)$ ,  $v(x) = 1/(1+x^2)$  and  $w(x) = 2/(3+x)$  on the interval  $[-1, 1]$ , using equispaced-points and Chebyshev-nodes. Almost the same maximum errors are obtained when the algebraic polynomial (3.2.6) is used as can be found in (Trefethen [209]). It clearly shows on equispaced points in  $[-1, 1]$ , the maximum error does not converge to 0 especially for large  $N$ . The wiggling or oscillations we noticed at the boundaries  $\pm 1$  for the interpolation of each function in Figure 3.1 is known as *Runge phenomena*. On the other side, using Chebyshev-nodes<sup>3</sup>, the effect of the error has been reduced. Moreover, this proves that there is a minimal degree for higher degree interpolating polynomials in enhancing the approximation accuracy.

With Chebyshev nodes in  $[a, b]$ , one proves

$$\max_{a \leq x \leq b} \left| \prod_{n=0}^N (x - x_n) \right| = 2^{-(2N+1)} (b-a)^{N+1} \quad (3.2.13)$$

<sup>3</sup>Chebyshev nodes are obtained by projecting points on the semi-circle in the complex plane onto the  $x$ -axis. See Appendix for details.

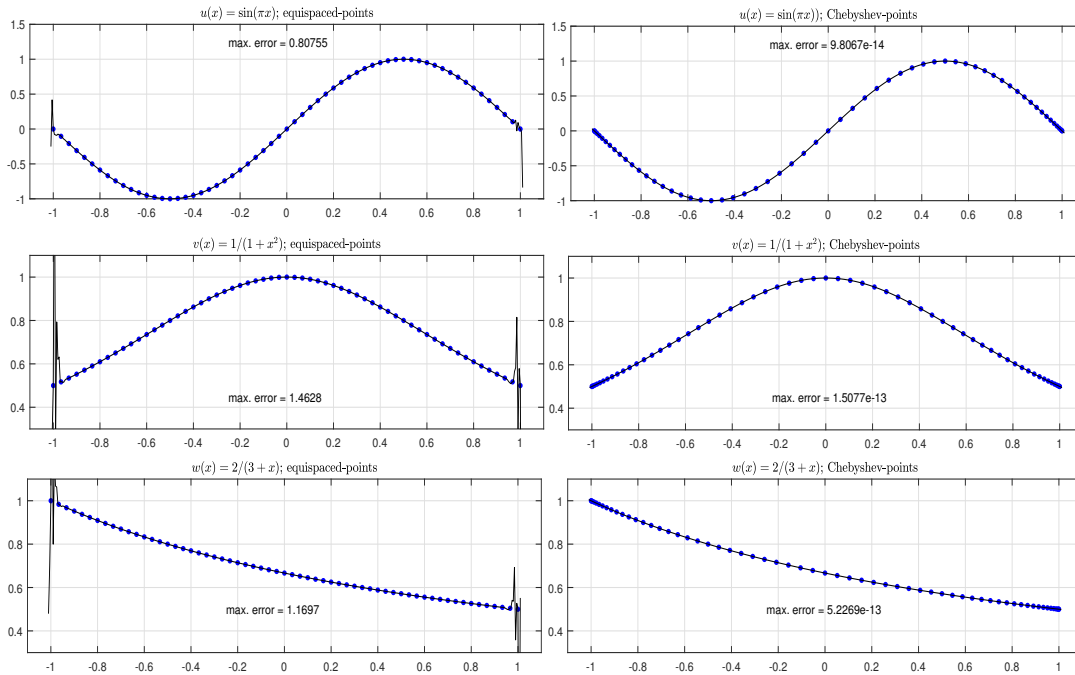


Figure 3.1: Comparison of Lagrange polynomial interpolations using 61 equispaced-points and 61 Chebyshev-points on  $[-1,1]$ . Left: the functions  $u, v, w$  are interpolated on equispaced with effect of error oscillations at the boundaries. Right: the effect of oscillations is damped out by interpolating  $u, v, w$  on Chebyshev nodes. Cf. [209]

with error bound  $2^{-(2N+1)}C/(N+1)!$  if  $u(x)$  is differentiable. It is not hard to verify that the errors in this case approach zero faster than the errors for equispaced-points. Analogously, we can check the conditioning, using Lebesgue function, of these different points distributions, where  $\Lambda_N = \max_{a \leq x \leq b} \lambda(x) = \max_{a \leq x \leq b} \sum_{n=0}^N |\ell_n(x)|$  in the Figure 3.2.

### 3.3 Numerical Differentiation Matrices

Given the set of discrete points  $\{x_n\}_{n=0}^N \in [a, b]$  with corresponding values  $\mathbf{u} = \{u(x_n)\}_{n=0}^N$ , we are interested in the values of the derivatives of  $u(x)$  at the discrete points, that is  $d^{(k)}(u) = \{d_n^{(k)}\}_{n=0}^N$  for  $d_n^{(k)} \approx u^{(k)}(x_n)$ , where  $d^{(k)}$  is the discrete differential operator. Exploiting the linearity property of differentiation, the relation between the  $k$ th derivative and  $u$  is given by the linear transformation

$$d_n^{(k)}(\mathbf{u}) = D_N^{(k)} \mathbf{u}, \quad k = 0, 1, 2, 3, \dots \quad (3.3.1)$$

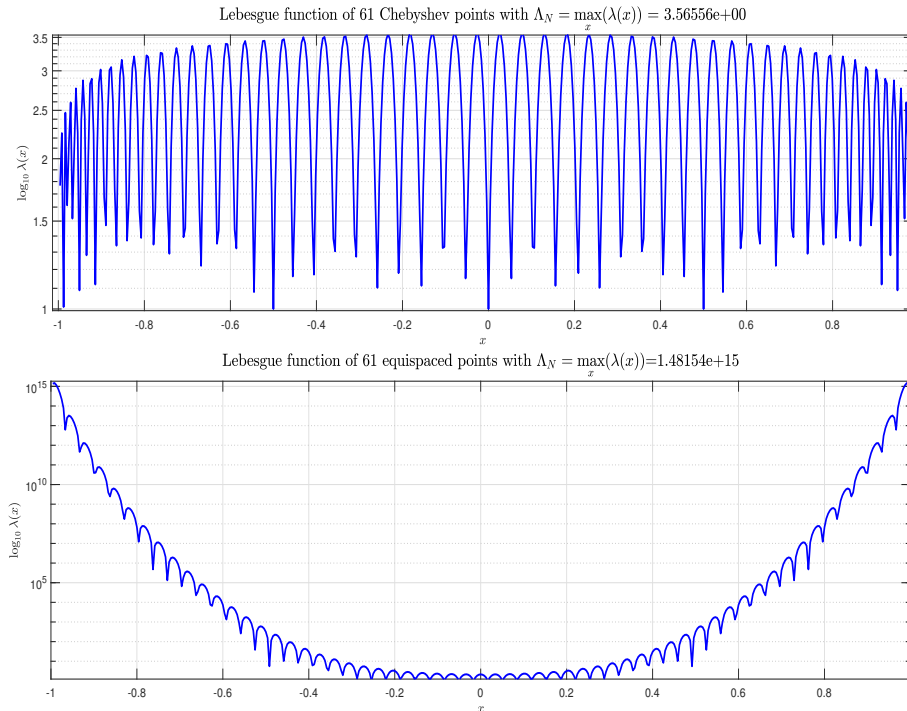


Figure 3.2: Comparison of Lebesgue functions for  $N + 1$  equispaced-points (top) and  $N + 1$  Chebyshev-points (bottom) on  $[-1,1]$ , with  $N = 60$  used. Cf. Trefethen [208].

where  $D_N^{(k)}$  is an  $(N + 1)$ -square matrix, which can be referred to as  $k$ th order *differentiation matrix*. The order  $k$  can be generated by recursive multiplication of  $D_N$   $k$ -times or derive them implicitly (see Gottlieb [75] and Weideman [217]).

Let  $p_N(x)$  interpolate  $u(x)$  at equispaced discrete points:  $x_{n+1} - x_n = \delta$  for each  $n$ , the first-derivative approximation to  $u(x)$ , by degree  $m \leq 2$  Lagrange polynomial form, at  $x_n$  can be obtained via the 3-points formula

$$u'(x_n) \simeq p'_m(x_n) = \sum_{j=0}^m \ell'_j(x_n) u(x_j) = \frac{u_{n+1} - u_{n-1}}{2\delta}, \quad 1 \leq n \leq N - 1, \quad (3.3.2)$$

where the sample points used are  $\{x_0, x_1, x_2\} = \{x - \delta, x, x + \delta\}$ ,<sup>4</sup>. Next, it remains to impose conditions on the boundary values at  $n = 0, N$ .

<sup>4</sup>Equivalently, let  $I = [a, b]$ , suppose  $u(x) \in C^3(I)$  in a neighbourhood  $[x - \delta_0, x + \delta_0]$  of  $x \in I$  for some  $\delta_0 > 0$ . Now, for  $\delta \in ]0, \delta_0[$  with some  $\zeta \in ]x, x + \delta[$ , the 3rd order Taylor expansion  $u(x + \delta) = u(x) + u'(x)\delta + u''(x)\frac{\delta^2}{2!} + u'''(\zeta)\frac{\delta^3}{3!}$ . Replacing  $\delta$  by  $-\delta$ , yet  $\zeta \in ]x - \delta, x[$ , in the expansion and subtracting the two results leads to the second order finite difference formula, where for  $\zeta \in ]x - \delta, x + \delta[$ : one gets  $p'_2(x) = \tilde{u}'(x) := \frac{u(x+\delta) - u(x-\delta)}{2\delta} = u'(x) + \frac{\delta^2}{3!}u'''(\zeta)$ , where  $\tilde{u}'(x)$  approximates the derivative  $u'(x)$  with error term  $\delta^2 u'''(\gamma)/3!$ . One may deduce the estimates  $|u'(x) - \tilde{u}'(x)| \leq C\delta^2$  directly, where  $C = \max_{y \in [x-\delta_0, x+\delta_0]} \frac{|u'''(y)|}{6}$ .

If  $u(x)$  is periodic with  $u_n = u(x_n)$ , we impose periodic boundary conditions  $u_0 = u_N$  and  $u_{N+1} = u_1$ . Constituting the entire evaluation process of the derivative at the nodes, in terms of matrix representation  $d(\mathbf{u}) = D_N \mathbf{u}$ , we explicitly write

$$\begin{pmatrix} d_0 \\ d_1 \\ \vdots \\ d_N \end{pmatrix} = \frac{1}{2\delta} \underbrace{\begin{pmatrix} 0 & 1 & 0 & \cdots & 0 & -1 \\ -1 & \ddots & \ddots & \ddots & \ddots & 0 \\ 0 & \ddots & \ddots & \ddots & \ddots & \vdots \\ \vdots & \ddots & \ddots & \ddots & \ddots & 0 \\ 0 & \ddots & \ddots & \ddots & \ddots & 1 \\ 1 & 0 & \cdots & 0 & -1 & 0 \end{pmatrix}}_{D_N} \begin{pmatrix} u_0 \\ u_1 \\ \vdots \\ u_N \end{pmatrix}, \quad (3.3.3)$$

the differentiation matrix  $D_N$  is as shown in the equation (3.3.3).

For non periodic functions, we must use the right and left-sided derivatives for the boundaries, where we take

$$d_0 = (-3u_0 + 4u_1 - u_2)/2\delta, \quad d_N = (3u_N - 4u_{N-1} + u_{N-2})/2\delta, \quad (3.3.4)$$

combined with (3.3.2) the differentiation matrix becomes

$$D_N = \frac{1}{2\delta} \begin{pmatrix} -3 & 4 & -1 & 0 & \cdots & 0 \\ -1 & 0 & 1 & 0 & \cdots & 0 \\ 0 & \ddots & \ddots & \ddots & \ddots & \vdots \\ \vdots & \ddots & \ddots & \ddots & \ddots & 0 \\ 0 & \cdots & 0 & -1 & 0 & 1 \\ 0 & \cdots & 0 & 1 & -4 & 3 \end{pmatrix}. \quad (3.3.5)$$

As  $\delta \rightarrow 0$ , the approximations (3.3.2) to the derivative  $u'(x_n)$  converges at the rate  $O(\delta^2)$ . Thus, 2nd order central finite difference approximation has an order of accuracy two, where  $\varepsilon_N(\delta) = O(\delta^2) \leq C\delta^2 = C \cdot (2/N)^2 = O(N^{-2})$ .

As we can see, in Figure 3.3, for the functions  $\sin(\pi x)$ ,  $1/(1+x^2)$  and  $2/(3+x)$  on  $[-1, 1]$  using equally-spaced points, the error in the first derivative dropped to  $10^{-10}$  and increases as  $N \geq 10^6$ . This shows significant loss of accuracy. The point where the theoretical errors and approximation errors disagree, the diminishing of the maximum errors ceased.

Similar behaviour is observed when a 4th order finite central scheme is implemented, where the differentiation matrix is sparse, Toeplitz and circulant like in (3.3.3). From the Figure 3.3 it apparently indicates that there exist some positive  $N_0$  for which the maximum absolute error  $\max_{x \in [-1, 1]} |d(\mathbf{u}) - D\mathbf{u}| \rightarrow \infty$  for  $N_0 \leq N$ .

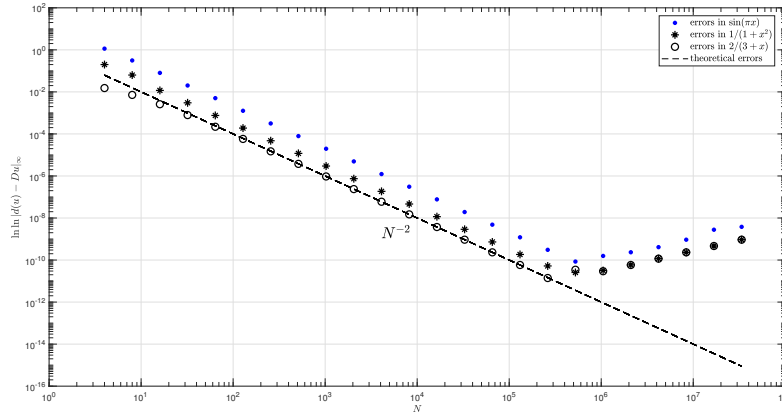


Figure 3.3: Convergence of the 2nd-order finite differences for an entire function  $\sin(\pi x)$  (shown  $\bullet$ ) and analytic functions  $2/(3+x)$  and  $1/(1+x^2)$  (shown in  $\circ$  and  $*$  respectively) defined on  $[-1,1]$ . (Cf. Trefethen [209]).

### 3.3.1 Chebyshev Differentiation Matrices

Construction of the Chebyshev differentiation matrices is done by simply considering the Lagrange interpolating polynomial  $p_N(x)$ , in Chebyshev nodes (3.2.12). A function  $u(x)$  defined on  $[-1,1]$  approximated as  $\mathbf{u} = \{u(x_n)\}_{n=0}^N$  for all discrete  $x_n \in [-1,1]$  has its first-derivative approximation written as  $p'_N = D_N \mathbf{u}$  for a differentiation matrix  $D_N$ . The  $(N+1)$ -square matrix  $D_N$  is generated as follows (see Trefethen [209]).

**Definition 3.3.1.** Let  $N \in \mathbb{N}$ ,  $c_n = 2$  for  $n = 1, N$  and  $c_n = 1$  otherwise. The entries  $(N+1)$ -square first order Chebyshev differentiation matrix  $D_N = (d_{nm})_{m,n=0}^N$  are

$$\begin{aligned} d_{00} &= (2N^2 + 1)/6, & d_{nn} &= \frac{-x_n}{2(1-x_n^2)}, & n &= 1, \dots, N-1 \\ d_{NN} &= -d_{00}, & d_{nm} &= \frac{c_n}{c_m} \frac{(-1)^{m+n}}{(x_n - x_m)}, & n \neq m; & n=1, \dots, N-1. \end{aligned} \quad (3.3.6)$$

Let us denote the  $k$ th derivative of  $p_N(x)$  at  $x_n$  by  $p_N^{(k)}$  and define  $p_N^{(k)} := D_N^{(k)} u$ . For the explicit formulas and the cost in computing  $D_N^{(k)}$  see (Gottlieb [75] and Peyret [181] and by recurrence formulas see (Weideman [217] and Welfert [220])).

In the Figure 3.4, the errors in the first two derivatives of the functions  $1/(1+x^2)$  and  $2/(3+x)$  on  $[-1,1]$  are compared. We visualise the loss of about 3 significant digits in the second derivatives compared to the first derivative, taking optimal degree  $N_0 = 40$ . There  $D_N^{(2)}$  is taken as  $D_N^2$ . This shows computing higher derivatives, for instance  $k \geq 10$ , is troublesome, as this the loss of accuracy increases with the number of derivatives.

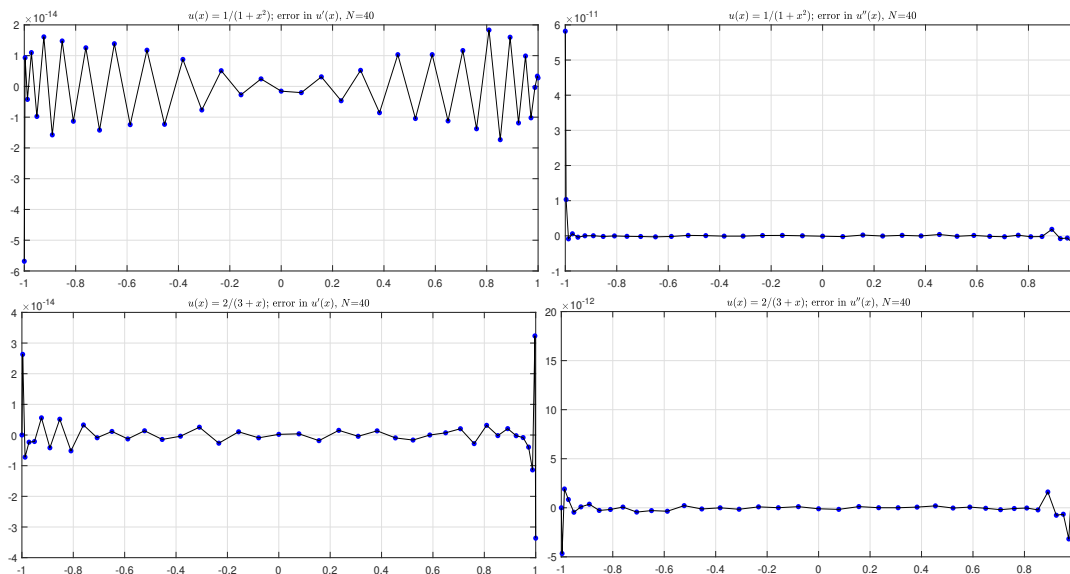


Figure 3.4: The Chebyshev spectral differentiations of functions defined on  $[-1,1]$ . At the top, absolute errors in the 1st and 2nd Chebyshev spectral derivatives of  $1/(1+x^2)$  and at the bottom for  $2/(3+x)$ , (cf. Trefethen[209]).

**Definition 3.3.2** (Spectral accuracy in Chebyshev spectral differentiation, Trefethen [209]).

Let  $u(x)$  be analytic inside and on a Bernstein ellipse of foci  $\pm 1$ . With  $N \rightarrow \infty$ ,  $k \geq 1$

$$|p_N^{(k)}(x_n) - u^{(k)}(x_n)| = O(c^{-N}); \quad c = 2 \exp(-N\phi_v) \quad (3.3.7)$$

where  $\phi_v$  is the value of the Chebyshev potential  $\phi(z) = \ln(|z - \sqrt{z^2 - 1}|/2)$  and  $c$  is the sum of the semi-major and semi-minor axes of the ellipse.

A "Bernstein ellipse" is an arbitrary ellipse of foci  $\pm 1$  on the  $\mathbb{C}$ -plane, which is the largest region for which an analytic function, say  $u(x)$ , remains analytic and bounded ([208], ch. 8). The values  $\phi_v$  of the Chebyshev potential  $\phi(z)$  are level curves that generate the ellipses on the complex plane ( see details in Trefethen [209], ch.5).

Even though one expects geometric convergence in theory but not so numerically. Thus, if  $u(x_n) = \tilde{u}_n + \epsilon_n$ , for  $0 \leq n \leq N$ , where  $\tilde{u}_n$  is the true computed value of  $u(x_n)$  with an error  $\epsilon_n$  for each  $n$ , the derivative  $u'(x_n)$  will encounter an error of  $\epsilon_n$  such that  $|\epsilon_n| \leq \epsilon_n$ , with  $\epsilon = \{\epsilon_n\}_{n=0}^N$  and  $\varepsilon = \{\varepsilon_n\}_{n=0}^N$ . The relationship between the  $D_N$ ,  $\mathbf{u}$  and the true derivative  $u'$  is shown in the *epsilon commutative diagram*, Fig. 3.3.1, where  $u'$  and  $\tilde{u}'$  are respectively the exact and numerically computed derivatives. The vertical arrows pointing down describe approximations while the horizontal ones show the differentiations. The

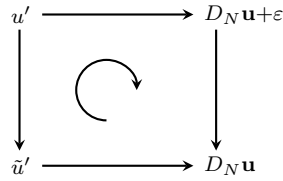


Figure 3.5: Epsilon commutative diagram.

diagram is commutative to a finite precision (depends on  $\epsilon$ ) that we are able to determine in advance.

### 3.3.2 Numerical differentiation for pseudo-spectral series

The Lagrange interpolating polynomial (3.2.9) interpolates  $u(x)$  at  $x_n$  by a series of overlapping low-degree local polynomials  $\phi_n(x) = \ell_n(x)$ , whereas the derivatives  $p'_N(x_n)$  (correspondingly finite difference formula) interpolates, using the  $m + 1$ -points weighted formula (3.3.2), the derivative of  $u(x)$  locally centered at  $x_n$ . Instead of representing the function by its sequence of discrete values on an interval, we might represent it in series form with basis function  $\phi_n(x)$  (differentiable), an  $n$  degree polynomial (a trig. or algebraic polynomial) that evaluates globally on the whole interval, and the (pseudo) spectral derivative comes from differentiating the higher-degree global interpolating polynomial.

**Definition 3.3.3.** Let  $u(x)$  be represented by an infinite series

$$u(x) = \sum_{n=0}^{\infty} c_n \phi_n(x), \quad x \in [a, b] \quad (3.3.8)$$

where  $\phi_n$  are the basis functions and  $c_n$  are the expansion coefficients for  $n = 0, 1, \dots$ . The series (3.3.8) has spectral (exponential) convergence if there exists a constant  $\alpha$  and a rate of convergence  $r > 0$  such that

$$c_n \sim O(\exp(-\alpha n^r)), \quad n \gg 1. \quad (3.3.9)$$

Let  $p_N(x)$  be the  $(N+1)$  partial sum of the series (3.3.8). A pseudo-spectral collocation utilizes the discrete values  $\{u(x_n)\}_{n=0}^N$  on discrete points  $\{x_n\}_{n=0}^N$  to determine the series expansion coefficients  $c_n$ . Then,  $p_N(x)$  and its derivatives are  $(N+1)$ -point formulas unlike the  $(m+1)$ -points formula (3.3.2). Therefore,  $p_N(x) \simeq u(x)$  is a spectral interpolating polynomial if the series (3.3.8) converges fast enough (exponentially) for sufficiently large  $N$ ,<sup>5</sup> In an  $m$ - ordered finite difference scheme,<sup>6</sup> the usual rate of convergence is  $O(N^{-m})$  for smooth

<sup>5</sup>Convergence, numerically, would mean if the required accuracy is attained.

<sup>6</sup>To balance the accuracy of an  $N$ -points (pseudo) spectral scheme for a function on  $[a, b]$ , one needs an

functions whereas for analytic functions the rate of convergence for spectral method is  $O(r^N)$  where  $0 < r < 1$ . *Spectral accuracy* is termed for the latter.

In this work we employ Fourier spectral method to semi-discretize the DS system. The method is very important especially for solving periodic problems. Recall, in one dimension, the continuous Fourier transform of a function  $u(x) \in L^2(\mathbb{R})$  and its inverse are defined by

$$\hat{u}(k) = \mathcal{F}[u](k) = \int_{-\infty}^{\infty} u(x)e^{-ikx} dx \quad k \in \mathbb{R}, \quad (3.3.10)$$

$$u(x) = \mathcal{F}^{-1}(u(k)) = \frac{1}{2\pi} \int_{-\infty}^{\infty} \hat{u}(k)e^{ikx} dk, \quad x \in \mathbb{R} \quad (3.3.11)$$

have their discrete versions (for a  $2\pi$ -periodic  $u$  where  $x_j = 2\pi j/N$  and  $v_j = u(x_j)$ ) taking  $x = \{x_1, \dots, x_N\}$ ,  $x_{j+1} - x_j = 2\pi/N$ ) defined as

$$\hat{v}_k = \frac{2\pi}{N} \sum_{j=1}^N e^{-ikx_j} v_j, \quad k = -\frac{N}{2} + 1 \cdots \frac{N}{2}, \quad (3.3.12)$$

$$v_j = \frac{1}{2\pi} \sum_{k=-\frac{N}{2}+1}^{\frac{N}{2}} e^{ikx_j} \hat{v}_k, \quad j = 1, \dots, N, \quad (3.3.13)$$

and they are called the Discrete Fourier Transform (DFT) and the inverse Discrete Fourier Transform (IDFT) respectively of the function  $u$ . See [208, 209] for more details. For the Fourier transform, the first derivative is determined by the spectral differentiation operator  $D : \ell^2 \rightarrow \ell^2$  defined as  $Dv = \mathcal{F}^{-1}(ik\mathcal{F}(v)) \approx u'(x)$ , where  $\ell^2$  is a space of square summable functions. The higher derivatives of order  $s \geq 1$  are generalized to  $D^{(s)}v = \mathcal{F}^{-1}((ik)^s \mathcal{F}(v))$  in order to approximate  $u^{(s)}(x)$ .

In terms of interpolant of  $u$ , the basis one uses are the Fourier basis  $\phi_n(x) = e^{inx}$  where  $c_n$  are the Fourier coefficients. Converting the  $x$ -interval into an interval  $[0, 2\pi) \ni \theta$  so that the interpolant  $p_N(\theta)$  and its derivatives evaluated at  $\theta_n$  are

$$p_N(\theta_n) = \sum_{n=-N}^N c_n e^{in\theta_n}, \quad p_N^{(k)}(\theta_n) = \sum_{n=-N}^N (in)^k c_n e^{in\theta_n}, \quad (3.3.14)$$

with equidistant  $\theta_n \in [0, 2\pi)$  and  $c_n = \mathcal{F}^{-1}(p_N(\theta_n))$ , where  $\mathcal{F}^{-1}$  is the inverse Fourier transform. The differentiation matrix in this case is dense for all the  $N + 1$  points, the derivative may behave like an  $N + 1$ -order finite difference scheme.

For non-periodic problem on  $[-1, 1]$ , the suitable choice of basis functions are  $\phi_n(x) = \cos(n \arccos(x))$ , the Chebyshev polynomials  $T_n(x)$ . Thus, the function  $u(x)$  on  $[-1, 1]$  can

$N$ -order finite difference scheme producing an error of  $O(\delta^N) = O[(b-a)/N]^N \sim O(N^{-N})$ .

be represented by

$$u(x) \simeq p_N^C(x) := \sum_{n=0}^N c_n T_n(x) = \sum_{n=0}^N c_n \cos(n \arccos(x)), \quad x \in [-1, 1] \quad (3.3.15)$$

with

$$\begin{aligned} c_n &= \frac{2}{\pi} \int_{-1}^1 \frac{u(x)T_n(x)}{\sqrt{1-x^2}} dx = 2 \int_0^1 u(\cos(\pi t)) \cos(n \cos(\pi t)) dt \\ &\simeq \frac{2}{N} \sum_{j=0}^N {}'' u\left(\cos \frac{j\pi}{N}\right) \cos\left(\frac{jn\pi}{N}\right) \end{aligned} \quad (3.3.16)$$

where the symbol  $''$  implies the terms for  $j = 0, N$  are to be multiplied by a factor of  $1/2$ . The Chebyshev coefficients  $c_n$  can be numerically determined using Fast cosine transform (FCT) implemented using the FFT- algorithm since we are approximating the integral of a periodic function via a trapezoidal rule.

With this  $N + 1$ -point formula (3.3.15) we encounter a dense matrix as in the Vandermonde matrix (3.2.7). In fact,  $T_n(x)$  are polynomials, orthogonal too, since by using the method of mathematical induction the sequence of  $n$ -degree Chebyshev polynomials

$$\begin{cases} T_0(x) = \cos(0) = 1, & T_1(x) = x, & n = 0, 1, \\ T_{n+1}(x) = 2xT_n(x) - T_{n-1}(x), & n \geq 1 \end{cases} \quad (3.3.17)$$

generates a polynomial of degree  $n$ . To show that let  $t = \arccos(x) \in \mathbb{R}$  using the identity  $2 \cos(nt) = e^{int} + e^{-int}$ , de Moivre's theorem:  $e^{ik\theta} = \cos(k\theta) + i \sin(k\theta)$  and the binomial theorem, with  ${}^n C_m = n! / [(n-m)!m!]$  we have

$$\begin{aligned} \cos(nt) &= \frac{1}{2} \sum_{m=0}^n \left[ {}^n C_m \cos^{n-m}(t) (i \sin^m(t)) + {}^n C_m \cos^{n-m}(t) (-i \sin^m(t)) \right] \\ &= \frac{1}{2} \sum_{m=0}^n {}^n C_m \cos^{n-m}(t) \sin^m(t) [i^{n-m} + (-i)^{n-m}] = \sum_{m=0}^{\lfloor n/2 \rfloor} {}^n C_m \cdot (-1)^m \cos^{n-2m}(t) \sin^{2m}(t) \\ &= \sum_{m=0}^{\lfloor n/2 \rfloor} {}^n C_m \cdot (-1)^m x^{n-2m} (1-x^2)^m = \sum_{m=0}^{\lfloor n/2 \rfloor} \sum_{r=m}^{\lfloor n/2 \rfloor} {}^n C_{2m} \cdot {}^m C_r \cdot (-1)^m x^{n-2r}, \end{aligned} \quad (3.3.18)$$

where  $\lfloor k \rfloor$  is the greatest integer  $\leq k$ . The result in (3.3.18) can further be simplified as found in (Clenshaw [36] and Snyder [198]) to

$$T_n(x) = \sum_{m=0}^{\lfloor n/2 \rfloor} \alpha_n^{(m)} x^{n-2m} = \begin{cases} \sum_{m=0}^{\lfloor n/2 \rfloor} (-1)^m \frac{2^{n-2m-1} n!}{(n-m)!} \cdot n^{-m} C_m x^{n-2m}; & m < n/2 \\ \sum_{m=0}^{\lfloor n/2 \rfloor} (-1)^m x^{n-2m}; & n = 2m. \end{cases} \quad (3.3.19)$$

An easy way to compute the  $k$ th derivative of the Chebyshev series (3.3.15) is to express it as

a superposition of the  $k$ th derivative of the basis function  $T_n(x)$ , however, bad conditioning kicks back again and it is not possible maintaining the same accuracy described in (3.3.15). In fact, the problem of oscillations at the boundaries  $\pm 1$  would reappear in large magnitude while the wavelength (of  $T_n(x)$ ) becomes small with an increase in degree  $N$  and order of the derivative  $k$ . This is evident, at the boundaries  $x = \pm 1$ , since the estimate

$$\left| T_N^{(k)}(\pm 1) \right| = \left| (\pm 1)^{N+k} \prod_{m=0}^{k-1} \frac{(N^2 - m^2)}{(2m + 1)} \right| \sim N^{2k} \prod_{m=0}^{k-1} \frac{1}{(2m + 1)} (1 + O(N^{-2})) \quad (3.3.20)$$

indicates that the conditioning of the  $k$ th order differentiation matrix of the Chebyshev interpolation problem goes to  $\infty$  at the rate  $N^{2k}$ , because the condition number for computing the  $k$ th derivative is  $O(N^{2k})$ . Henrichis [83] improved the conditioning by about the order  $O(N^k)$  by considering the "basis recombination". The modified basis used are  $\phi_n(x) = (1 - x^2)T_n(x)$  where the error contributions at the boundaries are rid-off. For instance, the conditioning of the 2nd derivative  $\phi_n''(x) = -4xT_n'(x) - 2T_n(x) + (1 - x^2)T_n''(x)$  near the boundaries grows like  $O(N^2)$ , same as that of 1st derivative instead of  $O(N^4)$  since  $T_n''(\pm 1)$  vanishes. Nevertheless, still higher derivatives, say 4th derivatives, also become ill-conditioned (Boyd [20], sec 7.7).

Another way to circumnavigate this issue is to compute the  $k$ th derivative of the series (3.3.15) recursively in terms of the values of the derivatives of the Chebyshev coefficients:

$$p_N^{(k)}(x) = \sum_{n=0}^N c_n^{(k)} T_n(x), \quad c_n^{(k)} = \begin{cases} 0, & n = N, N - 1; \\ (2(n + 1)c_{n+1}^{(k-1)} + c_{2n+1}^{(k)})/q_n, & n = N - 2, \dots, 0 \end{cases} \quad (3.3.21)$$

where  $q_0 = 2$  and for  $n > 0$ ,  $q_n = 1$ . For the evaluation of the derivatives see Clenshaw algorithm [36] or (William [185], sec. 5.5). Unfortunately, for higher derivatives, say 4th, we encounter ill-conditioned problem again even though the algorithm is stable, see Breuer and Everson [21], Merryfield and Shizgal [156].

An alternative method of differentiating (3.3.15) is via the combination Chebyshev-fast Fourier transform (chebfft) algorithm, see (Trefethen [209], ch. 8). Using the definition of  $c_n$  in (3.3.16), the Fourier series (3.3.14) coincides with the Chebyshev series (3.3.15), for that, given  $\{u_n\}_{n=0}^N$  with the Chebyshev nodes, one applies the chebfft algorithm in order to compute the derivatives of the Chebyshev series (3.3.15). The task is accomplished by extending the vector  $\mathbf{u} := (u_0, \dots, u_N)$  to  $\mathbf{v} := (v_{-N+1}, \dots, v_N)$  where  $\mathbf{v}_{-N+m} = v_m$  with  $m = 1, 2, \dots, 2N$ . This is equivalent to mapping the data  $\mathbf{u} \in \mathbb{C}^{N+1}$  to  $\mathbf{v} \in \mathbb{C}^{2N}$ . Next, by

the Fourier transform (equivalently the Fast-Fourier Transform) yields

$$\hat{\mathbf{v}}_n = \frac{\pi}{N} \sum_{m=1}^{2N} e^{-int_m} \mathbf{v}_m, \quad n = -N + 1, \dots, N$$

and define, in the Fourier space,  $\hat{\mathbf{w}}_n = in\hat{v}_n$  for all  $n \neq 0$  and  $\hat{\mathbf{w}}_N = 0$ . The inverse FFT

$$\mathbf{w}_m = \frac{1}{2\pi} \sum_{n=-N+1}^N e^{int_m} \hat{\mathbf{w}}_n, \quad m = 1, \dots, 2N$$

corresponds to the approximate derivative of a trig. interpolant on the data  $\{v_m\}_m$

$$\mathbf{p}(t) = \frac{1}{2\pi} \sum_{n=-N+1}^N e^{int} \hat{v}_n = \sum_{k=0}^N c_k T_k(x) = \sum_{k=0}^N c_k \cos(kt)$$

defined on equally space points  $t_m$  where  $c_k$  are the Chebyshev coefficients. Then, the first derivative of the algebraic, basically Chebyshev, interpolant is  $p_N(x) = \mathbf{p}(t)$  where  $x = \cos(t)$ . The derivative is therefore

$$p'_N(x) = \mathbf{p}'(t) \cdot \frac{dt}{dx} = \sum_{k=0}^N \frac{kc_k \sin(kt)}{\sqrt{1-x^2}} \quad (3.3.22)$$

which when evaluated at each  $x_m$  reads

$$p'_N(x_m) = w_m = \begin{cases} \frac{1}{2\pi} \sum'_{k=0}^N k^2 \hat{v}_k, & m = 0, \\ -w_m / \sqrt{1-x_m^2}, & m = 1, \dots, N-1 \\ \frac{1}{2\pi} \sum'_{k=0}^N (-1)^{k+1} k^2 \hat{v}_k, & m = N, \end{cases} \quad (3.3.23)$$

where the sum  $\sum'$  indicates the terms corresponding to the end points  $x_0 = 1$  and  $x_N = -1$  are having a factor of 1/2. The  $k$ th derivatives are obtained by successive differentiation of the first derivative where, in the Fourier space, the term  $\hat{\mathbf{w}}_n = in\hat{v}_n$  is replaced by  $\hat{\mathbf{w}}_n^{(s)} = (in)^s \hat{v}_n \forall n \neq 0$  and  $\mathbf{w}_N^{(s)} = 0$  for odd  $s$  (3.3.22) (see chebfft algorithm in appendix).

Figure 3.6 shows errors for the numerically computed derivatives of the function  $u(x) = \sin(\pi x)$  on  $[-1, 1]$ . In the first figure, Clenshaw's algorithm is implement to compute up to 4th derivative while in the second the chebfft algorithm is applied.

Even though Chebyshev series (3.3.15) reduce the errors, however, the oscillations at the boundaries return back whenever we try computing higher derivatives. This is equivalent to say that the condition number of Chebyshev differentiation matrices for higher derivatives can grow big even for not so large  $N$  and deprives us from getting required accuracy. In short, numerical differentiation through interpolation becomes ill-conditioned as well.

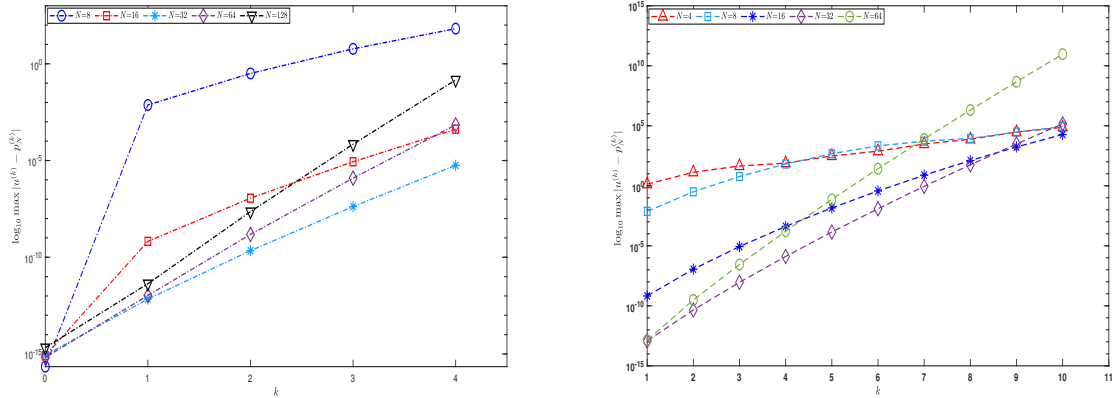


Figure 3.6: The maximum absolute error of the  $s$ th numerical derivative of the function  $u(x) = \sin(\pi x)$  on Chebyshev nodes in  $[-1, 1]$  for various degrees  $N$  of the polynomial interpolant using (left) Clenshaw's algorithm and (right) chebfft algorithm.

### 3.3.3 Discussion

In all the approaches we conclude that computational issues persevere and become even more intense in approximating higher-derivatives evident from the Figures 3.3-3.6. The errors generated while one attempts to balance the approximation errors and rounding errors are bound to blow up as the order  $s$  of the derivative increases. Therefore, attaining significant number of digits for the higher order derivatives  $s \geq 10$ , becomes a difficult task. One way around this undesirable situation is to use infinite summation formula, i.e. integration. However, this requires extension of  $u(x)$  analytically onto the complex plane in the neighbourhood of expansion point  $x_0$ , where one writes, via Cauchy integral formula (Gautschi [70], pg. 163-164), for the  $s$ th derivative

$$u^{(s)}(x_0) = \frac{s!}{2\pi i} \oint_{C_R} \frac{u(z)}{(z - x_0)^{s+1}} dz = \frac{s!}{2\pi R^s} \int_0^1 e^{-2\pi s i t} u(x_0 + R e^{2\pi i t}) dt \quad (3.3.24)$$

where  $C_R$  is assumed to be a closed circular contour about  $x_0$  with radius  $R$  to be chosen in a way that  $z = x_0 + R e^{2\pi i t}$  stays in the analytic region of  $u$ . If  $u(x)$  is real then we replace the integrand by its real part. The integral (3.3.24) matches the definition of the Fourier transform whose discrete counterpart, discrete Fourier transform (DFT), is efficiently approximated using a simple numerical quadrature, e.g. the Trapezoidal rule. The trapezoidal approximation would correspond to computing "fast Fourier transform (FFT)", (see Davis [42] and Appendix).

### 3.4 Numerical Time Integration Approaches

In this section, numerical techniques for time integrating non-linear dispersive PDEs are discussed. They consist of the implicit and explicit schemes.

#### 3.4.1 Stiff equations

A typical case of stiff equation in one dimension is the numerical solution to the equation

$$u'(t) = -50u(t), \quad u(0) = u_0 \in \mathbb{R} \setminus \{0\}, \quad t \geq 0 \quad (3.4.1)$$

whose exact solution is given as  $u(t) = u_0 \exp(-50t)$ . The reason of being stiff equation is that numerical solution as  $t \rightarrow \infty$  may diverge unlike the exact solution, where, for  $u_0 > 0$  one gets  $u(t) \rightarrow 0$  as  $t \rightarrow \infty$ . For instance, numerical solutions obtained by implementing explicit schemes, e.g. Euler's method exhibits such behaviour due to emergence of spurious errors, where they propagate to infinity except  $h$  is taken very small. In contrast to the explicit Euler's implementation, this is somewhat controlled, when the implicit one is used e.g. implicit 2nd order Runge-Kutta (IRK2) scheme. Already, as shown in the Fig. 3.7, the implicit RK2 does better than explicit Euler scheme for smaller time-step. It shows that explicit methods are costly to use since it demands more points, thus for stiff equation it is preferable to use implicit schemes with small  $h$ . However, stiffness is a subtle notion despite the fact that it is important to be aware of stiff equations for certain numerical scheme.

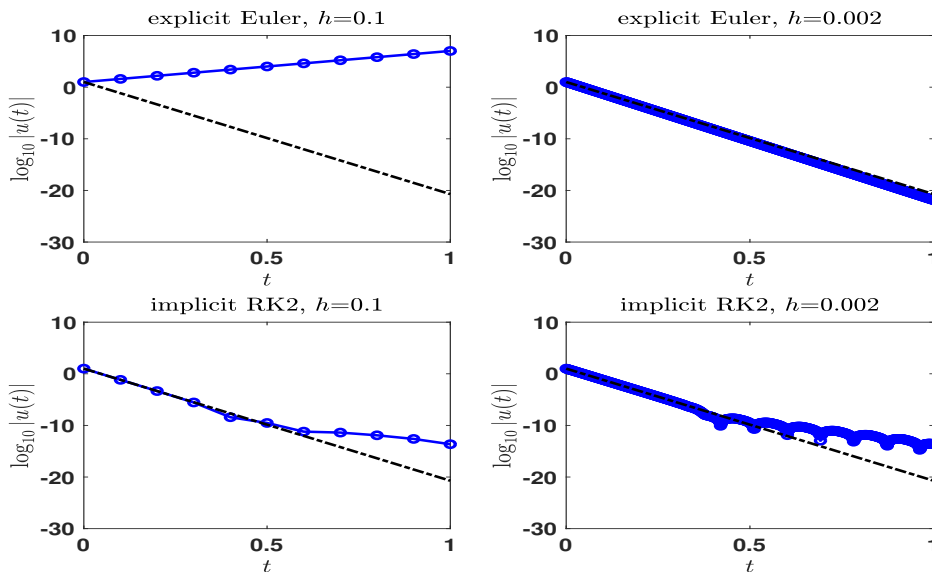


Figure 3.7: Logarithmic plots of the numerical (-o-) and exact (---) solutions of the problem (3.4.1), for  $y_0 = 10$ , by explicit (Euler) and implicit (RK2) schemes at time-steps  $h$ .

The eigen-value problem (3.4.1) has the general form  $u'(t) = \lambda u(t)$  where explicit Euler's scheme at each  $n$ th step with step-size  $h$  is  $u_{n+1} = (1 + h\lambda)^n u_0$ . If  $\lambda < 0$  (which is the case in (3.4.1)) and  $h > 0$  we will have  $|1 + h\lambda| < 1$ , requiring  $|u_n|$  to decrease monotonically, iff  $0 < h < 2/|\lambda|$ . This restricts  $h$  not to exceed  $2/|\lambda|$ , otherwise numerical solution oscillates with growing amplitude  $u(t_n) \rightarrow \infty$  as  $n \rightarrow \infty$ .

Now, in more general setting of such, consider a system of in-homogeneous equation:

$$\frac{d}{dt}\mathbf{u}(t) = \mathbf{A}\mathbf{u}(t) + \mathbf{w}(t), \quad \mathbf{u}, \mathbf{w} \in \mathbb{R}^d, \quad \mathbf{A} \in \mathbf{M}(\mathbb{R}^{d \times d}) \quad (3.4.2)$$

where  $\mathbf{M}$  is the space of  $d$ -square diagonalisable matrices in  $\mathbb{R}^d$ . Suppose the matrix  $\mathbf{A}$  has eigenvalues  $(\lambda_j)_{j=1}^d$  with corresponding eigenvectors  $\mathbf{v}_j \in \mathbb{C}^d$ . Solution to the (3.4.2) is

$$\mathbf{u}(t) = \sum_{j=1}^d a_j e^{\lambda_j t} \mathbf{v}_j + \mathbf{z}(t), \quad a_j \in \mathbb{R} \quad (3.4.3)$$

where  $\mathbf{z}(t)$  is obtained from the integration of  $\mathbf{w}(t)$ . Now, Assume  $\Re(\lambda_j) < 0$  for all  $j$ , then

$$\mathbf{u}(t) \rightarrow \mathbf{z}(t) \quad \text{as } t \rightarrow \infty. \quad (3.4.4)$$

Moreover, provided  $\lambda_j \in \mathbb{R}$  then each term  $|a_j e^{\lambda_j t} \mathbf{v}_j|$  decays monotonically and becomes sinusoidal for  $\lambda_j \in \mathbb{C}$ . On this note, it is possible to define stiffness in terms of the size of  $|\Re(\lambda_j)|$ . Its small value corresponds to slow-frequency term  $a_j e^{\lambda_j t} \mathbf{v}_j$  whereas the large value will correspond to the high-frequency term, sufficiently fast decaying.

Suppose that  $\lambda^1, \lambda^2 \in (\lambda_j)_{j=1}^d$  have corresponding slowest and fastest frequency terms  $a_j e^{\lambda^1 t} \mathbf{v}_j$  and  $a_j e^{\lambda^2 t} \mathbf{v}_j$  respectively. Then, for all  $j$  we have

$$|\Re(\lambda^1)| \leq |\Re(\lambda_j)| \leq |\Re(\lambda^2)| \quad (3.4.5)$$

and thus we define *stiff-ratio* as

$$R^{\text{stiff}} = |\Re(\lambda^1)| / |\Re(\lambda^2)|. \quad (3.4.6)$$

The stiff-ratio measures the stiffness of a system like (3.4.2) having several components with stiff terms. Hence, stiffness of the problem (3.4.2) is determined for large stiff-ratio.

### 3.4.2 Numerical Techniques for Stiff PDEs

A dynamical system put in the form of ODE system  $U_t = \mathcal{L}U + \mathcal{N}(U)$  can be solved using  $s$ -stage Runge-Kutta (RK) time integration IMEX-method. The advantage of this method is that the stiffness arising from the linear part of the ODE system is taken care of by the

$\mathbf{c}$	$\mathbf{A}$	$c_1$	$a_{11}$	$a_{21}$	$\cdots$	$a_{1s}$
		$c_2$	$a_{21}$	$a_{22}$	$\cdots$	$a_{2s}$
		$\vdots$				$\vdots$
		$c_s$	$a_{s1}$	$a_{s2}$	$\cdots$	$a_{ss}$
		$\mathbf{b}^T$	$b_1$	$b_2$	$\cdots$	$b_s$

Table 3.1: Butcher Tableau

implicit time scheme of the Runge Kutta- methods, while, the nonlinear part is explicitly solved. The range of applicable numerical techniques includes, Driscoll's composite RK4, Strang splitting, see [200] for details. One of the characteristics of stiff equations, as discussed in the previous section, is that if the explicit scheme is used for the linear term, stability issues set in and impose strict conditions on the time steps.

### 3.4.3 Runge-Kutta Method

An  $s$ -stage Runge-Kutta method for initial value problem (IVP)  $\dot{u} = F(t, u)$  is

$$u_{n+1} = u_n + h \sum_{j=1}^s b_j K_j, \quad K_j = u(t_n + c_j h, u_n + h \sum_{j=1}^s a_{jk} K_j) \quad (3.4.7)$$

where  $u_n = u(t_n)$  and  $b_j, a_{jk} \in \mathbb{R}$ , for  $j, k = 1, \dots, s$  and  $c_k = \sum_{j=1}^s a_{jk}$ . These coefficients  $a_{jk}$  are chosen from a Butcher Tableau introduced in Figure 3.1. We are interested in the fourth order implicit Runge-Kutta (IRK4) time integration technique. Particularly, the coefficients used are motivated by Hammer-Hollingworth approach which in turn is a 2-stage Gauss scheme. These are,

$$\begin{aligned} a_{11} = a_{22} &= \frac{1}{4}, & a_{12} &= \frac{1}{4} - \frac{\sqrt{3}}{6}, & a_{21} &= \frac{1}{4} + \frac{\sqrt{3}}{6} \\ c_1 &= \frac{1}{2} - \frac{\sqrt{3}}{6}, & c_2 &= \frac{1}{2} + \frac{\sqrt{3}}{6}, & b_1 = b_2 &= \frac{1}{2}. \end{aligned} \quad (3.4.8)$$

As it is noticeable, when  $a_{jk} = 0$  for  $j < k$ , i.e.  $\mathbf{A}$  is a lower triangular matrix, the method becomes an  $s$ -stage explicit Runge-Kutta (ERKs) method.

### 3.5 Driscoll's Composite Runge-Kutta Method

The DS system, in its non-local form,

$$i\psi_t + 2(\psi_{xx} + \psi_{yy}) + (\partial_x^{-1} \partial_y + \partial_y^{-1} \partial_x) |\psi|^2 \psi = 0$$

0	0								
$c_2$	$a_{21}$	$a_{22}$							
$c_3$	$a_{31}$	$a_{32}$	$a_{33}$						
$c_4$	$a_{41}$	$a_{42}$	$a_{43}$	$a_{44}$					
	$b_1$	$b_2$	$b_3$	$b_4$					


Table 3.2: Butcher tableau for Driscoll's composite RK Scheme

is solved using an IMEX method, i.e. applying for the stiff term, the linear part, a stable implicit method and an explicit scheme for the non-stiff term, the nonlinear part. This requires transforming the problem into the Fourier space using discrete Fourier transform (DFT). Then the solutions, in the Fourier space, are obtained by invoking the Driscoll's composite Runge-Kutta approach, [44] [92]. First, we put the equation in the form

$$\psi_t = \mathbf{L}\psi + \mathbf{N}[\psi] = 2i\partial_{xx}\psi + 2i\partial_{yy}\psi + i(\partial_x^{-1}\partial_y + \partial_y^{-1}\partial_x)|\psi|^2\psi. \quad (3.5.1)$$

In the Fourier space,

$$\hat{\psi}_t = \mathbf{L}\hat{\psi} + \hat{\mathbf{N}}[\hat{\psi}] = -2i(k_x^2 + k_y^2)\hat{\psi} + i\mathcal{F}_{xy}((\partial_x^{-1}\partial_y + \partial_y^{-1}\partial_x)|\psi|^2\psi). \quad (3.5.2)$$

The nonlinear term  $\hat{\mathbf{N}}[\hat{\psi}] = i\mathcal{F}_{xy}((\partial_x^{-1}\partial_y + \partial_y^{-1}\partial_x)|\psi|^2\psi)$  is evaluated by transforming  $\hat{\psi}$  to the coordinate space back and forth any time the nonlinear operation is to be applied. One writes the problem, for convenience, in the form

$$u_t = F(u(t)) + \lambda u(t), \quad v_t = G(u(t), v(t)) \quad (3.5.3)$$

where  $u$  and  $v$  characterize the *fast* and *slow* modes respectively and  $\lambda$  is a constant. The slower modes are usually subsumed in  $v$  equation. Therefore, several different RK methods are used in treating each mode of the linear and nonlinear parts. Then, the composite method for advancing in time from step  $m$  to  $m+1$  for a step-size  $k$  and  $i = 1, \dots, n$  is an  $n$ -stage RK method

$$U_i = u_m + k \left( \sum_{j=1}^{i-1} a_{ij} F(U_j, V_j) + \lambda \sum_{j=1}^i \tilde{a}_{ij} V_j \right), \quad V_i = v_m + k \sum_{j=1}^{i-1} \hat{a}_{ij} G(U_j, V_j) \quad (3.5.4)$$

$$u_{m+1} = u_m + k \left( \sum_{i=1}^n b_i F(U_i, V_i) + \lambda \sum_{i=1}^n \tilde{b}_i U_i \right), \quad v_{m+1} = v_m + k \sum_{i=1}^n \hat{b}_i G(U_i, V_i) \quad (3.5.5)$$

The RK method for the semi-linear problem at four stages reads

$$\begin{aligned}
U_1 &= u_1, & V_1 &= v_n \\
U_2 &= \left(1 - \frac{1}{3}k\lambda\right)^{-1} \left(u_n + \frac{1}{2}kF(U_1, V_1) + \frac{1}{6}k\lambda U_1\right), & V_2 &= v_n + \frac{k}{2}G(U_1, V_1) \\
U_3 &= \left(1 - k\lambda\right)^{-1} \left(u_n + \frac{1}{2}kF(U_2, V_2) + k\lambda\left(\frac{1}{2}U_1 - U_2\right)\right), & V_3 &= v_n + \frac{k}{2}G(U_2, V_2) \\
U_4 &= \left(1 - \frac{k\lambda}{3}\right)^{-1} \left(u_n + kF(U_3, V_3) + \frac{2}{3}k\lambda U_3\right), & V_4 &= v_n + kG(U_3, V_3)
\end{aligned}$$

so that  $u_m$  and  $v_m$  are updated via

$$\begin{aligned}
u_{m+1} &= u_m + \frac{k}{6}(F(U_1, V_1) + F(U_4, V_4) + \lambda(U_1 + U_4)) \\
&\quad + \frac{k}{3}(F(U_2, V_2) + F(U_3, V_3) + \lambda(U_2 + U_3))
\end{aligned} \tag{3.5.6}$$

$$v_{m+1} = v_m + \frac{k}{6}(G(U_1, V_1) + G(U_4, V_4)) + \frac{k}{3}(G(U_2, V_2) + G(U_3, V_3)) \tag{3.5.7}$$

The table 3.2 is as generated in [44]. To fit the linear term into the stability region, one chooses a slow wavenumber which satisfies

$$|\hat{\mathbf{N}}(\hat{\psi})| < 2.8/k. \tag{3.5.8}$$

### 3.5.1 Split-Stepping Approach

An alternate scheme is split-stepping approach. Regarding the requirements for implicit scheme for the linear part and explicit for the nonlinear part of the problem (4.6.3), hence the name IMEX-method, can be solved explicitly by solving each part independently through splitting method. That's to seek solutions of  $U_\tau = \mathbf{L}U$  and  $U_\tau = \mathbf{N}(U)$  independently. The idea behind the split-step approach is the solution to the problem  $U_\tau = (\mathcal{A} + \mathcal{B})U$ , for operators  $\mathcal{A}, \mathcal{B}$ , the numerical solution using  $n + 1$  time-steps takes the form

$$U(\tau_{n+1}) = \prod_{n=1}^N e^{(c_n\tau\mathcal{A})} \cdot e^{(d_n\tau\mathcal{B})} U(\tau_n) \tag{3.5.9}$$

where  $c_n$  and  $d_n$ ,  $n = 1, \dots, N$  are real numbers representing the fractional time steps  $\tau_n$ . The inspiration for this formula is from the Trotter-Kato formula

$$\lim_{n \rightarrow \infty} \left[ e^{-\tau\mathcal{A}/n} e^{-\tau\mathcal{B}/n} \right]^n = e^{-\tau(\mathcal{A}+\mathcal{B})},$$

where  $\mathcal{A}, \mathcal{B}$  are unbounded linear operators. An example of a split-step method is given in [230] for all any even order. One applies 4th-order splitting-step method for the nonlinear part  $U_\tau = \mathbf{N}[U]$ , corresponding to  $iu_t + |u|^{2\sigma}u = 0$ , and IRK4 to the linear part  $U_\tau = \mathbf{L}U$ ,

i.e.  $u_t = \Delta u$ , to produce a fourth order split-step scheme. Note that, by splitting, the independent solutions are approximations to the NLS solution in question. However, both steps can be done explicitly for equations like (4.6.3), see ([105], pp.6) for more details.

A convenient way of tracing accuracy of the numerical-time-integration technique is by investigating the behaviour of the conserved quantities of the problem, e.g. mass or energy.



### III

---

## Review on NLS equations

---

## Chapter 4

# The NLS equations: Existence Properties and Numerical Observations of Blow-ups

In this chapter, we review properties of solutions to the NLS equation. Further, we discuss several cases where blow-up of solutions to the NLS equation arises. Some of the blow-up results traced via dynamically re-scaling approach are reviewed. The NLS equation is among nonlinear evolution equations which blow-up solution or collapse [202],[52] of the solutions is possible. We have been interested in the NLS equation with power nonlinearity ( $\sigma \in \mathbb{N}^+$ ) in  $1 + d$  dimension

$$i\psi_t + \Delta\psi + \gamma|\psi|^{2\sigma}\psi = 0; \quad \psi : \mathbb{R}^+ \times \mathbb{R}^d \rightarrow \mathbb{C}, \quad \gamma = \pm 1. \quad (4.0.1)$$

Blow-up, in some dynamical systems, appears to be the consequence of the violent transfer of energy from lower scales to larger ones, for instance in fibre optics and related fields. Thus, understanding this behaviour, how, why and when it occurs, is a very important aspect to the mathematicians and physicists. One way to understand it is by observing the profile of its solution near the region of singularity.

When the nonlinearity is defocusing ( $\gamma = -1$ ) the solution is known to exist for all times  $t \in [0, \infty)$ , for instance see [202] and [206] with the references therein, where the global well-posedness of the problem (4.1.1) for initial data  $\psi_0 \in H^1$  in a critical dimension  $d < \sigma/2$  is proved. There the dispersion dominates the nonlinearity. However, in the focusing nonlinearity ( $\gamma = 1$ ) the critical and super critical dimension  $d \geq 2/\sigma$ , where the solution can blow-up even for initial data  $\psi_0 \in H^1$  [203],[126],[118] in a finite interval of time  $t \in [0, T^*)$ . This is as consequence of the interaction of the two effects, where the dispersion becomes dominated by non-linearity thereby leading to the blow-up, [119],[202].

We will use the radial coordinates to seek for radially symmetric solutions. This coordinate transformation allows one treats the NLS problem (4.0.1) as  $1 + 1$  dimensional problem. It has been proven in [144] that, the cubic NLS ( $\sigma d = 2$  with  $\sigma = 1$ ), at the blow-up time  $t = t_*$ , has a radially symmetric self-similar solution of the kind

$$\psi(t, |\mathbf{x}|) \equiv u(t, r) \sim \frac{\sqrt{C}e^{i\theta}}{(T^* - t)^{1/2}\alpha} Q\left(\frac{\sqrt{rC}}{(T^* - t)^{1/2}\alpha}\right) \cdot e^{(iC/\beta)\ln\left[\frac{C}{(T^* - t)}\right]}, \quad r = |\mathbf{x}|$$

---

where parameters  $\theta, \alpha, \beta, C$  are constants that depend on the choice of the initial data and ground-state solution  $Q(\eta)$ ,  $\eta \geq 0$ . This type of transformation is known as Pseudo-conformal, a kind of self-similar blow-up solution (see the sections 4.5.1 and 4.6).

An  $L^2$  critical blow-up is possible in dimension  $d = 2$  for  $\sigma = 1$  and dimension  $d = 3$  for  $\sigma = 2/3$ . The  $L^2$  critical NLS as a physical model appears in, many but we mention, two major principle settings: non-linear optics and condensed matter physics.

In the context of non-linear optics, NLS basically describes the propagation of a light beam in a kerr-medium in which the refractive index depends on the intensity of the beam. In this case, the paraxial approximation is made (i.e.  $t = z$  direction) and the beam travels along the  $z$ -direction. Moreover, the assumption being made on an electric field given in an ansatz form  $\psi e^{i(\mathbf{k}\cdot\mathbf{x}-\omega t)}$  in the derivation of the dynamics leads to NLS equation where the second derivative  $\partial^2/\partial t^2$  is negligible; this is to say that negligence of higher order terms  $\partial^2/\partial t^2$  indicates the absence of back-scattering assumption. The model in this context is focusing cubic NLS where  $\sigma = 2$  and  $\sigma = 1$  and  $\gamma = 1$ . The blow-up or the singularity in this context corresponds to the self-focusing and narrowing of the beam.

In the context of condensed matter physics, particularly Bose-Einstein-Condensates (BEC), the wave function  $\psi$  describes the collective or accumulation behaviour of atoms and nano-particles. In principle we work in three-dimensions, however, the strong confinement of the wave function  $\psi$  in one or two dimensions will effectively reduce to lower dimensions. The quantity  $\int |\psi|^2 d\mathbf{x}$  usually represents the probability density of the collective atoms. The presence of a dilute gas is one of the assumptions for the BEC model. Cornell & Wemann in 1995 were the first to discover the BEC equation experimentally while it was firstly developed by Einstein & Bose in the 1920s. The NLS equation can be focusing or defocusing in this context. Despite the fact that Schrödinger equation originates from quantum mechanics where electron/photon/whatever interaction of the active environment is taken into account and the superposition principle holds, there is no quantum mechanic involved for NLS equation.

The blow-up solution for NLS is not present in applications but rather an indication that the NLS approximation breaks down as it is an asymptotic model, see [96] and references there in. The blow-up phenomenon is recognized if the simulated solution develops a singularity and becomes concentrated near a point as the time of the blow-up is approached, e.g. the wave collapses that can possibly be experienced by *optical turbulence* and the saturation in the NLS solution necessitates the inclusion of some damping whenever the amplitude gets large. Consequently, the peak forms of the solution become and remain finite, and one observes outgoing circular wave-trains after the collapses of the NLS solution.

## 4.1 Local and Global Existence Properties

The Cauchy problem for the NLS equation with power nonlinearity ( $\sigma \in \mathbb{N}^+$ ) in  $1 + d$  dimension reads

$$\begin{cases} i\psi_t + \Delta\psi + \gamma|\psi|^{2\sigma}\psi = 0; & \psi : \mathbb{R}^+ \times \mathbb{R}^d \rightarrow \mathbb{C}, \quad \gamma = \pm 1 \\ \psi_0(\mathbf{x}) = \psi_0 : \mathbb{R}^d \rightarrow \mathbb{C}, & \psi_0 \in H^s(\mathbb{R}^d) \end{cases} \quad (4.1.1)$$

where  $\gamma = \pm 1$  corresponds to a focusing and defocusing nonlinearity respectively and  $\psi \rightarrow 0$  as  $|\mathbf{x}| \rightarrow \infty$ . The existence results of the solution to the NLS equation defined on the whole space  $\mathbb{R}^d$  are proved from the Duhamel integral formulation

$$\psi(t, \mathbf{x}) = e^{-it\Delta}\psi_0(\mathbf{x}) + i\gamma \int_0^t e^{-i(t-t')\Delta} |\psi|^{2\sigma}\psi(t', \mathbf{x}) dt' \quad (4.1.2)$$

where  $e^{-it\Delta}$  is a *one-parameter unitary group operator*. The proof that  $\psi(t, \mathbf{x})$  exists *locally* for a small time  $t$  is established by applying the Banach fixed Point theorem. Due to the dispersion properties of the linear operator  $\Delta$ , for any  $\psi(x, t)$  taken in an appropriate Banach space, the Duhamel formulation (4.1.2) defines a contraction map for a sufficiently small  $t$ . If the locally existing solution  $\psi(t, \mathbf{x})$  can be extended for all times, then the *global existence* (existence for all times) of  $\psi(t, \mathbf{x})$  is proved via important a priori estimates from Sobolev inequalities and some conservation laws on the norms of  $\psi(t, \mathbf{x})$ . There, the asymptotic behaviour of  $\psi(t, \mathbf{x})$  as  $t \rightarrow \infty$  becomes interesting.

Most interesting is the dynamic behaviour of the NLS equation with attracting nonlinearity, for that we will focus on the focusing NLS equation.

### 4.1.1 Conservation Properties of NLS

The focusing NLS equation in (4.1.1) being a Hamiltonian system has conserved quantities which include the *mass*

$$M[\psi] = \int_{\mathbb{R}^d} |\psi|^2 d\mathbf{x} := \|\psi\|_2^2, \quad (4.1.3)$$

the *energy* (also corresponding to *Hamiltonian*),<sup>1</sup>,

$$E[\psi] = \int_{\mathbb{R}^d} \left( |\nabla\psi|^2 - \frac{1}{\sigma+1} |\psi|^{2\sigma+2} \right) d\mathbf{x} := \|\nabla\psi\|_2^2 - \frac{1}{\sigma+1} \|\psi\|_{2(\sigma+1)}^{2(\sigma+1)}, \quad (4.1.4)$$

and the *momentum*

$$P[\psi] = \Im \int_{\mathbb{R}^d} (\psi^* \nabla\psi) d\mathbf{x}. \quad (4.1.5)$$

---

<sup>1</sup>The term  $\|\nabla\psi\|_2^2$  is the diffraction term competing with the nonlinearity  $\|\psi\|_{2(\sigma+1)}^{2(\sigma+1)}$ . The condition  $E[u_0] < 0$  corresponds to stronger nonlinearity than the diffraction and vice-versa for  $E[u_0] > 0$ . We will see later none of them is a sharp condition and both can lead to blow-up solution.

See appendix III for the proof. The mass and energy are in general conserved for a regular solution  $\psi$  of (4.1.1).

There are also corresponding symmetries such as spatial translation, spatial rotation and time-translation of  $\psi(t, \mathbf{x})$ . The Laplacian  $\Delta$  is invariant under rotation and the conjugate of the NLS equation will invert the time from  $t$  to  $-t$ . Among the most important invariances, especially for blow-up tracing, is the scaling-invariance.

The minimal regularity (smoothness) index  $s$  for local existence of solution in  $H^s(\mathbb{R}^d)$  depends on the nonlinearity exponent  $\sigma$ . This defines criticality at the level of the Sobolev space  $H^s(\mathbb{R}^d)$ . Thus, the Cauchy problem in  $H^s(\mathbb{R}^d)$  has a *critical exponent*  $\sigma$  provided the NLS equation (4.1.1) and the Sobolev norm  $\|\psi\|_{\dot{H}^s(\mathbb{R}^d)}$  stay invariant under scaling transformation.

For  $\lambda > 0$ , one chooses  $a, b, c \in \mathbb{R}$ , so that the focusing NLS equation remains invariant under the scaling transformation <sup>2</sup>

$$\psi_\lambda(\tilde{t}, \tilde{\mathbf{x}}) := \lambda^a \psi(\lambda^{-b}t, \lambda^{-c}\mathbf{x}), \quad t \rightarrow \tilde{t} = \lambda^b t, \quad \mathbf{x} \rightarrow \tilde{\mathbf{x}} = \lambda^c \mathbf{x}.$$

It is easy to check that the equation is invariant when  $a = 1/\sigma$ ,  $b = -2$  and  $c = -1$ . Therefore, if  $\psi$  solves the NLS (4.1.1), then

$$\psi_\lambda(\tilde{t}, \tilde{\mathbf{x}}) = \lambda^{1/\sigma} \psi(\lambda^2 t, \lambda \mathbf{x}) \quad (4.1.6)$$

solves the NLS equation (4.1.1), where  $t \rightarrow \tilde{t} = t/\lambda^2$  and  $\mathbf{x} \rightarrow \tilde{\mathbf{x}} = \mathbf{x}/\lambda$ .

Similarly, Since  $\dot{H}^s$  is a scale invariant, in Fourier domain, we have

$$\|\psi\|_{\dot{H}^s} = \left\| |\xi|^s \hat{\psi}(\xi) \right\|_{L_\xi^2} \quad (4.1.7)$$

with  $|\xi| = \sqrt{\xi_1^2 + \dots + \xi_d^2}$ , then for  $|\alpha| = s$ , using the scaled solution  $\psi_\lambda$  (4.1.6)

$$\begin{aligned} \|\psi_\lambda\|_{\dot{H}^s}^2 &= \int_{\mathbb{R}^d} |D^\alpha \psi_\lambda(\tilde{t}, \tilde{\mathbf{x}})|^2 d\tilde{\mathbf{x}} \equiv \int_{\mathbb{R}^d} \lambda^{2/\sigma} |D^\alpha \psi(t, \mathbf{x})|^2 \lambda^{-d} d\mathbf{x} \\ &= \lambda^{\frac{2}{\sigma}-d} \int_{\mathbb{R}^d} |D^\alpha \psi(t, \mathbf{x})|^2 d\mathbf{x} \equiv \lambda^{\frac{2}{\sigma}-d} \left\| |\xi|^s \hat{\psi}(\xi) \right\|_{L_\xi^2}^2 \equiv \lambda^{\frac{2}{\sigma}-d} \|\psi\|_{L_\xi^2}^2 \end{aligned} \quad (4.1.8)$$

and then  $\|\psi_\lambda\|_{\dot{H}^s} = \lambda^{\frac{d}{2}-\frac{1}{\sigma}} \|\psi\|_{L_\xi^2}$ . The last equality follows from the Plancherel identity. With  $\|\psi\|_{L_\xi^2(\mathbb{R}^d)} = \lambda^{\frac{d}{2}-\frac{1}{\sigma}} \|\psi_\lambda\|_{\dot{H}^s}$  let the *critical exponent* be

$$s = \sigma_c := \frac{d}{2} - \frac{1}{\sigma}$$

<sup>2</sup>Using the scaling for the NLS equation to be invariant one gets  $b - a = 2c - a = -2\sigma a - a$  yielding  $b = 2c$ . If  $c = -1$ , then  $b = -2$  and  $a = 1/\sigma$ .

The nonlinearity exponent takes the form  $\sigma = 2/(d - 2\sigma_c)$ .

This shows  $s < d/2$ . Furthermore, the condition on  $\sigma$  for local existence of solution in  $H^s(\mathbb{R}^d)$  is classified as *subcritical* if  $\sigma < 2/(d-2s)$ , *critical* for  $\sigma = 2/(d-2s)$  and *supercritical* when  $\sigma > 2/(d - 2s)$ . Nevertheless, the local existence theorem for any  $\psi_0 \in H^s(\mathbb{R}^d)$  can be employed only in the subcritical or critical case, for instance read [73] for more details.

As a result, we can classify the Cauchy problem for the focusing NLS equation at the level of the space  $H^{\sigma_c}$  for each  $\sigma_c$ . Thus,  $\sigma_c = 0$  corresponds to  $\sigma d = 2$  and preservation of the  $L^2$ -norm, hence the NLS equation is  $L^2$ -critical or mass-critical. Moreover, if for non-zero  $\psi \in L^2(\mathbb{R}^d)$  but  $\lim_{\lambda \rightarrow 0} \|\psi_\lambda\|_{L^2(\mathbb{R}^d)} = 0$  and  $\sigma d < 2$  then the NLS equation is  $L^2$ -subcritical and  $L^2$ -supercritical when  $\lim_{\lambda \rightarrow 0} \|\psi_\lambda\|_{L^2(\mathbb{R}^d)} = \infty$  and  $\sigma d > 2$ . Some common values of  $\sigma_c, \sigma$  and  $d$  are given in the following table:

	$d$	1	2	3	4	
$\sigma = 1$	$\sigma_c$	$-\frac{1}{2}$	0	$\frac{1}{2}$	1	$\begin{cases} H^s\text{-critical} & \sigma = 2/(d - 2s) \\ L^2\text{-critical} & \sigma d = 2 \\ H^1\text{-critical} & \sigma = 2/(d - 2) \end{cases}$
$\sigma = 2$		0	$\frac{1}{2}$	1	$\frac{3}{2}$	
$\sigma = 3$		$\frac{1}{6}$	$\frac{2}{3}$	$\frac{4}{3}$	$\frac{5}{3}$	

In a similar fashion,  $\sigma_c = 1$  corresponds to invariance of  $\|\psi\|_{\dot{H}^1}$  and  $\sigma = 2/(d - 2)$ . Therefore, the NLS equation is  $H^1$ -critical or energy-critical. Moreover, the NLS equation is  $H^1$ -subcritical (respectively supercritical) if  $\sigma < 2/(d - 2)$  (respectively  $\sigma > 2/(d - 2)$ ) and for nonzero  $\psi \in H^1$  and  $\lim_{\lambda \rightarrow 0} \|\psi_\lambda\|_{2(\mathbb{R}^d)} = 0$  (respectively  $= \infty$ ).

**Remark 4.1.1.** In the  $H^1$ -subcritical case, the condition on  $\sigma$  can be  $0 < \sigma < \infty$  for  $d \leq 2$  and  $0 < \sigma < 2/(d - 2)$  for  $d > 2$ .

**Theorem 4.1.1** (Existence in  $L^2$  and  $H^1$ ). *Given an initial data  $\psi_0 = \psi(0, \mathbf{x})$*

(i) *if  $\psi_0 \in L^2(\mathbb{R}^d)$  for  $0 \leq \sigma < 2/d$ , then  $\exists$  a unique solution*

$$\psi \in C([-T_*, T_*], L^2(\mathbb{R}^d)) \cap L^p([-T_*, T_*], L^{2(\sigma+1)}(\mathbb{R}^d))$$

*having  $\|\psi\|_{L^2(\mathbb{R}^d)}^2$  preserved, where  $p = 4(\sigma + 1)/d\sigma$ .*

(ii) *if  $\psi_0 \in H^1(\mathbb{R}^d)$  and  $0 \leq \sigma < 2/(d - 2)$  for  $d > 2$ ,  $\exists$  a positive  $T_* = T_*(\|\psi_0\|_{H^1})$  monotonically decreasing in  $\|\psi_0\|_{H^1}$  and a unique maximal solution  $\psi \in C([-T_*, T_*], H^1(\mathbb{R}^d))$  preserving the mass and energy. If moreover,  $\psi_0 \in \Sigma := \{u : u \in H^1(\mathbb{R}^d), |\mathbf{x}u| \in L^2(\mathbb{R}^d)\}$  with variance  $V(t) = \int_{\mathbb{R}^d} |\mathbf{x}|^2 |\psi|^2 d\mathbf{x} < \infty$  satisfying*

$$\frac{1}{8} \frac{d^2 V(t)}{dt^2} = E[\psi(t)] - \frac{d\sigma - 2}{2(\sigma + 1)} \int_{\mathbb{R}^d} |\psi|^{2(\sigma+1)} d\mathbf{x} = \|\nabla \psi\|_2^2 - \frac{\sigma d}{2(\sigma + 1)} \|\psi\|_{2(\sigma+1)}^{2(\sigma+1)}.$$

The first part of the theorem, as proved in [211], provides the condition for local existence of the solution in finite time  $T_*$  by requiring the  $L^2$ -norms be conserved in the subcritical case  $\sigma d < 2$ . While the second part, for  $\psi$  to exist in  $H^1(\mathbb{R}^d)$  satisfying the mass and energy equations, we need  $\sigma < 2/(d-2)$  for  $d > 2$ . If the virial identity holds with variance  $V(t) \in C^2(] - T_*, T_*[)$  then  $\psi$  exists in the space  $\Sigma$ . The maximal solution here implies that  $\|\psi(t)\|_{H^1(\mathbb{R}^d)} \rightarrow \infty$  as  $t \rightarrow T_* < \infty$ .

Existence may also depend on the size of initial data  $\psi_0$ . For large initial data in  $H^1(\mathbb{R}^d)$ , both the defocusing NLS equation (with  $0 \leq \sigma < 2/d$ ) and focusing NLS equation (with  $0 \leq \sigma < 2/(d-2)$ ) admit a global solution  $\psi \in C(\mathbb{R}, H^1(\mathbb{R}^d))$ , having finite mass and energy, that depends continuously on the  $\psi_0 \in H^1(\mathbb{R}^d)$ . These conserved quantities provide a uniform upper bound for  $\|\psi\|_{H^1(\mathbb{R}^d)}$ , see [128] and [72]. The key tool in the proof is the well-known "*Gagliardo-Nirenberg inequality*"

$$\|u\|_{2(\sigma+1)}^{2(\sigma+1)} \leq C_{\sigma,d} \|\nabla u\|_2^{\sigma d} \|u\|_2^{\sigma(2-d)+2} \quad (4.1.9)$$

applied on the conserved Hamiltonian (4.1.4) so that, provided the  $L^2$ -norm is conserved, a uniform upper bound for  $\|\nabla \psi\|_{L^2}$  is obtained in the subcritical case  $\sigma d < 2$  for the focusing case. However, having a bound on the  $\|\psi\|_{H^1}$ , global existence in  $H^1$  does not directly follow. This is because,  $\psi$  may cease to exist in  $H^1$  even though the solution  $\psi$  may be in  $L^2(\mathbb{R}^d)$ , but  $\psi$  tends to a delta function which is not in  $L^2(\mathbb{R}^d)$ .

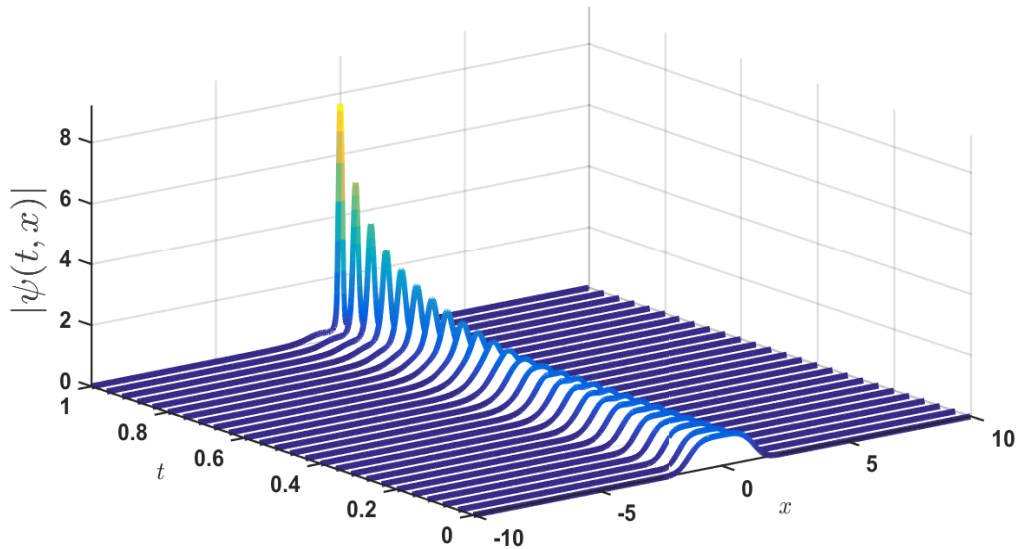


Figure 4.1: Blow-up solution to the focusing NLS equation (4.1.1) at the critical dimension  $d = 1$  with  $\sigma = 2$  for initial data  $\exp(-x^4/4) \in H^1(\mathbb{R})$ .

For  $\psi$  to remain in  $H^1(\mathbb{R}^d)$  for all  $t$ , we need an a priori estimate, i.e. variance identity to be discussed later <sup>3</sup>. Merle and Tsutsumi [155] proved that in the focusing NLS equation if  $\sigma d = 2$  and  $\lim_{t \rightarrow T_*} \|\psi\|_{H^1} = \infty$  then  $\psi$  has no limits in  $L^2(\mathbb{R}^d)$ . According to Weinstein [218], the sufficient condition for global existence of the focusing NLS equation is either  $0 < \sigma < 2/d$  or  $\sigma d = 2$  and  $\|\psi_0\|_2 < (C_{\sigma,d}/(\sigma + 1))^{-1/\sigma} := \kappa_{\sigma,d}$ . The latter result is obtained by inquiring that  $(\frac{C_{\sigma,d}}{\sigma+1}) \|\psi\|_2^{\sigma(2-d)+2} < 1$  as the sufficient condition for global existence in the uniform upper bound of  $\|\nabla\psi\|_2^2$  discussed earlier.

The  $H^1(\mathbb{R}^d)$  is particularly important since the NLS theory and applications heavily rely on the mass (4.1.3) and Hamiltonian (4.1.4). For that, these conserved quantities should be finite, and this would make it possible working in the space  $H^1(\mathbb{R}^d)$ . In fact, for NLS equation  $H^1(\mathbb{R}^d)$  is a natural choice for the study of the existence and blow-up.

## 4.2 Blow-up Alternative

Before we discuss about classical blow-up results, let us discuss some behaviour that can lead to an alternative to blow-up. Consider  $\psi \in H^1(\mathbb{R}^d)$  and the scaling  $\psi_\lambda = \lambda^{1-d/2}\psi(\lambda^{-1}\mathbf{x})$ , one can verify that the following estimates

$$\lim_{\substack{\lambda(t) \rightarrow 0 \\ t \rightarrow T_*}} \|\psi_\lambda\|_2^2 = 0, \quad \lim_{\substack{\lambda(t) \rightarrow 0 \\ t \rightarrow T_*}} \|\psi_\lambda\|_{H^1}^2 = \|\nabla\psi\|_2^2, \quad \lim_{\substack{\lambda(t) \rightarrow 0 \\ t \rightarrow T_*}} |\psi_\lambda| = \delta(\mathbf{x}) \|\nabla\psi\|_2^2,$$

imply that even if  $\psi$  has a bounded  $H^1(\mathbb{R}^d)$  norm,  $\psi$  could exit the space  $H^1(\mathbb{R}^d)$  at some time  $T_*$ . Therefore, in the absence of existence in  $H^1(\mathbb{R}^d)$ , the NLS equation is said to be singular since a priori estimate will reflect the nonexistence of  $\psi$ . In what follows, we will trace the singularity by investigating if the  $H^1$  norm diverges.

Singularity (blow-up) signifying the nonexistence of  $\psi$  as a particular time  $T_*$  is approached has a corresponding location in space of occurrence. Assume  $\psi_0 \in H^1(\mathbb{R}^d)$ , then according to the Theorem 4.1.1(ii) there exists a unique maximal solution  $\psi$  on the interval  $] - T_*, T_*[$ . We say that either  $T_* = \infty$  or  $0 < T_* < \infty$  and  $\lim_{t \rightarrow T_*} \|\psi\|_{H^1} = \infty$ . If a singularity occurs, its corresponding position can be denoted as  $\mathbf{x}_*$ .

To this end, we conclude that the NLS equation is singular if any norm of its solution blows-up. Based on the Weinstein [218] results, blow-up is possible whenever  $\sigma d \geq 2$  in the focusing NLS equation and global existence for  $\sigma d < 2$ . Thus,  $\sigma = 2/d$  is the critical exponent for blow-up in the NLS equation. Therefore, the NLS equation is classified as *subcritical* when  $0 < \sigma < 2/d$ , *critical* if  $\sigma d = 2$  and *supercritical* with  $\sigma d > 2$ . These

---

<sup>3</sup>An a priori estimates is the one that is derived from the given equation before we know existence of solution, which is the variance identity in this case. It will be useful in detailing if  $\psi$  remains in the said solution space. For  $\psi_0 \in L^2(\mathbb{R}^d)$  and  $\|\psi_0\|_2$ , of course  $\|\psi_0\|_2 = \|\psi\|_2$  that does not ensure existence for all  $t \geq 0$ . This clears air for blow-up existence in Theorem 4.1.1(i) when  $\sigma d = 2$ .

correspond to the classification of NLS equation at the level of  $L^2(\mathbb{R}^d)$ . In the subcritical case, the Weinstein results do not rule out existence of blow-up solution in the subcritical NLS equation (see why in Fibich [52])<sup>4</sup>. For the critical case, as we will see later the sufficient condition for blow-up is negative Hamiltonian  $E[0] < 0$  which is opposite to the case for global existence given by Weinstein [218] where  $0 < \|\psi_0\|_2^2 < \kappa_{\sigma,d}$  and  $E(0) > 0$  or  $\|\psi_0\|_2^2 \geq \kappa_{\sigma,d}$  and  $E(0) \leq 0$  for blow-up. In fact, in the critical and supercritical case, there exists  $\varepsilon > 0$  such that if  $\|\psi_0\|_{H^1} > \varepsilon$  then  $\psi$  blows up. See Theorem 6.2.1 in [32] for details. Therefore, this motivates the use of appropriate scaling of  $\psi$  to study its blow-up behaviour.

#### 4.2.1 Critical NLS: Sufficient condition for global existence

So far, we only know of the consequence of the Weinstein results on the sufficient condition of blow-up to the focusing NLS equation in the critical dimension, that is  $\|\psi_0\|_2^2 \geq \kappa_{\sigma,d}$  and  $E(0) \leq 0$ . Let us advance by exploring what the Gagliardo-Nirenberg inequality (4.1.9) entails. Using the inequality, for any non-zero  $u \in H^1(\mathbb{R}^d)$ , we define the functional

$$I[u] = \frac{\|\nabla u\|_2^{\sigma d} \|u\|_2^{2\sigma - (\sigma d - 2)}}{\|u\|_{2(\sigma+1)}^{2(\sigma+1)}} \quad (4.2.1)$$

so that  $0 < 1/C_{\sigma,d} \leq I[u]$  for positive constant  $C_{\sigma,d} = C(\sigma, d)$ , see [67, 68, 164] for instance. If  $C_{\sigma,d}$  is large, the inequality (4.2.1) still holds but could fail for smaller  $C_{\sigma,d}$  for some  $u$ . Searching for optimal  $C_{\sigma,d}$  in which the inequality (4.1.9) holds for all  $u \in H^1(\mathbb{R}^d)$  becomes necessary. We therefore define an optimization problem on  $\psi$ :

$$\tilde{C}_{\sigma,d} = \left[ \min_{H^1 \ni \psi \neq 0} I[\psi] \right]^{-1}. \quad (4.2.2)$$

If such a minimizer  $\tilde{\psi}$  exists, then the inequality (4.1.9) holds for  $\tilde{\psi}$  and we will have  $\tilde{C}_{\sigma,d} = 1/I[\tilde{\psi}]$ , see [218, 159]. It turns out that, as found in the proof of existence of the minimizer by Weinstein [218] and Nawa [159] in the  $H^1(\mathbb{R}^d)$ , the minimizer takes the form of real-valued function  $Q(\mathbf{x})$  up to a phase factor  $e^{i\omega(t)}$ :

$$\tilde{\psi}(t, \mathbf{x}) = Q(\mathbf{x})e^{i\omega(t)}. \quad (4.2.3)$$

See Fibich ([51], section 5.12), the Theorems, Lemmas, corollaries and the references therein. The Function  $Q(\mathbf{x})$  is known as the *ground state*. It has the minimal mass ( $L^2$  norm) of the non-zero solution in  $H^1(\mathbb{R}^d)$  and any solution with larger mass is considered as an *excited*

---

<sup>4</sup>Fibich [52] shows that an explicit singular solution can be constructed in which  $\|\psi\|_p < \infty$  but  $\lim_{t \rightarrow T_*} \|\psi\|_p = \infty$  for any  $2 < p < \infty$ .

state. Thus, the ground state  $Q$  is crucial in the blow-up study of the NLS equation since it contains the minimal mass of  $\psi$  required for blow-up.

In the critical dimension  $\sigma d = 2$ , as one may observe, the ground state solution  $Q^{(0)}$  of the equation

$$\Delta Q + |Q|^{4/d}Q - \omega_t Q = 0 \quad (4.2.4)$$

attains the minimizer of the functional  $I[Q]$ , i.e.  $I[Q^{(0)}] = \inf_{H^1 \ni Q \neq 0} I[Q]$ . In fact,

$$I[Q^{(0)}] = \inf_{H^1 \ni Q \neq 0} I[Q] = \frac{1}{\sigma + 1} \|Q^{(0)}\|_2^{2\sigma}$$

and the optimal constant  $\tilde{C}_{\sigma,d}$  is

$$\tilde{C}_{\sigma,d} = (\sigma + 1) / \|Q^{(0)}\|_2^{2\sigma} = (d + 2) / \left( d \|Q^{(0)}\|_2^{4/d} \right).$$

These obtained results joined together with the sufficient conditions for global existence (resp. for blow-up) in the critical case translate to sufficient conditions for global existence (resp. blow-up) in terms of ground state  $Q^{(0)}$

$$\|\psi_0\|_2^2 < \|Q^{(0)}\|_2^2 \quad \text{resp.} \quad \|\psi_0\|_2^2 \geq \|Q^{(0)}\|_2^2. \quad (4.2.5)$$

Therefore, the critical-mass for blow-up is given by norm of the ground state  $\|Q^{(0)}\|_2^2$ .

### 4.3 Ground state

Having seen, in the previous section, the role that the ground-state plays, it is important to know that the blow-up profile of  $\psi$  is completely described by  $Q$ . In order to study this blow-up profile, we plug into the NLS equation, the stationary or solitary wave solution

$$\psi(t, \mathbf{x}) = e^{i\omega t} Q(\mathbf{x}) \quad (4.3.1)$$

in the ground-state equation (4.2.4), where  $\omega(t) = \omega t$  for real  $\omega$ . This yields

$$\Delta Q + |Q|^{4/d}Q = \omega Q. \quad (4.3.2)$$

We are interested in the positive, smooth, radially symmetric solution in  $H^1$ . However, the necessary condition for existence <sup>5</sup> of  $\psi \in H^1(\mathbb{R}^d)$  can be shown to be  $\omega > 0$ . Roughly speaking, as  $|\mathbf{x}| \rightarrow \infty$  the nonlinear term is negligible since  $\lim_{|\mathbf{x}| \rightarrow \infty} Q = 0$ . Therefore we deal

---

<sup>5</sup>This condition may not hold for unbounded domains.

with only the linear eigen-value equation

$$\Delta Q = \omega Q. \quad (4.3.3)$$

Solutions to the linear equation oscillate for  $\omega < 0$  and may decay slowly but not sufficiently enough to be in the space  $H^1$ . For instance, in one-dimension  $Q = \cos(\sqrt{-\omega}x)$  oscillate as  $x \rightarrow \infty$  but the radial solution for  $d \geq 1$  decays to zero at a slow rate of  $1/r^{(d-1)/2}$ . Thus,  $Q_{\omega < 0} \notin H^1$ .

From now on, we will refer to the ground state equation as the profile equation since it governs the profile of the solitary wave solution, it also represent the self-similar explicit blow-up solution of the focusing NLS equation. Moreover, the minimizer of the functional  $I[\psi]$  satisfies this profile equation.

There are infinitely many solution to the profile equation, even if we restrict ourselves to the positive smooth ones. However, it can be proved that the profile equation admits a unique, strictly positive, analytic, radially symmetric about a point  $\mathbf{x}_0 \in \mathbb{R}^d$  solution. See section 6.3 of [51].

Before we go further, we will discuss about important identities of Pohozaev. The Pohozaev identities for the NLS equation firstly appeared in the work [183]. It is useful in deducing estimates associated to the ground state  $Q$ .

### 4.3.1 Pohozaev Identities

Let  $Q(\mathbf{x})$  solves the profile equation (4.3.4)

$$\Delta Q + |Q|^{2\sigma}Q - \omega Q = 0 \quad (4.3.4)$$

then, with  $\omega > 0$  we have

$$\|Q\|_2^2 = \frac{2\sigma - (\sigma d - 2)}{2\omega(\sigma + 1)} \|Q\|_{2(\sigma+1)}^{2(\sigma+1)}, \quad \|\nabla Q\|_2^2 = \frac{\sigma d}{2\sigma + 2} \|Q\|_{2(\sigma+1)}^{2(\sigma+1)}. \quad (4.3.5)$$

These are called the *Pohozaev identities* and their proofs are provided in the appendix III section C.0.2. Consequent to the 2nd part of this identity is the following.

If the solitary wave solution (4.3.1) satisfies the Hamiltonian (4.1.4) and the ground-state satisfying the Pohozaev identity, it then follows that

$$E[Q] = \frac{\sigma d - 2}{2\sigma + 2} \|Q\|_{L^{2(\sigma+1)}}^{2(\sigma+1)} \quad (4.3.6)$$

and we can easily deduce that  $E[Q] < 0$  if  $\sigma d < 2$ ,  $E[Q] = 0$  when  $\sigma d = 2$  and  $E[Q] > 0$  when  $\sigma d > 2$ . This implies that  $H[Q]$  is negative in the subcritical case. Relations for the

functional  $I[Q]$  can be derived using the Pohozaev identities.

### 4.3.2 Critical NLS: Variational Characterization

In the critical NLS equation,  $\sigma d = 2$ , as we know, there exist a minimal critical mass  $M_{\min}$  with  $\|\psi_0\|_2^2 = M_{\min}$  so that  $E[\psi_0] \leq 0$ . The critical ground state  $Q^{(0)}$  is not only the minimizer of the variational problem given by the functional  $I[Q]$  but also minimizes many related variational problems, such stated as follows:

**Lemma 4.3.2.1** (Variational characterization). *Assume  $\sigma d = 2$ , then the ground state  $Q^{(0)}$  attains the infimums*

$$(i) \quad \inf_{H^1 \ni Q \neq 0} \{\|Q\|_2^2 : E[Q] \leq 0\} := M_{\min}; \quad (ii) \quad \inf_{H^1 \ni Q \neq 0} \{E[Q] : \|Q\|_2^2 = M_{\min}\} = 0.$$

The first part can be proved using the assumption that such  $I[Q]$  exists and  $E[Q] \leq 0$ . Then  $\|Q\|_2^2 \geq M_{\min}$ . However, this is the zero Hamiltonian case, hence  $E[Q^{(0)}] \geq 0$  and  $\|Q^{(0)}\|_2^2 = M_{\min}$ , but using the (4.3.6) we have  $E[Q^{(0)}] = 0$ . The second part follows directly from (4.3.6) when  $\sigma d = 2$ .

To this end, the variational characterization for  $Q$  of (4.3.4) suggests that, in the critical case, the blow-up solution  $\psi(t)$  can be constructed in terms of  $Q$  with  $\|\psi_0\|_2$  slightly larger than  $\|Q\|_2$ . While  $\psi(t)$  has to match  $Q$  asymptotically, however, the spectral analysis of the linearized NLS equation in the neighbourhood of  $Q$  exhibits a missing direction which indicates the needs of  $Q$  to be extended as complex-valued function [233].

### 4.4 Virial theorem (Variance Identity)

A virial theorem is a useful tool that provides us with conditions that suffice to trace classical blow-up solutions to the NLS equation (4.1.1). Suppose  $u(t, \mathbf{x}) \equiv \psi(t, \mathbf{x})$  solves the NLS equation (4.1.1) and  $u_0 \in \Sigma = \{f : f \in H^1, \mathbf{x}f \in L^2\}$ , the variance of the solution  $u$  is given by  $V(t) = V[u(t, \mathbf{x})] = \int_{\mathbb{R}^d} |\mathbf{x}|^2 |u|^2 \mathbf{d}\mathbf{x}$ , i.e.  $V(t)$  is a *moment of inertia* of  $u$ . For  $0 \leq t < T_*$ , the *variance identity* is defined by the quantity

$$\frac{d^2 V(t)}{dt^2} = 8E[u] - 4 \left( \frac{\sigma d - 2}{\sigma + 1} \right) \int_{\mathbb{R}^d} |u|^{2\sigma+2} \mathbf{d}\mathbf{x}. \quad (4.4.1)$$

It is particularly important in checking the finite time existence of solution to NLS equations. The virial theorem confirms the presence of blow-up in the critical and supercritical dimensions  $\sigma d \geq 2$  even for smooth initial conditions and large class of initial data having negative Hamiltonian. The requirement  $u_0 \in \Sigma$  is to ensure that  $V(0) < \infty$ . See section C.0.1 of Appendix III for the the derivation of virial identity for NLS equation. The variance identity was derived in the work [215] and is also known as virial theorem .

#### 4.4.1 Critical NLS: sufficient conditions for blow-up

The sufficient, not necessary, conditions for collapse are stated in the theorem:

**Theorem 4.4.1.** *Let  $u_0 \in H^1$ , and  $E[u_0] < 0$  with  $V(0) < \infty$ , in the critical and supercritical case  $\sigma d \geq 2$  satisfying any of the conditions*

(i)  $E[u_0] < 0$

(ii)  $E[u_0] = 0$  and  $\Im \int_{\mathbb{R}^d} \mathbf{x} \cdot u^* \nabla u \, d\mathbf{x} < 0$

(iii)  $E[u_0] > 0$  and  $\Im \int_{\mathbb{R}^d} \mathbf{x} \cdot u^* \nabla u \, d\mathbf{x} < -4\sqrt{E[u_0]} \|\mathbf{x}u_0\|_2$ . Then, blow-up occurs in finite time, i.e. there exists some  $T^* < \infty$  such that

$$\lim_{t \rightarrow T^*} \|u(t)\|_\infty = \infty, \quad \text{or} \quad \lim_{t \rightarrow T^*} \|\nabla u(t)\|_2 = \infty. \quad (4.4.2)$$

*Proof.* Obviously, if  $\sigma d \geq 2$ , we have  $d^2V(t)/dt^2 \leq 8E$ . Therefore,

$$V(t) \leq P(t) := 4E[u_0]t^2 + C_1t + C_0. \quad (4.4.3)$$

If  $C_0 = V(0) < \infty$  and positive, the polynomial  $P(t)$  has at least a positive root  $t_0$ , that  $\lim_{t \rightarrow t_0} P(t) = 0$ , based on any of the conditions on its coefficients <sup>6</sup>.

(i) That  $4E[u_0] < 0$  or  $E[u_0] < 0$  implies  $V(t) < 0$ .

(ii) That  $4E[u_0] = 0$  and  $C_1 < 0$  or

$$E[u_0] = 0 \text{ and } V'(0) = 2i \int_{\mathbb{R}^d} (\mathbf{x} \cdot [u_0 \nabla u_0^* - u_0^* \nabla u_0]) \, d\mathbf{x} = 4\Im \int_{\mathbb{R}^d} (\mathbf{x} \cdot u_0 \nabla u_0^*) \, d\mathbf{x} < 0.$$

(iii) That  $4E[u_0] > 0$  and  $C_1 < 0$  and the discriminant  $C_1^2 - 4(4E[u_0])C_0 \geq 0$  or equivalently

$$E[u_0] > 0 \text{ and } C_1 \leq -4\sqrt{E[u_0]}C_0.$$

With  $C_0 = V(0) = \|\mathbf{x}u_0\|_2^2 = \int_{\mathbb{R}^d} |\mathbf{x}u_0|^2 \, d\mathbf{x}$ , we rewrite the above condition as

$$E[u_0] > 0 \text{ and } \Im \int_{\mathbb{R}^d} \mathbf{x} \cdot u_0^* \nabla u_0 \, d\mathbf{x} < -4\sqrt{E[u_0]} \|\mathbf{x}u_0\|_2.$$

In all the cases, the quantity in the right-hand-side of variance identity (4.4.1) imposes conditions on the variance  $V(t)$ . It is the point at which the  $V(t)$  attains a local maximum since  $V''(t) < 0$ , i.e. there is some  $t = t_0$  with  $0 \leq t \leq t_0$ , the root of the parabola  $P(t)$  such that  $V(t) \leq P(t)$  for all  $t \in [0, t_0]$ . <sup>7</sup>That is,  $V(t_0) \leq 0$  in any of the three conditions. This is false, because  $V(t) \geq 0$  and  $V(t) = 0$  only if  $u \equiv 0$ . However, none of the three conditions holds with  $u \equiv 0$ . Hence, we conclude that, there is some  $t_1 \leq t_0$  so that  $\lim_{t \rightarrow t_1} V(t) = 0$ .  $\square$

<sup>6</sup>Use Descartes' rule of signs applied to polynomials, to see the number of positive and negative roots of the parabola  $P(t)$ .

<sup>7</sup>By definition,  $V(t)$  should be positive, besides the roots of  $P(t)$  must be positive since  $t \geq 0$ .

Moreover, to emphasize the vanishing of the variance we employ the inequality due to uncertainty principle by assuming the norm  $\|u\|_2$  is conserved. Applying integration by part on the  $L^2$ -norm and use the identity  $\nabla \cdot (\varphi \vec{A}) = \varphi \nabla \cdot \vec{A} + \vec{A} \cdot \nabla \varphi$ :

$$\int_{\mathbb{R}^d} |u|^2 \mathbf{d}\mathbf{x} = -\frac{1}{d} \int_{\mathbb{R}^d} \left[ \nabla \cdot (\mathbf{x}|u|^2) - \mathbf{x} \cdot \nabla(|u|^2) \right] \mathbf{d}\mathbf{x} = -\frac{1}{d} \int_{\mathbb{R}^d} \mathbf{x} \cdot \nabla(|u|^2) \mathbf{d}\mathbf{x} \quad (4.4.4)$$

where  $\mathbf{x} \cdot \nabla(|u|^2) = 2\Re(u^* \mathbf{x} \cdot \nabla u)$  and by Cauchy-Schwartz inequality we can derive the uncertainty-principle applied to the solution  $u$ :

$$\|u\|_2^2 \leq \frac{2}{d} \|\nabla u\|_2 \|\mathbf{x}u\|_2. \quad (4.4.5)$$

According to the inequality (4.4.5), if  $V(t) = \|\mathbf{x}u\|_2^2$  is to vanish, there exists some  $T_* \leq t_1$  such that  $\lim_{t \rightarrow T_*} \|\nabla u(t)\|_2 = \infty$ , [212]. If in addition, the  $E[u_0]$  is conserved, then  $\lim_{t \rightarrow T_*} \|u\|_{2\sigma+2}^{2\sigma+2} = \infty$  and  $\lim_{t \rightarrow T_*} \|u\|_\infty = \infty$  because  $\|u\|_2^2$  is conserved. Thus vanishing of  $V(t)$  yields an upper bound for the blow-up time, i.e.  $0 < T_* \leq t_0 \leq t_1$ . Therefore, the parabola  $P(t)$  vanishes at  $t_0$ , the variance  $V(t)$  approaches 0 at  $t_1$  while the blow-up of  $u$  is at  $T_*$ .<sup>8</sup>

**Remark 4.4.1.** Blow-up to the critical NLS equation can occur without having any of the conditions in the theorem (4.4.1) satisfied.

As mentioned in the previous section, defocusing NLS solutions still develop singularity. Similar scenario, as above, can be followed in the verification of this<sup>9</sup>.

The variance identity is an a priori estimate derived based on the assumption that the NLS equation has a solution. This can best be viewed from the critical case where the equation  $V''(t) = 8E[u_0]$  admits a solution for all  $t > 0$ , but, imposing that  $V(t) \geq 0$  makes the variance identity indicates the NLS equation has blow-up at  $t_0$  where  $P(t) \rightarrow 0$  as  $t \rightarrow t_0$  and the variance bifurcates from being that of the NLS equation when  $t \geq T_*$ .

Variance as a global quantity is not in general a reliable measure for local phenomena like the blow-up in the NLS equation. For instance, a solution to the NLS equation in the cases  $\sigma d \geq 2$  with the radial initial data  $u_0(\mathbf{x}) = ce^{-|\mathbf{x}|^2}$  does not have a vanishing variance at the blow-up time  $T_*$  if slightly larger mass than critical mass is taken, i.e.  $\|u_0\|_2^2 = \kappa_{\sigma,d} + \varepsilon$

<sup>8</sup>Note that, the direct statement  $\lim_{t \rightarrow T_*} \|\nabla u\|_2^2 = \infty$  in (4.4.5) has two implications:  $\lim_{t \rightarrow T_*} V(t) \geq 0$ , however,  $V(t)$  is undefined if  $t > T_*$ . Thus, if  $\lim_{t \rightarrow T_*} V(t) > 0$  no such  $t_1$  which yields  $\lim_{t \rightarrow T_*} V(t) = 0$ . If it exists, it is  $t_1 = T_*$ . Hence, if  $t_1 < \infty$  then  $T_* = t_1$  and the bound on  $T_*$  is  $0 < T_* \leq t_0$ .

<sup>9</sup>If  $\sigma d < 2$ , it then implies that  $d^2 V/dt^2 > 8E[u_0]$  from virial theorem  $\frac{d^2}{dt^2} V = 8E[u] + \frac{(\sigma d - 2)}{(2\sigma + 2)} \|u\|_{2\sigma+2}^{2\sigma+2}$ . This leads to  $P(t) = 4E[u_0]t^2 + V'(0)t + V(0)$  whose positive root is given by  $t = \left( -V'(0) + \sqrt{V'^2(0) - 16E[u_0]V(0)} \right) / 8E[u_0]$  and holds only when  $V'(0) < \sqrt{V'^2(0) - 16E[u_0]V(0)}$ . Therefore,  $E[0] < 0$  if  $V(0) \neq 0$  reflects the first hypothesis of Theorem 4.4.1. Hence singularity shows up because  $V(t)$  would become negative again.

for small  $\varepsilon > 0$ . In fact, as numerical simulation will show,  $\lim_{t \rightarrow T_*} V(t) > 0$  for  $\sigma d = 2$ .<sup>10</sup> However, the only known blow-up solution whose variance vanishes at  $T_*$  is the explicit blow-up solution of the critical NLS equation, such as the Pseudo-conformal transform of  $u(t, r)$ . Moreover, in [160, 161], it is shown that, for beam input initial data, if  $V(t)$  vanishes at  $T_*$ , then the solution experiences a strong or whole beam collapse and a weak or partial beam collapse for non-vanishing variance<sup>11</sup>.

In the supercritical case, sharper conditions than that of the Theorem 4.4.1 are obtained by using the Gagliardo-Nirenberg inequality (4.1.9) to bound the term  $\frac{\sigma d - 2}{2\sigma + 2} \|u\|_{2\sigma + 2}^{2\sigma + 2}$ , see [112, 214]. There, in terms of the ground-state, it is proved that the conditions for the blow-up solution  $u$  at  $T_*$  are: if  $Q_\omega$  satisfies the profile equation (4.2.4), then there exist unique  $\omega$  such that  $\|u_0\|_2^2 = \|Q_\omega^{(0)}\|_2^2$  and if  $\|\nabla u_0\|_2^2 > \|\nabla Q_\omega^{(0)}\|_2^2$  then  $E(u_0) < E(Q_\omega^{(0)})$ . Nevertheless, the latter alone is not a sufficient condition for blow-up if  $\sigma d > 2$ , see [202] pg. 97-98 and references therein for further results on various domains.

Further studies have shown that results can be extended to infinite variance, i.e. the situation in which the variance  $V(t)$  is allowed pass the blow-up time  $T_*$ . Some of the results include that of Ogawa and Tsutsumi [170, 171] in the critical and supercritical dimensions. Read also [202] sect. 5.1.2. and the references there in.

## 4.5 Numerical observations of blow-up

Numerical experiments as found in [202] and [52] suggest that in the dimensions  $d \geq 2$  for an initial data (symmetric or non-symmetric) the blow-up appeared to be a radial phenomenon. Therefore, we consider in this section only the radial setting of the NLS equation. In the critical dimension, the ground state (profile) equation (4.3.2) has a positive radial solution [218] and a unique solution [188]. Thus, there exists a unique positive radial solution to the focusing NLS equation (4.1.1). Setting  $\psi(t, \mathbf{x}) \equiv u(t, r)$  where  $r := |\mathbf{x} - \mathbf{x}_0|$ , the radial equivalent of the NLS equation (4.1.1) in  $\Omega \subset \mathbb{R}^+$  with  $u : \mathbb{R} \times \mathbb{R}^+ \rightarrow \mathbb{C}$  for  $0 < r < \infty$  is

$$iu_t + \Delta u + |u|^{2\sigma} u = 0, \quad u(r, 0) = u_0(r) \in H^1(\mathbb{R}^d) \quad \text{for } r > 0. \quad (4.5.1)$$

$$u(r) \rightarrow 0, \quad \text{as } r \rightarrow \infty, \quad \partial\Omega = \{u \in \mathbb{C} : u(t, 0) = u'(t, 0) = 0\} \quad (4.5.2)$$

<sup>10</sup>At the point of collapse, for critical NLS equation, the mass is conserved but becomes concentrated and focused at the position  $\mathbf{x}_*$ . The amount of mass absorbed in the singularity at  $\mathbf{x}_*$  is the limiting lower bound of the critical mass near  $\mathbf{x}_*$ , i.e.  $\lim_{\varepsilon \rightarrow 0} \left[ \liminf_{t \rightarrow T_*} \int_{\mathbf{B}_\varepsilon(\mathbf{x}_*)} |u|^2 d\mathbf{x} \right]$  over  $\mathbf{B}_\varepsilon(\mathbf{x}_*) = \{\mathbf{x} \in \mathbb{R}^d : |\mathbf{x} - \mathbf{x}_*| = \varepsilon\}$ .

<sup>11</sup>The partial beam collapse, as an example, is one with delta function as a singularity, [51] pg. 163.

where  $\Delta u = r^{1-d}\partial_r(r^{d-1}\partial_r)u = (\partial_{rr}^2 + ((d-1)/r)\partial_r)u$ . By applying the solitary wave solution ansatz  $u = e^{i\omega t}Q(r)$  without loss of generality  $\omega = 1$  one gets, for  $Q : \Omega \subset \mathbb{R}^+ \rightarrow \mathbb{C}$ ,

$$\Delta Q + |Q|^{2\sigma}Q - Q = 0, \quad r > 0, \quad Q(r) \in H^1(\mathbb{R}^d) \quad (4.5.3)$$

$$Q(r) \rightarrow 0, \quad \text{as } r \rightarrow \infty, \quad \partial\Omega = \{Q \in \mathbb{C} : Q(0) = Q'(0) = 0\}. \quad (4.5.4)$$

If  $Q$  and the nonlinear part are continuous, the solution to the problem (4.5.3)-(4.5.4) is unique. See chapter 6 of [51] for the existence of  $Q$  and its asymptotic results in the section C.1. Furthermore, in the non-radial setting, the equation (4.5.3) can have a complex solution, for example take  $Q = Q_n e^{in\theta}$ ,  $n \in \mathbb{Z}$ . See section 15.2 of [51].

In the dimension  $d = 1$ , the ground-state equation for  $Q(r)$  has an explicit solution

$$Q(r) = \pm(\sigma + 1)^{1/(2\sigma)} \operatorname{sech}^{1/(2\sigma)}(\sigma r). \quad (4.5.5)$$

At the critical dimension  $\sigma = 2$  we have  $Q(r) = \pm 3^{1/4} \operatorname{sech}^{1/4}(2r)$  or at the subcritical dimension we have  $Q(r) = \pm\sqrt{2} \operatorname{sech}^{1/2}(r)$  with  $\sigma = 1$ . In the higher dimensions  $d > 1$ , no explicit ground-state solutions are known. Therefore, one resorts to numerical methods.

#### 4.5.1 NLS: Self-Similarity

Self-similarity is a crucial property of the solutions to the NLS equation especially in the study of the asymptotic behaviour of the solution  $u$  near collapse. Self-similarity for NLS equation implies the existence of the profile  $U(t, r)$  and the scaling functions  $a(t)$ ,  $b(t)$  such that, in the dimensions  $d > 2$ , solutions  $u$  takes the form

$$u(t, r) = \frac{1}{a(t)} U\left(\frac{r}{b(t)}\right) \quad (4.5.6)$$

with  $\lim_{t \rightarrow T_*} a(t) = 0$  and  $\lim_{t \rightarrow T_*} b(t) = 0$  where  $a(t)$  provides the blow-up rate and the  $b(t)$  plays the role of spatial rescaling factor. However, a solution to the NLS equation in dimension  $d = 2$  is approximately self-similar [188], where with the incorporation of the small correction term, quasi-self-similar solutions are given as

$$u(t, r) = \frac{1}{a(t)} U\left(\frac{r}{b(t)}\right) + O(a(t)). \quad (4.5.7)$$

The NLS equation is known to admit the (approximate) self-similar solutions of the form

$$u(t, \mathbf{x}) = \frac{1}{t^\alpha} U\left(\frac{\mathbf{x}}{t^\beta}\right) + O(t^\alpha), \quad \alpha = \frac{q}{2} \in \mathbb{C} \text{ with } \Re(q) = \frac{1}{\sigma}, \quad \beta = \frac{1}{2}. \quad (4.5.8)$$

Except at the critical dimensions  $\sigma d = 2$ , the self-similar solution (4.5.8) is not in  $H^1(\mathbb{R}^2)$  since one requires conserved  $L^2$  norm. This follows from  $\|u\|_2^2 = t^{\frac{\sigma d - 2}{2\sigma}} \|U\|_2^2$ ,<sup>12</sup> and ensures that in the super critical case ( $\sigma d > 2$ ),  $H^1(\mathbb{R}^d)$  is not suitable space for self-similar solution (4.5.8). Thus, it caused to seek self-similar solution  $u$  having  $U \notin L^2(\mathbb{R}^d)$  so that  $\|\nabla U\|_2^2 < \infty$  and  $\|U\|_{2\sigma+2}^{2\sigma+2} < \infty$ . Moreover, for  $\sigma d \geq 2$  the energy  $E[u]$  scales like

$$E[u] = \|\nabla u\|_2^2 - \frac{\sigma d - 2}{2\sigma + 2} \|u\|_{2\sigma+2}^{2\sigma+2} = t^{-1/\sigma - 1 + d/2} E[U]. \quad (4.5.9)$$

When  $\sigma d = 2$ , the energy in (4.5.9) associated to the self-similar solution (4.5.8) scales  $U$  by an amplitude  $t^{-1}$  which proves the non-existence of  $u$  in  $H^1(\mathbb{R}^d)$ .<sup>13</sup> For the energy  $E[u]$  to be conserved  $\sigma = \frac{2}{d-2}$  must be taken, hence  $u$  is confirmed to exist in  $H^1(\mathbb{R}^d)$  only in the dimensions  $d > 2$ . Furthermore, since  $\|u\|_{2\sigma+2} = t^{\frac{d}{4(\sigma+1)} - \frac{1}{2\sigma}} \|U\|_{2\sigma+2}$ ,<sup>14</sup> a suitable space to study the self-similar solution of the NLS equation introduced in [25, 26] is

$$W_\sigma = \left\{ u \in L_{\text{loc}}^\infty((0, \infty), L^{2\sigma+2}) : \sup_{t \in (0, \infty)} t^{-\alpha} \|u(t)\|_{L^{2\sigma+2}} < \infty \right\} \quad (4.5.10)$$

where  $\alpha = \frac{d}{4(\sigma+1)} - \frac{1}{2\sigma}$ , see (Sulem-Sulem [202] sect. 3.2.4 and Cazenave [25]) and details on the condition of the existence of solutions for initial data taken from the space of tempered distributions for both linear and nonlinear Schrödinger equations.

## 4.6 Critical NLS: Asymptotic Self-similar blow-up solution

In order to handle and treat fairly the numerical instability that could rise near singularity in the blow-up numerical simulations, there is need for reliable improved adaptive refinement of the spatial resolution near singularity. For this requirements, a theoretical understanding given in [144] and [177] recommends that asymptotically self-similar solutions, near blow-up, are furnished by method of dynamic rescaling. The method entails the rescaling of the variables involved in the NLS equation by the self-consistent factors given in terms of appropriate norms of the blow-up solution at the singularity [177]. It is expected that the rescaled solution has a constant norm which will result to a non-singular problem and allow numerical time integration near blow-up possible. Furthermore, due to scaling invariance property of the NLS equation the blow-up rate and blow-up profile are consequently captured from the obtained results of dynamically rescaled equation.

Furthermore, one constructs, as suggested by Zakharov [239], a family of solutions blowing up via a solitary wave transform  $e^{i\omega t} Q(r)$  of the dynamically rescaled equation,

<sup>12</sup>Note that  $|t^{-\frac{q}{2}}|^2 = |e^{-q \ln t}| = |e^{-a \ln t - ib \ln t}| = e^{-\Re q \ln t} = t^{-1/\sigma}$  where  $q = a + bi \in \mathbb{C}$ .

<sup>13</sup>Using the transformation (4.5.8) one gets  $2\alpha - \beta d + 2\beta = 2\alpha(\sigma + 1) - \beta d$  or  $\alpha = \beta/\sigma$ . If  $\beta = 1$ , we have  $\alpha = 1/\sigma$ . Then, the scaling factor simplifies to  $t^{\frac{1}{\sigma} - \frac{d}{2} + 1}$ .

<sup>14</sup>This is obtained by taking the  $\frac{1}{(2\sigma+2)}$  power of the relation  $\|u\|_{2\sigma+2}^{2\sigma+2} = t^{-1/\sigma - 1 + d/2} \|U\|_{2\sigma+2}^{2\sigma+2}$ .

where  $Q(r)$  is a ground state. A pseudo-conformal transformation  $u_c(r, t)$  of the standing wave solution  $u(r, t) = e^{it}Q(r)$  yields an explicit blow-up solution

$$u_c(r, t) = \frac{1}{(T_* - t)^{1/\sigma}} e^{\frac{i}{(T_* - t)}} Q\left(\frac{|\mathbf{x} - \mathbf{x}_*|}{(T_* - t)}\right) e^{\frac{-i|\mathbf{x} - \mathbf{x}_*|^2}{4(T_* - t)}}. \quad (4.6.1)$$

At the critical dimension,  $1/\sigma = d/2$  and  $\|u_0\|_2^2 = \|Q\|_2^2$ . Numerical simulation can show that solutions with critical mass behaves like  $u(r, t) \sim \frac{1}{\gamma(t)} Q\left(\frac{|\mathbf{x}|}{\gamma(t)}\right)$  where  $\gamma(t) = (T_* - t)^{1/2}$ . In this regards, the mass  $\|Q\|_2^2$  defines the threshold for the  $\|u_0\|_2^2$ .

With these, we summarize the results of the self-similar solution of the critical NLS equation. If  $\|u_0\|_2^2 < \|Q\|_2^2$ , global solutions exist and decay to zero at the rate which free Schrödinger equation will so that  $\sup_t |t|^{d/2-d/p} \|u(t)\|_p < \infty$ . When  $\|u_0\|_2^2 = \|Q\|_2^2$ , solutions blow-up at the rate  $(T_* - t)^{-d/2}$ ; whereas when  $\|u_0\|_2^2 > \|Q\|_2^2$  the solution blows-up with mass  $\|u_0\|_2^2$  concentrated near the point of singularity by an amount with lower bound given by  $\|Q\|_2^2$ .

Following the analysis given in [202], [144] and [177] we study the asymptotic behaviour of the dynamically rescaled radially symmetric NLS equation (4.5.1).

#### 4.6.1 NLS: Dynamic rescaling

The general dynamic rescaling of the radial equation (4.5.1) takes the form

$$\tau = \int_0^t \lambda^{-2}(s) ds, \quad \rho = \frac{r}{\lambda(t)}, \quad u(t, r) = \frac{1}{\lambda^{1/\sigma}(t)} U(\tau, \rho). \quad (4.6.2)$$

If  $\lambda = \text{constant}$ , the equation (4.5.1) is invariant <sup>15</sup>:

$$iU_\tau + U_{\rho\rho} + \frac{(d-1)}{\rho} U_\rho + |U|^{2\sigma} U = 0, \quad U(0, \rho) = \lambda^{1/\sigma} u_0(\lambda\rho).$$

However, if  $\lambda = \lambda(\tau)$  with  $\frac{d\tau}{dt} = \lambda^{-2}(\tau)$ , letting  $\alpha = \alpha(\tau) = -\frac{1}{\lambda(\tau)} \frac{d\lambda(\tau)}{d\tau} = -(\ln \lambda)_\tau \neq 0$ , the terms transform respectively as follows:

$$\begin{aligned} iu_t &= i \left[ -\frac{U}{\sigma} \lambda^{-\frac{1}{\sigma}-1}(\tau) \frac{d\lambda(\tau)}{d\tau} \frac{d\tau}{dt} + \lambda^{-\frac{1}{\sigma}}(\tau) \left( U_\tau \frac{d\tau}{dt} + U_\rho \frac{d\rho}{d\tau} \frac{d\tau}{dt} \right) \right] \\ &= i \left[ -\frac{U}{\sigma} \lambda^{-\frac{1}{\sigma}-2}(\tau) \frac{1}{\lambda(\tau)} \frac{d\lambda(\tau)}{d\tau} + \lambda^{-\frac{1}{\sigma}-2}(\tau) \left( U_\tau + \lambda(\tau)\rho \cdot \left( -\frac{1}{\lambda^2(\tau)} \frac{d\lambda(\tau)}{d\tau} \right) U_\rho \right) \right] \\ &= i \lambda^{-\frac{1}{\sigma}-2} \left[ U_\tau + \alpha(\tau) \left( \frac{U}{\sigma} + \rho U_\rho \right) \right]; \\ \frac{u_r}{r} &= \frac{\lambda^{-1/\sigma}(\tau)}{\rho \lambda(\tau)} U_\rho \cdot \frac{d\rho}{dr} = \lambda^{-\frac{1}{\sigma}-2}(\tau) \frac{U_\rho}{\rho}; \quad u_{rr} = \lambda^{-\frac{1}{\sigma}-2}(\tau) U_{\rho\rho}, \end{aligned}$$

<sup>15</sup>The parameter  $\lambda = \lambda(\tau)$  represents the width of the blow-up solution  $u(r, t)$ .

In this case, the equation (4.5.1) transforms to

$$iU_\tau + U_{\rho\rho} + i\alpha(\tau)\left(\frac{U}{\sigma} + \rho U_\rho\right) + \frac{(d-1)}{\rho}U_\rho + |U|^{2\sigma}U = 0, \quad \rho > 0 \quad (4.6.3)$$

$$U_0(\rho) = U(0, \rho) = \lambda^{1/\sigma}(0)u_0(\lambda(0)\rho); \quad U \rightarrow U^\infty, \tau \rightarrow \infty. \quad (4.6.4)$$

The scaling factor  $\lambda := \lambda(\tau)$  is chosen such that certain spatial norm  $\|\cdot\|_p$  is bounded, e.g. the  $\|u\|_p$  and  $\|\nabla u\|_p$  for  $p = 2, \infty$ . The idea, for smooth  $U$ , is to have  $\lambda(\tau) \rightarrow 0$  as  $\tau \rightarrow \infty$  while the  $t \rightarrow T^*$ . For instance, since  $u(t, r) = \lambda^{-1/\sigma}U(\tau, \rho)$ , requiring  $\|U\|_\infty$  to be constant would mean if  $|U| = \|U\|_\infty = \max_\rho |U(\tau, \rho)|$ , then differentiating

$$|u(r, t)|^2 = \lambda^{-2/\sigma}|U(\tau, \rho)|^2$$

w.r.t. time  $\tau$ , one gets  $0 = \lambda(\tau)^{-2/\sigma} \left[ \frac{2\alpha(\tau)}{\sigma}|U(\tau, \rho)|^2 + (|U(\tau, \rho)|^2)_\tau \right]$ , where by assuming that  $U$  satisfies (4.1.1) and its conjugate

$$(|U(\tau, \rho)|^2)_\tau = U_\tau \bar{U} + U \bar{U}_\tau = i(U\Delta \bar{U} - \bar{U}\Delta U) = 2\Im(\bar{U}\Delta U)$$

which yields, noting the infinity norm of  $U(\tau, 0)$  is constant for all  $\tau$  at  $\rho = 0$ ,

$$\alpha(\tau) = -\frac{\sigma}{\|U_0(0)\|_\infty^2} \Im(\bar{U}\Delta U)(\tau, 0) \quad (4.6.5)$$

This ensures that  $\lambda(\tau) = (|U_0(0)|/\|u(t, r)\|_\infty)^\sigma \sim \|u(t, r)\|_\infty^{-\sigma}$  is taken. This choice of uniform norm in  $\tau$ , however, allows numerical instability due to accumulation of local errors from the local behaviour of  $\lambda(\tau)$ , see (LeMesurier et. al. [126]).

Another approach, which fixes accumulation of local errors, is by fixing  $\|\nabla U(\tau, :)\|_2$  to be constant for all  $\tau$ . Using the scaled solution  $u(t, r) = \lambda^{-1/\sigma}(\tau)U(\tau, \rho)$ , then  $\nabla u(t, r) = \lambda^{-(1/\sigma+1)}\nabla U(\tau, \rho)$  so that we get  $|\nabla u|^2 r^{d-1} dr = \lambda^{-2/\sigma-2+d}|\nabla U|^2 \rho^{d-1} d\rho$ , since  $u \in H^1$  blows-up. On integrating over  $\rho \in [0, \infty)$ , assuming the scaling (4.6.2) holds, we get by fixing  $\rho = \rho_0$ ,

$$\int_0^\infty |\nabla u|^2 r^{d-1} dr = \lambda^{-q} \int_0^\infty |\nabla U|^2 \rho^{d-1} d\rho, \quad \text{where } q = 2 + \frac{2}{\sigma} - d,$$

equivalent to  $\|\nabla u(t, :)\|_2 = \lambda^{-q} \|\nabla U(\tau, :)\|_2$ , and we can take for fixed  $\rho$  (say  $\rho$  equals 0):

$$\lambda(\tau) = \left( \frac{\|\nabla U(\tau, 0)\|_2}{\|\nabla u(t, :)\|_2} \right)^{2/q}.$$

At the critical dimension  $d = 2/\sigma$  the  $\lambda(\tau)$  scales like  $\|\nabla u\|_2^{-1}$ . By differentiating w.r.t.  $\tau$

one gets, with  $\alpha(\tau) = -(\ln \lambda(\tau))_\tau$  and  $\lambda^{-q} \neq 0$ ,

$$\begin{aligned}
 0 &= -q\lambda^{-q-1}\frac{d\lambda}{d\tau} \|\nabla U\|_2 + \lambda^{-q} \int_0^\infty (\nabla U_\tau \nabla \bar{U} + \nabla U \nabla \bar{U}_\tau) \rho^{d-1} d\rho \\
 &= q\alpha(\tau) \|\nabla U\|_2 - \int_0^\infty (U_\tau \Delta \bar{U} + \bar{U}_\tau \Delta U) \rho^{d-1} d\rho \\
 &= q\alpha(\tau) \|\nabla U\|_2 - i \int_0^\infty |U|^{2\sigma} (U \Delta \bar{U} - \bar{U} \Delta U) \rho^{d-1} d\rho \\
 &= q\alpha(\tau) \|\nabla U\|_2 - i(2i) \int_0^\infty |U|^{2\sigma} \Im(U \Delta \bar{U}) \rho^{d-1} d\rho.
 \end{aligned} \tag{4.6.6}$$

The integral in the second equality is obtained through integration-by-parts and the third one is from using the equation (4.1.1) and its conjugate. We, therefore, get

$$\alpha(\tau) = -\frac{2}{q \|\nabla U(\rho, 0)\|_2} \int_0^\infty |U|^{2\sigma} \Im(U \Delta \bar{U}) \rho^{d-1} d\rho. \tag{4.6.7}$$

It is noted, in [202], that in the case of computing  $\|\nabla U(\tau)\|_2$  that we do not worry about accumulation of numerical errors, whereas the latter is expected for  $\|U\|_\infty$  due to the presence of instability introduced by the local behaviour of the scaling factor  $\lambda(\tau)$  (see [144], sec. III). Furthermore, if we differentiate  $\|\nabla U(\tau, \rho)\|_2^2$  w.r.t.  $\tau$ , one obtains

$$\begin{aligned}
 \frac{d}{d\tau} \int_0^\infty |\nabla U|^2 \rho^{d-1} d\rho &= \int_0^\infty (\nabla U_\tau \nabla \bar{U} + \nabla U \nabla \bar{U}_\tau) \rho^{d-1} d\rho + q\alpha(\tau) \int_0^\infty |\nabla U|^2 \rho^{d-1} d\rho \\
 &= q\alpha(\tau) \|\nabla U(\rho, 0)\|_2^2 - q\alpha(\tau) \|\nabla U(\rho, \tau)\|_2^2 \\
 &= q\alpha(\tau) \left( \|\nabla U(\rho, 0)\|_2^2 - \|\nabla U(\rho, \tau)\|_2^2 \right).
 \end{aligned} \tag{4.6.8}$$

In the case of blow-up (singular) solution, the  $\lambda(\tau)$  decreases and this requires  $\alpha(\tau)$  to be positive. Hence,  $\frac{d}{d\tau} \|\nabla U\|_2^2 = 0$  so that  $\|\nabla U(\rho, 0)\|_2^2 = \|\nabla U(\rho, \tau)\|_2^2$  established stable solution.

For general norms such as  $\|\nabla U\|_p$  for  $p > 2$  (or even  $\|\Delta u\|_p$ ), similar approach (also useful in the non-radial symmetric settings) can be applied to choose  $\lambda(\tau)$  by keeping certain quantity  $\mathcal{Q}(\tau)$  bounded (see [202], sec. 6.1.2) defined as:

$$\mathcal{Q}(\tau) = \int_0^\infty \rho^2 |U|^{2q} \rho^{d-1} d\rho / \int_0^\infty |U|^{2q} \rho^{d-1} d\rho, \quad q \geq 2. \tag{4.6.9}$$

Using the scaling (4.6.2), the mass and energy equations (4.1.3)-(4.1.4)

$$\begin{aligned}
 \|U\|_2^2 &= \int_{\mathbb{R}^d} |\lambda^{1/\sigma} u(t, r)|^2 \rho^{d-1} d\rho = \lambda^{2/\sigma-d} \int_{\mathbb{R}^d} |u(t, r)|^2 dr = \lambda^{2/\sigma-d}(\tau) \|u\|_2^2 \\
 E[U] &= \left[ \int_{\mathbb{R}^d} \left( |\nabla U|^2 - \frac{1}{\sigma+1} |U|^{2\sigma+2} \right) \rho^{d-1} d\rho \right] = \lambda^{2+\frac{2}{\sigma}-d}(\tau) E[u].
 \end{aligned}$$

Therefore, the equation (4.6.3) is  $L^2$ -critical if  $\sigma d = 2$  and supercritical for  $\sigma d > 2$ . It is energy-critical when  $d = 2 + 2/\sigma > 2$ .

In the case of self-similar blow-up for  $\tau \rightarrow \infty$ , the scaling factor should approach zero while  $U$  tends to the blow-up profile, i.e.  $U \rightarrow U^\infty$ . The profile equation (4.6.3), with  $U_\tau^\infty \rightarrow 0$ , becomes

$$U_{\rho\rho}^\infty + i\alpha^\infty \left( \frac{U^\infty}{\sigma} + \rho U_\rho^\infty \right) + \frac{(d-1)}{\rho} U_\rho^\infty + |U^\infty|^{2\sigma} U^\infty = 0 \quad (4.6.10)$$

In the  $L^2$ -critical case, one expects  $\alpha^\infty = 0$ . In this case the profile is just given by the ground state. Exact solution to (4.6.10) is not known even in lower dimension  $d = 1$ .

To numerically solve the equation (4.6.3), one may choose to employ several possible strategies. One possibility is to introduce the variable  $s = \rho^2$  and solve a less singular equation numerically by Fourth order Runge-Kutta (Rk4) scheme on a multi-domains or apply the RK4 scheme on the equation (4.6.10). It turns out, numerical experiments show not much is gained as a result of (numerical) radiation coming from infinity will destroy the accuracy of the solution. In what follows, the equation (4.6.3) is then put in the form of semilinear equation  $U_\tau = \mathbf{L}U + \mathbf{N}[U]$ .

In a particular domain  $[0, \kappa]$ , for  $\kappa$  finite or  $\infty$ , a Chebyshev collocation method can be applied on the spatial coordinates. The time integration is done as in [105] with a fourth order splitting scheme. To this end equation (4.6.3) is split into two equations, first the linear equation

$$U_\tau = iU_{\rho\rho} + i\frac{(d-1)}{\rho}U_\rho, \quad (4.6.11)$$

which will be numerically integrated using a 4th order implicit Runge-Kutta method. Secondly the equation

$$U_\tau = -\alpha(\tau) \left( \rho U_\rho + \frac{U}{\sigma} \right) + i|U|^{2\sigma}U \quad (4.6.12)$$

which is equivalent to

$$iu_t + |u|^{2\sigma}u = 0$$

has the solution  $u(t, r) = u_0(r) \exp(i|u_0(r)|^{2\sigma}t)$  since  $|u(t, r)| = \text{const}$  with respect to time ( $u_0 = u(r, 0)$ ). Thus we get for  $U$

$$U(\rho/\lambda(\tau), \tau) = U(\rho/\lambda(0), 0) \left( \frac{\lambda(\tau)}{\lambda(0)} \right)^{1/\sigma} \exp(i|U(\rho/\lambda(0), 0)|^2 t(\tau) \lambda(0)^{-2/\sigma}). \quad (4.6.13)$$

This means that the second equation can be integrated exactly up to the integration of the scaling factor  $\lambda$  and the time  $t$ , both with respect to  $\tau$  only.

Alternatively, one may choose to solve the profile equation (4.6.17) in terms of the ground state as described in section 4.6.3 in terms of the blow-up profile.

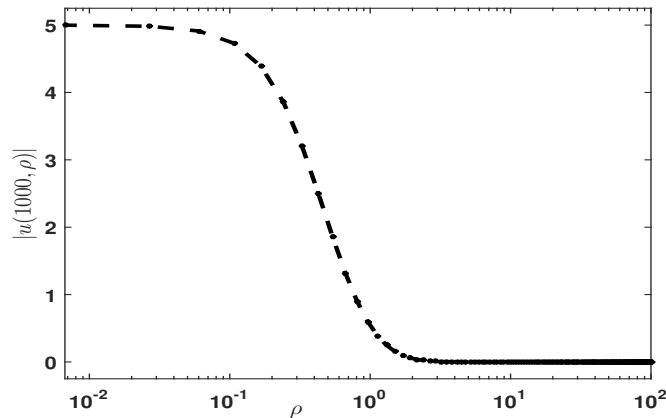


Figure 4.2: Asymptotic profile of the blow-up solution at the critical dimension, where  $d = 2$  and  $\sigma = 1$  on the domain  $[0, 100]$  for an initial data  $u(0, \rho) = 5e^{-\rho^2/d}$

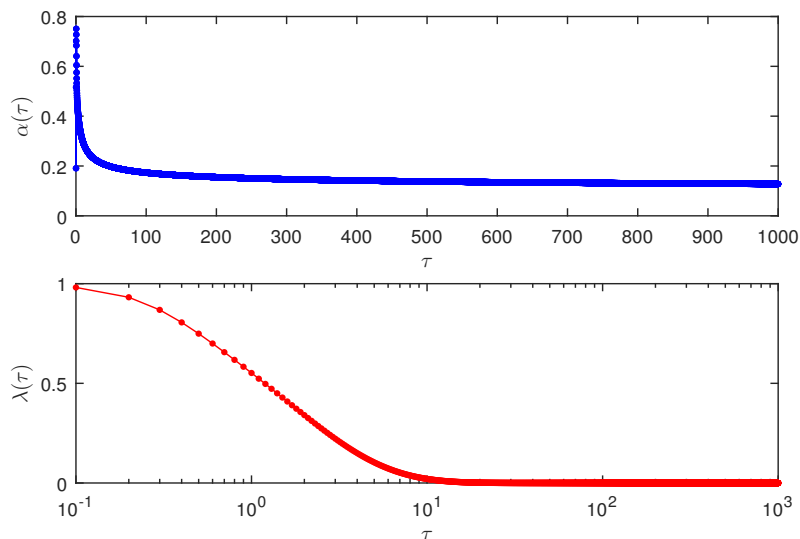


Figure 4.3: The behaviour of  $\alpha(\tau)$  (top panel) and  $\lambda(\tau)$  (lower panel) for  $|u(\tau, \rho)|$  as  $\tau$  approaches  $\tau_{max} = \infty$ , in the critical case with  $d = 2$  and  $\sigma = 1$  on  $[0, \infty]$ .

#### 4.6.2 Blow-up rate

From the motivation by the dynamic rescaling and conservation of energy, in the critical and supercritical cases ( $\sigma d \geq 2$ ), associated to the blow-up solution of NLS equation is its blow-up rate property, i.e. the rate at which, as  $t \rightarrow T_*$ ,

$$\lambda_*(t) := \|\nabla u\|_2^{-1} \rightarrow 0 \quad \text{or} \quad \lambda_*(t) := \left[ (\sigma + 1) / \|u\|_{2\sigma+2}^{2\sigma+2} \right]^{\frac{1}{2}} \rightarrow 0. \quad (4.6.14)$$

The latter rate comes from the conservation of energy (4.1.4) where we have the quantity  $(\sigma + 1) \|\nabla u\|_2^2 / \|u\|_{2\sigma+2}^{2\sigma+2} \sim (\sigma + 1) / \|u\|_{2\sigma+2}^{2\sigma+2}$  since  $\lim_{t \rightarrow T_*} (\sigma + 1) \|\nabla u\|_2^2 / \|u\|_{2\sigma+2}^{2\sigma+2} = 1$ . Furthermore, it is generalization of blow-up rate for blow-up solution in the space  $L^{2\sigma+2}(\mathbb{R}^d)$  not in  $H^1(\mathbb{R}^d)$ . When it is generalized to the  $L^q$  space for  $2\sigma + 2 \leq q \leq \infty$ , there exists a constant  $\alpha_q = \alpha_q(\|u\|_q)$  such that

$$\|u\|_q \geq \lambda_*(t), \quad \lambda_*(t) := \alpha_q \cdot (T_* - t)^{-(q-2)/(2\sigma)}, \quad 0 \leq t < T_* \quad (4.6.15)$$

where the  $L^\infty(\mathbb{R}^d)$  has  $\|u\|_\infty \geq \alpha_\infty \cdot (T_* - t)^{-1/(2\sigma)}$  for  $0 \leq t < T_*$ .

**Proposition 4.6.1.** *If the ground state  $Q(\rho)$  attains a global minimum at  $0 < \rho_{\max} < \infty$ , then the blow-up rate is  $\lambda(t) \sim \alpha \cdot (T_* - t)^{1/2}$  as  $t \rightarrow T_*$  with  $\alpha = \alpha(\|u_0\|_2^2) > 0$ .*

A clear suggestion from this proposition 4.6.1 is the self-similarity of NLS as described in (4.5.8). Moreover, for singular solution to NLS equation at  $T_*$ , there exists a constant  $\alpha = \alpha(\|u_0\|_2^2) > 0$  such that  $\|\nabla u\|_2 \geq \alpha / \sqrt{T_* - t}$  for  $0 \leq t < T_*$ . See [31] for details and the proof in [202] chp.5 and Theorem 13.1 of [51].

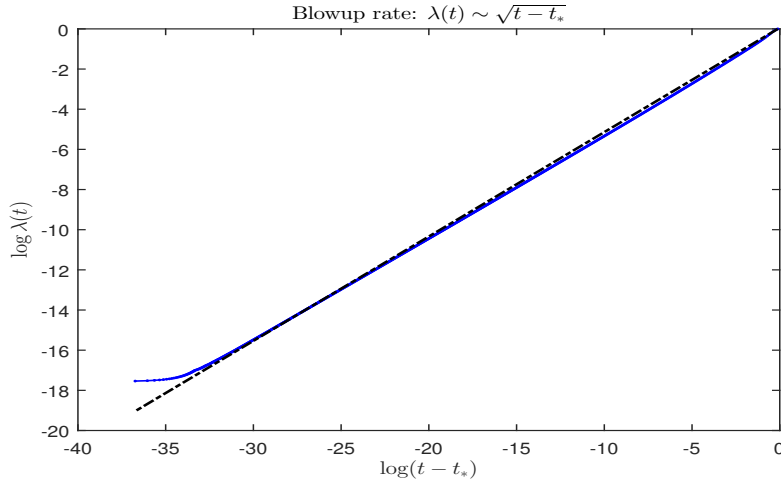


Figure 4.4: Blow-up rate in the critical dimension, where  $d = 2$  and  $\sigma = 1$ . The bold dashed line represents the equation of the line  $y = 0.5198x - 0.04623$  while the bold-line represents the  $\log \lambda(t)$ . This is equivalent to  $\log \lambda(t) \sim 0.5198 * \log(T_* - t)$ .

According to the Chebyshev coefficients in Figure 4.6.2, the Chebyshev approximation near infinity is less accurate compared to approximation near zero. This is a reflection of numerical radiation as a result of error amplification in approximate  $u(\tau, \rho)$  towards infinity.

The method of dynamic rescaling is used in [144] to study the solution to the NLS equation near singularity which can attain amplitude (focusing level) up to  $10^{15}$ , originally

meant to approximate boundaries [108]. Nevertheless, the loglog correction is not reachable and one cannot show that the blow-up rate is faster than the square root, which, mostly, is the case. Unfortunately, the loglog correction to the square root blow-up rate is not observable numerically.

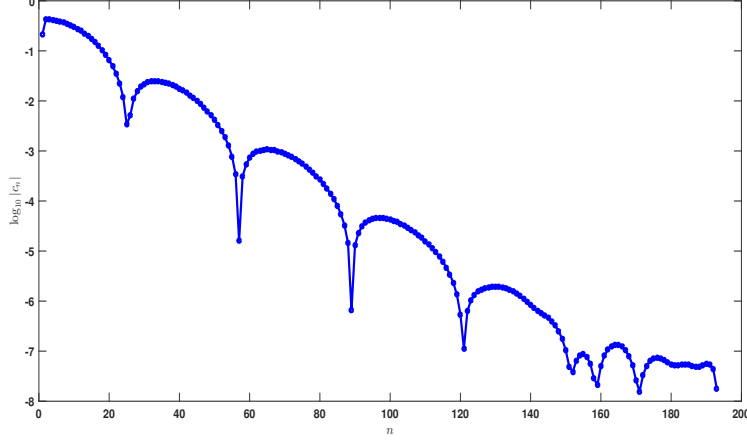


Figure 4.5: Chebyshev coefficients of  $|u(1000, \rho)|$  on the domain  $[0, 100]$  in the critical dimension,  $d = 2$  and  $\sigma = 1$ .

### 4.6.3 Blow-up profile

All singular solutions to the focusing NLS equation experience quasi-self-similar blow-up with self-similar-profile possessing mass not less than the  $\kappa_{\sigma,d}$ . A faster, than square root, blow-up rate was proved by Merle and Raphaël stated and summarized in the Theorem 4.6.1 due to the results in [155]-[150] and [186], modified to radial form.

The blow-up profile is best described by  $Q$  by  $U(\tau, \rho) = e^{i\tau}Q(\rho)$  equivalent to

$$u(r, t) = \frac{1}{\lambda^{1/\sigma}(\tau(t))}Q\left(\frac{r}{\lambda(t)}\right)e^{i\tau(t)} \quad (4.6.16)$$

with  $Q$  satisfying the profile equation

$$Q_{\rho\rho} + \frac{(d-1)}{\rho}Q_{\rho} - Q + i\alpha(t)\left(\rho Q_{\rho} + Q/\sigma\right) + |Q|^{2\sigma} = 0, \quad \rho > 0 \quad (4.6.17)$$

$$Q_{\rho}(0) = 0 \quad Q(\rho) \rightarrow 0 \quad \text{as } \rho \rightarrow \infty. \quad (4.6.18)$$

where we shall assume that, for limiting profiles of blow-up solution  $u(t, r)$ , an *admissible* complex valued solution to the equation (4.6.17) to be one with  $|Q|$  monotonically decreasing function with  $\rho$  and  $E[Q] = 0$  and possibly  $E[Q] > 0$ . The  $\alpha$  may depend on the  $\sigma$  or

dimension  $d$ . See section 4.7 for more details.

**Theorem 4.6.1** ([155]-[150]). *Given that  $1 \leq d \leq 10$ , and  $u$  blows up at the point  $T_*$ . Then there exists a positive <sup>16</sup> universal constant  $\alpha_* = \alpha_*(d)$  such that for  $u_0 \in \{f : f \in H^1, \kappa_{\sigma,d} \leq \|f\|_2^2 \leq \kappa_{\sigma,d} + \alpha_*\}$ . Suppose also*

$$\tilde{u}(t, r) = \frac{1}{\lambda^{1/\sigma}(t)} Q^{(0)}\left(\frac{r}{\lambda(t)}\right) e^{i\zeta(t)} \quad (4.6.19)$$

then the following hold:

- (i) **Universal blow-up profile.** *There exist parameters  $(\lambda(t), \mathbf{x}_0(t), \zeta(t)) \in \mathbb{R} \times \mathbb{R}^+ \times \mathbb{R}^d$  and  $\varphi(r) \in L^2$  and ground state  $Q^{(0)}$  such that (4.6.19) is a universal profile for blow-up at the critical and supercritical dimensions and*

$$u(t, r) - \tilde{u}(t, |\mathbf{x} - \mathbf{x}_0|) \xrightarrow{L^2} \varphi(r) \quad (4.6.20)$$

and the blow-up occur at the position  $\mathbf{x}_* = \lim_{t \rightarrow T_*} \mathbf{x}_0(t) \in \mathbb{R}^d$ .

- (ii) **Blow-up rate.** *As  $t \rightarrow T_*$ , then the blow up rate of the profile (4.6.19) is a loglog law*

$$\|\nabla u\|_2 \sim \frac{(\log |\log(T_* - t)|)^{1/2}}{(T_* - t)^{1/2}} \cdot \frac{\|\nabla Q^{(0)}\|_2}{\sqrt{2\pi}} \quad (4.6.21)$$

or a linear rate

$$\|\nabla u\|_2 \geq M \cdot (E_c[u_0])^{-1/2} (T_* - t)^{-1} \quad (4.6.22)$$

where  $E_c[u_0] = E[u_0] - \left( \int_{\mathbb{R}^d} u^* \nabla u / \|u\|_2 \right)^2$  and a universal constant  $M$ .

- (iii) **Sufficient condition for log log blow-up.** *If  $E_c[u_0] < 0$  and  $\kappa_{\sigma,d} \leq \|u_0\|_{L^2}^2 \leq \kappa_{\sigma,d} + \alpha_*$ , then  $u(r, t)$  has a blow-up rate (4.6.21).*

This Theorem 4.6.1 describes the stable blow-up dynamics of the focusing NLS equation and is based on the assumptions that spectral property of the Nonlinear operator acting on the ground state holds true. The spectral property is stated in [53] and [142] and is proved in several dimensions  $1 \leq d \leq 10$  in the non-radial setting [155]-[150] and  $d = 11, 12$  in the radial setting [228]. Explicit blow-up solutions by Bourgain and Wang according to Merle [154] is known to have linear blow-up rate and singular solutions with linear blow-up rate are in general unstable.

<sup>16</sup>Universal constant here implies  $\alpha_*$  is independent of the initial data  $u_0$ . And experiment shows that the constant  $\kappa$  is only universal in the generalized loglog law  $\lambda(t) \sim \kappa \cdot (T_* - t)^p (\log |\log(T_* - t)|)^q$  for  $p > 0$  and  $q \in \mathbb{R}$  but not true for the square root law only.

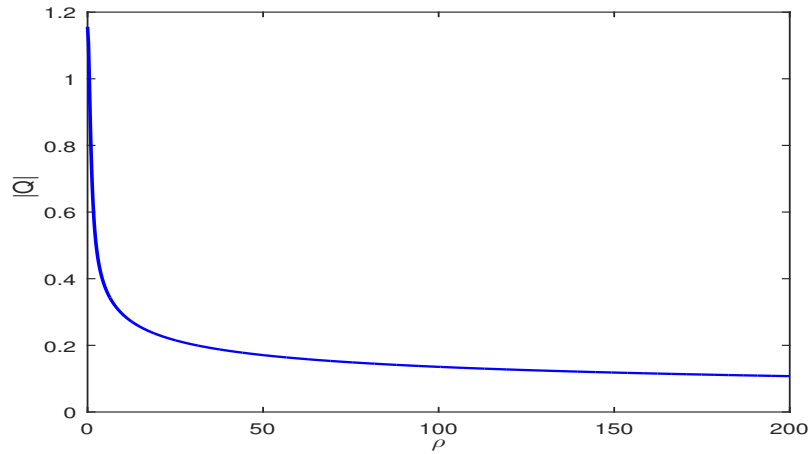


Figure 4.6: An admissible solution to the profile equation (4.6.17) at the supercritical dimension, where  $d = 1$  and  $\sigma = 3$ .

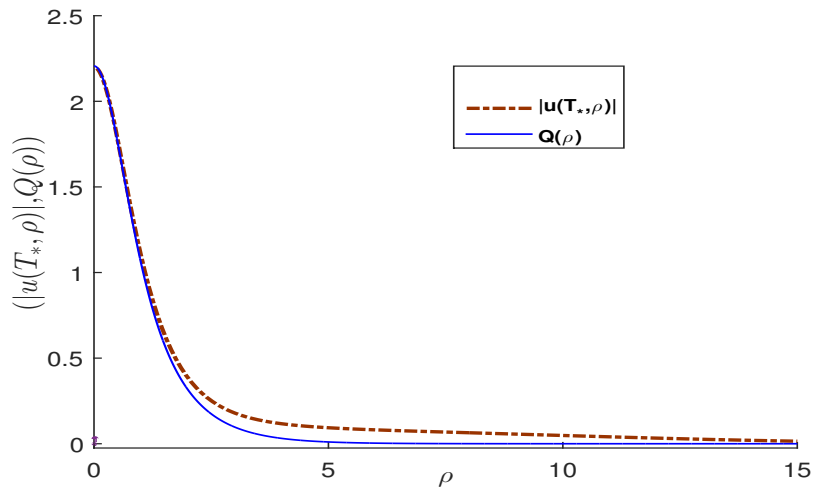


Figure 4.7: Convergence of the blow-up solution, at  $\tau = 1$ , to the focusing NLS equation to the self-similar blow-up profile  $Q$  with  $u_0(\rho) = 2.2e^{-\rho^2/d}$  at dimensions  $d = 2$  and  $\sigma = 1$ .

In the Figure 4.6.3, we can show that the ratio  $|u(0, \tau)|/\lambda(\tau)$  approaches a constant for various times  $\tau$  where  $\lambda(\tau) = |u(0, \tau)|/Q(0)$ .

## 4.7 Convergence of Asymptotic Profile near Blow-up Regime

As the previous experiments show at the critical dimension, the function  $\alpha(t)$  is slowly varying as the blow-up time is approached and does not reach a finite limit. This indicates the presence of correction to the rate of blow-up related to the self-similar profile. This implies that, the rescaled solution  $U$  does not quite converge uniformly to the self-similar blow-up solution. Thus, there is need for the construction of an asymptotic solution profile near blow-up at the critical and supercritical dimensions. Sequel to the slow variation of  $\alpha(t)$  it is sensible to maintain slow variation too in the self-similar profile. This is achieved by adding a correction term to the phase of the self-similar profile  $u(t, r) = \lambda^{-1/\sigma} e^{i\tau} Q(\rho, \alpha)$ . In [126] and [119] it is shown that construction of the blow-up profile should take into consideration the relation between  $\alpha$  and  $d$  or  $\sigma$  depending on the existence of blow-up solution of the self-similar blow-up solution. Moreover, the blow-up rate is determined as a solvability condition in an expansion near the quasi-self-similar blow-up profile.

### 4.7.1 Critical and supercritical collapse

The self-similar profile equation (4.6.17), in the critical dimensions, possesses no admissible solution if  $\alpha$  takes values on  $(0, \infty)$ . More precisely, plugging into the equation (4.6.17) the term  $Q = Re^{i\theta}$ , assuming that the amplitude  $R = R(\rho)$  is real with phase  $\theta = \theta(\rho)$ . This lead to real and imaginary parts

$$R_{\rho\rho} + \frac{(d-1)}{\rho} R_{\rho} - R - (\theta_{\rho} + \alpha\rho)\theta_{\rho}R + R^{2\sigma+1} = 0 \quad (4.7.1)$$

$$\left(\theta_{\rho\rho} + \frac{(d-1)}{\rho}\theta_{\rho} + \frac{\alpha}{\sigma}\right)R + 2R_{\rho} \cdot \left(\theta_{\rho} + \frac{\alpha\rho}{2}\right) = 0. \quad (4.7.2)$$

The equation (4.7.2) is simplified to <sup>17</sup>

$$\frac{(\sigma d - 2)}{\sigma}\theta_{\rho}R^2\rho^{\frac{2}{\sigma}-2} + \partial_{\rho}\left(\left(\theta_{\rho} + \frac{\alpha}{2}\rho\right)\rho^{\frac{2}{\sigma}-1}R^2\right) = 0. \quad (4.7.3)$$

If  $\sigma d = 2$ , critical case, one finds the exact solution to the equation (4.7.3) leads  $\theta$  to be the quadratic phase  $\theta(\rho) = -\alpha\rho^2/4$  for smooth even solution  $Q$  to (4.6.17). However, this property is missing on  $Q$  for sufficiently large  $\rho$ , even though  $|Q|$  is monotonically decaying

<sup>17</sup>Multiplying equation (4.7.2) by  $R$  will result to

$$\frac{(d-1)}{\rho}\theta_{\rho}R^2 + \frac{\alpha}{2}\left(\frac{2}{\sigma} - 1\right)R^2 + \partial_{\rho}\left(\left(\theta_{\rho} + \frac{\alpha}{2}\rho\right)R^2\right) = 0$$

suggesting to obtain an expression in terms of  $\partial_{\rho}\left(\left(\theta_{\rho} + \frac{\alpha}{2}\rho\right)\rho^{\frac{2}{\sigma}-1}R^2\right)$ . Thus, the equation (4.7.3).

to zero, as some of the solutions would be non-smooth as  $\rho \rightarrow \infty$ , see Proposition C.1.1 in the appendix. Consequently, in the critical case,  $Q$  has no admissible solution for  $\alpha(\tau) > 0$ . See Sect. 8.1.1 of [202]. According to the Propositions 8.1 of [202], the conditions for admissibility of the profile  $|Q|$  requires the values of  $\alpha$  to be adjusted to a distance near or closed to criticality at fixed nonlinearity. The  $\alpha$  and  $d$  are shown to be related in the limit  $d(\alpha) \downarrow 2/\sigma$  as  $\alpha \rightarrow 0^+$ .

A proposition 8.4 in [202], restated in the appendix, Proposition C.1.3, states that such admissible  $|Q|$ , in the limit  $d(\alpha) \downarrow 2/\sigma$  as  $\alpha \rightarrow 0^+$  satisfies the asymptotic behaviour of  $d(\alpha)$  given as

$$\frac{\sigma d - 2}{2\sigma} \approx \frac{\nu_0^2}{M_c} \frac{1}{\alpha} e^{-\frac{\pi}{\alpha}} \quad (4.7.4)$$

where the critical mass for blow-up is represented by  $M_c := \int_{\mathbb{R}^+} R^2 \rho^{d-1} d\rho$  and  $\nu_0 := \lim_{\rho \rightarrow \infty} \rho^{(d-1)/2} R(\rho)$ . If we further define  $\nu(\alpha) := \alpha(\sigma d - 2)/(2\sigma)$  as a function controlling the distance to criticality, then in the  $\alpha$ -limit, one gets

$$\nu(\alpha) \approx \frac{\nu_0^2}{M_c} e^{-\frac{\pi}{\alpha}} \quad (4.7.5)$$

Therefore, to capture closely, the blow-up rate and its profile near collapse we apply the change of variables  $U(\tau, \rho) = e^{i\tau} e^{-i\frac{\alpha(\tau)\rho^2}{4}} V(\tau, \rho) = e^{i(\tau - \frac{\alpha(\tau)\rho^2}{4})} V(\tau, \rho)$  with the second order correction term. As a result, this transforms (4.6.3) to

$$iV_\tau + V_{\rho\rho} + \frac{(d-1)}{\rho} V_\rho - V + \frac{1}{4}(\alpha^2(\tau) + \alpha_\tau(\tau))V + i\frac{(\sigma d - 2)}{2\sigma} \alpha(\tau)V + |V|^{2\sigma}V = 0. \quad (4.7.6)$$

where  $\alpha_\tau$  is negligible with  $\alpha$  satisfying

$$\alpha_\tau + \alpha^2 = -\lambda^3 \lambda_{\tau\tau}. \quad (4.7.7)$$

Letting  $\beta = \alpha_\tau + \alpha^2$ , it can be shown that  $\alpha_\tau$  is negligible<sup>18</sup> as  $\alpha \rightarrow 0$  and  $\beta \approx \alpha^2$ . If we further seek for quasi-stationary solution at leading order in the limit  $\tau \rightarrow \infty$ , one gets

$$V(\tau, \rho) = P(\beta(\tau), \rho) + W(\tau, \rho) \quad \text{with } W \ll P, \quad (4.7.8)$$

where, by taking correction terms negligible [45],  $P$  satisfies the boundary valued problem

$$P_{\rho\rho} + \frac{(d-1)}{\rho} P_\rho - P + \frac{\beta\rho^2}{4} P - i\nu(\sqrt{\beta})P + |P|^{2\sigma}P = 0 \quad (4.7.9)$$

$$P_\rho(0) = 0, \quad P(\rho) \rightarrow 0 \quad \text{as } P(0) \text{ real}, \quad (4.7.10)$$

<sup>18</sup>Roughly, if the relation (4.7.4) is differentiated w.r.t.  $\tau$  one gets  $(\alpha + \pi)\alpha_\tau \approx 0$ . Since, as  $\tau \rightarrow \infty$ ,  $\alpha + \pi \neq 0$  then  $\alpha_\tau \approx 0$ .

and the zero Hamiltonian condition

$$\int_0^\infty \left( |P_\rho|^2 - \frac{1}{(\sigma+1)} |P|^{2\sigma+2} + \sqrt{\beta} \Im(\rho P \bar{P}_\rho) + \frac{\beta \rho^2}{4} |P|^2 \right) \rho^{d-1} \rho = 0, \quad (4.7.11)$$

with  $\nu$  defined in (4.7.5) and  $\alpha \approx \sqrt{\beta}$  as  $\alpha \rightarrow 0$ . There, we have  $(\sigma d - 2)/2\sigma = \nu(\sqrt{\beta})/\sqrt{\beta}$ . Considering (4.7.8) as an asymptotic solution to the equation (4.7.6) the function  $\beta(\tau)$  is determined to be the solution to the equation

$$\beta_\tau(\tau) = -\frac{2M_c}{M} \nu(\beta) \approx -\frac{2\nu_0^2}{M} e^{-\pi/\sqrt{\beta}}, \quad \text{for } M = \frac{1}{4} \int_0^\infty R^2 \rho^2 \rho^{2/\sigma-1} d\rho. \quad (4.7.12)$$

In the propositions C.1.4 and C.1.5 it is proved that

$$\alpha(t) \approx \pi / \ln \tau$$

and by maintaining the correction terms one gets

$$\alpha(t) \approx \pi / (\ln \tau + 3 \ln \ln \tau).$$

#### 4.8 The 2D NLS and DS I

Questions related to the 2D NLS and DS I are the self-similarity, rate and profile of their blow-up solutions. It is shown in the figure 4.6.3 that, the blow-up solution to the two dimensional critical cubic NLS equation is quasi-self-similar. The blow-up rate for 2D NLS is quite the loglog law (4.6.21) and the profile is modelled by the ground-state  $Q$  [72]. Therefore, because the DS system is also a particular critical cubic NLS, we can study its blow-up behaviour. Blow-up studies in other DS systems include blow-up in the elliptic-elliptic type [174], blow-up mechanism for DS II [105]. For global and local wellposed and blow-up solutions in the elliptic-elliptic and hyperbolic-elliptic (DS II), hyperbolic-hyperbolic and DS I see [71],[82, 34, 81, 80] and the references therein. The DS system of the type

$$i\psi_t + \partial_{xx}\phi + \partial_{yy}\psi = -2(|\psi|^2 + \phi)\psi \quad (4.8.1)$$

$$\partial_{xx}\phi - \partial_{yy}\phi = -2\partial_{xx}(|\psi|^2) \quad (4.8.2)$$

in the new coordinates  $\xi = x - y$  and  $\eta = x + y$  is given in the form

$$i\psi_t + 2(\partial_\xi^2 + \partial_\eta^2)\psi = -2(|\psi|^2 + \phi)\psi \quad (4.8.3)$$

$$2\phi_{\xi\eta} = -(\partial_{\xi\xi} + 2\partial_{\xi\eta} + \partial_{\eta\eta})|\psi|^2. \quad (4.8.4)$$

The dynamical rescaling

$$X = \frac{\xi}{L(\tau)}, \quad Y = \frac{\eta}{L(\tau)}, \quad \tau = \int_0^t L^{-2}(s)ds, \quad (4.8.5)$$

$$\psi(t, \xi, \eta) = \frac{1}{L(\tau)}V(\tau, X, Y)e^{i(\tau - \alpha(\tau)|\rho|^2/4)}, \quad \phi(t, \xi, \eta) = \frac{1}{L^2(\tau)}W(\tau, X, Y) \quad (4.8.6)$$

of the equation (4.8.3) yields

$$iV_\tau + 2(V_{XX} + V_{YY}) + \frac{V}{4}(a_\tau - 2a^2)(X^2 + Y^2) + \frac{a^2V}{2}(X + Y) = -2(V + W)|V|^2 \quad (4.8.7)$$

$$2W_{XY} = -(\partial_{XX} + \partial_{XY} + \partial_{YY})|V|^2 \quad (4.8.8)$$

where  $\rho = (X, Y)$  and  $|\rho|^2 = X^2 + Y^2$ . Following similar calculations for NLS equation, with the radial phase factor, we have instead

$$iV_\tau + \Delta V - V + \frac{b(\tau)}{4}\rho^2V = -2(|V|^2 + W)V \quad (4.8.9)$$

$$2W_{XY} = -(\partial_{XX} + \partial_{XY} + \partial_{YY})|V|^2, \quad (4.8.10)$$

where  $a = \partial_\tau L$ ,  $b = a^2 + a_\tau$  and  $\nu(\sqrt{b})$  is as defined earlier. Since DSI can be viewed as a perturbation of 2D NLS, according to the studies in [14] and [174], when we sought for quasi-stationary solution to the DS I equations (4.8.1)-(4.8.2) similar to (C.1.28), (C.1.29), (C.1.30) and (C.1.31) are obtained, see section 9.3 of [202] for details. In fact, findings, in [14] and ([202] sect. 12.5), suggest that, the result of dynamically rescaling DSI equation comes down to the 2D critical cubic focusing NLS equation and therefore yields the same blow-up rate for DSI.

## IV

---

# Numerical Study: Blow-up in Davey-Stewartson I systems

---

# Chapter 5

## The DS I: Numerical Study of blow-up

In this chapter, we introduce in a nutshell the Davey-Stewartson (DS) systems and some of associated properties of the related DS system, specifically the so-called integrable DS I equations. Then, we present a detailed numerical study concerning the emergence of blow-up structure of solutions to the DS I system.

### 5.1 Davey-Stewartson System: The general setting

DS system is a system of two PDEs that was initially derived to depict the evolution of progressive (travelling) waves with slowly varying amplitude travelling under the influence of gravity on the surface of water of finite depth. The general DS system is the coupled equations

$$\begin{aligned} i\partial_t\Psi + \lambda\partial_{xx}\Psi + \mu\partial_{yy}\Psi &= \nu|\Psi|^2\Psi + \nu_1\Psi\Phi \\ \lambda_1\partial_{yy}\Phi + \mu_1\partial_{yy}\Phi &= \kappa\partial_{xx}|\Psi|^2 \end{aligned} \quad (5.1.1)$$

where the indices of  $\partial$  denote partial derivatives,  $\mathbf{x} = (x, y) \in \mathbb{R}^2$ , and  $\lambda, \lambda_1, \mu, \mu_1, \nu, \nu_1, \kappa$  are constants,  $\Psi : \mathbb{R} \times \mathbb{R}^2 \rightarrow \mathbb{C}$  is called the *main field*, and  $\Phi : \mathbb{R}^2 \rightarrow \mathbb{R}$  is the *mean velocity potential field* like e.g. in the Navier-Stokes. The DS system was firstly derived in the work of Davey & Stewartson [41] using a method of multiple-scales to describe the evolution of a 3-dimensional wave-packet with wave-number  $k$  on finite depth water. The formulation allowed them to study the stability of uniform wave-train of Stokes wave. The system had then received lot of attentions in the context of water waves [43, 3, 122] in particular in the study of the modulation of plane waves.

The Davey-Stewartson systems are of importance in many other applications since they can be seen as simplifications of the Benney-Roskes [12] and Zakharov-Rubenchik [236] systems, ‘universal’ models for the description of the interaction of short and long waves. DS systems also appear in ferromagnetism [123], plasma physics [158], and nonlinear optics [162]. For more details on DS and its applications the reader is referred to [99, 98] where a comprehensive list of references is given.

Ghidaglia and Saut [71] classified the equations (5.1.1) as a system of elliptic and hyperbolic equations. These are elliptic-elliptic or hyperbolic-hyperbolic if the quadruple  $(\lambda, \lambda_1, \mu, \mu_1)$  is  $(+1, +1, +1, +1)$  or  $(+1, +1, -1, -1)$  respectively and hyperbolic-elliptic or elliptic-hyperbolic for  $(+1, +1, -1, +1)$  or  $(+1, +1, +1, -1)$  respectively.

## 5.2 Numerical Study of Davey-Stewartson I System

The DS system is proved to be integrable via the method of inverse scattering [56] in the case  $\mu_1 = -\mu = 1$  for  $\lambda = \lambda_1 = 1$  or  $\lambda_1 = -\lambda = 1$  for  $\mu = \mu_1 = 1$ . In this section, we are concerned with the numerical study of the integrable version of the Davey-Stewartson system, more specifically the Davey-Stewartson (DS) I system written in the form

$$\begin{aligned} i\Psi_t + \Psi_{xx} + \Psi_{yy} + 2(\Phi + |\Psi|^2)\Psi &= 0, \\ \Phi_{xx} - \Phi_{yy} + 2|\Psi|_{xx}^2 &= 0, \end{aligned} \quad (5.2.1)$$

obtained from (5.1.1) for specific choice of the constants coefficients. In the classification of Ghidaglia and Saut [71], this is an elliptic-hyperbolic equation since the second order operator acting on  $\Psi$  in the first equation of (5.2.1) is elliptic whereas the one acting on  $\Phi$  in the second equation of (5.2.1) is hyperbolic.

Note that DS I is also interesting from a purely mathematical point of view, since it is a nonlinear dispersive partial differential equation, and since it is one of the few completely integrable equations in two spatial dimensions, see [55, 57]. Local existence results for Cauchy problems with small initial data were proven in [82, 34, 81], and without a smallness assumption in [80].

Below we present some properties of DS I solutions:

- (I) **Translation invariance:** with  $\Psi(t, \xi, \eta)$  a solution to equation (5.2.3), also  $\Psi(t + t_0, \xi + \xi_0, \eta + \eta_0)$  is a solution, where  $t_0, \xi_0,$  and  $\eta_0$  are real constants.
- (II) **Galilei invariance:** with  $\Psi(t, \xi, \eta)$  a solution to equation (5.2.3),  $\Psi(t, \xi - v_\xi t, \eta - v_\eta t) \exp(\frac{i}{2}(v_\xi(\xi - tv_\xi/2) + v_\eta(\eta - tv_\eta/2)))$  with  $v_\xi, v_\eta$  real constants is also a solution. Thus a stationary localized solution can be seen as a soliton to the equation after a Galilei transformation.
- (III) **Scaling invariance:** with  $\Psi(t, \xi, \eta)$  a solution to equation (5.2.3),  $\lambda\Psi(\lambda^2 t, \lambda\xi, \lambda\eta)$  with  $\lambda \in \mathbb{R}/\{0\}$  is also a solution. Note that the  $L^2$  norm of  $\Psi$  is invariant under these rescalings. Therefore these equations are called  $L^2$  critical. Note that these properties apply both to the cubic NLS equation in 2D and to Davey-Stewartson systems. It is known for the NLS equations in this case that there can be a blow-up in finite time of the  $L^\infty$  norm of the solution for smooth initial data with sufficiently large  $L^2$  norm, see [152, 202]. However, there does not appear to be a theorem on whether DS I or DS II solutions can blow up for generic initial data of sufficient mass.

(IV) **Pseudo-conformal invariance:** with  $\Psi(t, \xi, \eta)$  a solution to (5.2.3), also

$$\frac{1}{t}\Psi(1/t, \xi/t, \eta/t) \exp\left(i\frac{\xi^2 + \eta^2}{t}\right)$$

is a solution. This implies together with the translation invariance of DS I that a stationary localized DS I solution under a pseudo-conformal transformation becomes a solution with a blow-up in finite time. This has been used in the context of DS II by Ozawa [173] to construct an explicit blow-up solution. Note that due to the oscillatory terms, the solution will not be in  $H^1(\mathbb{R}^2)$  after a pseudo-conformal transformation even if the original solution is in  $L^2(\mathbb{R}^2)$  for all  $t$ . For standard  $L^2$  critical NLS equations, this blow-up mechanism is unstable, see [202] for references.

The hyperbolic form of the second equation in (5.2.1) makes it convenient to introduce characteristic coordinates

$$\xi = x - y, \quad \eta = x + y. \quad (5.2.2)$$

In these coordinates DS I (5.2.1) takes the form of a non-local nonlinear Schrödinger (NLS) equation,

$$i\Psi_t + 2(\partial_\xi^2 + \partial_\eta^2)\Psi + [(\partial_\xi^{-1}\partial_\eta + \partial_\eta^{-1}\partial_\xi)|\Psi|^2]\Psi = 0, \quad (5.2.3)$$

where we have formally inverted the d'Alembert operator in the second equation of (5.2.1). In order to do so, one has to specify boundary conditions at infinity, a problem analytically discussed in [2] for the multiscales approach to the Kadomtsev-Petviashvili (KP) equation (for a numerical implementation see [102]). In [58] it was shown that *radiating boundary conditions* allow for stable localized travelling waves called *dromions* which appear in the long-time behaviour of the solutions to certain initial value problems for DS I. Another possibility applied in this context are vanishing boundary conditions for  $\Phi$  in (5.2.1) for  $\xi, \eta \rightarrow -\infty$  (or  $\xi, \eta \rightarrow \infty$ ). We define the operator  $\partial_\xi^{-1}$  (as is standard for the KP equation) via its Fourier symbol,

$$\partial_\xi^{-1} = \mathcal{F}_\xi^{-1} \frac{1}{ik_\xi} = \frac{1}{2}\mathcal{P} \left( \int_{-\infty}^\xi - \int_\xi^\infty \right), \quad (5.2.4)$$

where  $\mathcal{P}$  denotes the *Cauchy principal value*<sup>1</sup> and  $\mathcal{F}_\xi$  the Fourier transform in  $\xi$  with  $k_\xi$  being the dual Fourier variable, and likewise for  $\partial_\eta^{-1}$ . Note that a consequence of this

---

<sup>1</sup>The Cauchy principle value approach is used for singular integrals, e.g. the integral  $\int_a^b u(x)dx$  with singular value at  $b$  has its Cauchy principal value defined as  $\lim_{\varepsilon \rightarrow 0^+} \left\{ \int_a^{c-\varepsilon} u(x)dx + \int_{c+\varepsilon}^b u(x)dx \right\}$  for  $a < c < b$ .

definition is that for  $f \in L^1(\mathbb{R})$ , one has

$$(\partial_\xi^{-1} f(\xi))(+\infty) = -(\partial_\xi^{-1} f(\xi))(-\infty) = \frac{1}{2} \int_{-\infty}^{\infty} f(\xi) d\xi. \quad (5.2.5)$$

These *trivial boundary conditions*<sup>2</sup> will be the only ones studied in this work. Numerical studies of DS I solutions have been mainly performed for radiating boundary conditions, see [221, 167, 168, 14, 143]. In this part we will perform a similar study, but for the trivial boundary conditions (5.2.4). Since no explicit solitons are known for this case, we first construct localized stationary solutions numerically and show that they are also exponentially localized. We study the stability of these solutions, which we will also call dromions for simplicity.

In [93, 95] it is shown how to regularize terms of the type (5.2.4) arising in the context of D-bar equations with a hybrid approach: we subtract a singular term for which the Fourier transform can be analytically found. The term is chosen in a way that what is left is smooth *within finite numerical precision*, and that its Fourier transform can be numerically computed (we work here with *double precision* which is roughly of the order of  $10^{-16}$ ). Note that the terms treated in this way in [93, 95, 94] are less singular (they lead to cusps in the Fourier domain, but are bounded) than the simple poles considered here. Therefore, the regularization approach for DS I is more important than for DS II if high accuracy is to be achieved. We show that we can reach machine precision in the studied examples. Since we want to numerically study blow-up scenarios, an approach of high accuracy as presented here is crucial in order to obtain reliable results.

### 5.2.1 Main Results: Conjectures

With this particular numerical approach, we first construct numerically localized stationary solutions to DS I and propose

**Conjecture 5.2.1 (Main Conjecture (Part I)).** *The DS I equation has stationary solutions  $\Psi(\xi, \eta, t) = Q_\omega(\xi, \eta)e^{i\omega t}$  for  $\omega > 0$ , where  $Q_\omega$  can be chosen to have values in  $\mathbb{R}^+$ . The solutions are exponentially localized.*

It is unknown whether these solutions are ground states for the energy (5.2.8). Then we study the time evolution of localized perturbations of these stationary solutions and

---

<sup>2</sup>The general boundary conditions are described by the arbitrary functions  $f(\xi)$  and  $g(\eta)$  fixable for a boundary value problem (compare with (1.1.3) for classical wave equation in the introduction chapter and how  $f$  and  $g$  are fixed). For  $\xi, \eta \rightarrow \pm\infty$  we have  $\partial_\xi^{-1} \rightarrow \tilde{\partial}_\xi^{-1} + f(\eta)$  and  $\partial_\eta^{-1} \rightarrow \tilde{\partial}_\eta^{-1} + g(\xi)$ . The trivial boundary conditions correspond to  $\Phi(\xi = \pm\infty, \eta) = 0$  and  $\Phi(\xi, \eta = \pm\infty) = 0$ , i.e.  $\partial_\eta^{-1} \rightarrow 0$  and  $\partial_\xi^{-1} \rightarrow 0$  resp., while radiating (non-trivial) boundary conditions are  $\Phi(\xi = \pm\infty, \eta) = f(\eta)$  and  $\Phi(\xi, \eta = \pm\infty) = g(\xi)$ , i.e.  $\partial_\xi^{-1} \rightarrow f(\eta)$  and  $\partial_\eta^{-1} \rightarrow g(\xi)$  resp. Moreover, the main-field  $\Psi(t, \xi, \eta) \rightarrow 0$  as  $\eta^2 + \xi^2 \rightarrow \infty$ .

initial data from the Schwartz class  $\mathcal{S}(\mathbb{R}^2)$  of rapidly decreasing smooth functions with a single hump. We find

**Conjecture 5.2.2 (Main Conjecture (Part II)).** *Initial data  $\Psi(\xi, \eta, 0) \in \mathcal{S}(\mathbb{R}^2)$  with a single hump lead to one of the following 3 cases:*

- if  $\Psi(\xi, \eta, 0) = Q_\omega(\xi, \eta)$ , the DS I solution is stationary;
- if the mass  $\|\Psi(\xi, \eta, 0)\|_2^2 < m_Q := \|Q\|_2^2$  ( $Q := Q_1$ ), the solution is simply dispersed to infinity;
- if the mass  $\|\Psi(\xi, \eta, 0)\|_2^2 > m_Q$ , there is a blow-up of the  $L^\infty$  norm of  $\Psi$  at a finite time  $t^*$  such that

$$|\Psi(\xi, \eta, t)| = \frac{Q(X, Y)}{L(t)} + P(\xi, \eta, t), \quad (5.2.6)$$

where  $X, Y$  are defined in (5.2.12), where  $\|P\|_2 < \infty$  for all times, and where

$$L(t) \propto t^* - t. \quad (5.2.7)$$

This means that as in the DS II case conjectured in [105], the blow-up is of the type being unstable for standard NLS equations.

## 5.2.2 DSI: Basic Facts

In this section we collect some basic facts on the DS I equation.

We will always study the DS I equation in characteristic coordinates, i.e., in the form (5.2.3) of a non-local NLS equation. Note that the sign of the nonlinearity is not important as in the case of the DS II equations, where it distinguishes a focusing and defocusing variant of the equation, see e.g., [98]. For DS I, a change of sign of the nonlinearity can be compensated by a change of sign of either  $\xi$  or  $\eta$  and does not affect the behaviour of the solutions otherwise.

The DS I equation is completely integrable and thus has an infinite number of formally conserved quantities. In this section, we will consider the  $L^2$  norm and the *energy*

$$E = \int_{\mathbb{R}^2} d\xi d\eta \left\{ |\Psi_\xi|^2 + |\Psi_\eta|^2 + \frac{1}{4} \left( \partial_\eta^{-1} |\Psi|^2 \partial_\xi |\Psi|^2 + \partial_\xi^{-1} |\Psi|^2 \partial_\eta |\Psi|^2 \right) \right\}. \quad (5.2.8)$$

This form of the energy has been chosen in accordance to the definition of the anti-derivatives (5.2.4). It can be shown by direct computation that the energy is conserved in this case.

The DS I equation is expected to have stationary solutions of the form  $\Psi(\xi, \eta, t) = Q_\omega(\xi, \eta)e^{i\omega t}$ , where  $\omega \in \mathbb{R}^+$ , and where we get with (5.2.3) the following equation for  $Q$ ,

$$-\omega Q + 2(\partial_\xi^2 + \partial_\eta^2)Q + [(\partial_\xi^{-1} \partial_\eta + \partial_\eta^{-1} \partial_\xi)|Q|^2]Q = 0. \quad (5.2.9)$$

We are interested in localized solutions to this equation. Note that if the solution  $Q := Q_1$  of (5.2.9) is known for  $\omega = 1$ , the solution for arbitrary  $\omega > 0$  follows from  $Q_\omega = \sqrt{\omega}Q(\sqrt{\omega}\xi, \sqrt{\omega}\eta)$ . For the same reasons as for the standard NLS equation,  $Q$  can be chosen to be real for localized solutions of this equation. Note that there is an explicit solution to (5.2.9) called dromion [109], which reads for  $\omega = 1$

$$\tilde{Q} = \frac{1}{4 \cosh \xi/2 \cosh \eta/2 + e^{(\xi+\eta)/2}}, \quad (5.2.10)$$

if radiating boundary conditions at infinity are used, i.e., if

$$\partial_\xi^{-1} \mapsto \tilde{\partial}_\xi^{-1} + f(\eta), \quad \partial_\eta^{-1} \mapsto \tilde{\partial}_\eta^{-1} + f(\xi),$$

where

$$f(\xi) = \frac{4}{4(1+e^\xi)} + \frac{1}{4(1+2e^\xi)}. \quad (5.2.11)$$

Here the anti-derivatives for the radiating boundary conditions are denoted with a tilde, the difference to the anti-derivatives for the trivial boundary conditions (without tilde) used just being the functions  $f(\xi)$  and  $f(\eta)$  of (5.2.11). It is remarkable that the dromions are exponentially decaying towards infinity in all directions in contrast to the lump solution, the localized stationary solution to DS II which has an algebraic decrease towards infinity. Furthermore, again in contrast to the lump, the dromion is not radially symmetric. Note that it is unknown whether there is an exponentially localized solution to (5.2.9) for trivial boundary conditions at infinity.

The generic blow-up mechanism for NLS solutions is self-similar, which means one uses the above scaling invariance in  $\lambda$  with a time dependent factor  $L(t)$  in a *dynamic rescaling*,

$$X = \frac{\xi}{L(t)}, \quad Y = \frac{\eta}{L(t)}, \quad \tau = \int_0^t \frac{dt'}{L^2(t')}, \quad \psi(X, Y, \tau) = L(t)\Psi(\xi, \eta, t). \quad (5.2.12)$$

The dynamically rescaled DS I equation (5.2.3) then reads

$$i\psi_\tau + ia(X\partial_X\psi + Y\partial_Y\psi + \psi) + 2(\partial_X^2 + \partial_Y^2)\psi + [(\partial_X^{-1}\partial_Y + \partial_Y^{-1}\partial_X)|\psi|^2]\psi = 0, \quad (5.2.13)$$

where  $a = \partial_\tau \ln L$ . In the case of a blow-up, the scaling factor  $L(t)$  is chosen in a way to keep certain norms constant during the time-evolution, for instance the  $L^\infty$  norm of  $\psi$ . If the blow-up is reached for a finite time  $t^*$ , then  $\lim_{t \rightarrow t^*} L(t) = 0$  and  $\lim_{t \rightarrow t^*} \tau = \infty$ . For  $L^2$  critical NLS equations, it is expected that  $\lim_{t \rightarrow t^*} a(t) = 0$ . In this case, equation (5.2.13) reduces to the equation for the stationary solution (5.2.9) in the limit which would indicate that the blow-up is self-similar with  $Q$  giving the blow-up profile. Note, that the generic

blow-up rate for  $L^2$  critical NLS is given by (see [63, 126, 152, 153])

$$L(t) \propto \sqrt{\frac{t^* - t}{\ln |\ln(t^* - t)|}}. \quad (5.2.14)$$

One of the questions to be addressed in this section numerically is whether there is blow-up in DS I solutions, and whether it follows the behaviour (5.2.14) or the pseudoconformal rate as in DS II, see the conjecture in [105]. To this end we will trace the  $L^\infty$  norm of  $\Psi$  and the  $L^2$  norm of  $\Psi_\xi$ . Both are proportional to  $1/L(t)$  and can thus be used to identify the scaling factor  $L(t)$ .

**Remark 5.2.1.** In the numerical study in the following sections, we will always use the not rescaled DS I system. The reason for this is that radiation leads for the equations (5.2.13) to problems at the boundaries of the computational domain because of the terms  $X\partial_X\psi + Y\partial_Y\psi$  as discussed in detail in [100] for generalized Korteweg-de Vries equations; being the reason why dynamic rescaling is not possible for the DS I. Whereas such problems can be controlled for NLS equations, the nonlocality in DS systems is an issue in this context. Thus we have shown for DS II in [105] that a direct integration of DS yields the same information on a blow-up after a postprocessing of the data according to (5.2.13). The same approach will also be applied here.

### 5.2.3 Numerical approach for DS I

In this section we briefly describe the numerical approach for the DS I equation, in particular how the antiderivatives in (5.2.3) are computed. We will concentrate here on functions in the Schwartz class  $\mathcal{S}$  of smooth, rapidly decreasing functions.

The Fourier transform of a 1D function  $f(\xi)$  and its inverse are defined via

$$\begin{aligned} \hat{f}(k_\xi) &= \mathcal{F}_\xi f := \int_{\mathbb{R}} e^{-i\xi k_\xi} f(\xi) d\xi, \\ f(\xi) &= \mathcal{F}_\xi^{-1} f = \frac{1}{2\pi} \int_{\mathbb{R}} e^{i\xi k_\xi} \hat{f}(k_\xi) dk_\xi. \end{aligned} \quad (5.2.15)$$

The 2D Fourier transform of a function  $\Phi(\xi, \eta)$  is defined as

$$\begin{aligned} \hat{\Phi}(k_\xi, k_\eta) &= \mathcal{F}_{\xi\eta} \Phi := \int_{\mathbb{R}^2} \Phi(\xi, \eta) e^{-i(\xi k_\xi + \eta k_\eta)} d\xi d\eta, \\ \Phi(\xi, \eta) &= \mathcal{F}_{\xi\eta}^{-1} \Phi = \frac{1}{(2\pi)^2} \int_{\mathbb{R}^2} e^{i(\xi k_\xi + \eta k_\eta)} \hat{\Phi}(k_\xi, k_\eta) dk_\xi dk_\eta. \end{aligned} \quad (5.2.16)$$

The basic idea of the Fourier spectral method, which we are going to apply here, is to express every function in terms of a Fourier series and approximate the latter via a

truncated Fourier series. This is equivalent to approximating the Fourier transform (5.2.15) via a *discrete Fourier transform* which can be efficiently computed via a *fast Fourier transform* (FFT). It is well known that the Fourier coefficients of an analytic periodic function decrease exponentially, and thus the numerical error due to the truncation of the series will also decrease exponentially, see for instance the discussion in [208]. Thus Fourier spectral methods show exponential convergence for analytic functions, sometimes called *spectral convergence*. Here we only consider functions in the Schwartz class which can be efficiently treated as smooth periodic functions on sufficiently large tori within the chosen finite numerical precision (the function and all relevant derivatives have to vanish at the domain boundaries to the chosen numerical precision, here  $10^{-16}$ ).

Derivatives of a function  $f(\xi) \in \mathcal{S}(\mathbb{R})$ , i.e.,

$$f'(\xi) = \mathcal{F}_\xi^{-1}(ik_\xi \hat{f}(k_\xi)),$$

can then be approximated as mentioned above by approximating the standard Fourier transform via a discrete Fourier transform. However, for the antiderivative

$$\partial_\xi^{-1} f(\xi) = \mathcal{F}_\xi^{-1} \left( \frac{1}{ik_\xi} \hat{f}(k_\xi) \right),$$

the singular Fourier symbol will not lead to an exponentially decreasing numerical error if the Fourier transform is approximated via an FFT (it follows from a Payley-Wiener type argument that the singular symbol of the anti-derivative that the latter is not generically in the Schwartz class). Thus we use a hybrid approach, a combination of numerical and analytical techniques, similar to the approach in [94] for the DS II equation. Concretely we write

$$\mathcal{F}_\xi^{-1} \left( \frac{1}{ik_\xi} \hat{f}(k_\xi) \right) = \mathcal{F}_\xi^{-1} \left( \frac{\hat{f}(k_\xi) - \hat{f}(0) \exp(-k_\xi^2/4)}{ik_\xi} \right) + \hat{f}(0) \frac{1}{2} \text{erf}(\xi), \quad (5.2.17)$$

where the *error function*  $\text{erf}(x)$  is defined as

$$\text{erf}(x) = \frac{2}{\sqrt{\pi}} \int_0^x \exp(-y^2) dy. \quad (5.2.18)$$

The error function can be computed to machine precision with the techniques of [104] since the integral is essentially a Hilbert transform in Fourier space. But for simplicity we use the Matlab implementation of the error function here.

The first term on the right hand side of (5.2.17) is a smooth function if the limit

$$\lim_{k_\xi \rightarrow 0} \frac{\hat{f}(k_\xi) - \hat{f}(0) \exp(-k_\xi^2)}{ik_\xi} = \frac{\hat{f}'(0)}{i} \quad (5.2.19)$$

is taken into account via de l'Hospital's rule. Since  $\hat{f}'(0) = \int_{\mathbb{T}} i\xi f(\xi) d\xi$ , this term can be computed again with Fourier techniques (just the sum of  $\xi f(\xi)$  sampled on the collocation points). In this way the first term on the right hand side of (5.2.17) is in the Schwartz class if  $f(\xi)$  is. Thus it can be efficiently computed with Fourier techniques on a large enough torus. Note that a Gaussian was introduced in (5.2.17) in order to have an integrand in the Schwartz class to ensure the rapid convergence of the numerical approach. Thus the first term in (5.2.17) is computed to machine precision with Fourier techniques whereas the second is obtained with a Matlab algorithm with the same precision.

We illustrate the efficiency of the algorithm for some examples: for a Gaussian  $f(\xi) = \exp(-(\xi+1)^2)$  we work with  $N = 2^9$  Fourier modes on the interval  $10[-\pi, \pi]$ . In this case the Fourier coefficients decrease to machine precision. Note that we have considered a shifted Gaussian here in order to have a non-vanishing derivative at the origin in (5.2.19). The difference between the error function (times the factor  $\sqrt{\pi}/2$ ) is of the order of  $10^{-16}$ . If we consider with the same numerical parameters  $f(\xi) = \sinh(\xi + 1)/\cosh(\xi + 1)^2$ , the Fourier coefficients decrease to the order of  $10^{-14}$ , and the difference to the exact anti-derivative  $-\text{sech}(\xi + 1)$  is of the same order.

In the context of DS I, we are obviously mainly interested in the accurate numerical computation of the action of the operator  $\partial_\xi^{-1}\partial_\eta + \partial_\eta^{-1}\partial_\xi$  on some function in  $\mathcal{S}(\mathbb{R}^2)$ . To this end we simply apply the above approach in both dimensions. As an example we consider the dromion solution  $\tilde{Q}_2$  for  $\omega = 2$  in the case of radiating boundary conditions,

$$|\tilde{Q}_2|^2 = \frac{4}{(4 \cosh(\xi) \cosh(\eta) + \exp(\xi + \eta))^2}. \quad (5.2.20)$$

The action of the operator  $\partial_\xi^{-1}\partial_\eta + \partial_\eta^{-1}\partial_\xi$  on the dromion can be obviously computed explicitly. We work with  $N_\xi = N_\eta = 2^9$  Fourier modes in  $\xi$  and  $\eta$  respectively  $\partial_\xi^{-1}\partial_\eta + \partial_\eta^{-1}\partial_\xi$  on  $10[-\pi, \pi] \times 10[-\pi, \pi]$ . The Fourier coefficients of the function (5.2.20) can be seen on the left of Fig. 5.1. They decrease to machine precision. The difference (denoted by err) between the numerically computed action of the operator  $\partial_\xi^{-1}\partial_\eta + \partial_\eta^{-1}\partial_\xi$  on (5.2.20) and the exact expression can be seen on the right of the same figure. It is as expected of the same order ( $10^{-15}$ ) as the highest Fourier coefficients.

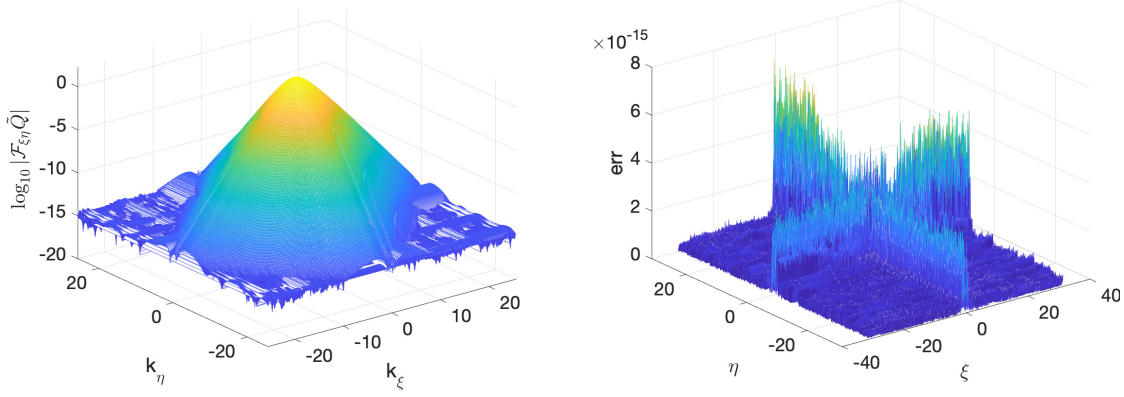


Figure 5.1: The Fourier coefficients of the function (5.2.20) on the left, and the difference of the numerically computed action of the operator  $\partial_\xi^{-1}\partial_\eta + \partial_\eta^{-1}\partial_\xi$  on (5.2.20) and the exact expression on the right.

#### 5.2.4 Localized stationary DS I solutions

In this section we numerically construct stationary localized solutions to DS I. This is done with the Fourier discretisation introduced in the previous section for equation (5.2.9) with  $\omega = 1$ . The resulting algebraic equation is then iteratively solved with a Newton-Krylov method.

The task is to find a localized solution to (5.2.9) where we restrict ourselves to  $\omega = 1$  without loss of generality. In Fourier space, equation (5.2.9) reads

$$(1 + 2k_\xi^2 + 2k_\eta^2)\hat{Q} = \mathcal{F}_{\xi\eta} \left( [(\partial_\xi^{-1}\partial_\eta + \partial_\eta^{-1}\partial_\xi)|Q|^2]Q \right). \quad (5.2.21)$$

As in the previous section, the Fourier transform is approximated via a discrete Fourier transform. This implies that (5.2.21) leads to an  $N_\xi N_\eta$  dimensional nonlinear equation system of the form  $F(\{\hat{Q}\}) = 0$  for  $\hat{Q}$  (in an abuse of notation, we denote the discrete Fourier transform as the standard Fourier transform). This system is solved iteratively with a Newton method,

$$\hat{Q}^{(n+1)} = \hat{Q}^{(n)} - \text{Jac}(F)^{-1}|_{\hat{Q}^{(n)}} F(\hat{Q}^{(n+1)}). \quad (5.2.22)$$

The action of the Jacobian on  $F$  is computed with the Krylov subspace method GMRES [194]. Note that the Jacobian has a finite dimensional kernel because of the translation invariance of the DS I equation. But the iteration converges nonetheless, just the maximum of the resulting solution  $Q$  will in general not be at the origin. In the plots below we have shifted the maximum back to the origin.

We use  $N_\xi = N_\eta = 2^{10}$  Fourier modes for  $(\xi, \eta) \in 20[-\pi, \pi] \times 20[-\pi, \pi]$  and  $Q^{(0)} = 6/(4 \cosh(\xi/2) \cosh(\eta/2) + \exp((\xi + \eta)/2))$  as the initial iterate, i.e., 6 times the dromion (5.2.10) for radiating boundary conditions. The iteration is stopped once  $\|F\|_\infty < 10^{-10}$ . The resulting solution can be seen in Fig. 5.2 on the left.

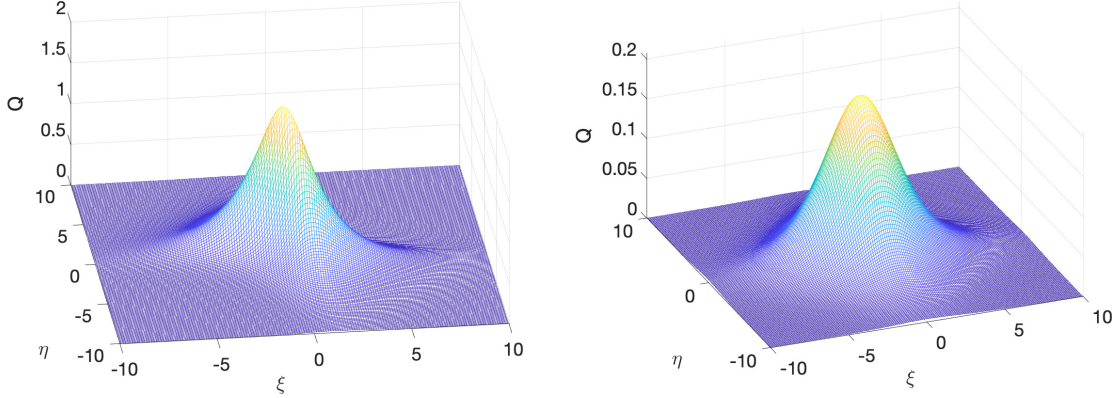


Figure 5.2: Localized stationary solution to DS I (5.2.9) for  $\omega = 1$  on the left, dromion solution (5.2.10) for radiating boundary conditions on the right.

The solution on the left of Fig 5.2 is again not radially symmetric, but has a symmetry with respect to an exchange of  $\xi$  and  $\eta$  as can be clearly seen from the contour plot on the left of Fig. 5.3. The Fourier coefficients of the solution on the right of the same figure decrease to machine precision and thus indicate that the solutions is numerically well resolved. In fact the numerical parameters have been chosen in a way to ensure this. Note that the

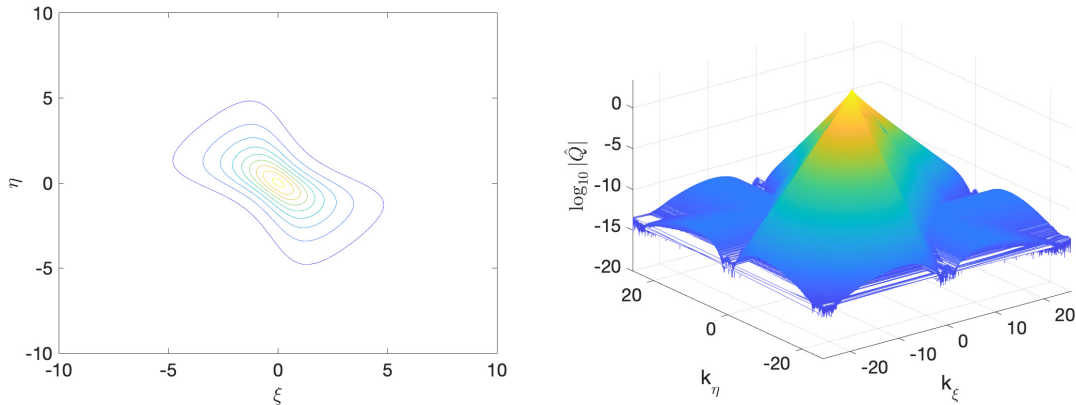


Figure 5.3: Contour plot of the solution in Fig. 5.2 on the left, and its Fourier coefficients on the right.

solution is much more peaked than the corresponding one (5.2.10) for radiating boundary

conditions which can be seen on the left of Fig. 5.4. In the middle of the same figure, we show the solution of Fig. 5.2 and (5.2.10) on the  $\xi$ -axis in one figure. Obviously the solution constructed in this section has a considerably larger maximum (which is why the initial iterate had to be chosen with a factor of 6). It is also more slowly decaying. However, it is also exponentially decaying as can be seen from the logarithmic plot on the right of Fig. 5.4 on the  $\xi$ -axis. We only show the plot on the  $\xi$ -axis here, but the same behaviour is observed for all values of  $\eta$ , and for the  $\eta$ -dependence for all values of  $\xi$ . Thus the stationary solutions to DS I are exponentially localized in contrast to the lumps of DS II which are algebraically decaying, and this not only for radiating boundary conditions. Therefore we will call this solution also dromion in the following even though it is not identical to the classical one in (5.2.10). Note that the numerical parameters in this section have been chosen in a way that both the solution and its Fourier coefficients decrease to machine precision.

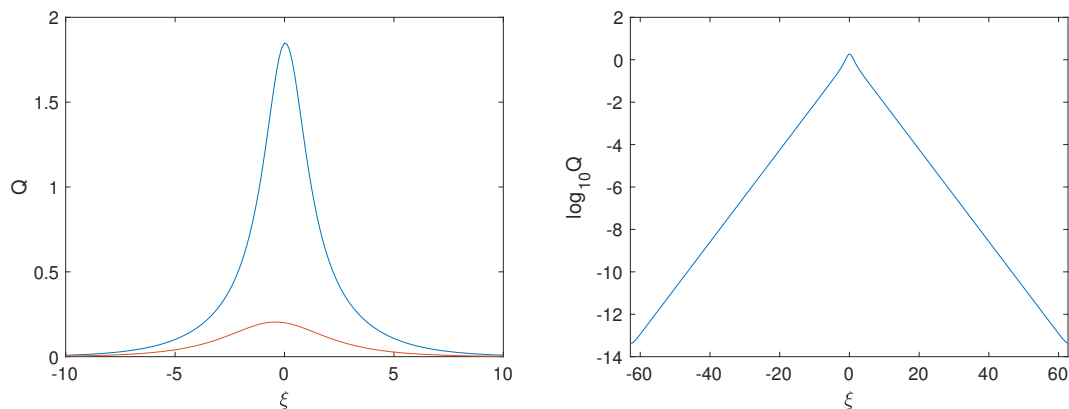


Figure 5.4: The solution  $\tilde{Q}$  of Fig. 5.2 on the right on the  $\xi$ -axis (red) together with the  $Q$  of Fig. 5.2 (blue) on the left, and a logarithmic plot of the solution of Fig. 5.2 on the  $\xi$ -axis on the right.

### 5.2.5 Time evolution

In this section we outline how the time integration of DS I is handled for the discretisation in the spatial coordinates explained in the previous sections. We discuss how the accuracy of the time integration is controlled and test the code for the example of the stationary solution of the previous section.

We work on  $\mathbb{R} \times \mathbb{T}_\xi \times \mathbb{T}_\eta$  where  $\mathbb{T}_\xi = \mathbb{R}/(2\pi L_\xi \mathbb{Z})$ ,  $\mathbb{T}_\eta = \mathbb{R}/(2\pi L_\eta \mathbb{Z})$ . After the FFT discretisation in  $\xi$  and  $\eta$  of the previous sections, the DS I equation (5.2.3) becomes an  $N_\xi N_\eta$  dimensional system of ordinary differential equations of the form (in an abuse of

notation, we denote the  $N_\xi \times N_\eta$  matrix obtained for  $\Psi(\xi, \eta)$  with the same symbol)

$$\hat{\Psi}_t = \mathcal{L}\hat{\Psi} + \mathcal{N}(\Psi), \quad (5.2.23)$$

where

$$\mathcal{L} = -2i(k_\xi^2 + k_\eta^2), \quad \mathcal{N} = i\mathcal{F}_{\xi\eta} \left( [(\partial_\xi^{-1}\partial_\eta + \partial_\eta^{-1}\partial_\xi)|\Psi|^2]\Psi \right). \quad (5.2.24)$$

The linear part proportional to  $\mathcal{L}$  is diagonal and *stiff* since it is quadratic in  $k_\xi$  and  $k_\eta$ , which means that explicit time integration schemes are not efficient. For such cases there are many efficient time integration schemes, see for instance the references in [92, 101]. Since it was found in [101] that Driscoll's composite Runge-Kutta method [44] is very efficient for DS equations, we apply it also here.

We use the relative conservation of the mass to control the accuracy in the time integration. Because of unavoidable numerical errors, the numerically computed mass will depend on time even though it is a conserved quantity. Thus  $\Delta = \log_{10} |1 - m/m_0|$ , where  $m_0$  is the initial mass and  $m$  the computed mass can be used to control the accuracy of the temporal discretisation. As discussed in detail in [101],  $\Delta$  overestimates the temporal resolution by two orders of magnitude. The relative mass conservation stays well below  $10^{-12}$  throughout most of the runs and sharply increases close to the time  $t^*$  of a potential finite time blow-up. Such a jump indicates a loss of precision, and we generally discard results with a value of  $\Delta$  greater than  $-3$ . Note that we could also use the conserved energy (5.2.8) to this end, but the anti-derivatives in (5.2.8) make this quantity numerically problematic if resolution in Fourier space is lost near a blow-up. The effect is worse for the energy than for the DS I solution since in the latter, the anti-derivative  $\partial_\xi^{-1}$  is multiplied with  $\partial_\eta$  which has a smoothing effect in the space of Fourier coefficients. Thus the energy would underestimate the accuracy near a blow-up which is why we use only mass conservation in the following, where such problems do not appear.

As an example we consider the dromion constructed in the previous section as initial data for DS I. We use  $N_t = 10^3$  time steps for  $t \leq 1$ . The relative conservation of the mass is always to the order of  $10^{-15}$  (the relative energy conservation is of the same order since the solution is fully resolved in Fourier space during the whole computation). Note that the solution is not static, there is a harmonic time dependence. We show the difference between the initial data times  $\exp(it)$  and the numerical DS I solution in Fig. 5.5, on the left the  $L^\infty$  norm of the difference between both solutions in dependence of time, on the right the modulus of the difference for  $t = 1$  (where the difference is denoted with 'err').

It can be seen that the difference is during the whole computation of the order of  $10^{-12}$  or better which is a remarkable result since it not only shows the accuracy of the

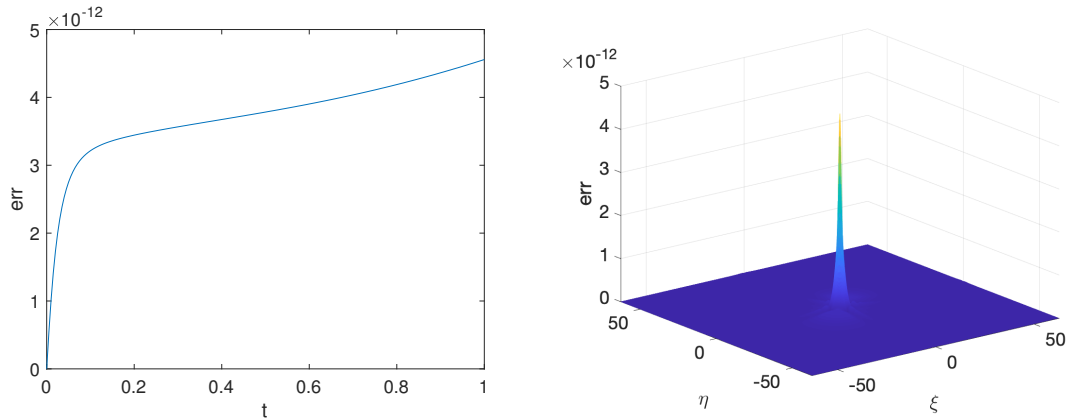


Figure 5.5: Difference of the DS I solution for the initial data  $\Psi(\xi, \eta, 0) = Q(\xi, \eta)$  and  $Qe^{it}$ , on the left the  $L^\infty$  norm of the difference in dependence of time where  $\text{err} = \|\Psi(t, \xi, \eta) - e^{it}Q(\xi, \eta)\|_\infty$ , on the right is just the difference for  $t = 1$ .

time evolution code, but also of the dromion numerically constructed in the previous section. It also shows that the dromion can be stably evolved in time although, as we will show in the following section, it is unstable against perturbations.

### 5.2.6 Time evolution of the dromion

In this section we study localized perturbations of the dromion, mainly of the form

$$\Psi(\xi, \eta, 0) = \mu Q, \quad \mu > 0. \quad (5.2.25)$$

It is shown that perturbations with a mass smaller than the mass of the dromion are just dispersed, whereas perturbations with a mass larger than the dromion will have a blow-up in finite time.

We first consider the case  $\mu = 0.9$  in (5.2.25) with  $N_\xi = N_\eta = 2^{10}$  Fourier modes and  $(\xi, \eta) \in 20[-\pi, \pi] \times 20[-\pi, \pi]$ , and with  $N_t = 5000$  time steps for  $t \leq 5$ . In this case the initial hump simply gets dispersed, it gets wider and flatter over time. The solution for  $t = 5$  can be seen on the left of Fig. 5.6. On the right of the same figure the  $L^\infty$  norm of the solution appears to be decreasing monotonically. Note that since we approximate a situation on  $\mathbb{R}^2$  with a setting on  $\mathbb{T}^2$ , radiation cannot escape to infinity and thus cannot leave the computational domain. Thus the solution cannot tend to zero even for longer times. However we do not find an indication of a stable structure in DS I solutions for trivial boundary conditions, in contrast to the result in [58] for radiative boundary conditions.

Then we use the same numerical parameters for the initial data  $\Psi(\xi, \eta, 0) = Q -$

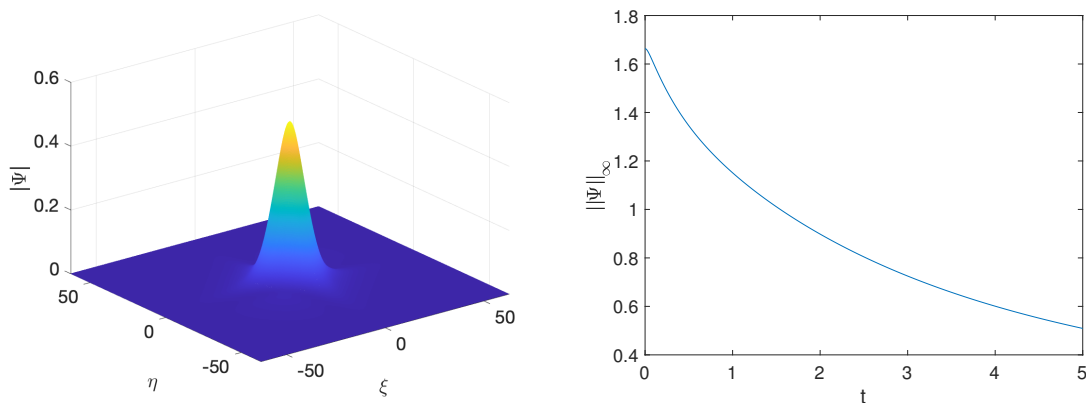


Figure 5.6: Solution to DS I for the initial data  $\Psi(\xi, \eta, 0) = 0.9Q$ , on the left for  $t = 5$ , on the right the  $L^\infty$  norm in dependence of time.

$0.1 \exp(-\xi^2 - \eta^2)$ . Note that the mass of these data is roughly  $0.96M_Q$  where  $M_Q$  is the mass of the dromion and thus larger than the mass in Fig. 5.6. We show the solution for  $t = 5$  on the left of Fig. 5.7. Again the initial hump gets just dispersed. This is also confirmed by the  $L^\infty$  norm of the solution on the right of the same figure which after some initial oscillation appears to be monotonically decreasing.

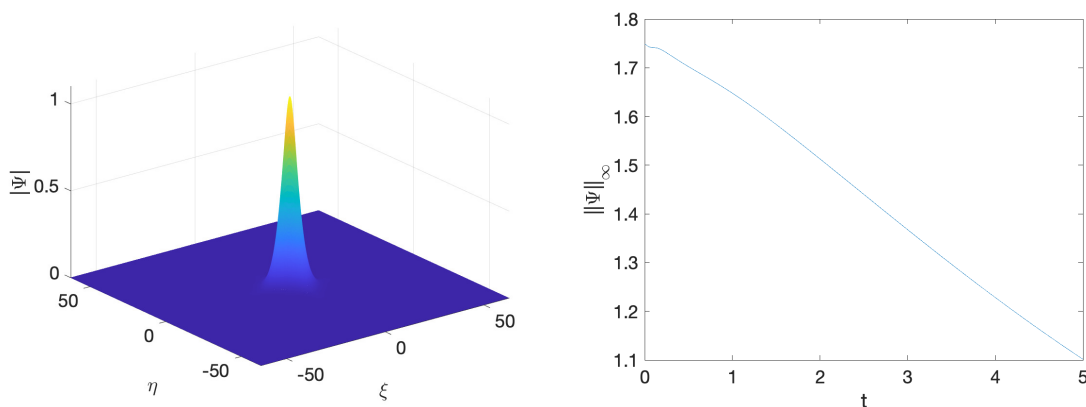


Figure 5.7: Solution to DS I for the initial data  $\Psi(\xi, \eta, 0) = Q - 0.1 \exp(-\xi^2 - \eta^2)$ , on the left for  $t = 5$ , on the right the  $L^\infty$  norm in dependence of time.

The situation changes considerably if we consider perturbations of the dromion with larger mass. Here the  $L^\infty$  norm appears to diverge in finite time which obviously cannot be captured numerically. However we will trace certain norms in this case and fit the found results to the self similar model (5.2.12) for blow-up. This allows us to extend data from the region, where the numerical error is still controlled to essentially the full blow-up scenario,

i.e., to identify the blow-up time  $t^*$  as well as the blow-up rate.

Nonetheless the numerical treatment of a blow-up is a delicate problem. In order to capture the phenomena, we need to make sure to have enough numerical resolution to get close enough to the blow-up in order to identify the mechanism. As before, we use  $L_\xi = L_\eta = 20$ , but now with  $N_\xi = N_\eta = 2^{12}$  Fourier collocation points in each direction. High-index Fourier coefficients, which are used to estimate the space resolution, stay below machine precision throughout the run. In time we use two consecutive runs, one up to  $\sim 0.9t^*$ , and a second one, with a much finer time step that runs beyond the  $t^*$  as estimated from the first run.

In Fig. 5.2.6 we show on the left the  $L^\infty$  norm of the solution which appears to indicate a finite time blow-up. On the right we trace the quantity  $\Delta$  indicating the relative conservation of the computed mass. It can be seen to be conserved to better than  $10^{-5}$  during the whole computation. We show the solution close to the blow-up in Fig. 5.2.6.

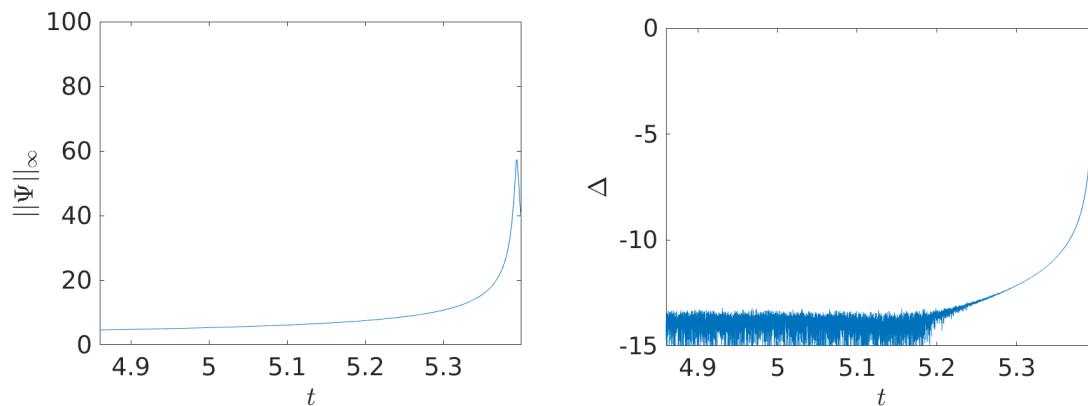


Figure 5.8: DSI solution close to blow-up for initial data  $\Psi(\xi, \eta, 0) = 1.1Q$ . On the left the evolution of the  $L^\infty$  norm of the solution, on the right the conservation of mass  $\Delta = \log_{10}(1 - m(t)/m(0))$ , which stays below  $-14$  until we get close to the critical time. The fitted blow-up time is  $t^* = 5.332$ .

To study the mechanism of the blow-up, we trace the  $L^\infty$  norm of the solution as well as the  $L^2$  norm of the  $\xi$  derivative. The fitting of these norms is done for the last several thousand recorded time steps before we start losing temporal resolution. Further we use stabilization of the fit to more precisely judge the data cut off point. Concretely we fit the logarithm of the considered norms, for instance the  $L^\infty$  norm according to  $\ln \|\Psi\|_\infty = a \ln(t^* - t) + b$  (and similarly for  $\|\Psi_\xi\|_2$ ). The fitting is performed with the algorithm [162] implemented in Matlab as the command `fminsearch`. For the example with the initial data  $1.1Q$ , the results can be seen in Fig. 5.10.

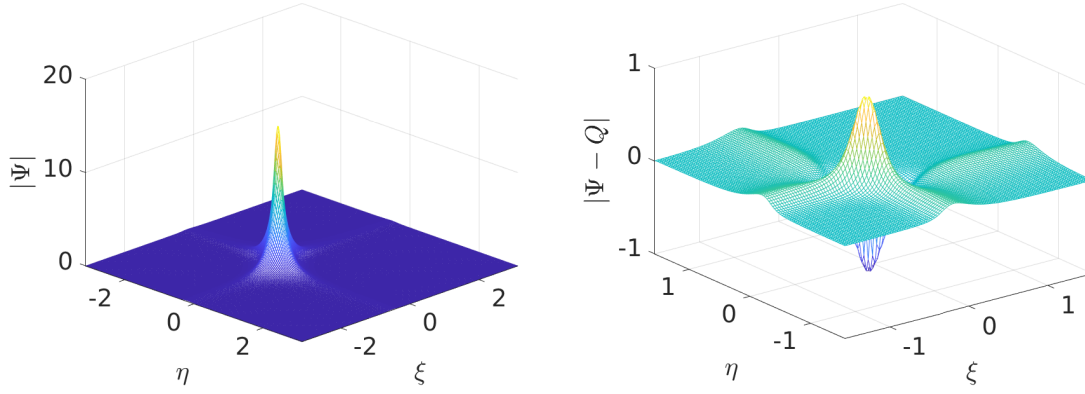


Figure 5.9: Left: DSI solution close to blow-up for initial data for  $\Psi(\xi, \eta, 0) = 1.1Q$ . Right: Difference of the DS I solution close to blow-up and a scaled dromion.

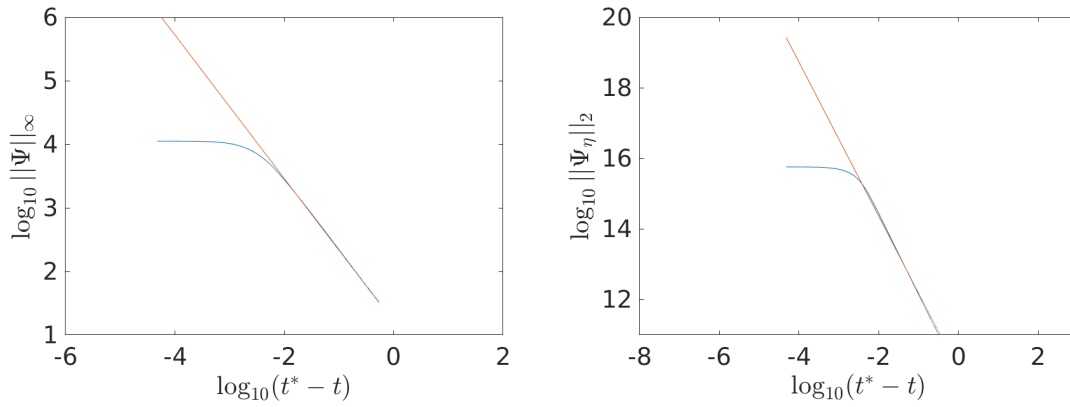


Figure 5.10: Blow-up rate for initial data  $\Psi(\xi, \eta, 0) = 1.1Q$ . On the left  $\|\Psi\|_\infty$ , the red lines have the form  $a \log_{10}(t^* - t) + b$ , with values obtained by fitting the last several thousand points before we lose precision,  $a_\infty = 1.13$ ,  $a_{\Psi_x} = 2.18$  and  $b_\infty = 1.2$ ,  $b_{\Psi_x} = 10.0$  and  $t^* = 0.5394$ .

The asymptotic profile of the solution appears to be a scaled dromion according to (5.2.12) as can be seen from Fig. 5.2.6. The residual  $P$  is defined in (5.2.6), and the  $L$  in the rescaled dromion there is determined via  $\max(Q)/\max(\Psi)$ . It can be seen in Fig. 5.2.6 that  $P$  is of the order of 10% of the maximum of the fitted solution which shows that one cannot get arbitrarily close to the blow-up numerically, but sufficiently to identify the asymptotic profile.

Note that one can also fit a phase factor  $\phi_0$  in  $\Psi \sim \frac{Q(X,Y)}{L(t)} e^{i\phi}$  which can be determined once more at the maximum of  $\Psi$ . The residual  $\Psi \sim \frac{Q(X,Y)}{L(t)} e^{i\phi}$  is very similar in modulus to the modulus of the residual in the Fig. 5.2.6 on the right.

### 5.2.7 Gaussian initial data

In this section, we study more examples from the Schwartz class of functions with a single hump. Since the dromion is not radially symmetric, we concentrate here on standard Gaussians, i.e., initial data of the form

$$\Psi(\xi, \eta, 0) = \kappa \exp(-\xi^2 - \eta^2), \quad \kappa > 0. \quad (5.2.26)$$

Once more we find that initial data with a mass smaller than the dromion will be simply dispersed, whereas initial data with a larger mass will lead to a blow-up in finite time.

First we consider the case  $\kappa = 3$  in (5.2.26) with a mass of roughly  $0.65M_Q$ . We use  $N_\xi = N_\eta = 2^{10}$  Fourier modes for  $(\xi, \eta) \in 10[-\pi, \pi] \times 10[-\pi, \pi]$  and  $N_t = 10^3$  time steps for  $t \leq 1$ . The solution for  $t = 1$  is shown on the left of Fig. 5.11. The initial hump is clearly dispersed. This is also confirmed by the  $L^\infty$  norm of the solution on the right of the same figure which after some initial growing appears to decrease monotonically.

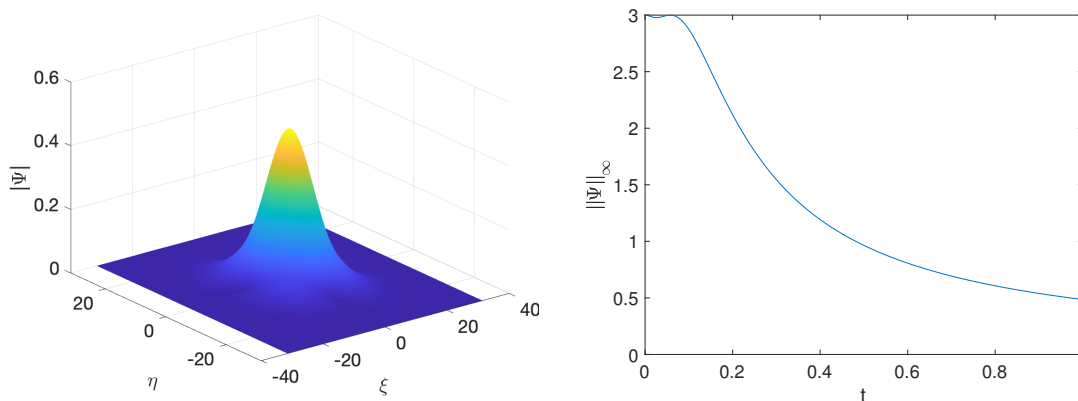


Figure 5.11: Solution to DS I for the initial data  $\Psi(\xi, \eta, 0) = 3 \exp(-\xi^2 - \eta^2)$ , on the left for  $t = 1$ , on the right the  $L^\infty$  norm in dependence of time.

If we take initial data with a mass larger than the dromion, say  $\kappa = 4.5$  in (5.2.26) where the mass is roughly  $1.45M_Q$ , we again seem to get a finite time blow-up. The solution for  $t = 0.1570$  in Fig. 5.12 is already close to the blow-up on the left.

The  $L^\infty$  norm of the solution is monotonically increasing until numerical precision is lost.

A fitting of the  $L^\infty$  norm of the solution as well as the  $L^2$  norm of  $\Psi_\xi$  as before in Fig. 5.14 indicates that the blow-up is generic, with blow-up rates

$$\|\Psi\|_\infty \sim |t^* - t|^{-1}, \quad \|\Psi_\xi\|_2^2 \approx |t^* - t|^{-2}.$$

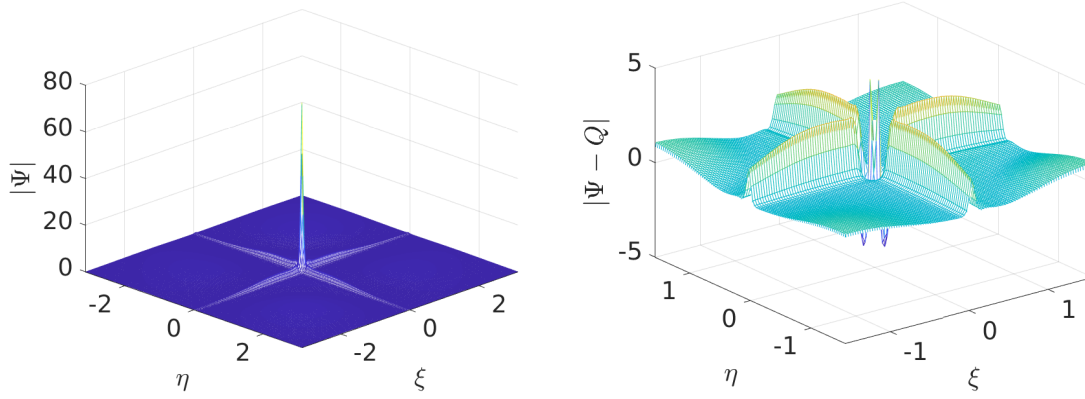


Figure 5.12: Left: DS I solution close to blow-up for Gaussian initial data  $\Psi(\xi, \eta, 0) = 4.5e^{-\xi^2 - \eta^2}$ . Right: difference of the DS I solution and a rescaled dromion close to blow-up for Gaussian initial data.

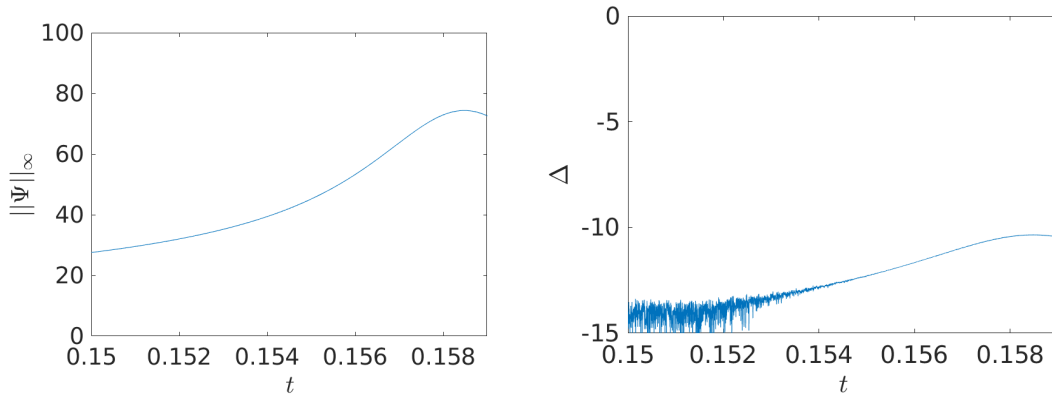


Figure 5.13: DS I solution close to blow-up for Gaussian initial data  $\Psi(\xi, \eta, 0) = 4.5e^{-\xi^2 - \eta^2}$ . Blow up time at  $t = 0.1583$

The blow up is self-similar with the profile close to the blow-up being a dynamically rescaled dromion as can be seen from the difference  $P$  in (5.2.6) between the solution at the final recorded time and rescaled dromion (again the scaling factor  $L$  is just taken as  $\max(Q)/\max(|\psi|)$  in Fig. 5.12. The residual is of the order of 10% which once more indicates a good agreement with the model.

### 5.3 Conclusion and Further studies

In conclusion, the thesis provides detailed numerical study of integrable DS I equations with trivial boundary conditions at infinity for initial data from the Schwartz class of rapidly decreasing smooth functions. By similar approach described in [94] we have presented a

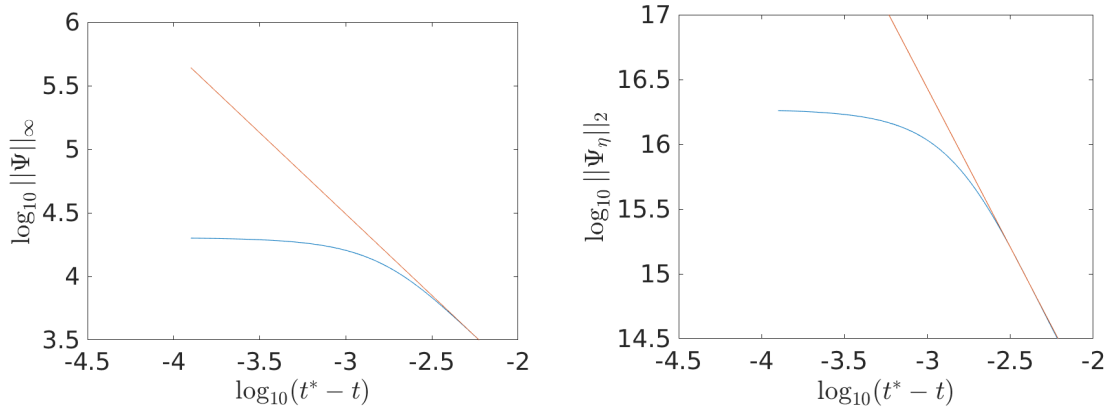


Figure 5.14: Blow-up rate for initial data  $\Psi = 4.5e^{-\xi^2 - \eta^2}$ . Left:  $\|\Psi\|_\infty$ , the red lines have the form  $a \log_{10}(t^* - t) + b$ , with values obtained by fitting the last several thousand points before we lose precision,  $a_\infty = 1.28$ ,  $a_{\Psi_x} = 2.45$  and  $b_\infty = 0.65$ ,  $b_{\Psi_x} = 9.08$  and  $t^* = 0.1583$ .

hybrid approach based on a Fourier spectral method with an analytic (up to the use of the error function) regularisation of the singular Fourier symbols. With this approach, it was possible to identify a localized stationary solution to DS I which was shown to be exponentially localized as the analytically known dromion for radiative boundary conditions. Strong numerical evidence has been presented that the dromion is unstable against localized perturbations, and that perturbations leading to a smaller mass of the initial data than the dromion mass will be simply dispersed. Perturbations with a larger mass than the dromion will lead to blow-up in finite time. We presented numerical evidence that the blow-up is self-similar with the dromion as the asymptotic profile. The same behaviour was observed for initial data from the Schwartz class with a single hump.

The future studies relevant to the family of DS systems are more of two concerns. One is the theoretical related and the second is on the numerical solution schemes.

Firstly, an interesting theoretical question to be studied in the future is whether dromions also exist for non-integrable generalisations of DS I and DS II, and whether a blow-up is still observed in such cases. A first study of these questions for DS II was presented in [99] and should also be redone with the methods of [94].

Secondly and finally, concerning with numerical schemes, it would be interesting to consider larger time-steps schemes so that solutions for longer time look the same as when smaller time-steps are used. In addition, time steppers techniques for irregular type of initial data, for instance characteristic function. Some possibilities include exponential-time integration schemes for water-dam problem since DS systems appeared in the context of water-waves.

# Appendix A

## Notations and blow-up

In this section, we provide definitions and notations used in the thesis.

### A.1 Function spaces: $L^p$ , $W^{k,p}$ and $H^k$

The following function spaces are used throughout the thesis [189]. Let  $\mathcal{F}$  be a general function space.

**Definition A.1.1** ( $L^p$  space). *The  $L^p$  function  $u(\mathbf{x})$  is one defined by*

$$L^p(\mathbb{R}^d) := \{u \in \mathcal{F} : \|u\|_p < \infty, \quad 1 \leq p \leq \infty\}$$

where

$$\|u\|_p := \begin{cases} (\int_{\mathbb{R}^d} |u|^p d\mathbf{x})^{1/p}, & 1 \leq p < \infty, \\ \sup_{\mathbf{x} \in \mathbb{R}^d} |u(\mathbf{x})|, & p = \infty. \end{cases} \quad (\text{A.1.1})$$

When the domain  $\Omega$  is known we denote the norm  $\|\cdot\|_{L^p(\Omega)}$  by  $\|\cdot\|_p$ .

**Definition A.1.2.** *The Schwartz space for function on  $\Omega \subset \mathbb{R}^d$  is defined, for multi-indices  $\alpha$  and  $\beta$ , by*

$$\mathcal{S}(\Omega) := \{u \in C^\infty(\mathbb{R}^d) : \|u\|_{\alpha,\beta} < \infty \quad \forall \alpha, \beta\} \quad (\text{A.1.2})$$

where  $\|u\|_{\alpha,\beta} := \sup_{\mathbb{R}^d} |x^\alpha \partial^\beta u|$  is a semi-norm.

**Definition A.1.3** (homogeneous space). *A normed linear space is homogeneous space if for any  $u \in X$  such that  $\|\lambda u\|_X = |\lambda| \|u\|_X$  for any  $\lambda \in \mathbb{C} \setminus \{0\}$ .*

**Definition A.1.4** (Sobolev space). *A space*

$$W^{k,p}(\Omega) := \{u \in L^p(\Omega) : D^\alpha u \in L^p(\Omega) \quad \forall |\alpha| \leq k\} \quad (\text{A.1.3})$$

with  $D^\alpha u = \frac{\partial^{|\alpha|} u}{\partial x_1^{\alpha_1} \dots \partial x_d^{\alpha_d}}$  is a Sobolev space endowed with the norm

$$\|u\|_{W^{k,p}(\Omega)}^p := \sum_{|\alpha| \leq k} \|D^\alpha u\|_{L^p(\Omega)}^p = \sum_{|\alpha| \leq k} \int_{\Omega} |D^\alpha u|^p d\mathbf{x}, \quad 1 \leq p < \infty. \quad (\text{A.1.4})$$

When  $p = \infty$  we have  $\|u\|_{W^{k,\infty}(\Omega)} = \max_{|\alpha| \leq k} \|D^\alpha u\|_{\infty(\Omega)}$  or its variant  $\sum_{|\alpha| \leq k} \|D^\alpha u\|_{\infty(\Omega)}$ . With respect to any of these norms, the space  $W^{k,p}$  is a Banach space. It is a common notation to take  $W^{k,2}(\Omega) := H^k(\Omega)$  as a Hilbert space, where  $p = 2$ .

More explicitly, these norms are defined as

$$\|u\|_{H^1}^2 := \|u\|_2^2 + \|\nabla u\|_2^2 = \int_{\mathbb{R}^d} |u(\mathbf{x})|^2 d\mathbf{x} + \int_{\mathbb{R}^d} |\nabla u(\mathbf{x})|^2 d\mathbf{x} \quad (\text{A.1.5})$$

where  $\nabla = (\partial_{x_1}, \dots, \partial_{x_d})$  and  $|\nabla u|^2 = |\partial_{x_1} u|^2 + \dots + |\partial_{x_d} u|^2$ . Plus, the  $H^2$  norm of  $u(\mathbf{x})$  is given by

$$\begin{aligned} \|u\|_{H^2}^2 &:= \|u\|_2^2 + \|\nabla u\|_2^2 + \|\Delta u\|_2^2 \\ &= \int_{\mathbb{R}^d} |u(\mathbf{x})|^2 d\mathbf{x} + \int_{\mathbb{R}^d} |\nabla u(\mathbf{x})|^2 d\mathbf{x} + \int_{\mathbb{R}^d} |\Delta u(\mathbf{x})|^2 d\mathbf{x}. \end{aligned} \quad (\text{A.1.6})$$

If  $\|u\|_p < \infty$ , we say that  $u$  is in  $L^p$ , similarly, the same holds for  $H^1$  and  $H^2$ .

**Definition A.1.5** (Homogeneous and inhomogeneous Sobolev spaces  $\dot{H}^k(\Omega), H^k(\Omega)$ ). For  $\Omega \subset \mathbb{R}^d$ , a homogeneous Sobolev space is the completion of the compact smooth space of functions  $C_c^\infty(\Omega)$  endowed with the norm, in the Fourier space

$$\|u\|_{\dot{H}^k(\Omega)} := \left\| |\omega|^k \hat{u}(\omega) \right\|_{2(\Omega)}, \quad (\text{A.1.7})$$

where  $\omega = (\omega_1, \dots, \omega_d)$  and  $|\omega| = \sqrt{\omega_1^2 + \dots + \omega_d^2}$ . The inhomogeneous space  $H^k(\Omega)$  is the completion of  $C_c^\infty(\Omega)$  under the norm

$$\|u\|_{H^k(\Omega)} := \left\| \langle \omega \rangle^k \hat{u}(\omega) \right\|_{2(\Omega)}, \quad (\text{A.1.8})$$

with  $\langle \omega \rangle = \sqrt{1 + |\omega|^2}$ .

**Remark A.1.1.** If  $k \in \mathbb{N}$ , then

$$\dot{H}^k(\Omega) = \{u \in L^2(\Omega) : \partial^\alpha u \in L^2(\Omega) \quad \forall |\alpha| = k\} \quad (\text{A.1.9})$$

and

$$H^k(\Omega) = \{u \in L^2(\Omega) : \partial^\alpha u \in L^2(\Omega) \quad \forall |\alpha| \leq k\} \quad (\text{A.1.10})$$

## A.2 The Laplacian

The usual Laplacian  $-\Delta$  defined in  $\mathbb{R}^d$  is denoted by

$$-\Delta = -\sum_{j=1}^d \frac{\partial^2}{\partial x_j^2} \equiv -\nabla \cdot \nabla \equiv -\nabla^2. \quad (\text{A.2.1})$$

In Fourier space, it is equivalent to

$$(\widehat{-\Delta \varphi})(\xi) = |\xi|^2 \hat{\varphi}(\xi) \quad (\text{A.2.2})$$

for any function  $\varphi$  where  $\xi := (\xi_1, \dots, \xi_d)$  and  $|\xi|^2 := \xi_1^2 + \dots + \xi_d^2$ . If the function  $\varphi$  is in the Schwartz space  $\mathcal{S}(\mathbb{R}^d)$ , the  $L^p$  norm of the Laplacian becomes

$$\left\| \widehat{(-\Delta\varphi)}(\xi) \right\|_p^p = \int_{\mathbb{R}^d} \|\xi\|^2 |\hat{\varphi}(\xi)|^p dx \quad (\text{A.2.3})$$

### A.3 Blow-up in Hopf equation

The inviscid Burgers equation (also Hopf equation) in 1d, for  $x \in \mathbb{R}$  and  $u(t, x) \in \mathbb{R}$

$$u_t + (u^2/2)_x = 0; \quad u(0, x) = u_0(x); \quad (\text{A.3.1})$$

admits no global solution if  $u'_0 < 0$  at any point, i.e. it has blow-up solution. Suppose by contradiction, the equation has a solution  $u(t, x)$  that is smooth. On differentiating the main equation in (A.3.1) w.r.t.  $x$ , one gets

$$u_{tx} + u_x^2 + uu_x = 0$$

which, when the substitution  $v = u_x$  is made, becomes

$$v_t + uv_x = -v^2. \quad (\text{A.3.2})$$

Along the characteristic curves associated with  $u$  let  $\tau = t + x/u$  so that  $v(t) \equiv v(\tau)$  and  $\partial_\tau = \partial_t + u\partial_x$ . The equation (A.3.2) takes the form of Ricatti differential equation

$$v_\tau = -v^2 \quad (\text{A.3.3})$$

whose solution reads

$$v = \frac{1}{\tau + \frac{1}{v_0}}.$$

The characteristic curves blow up whenever the time  $\tau = -1/v_0$  is approached. If  $v < 0$  at  $\tau = 0$ , i.e.  $v(0) < 0$ , blow-up to the equation (A.3.3) occurs at some positive  $\tau$ . Hence global solution cannot exist. Unless,  $u_0$  is a monotonically decreasing function, otherwise solution to the Hopf equation (A.3.1) will cease to exist beyond the critical time

$$\tau_c = -1/\inf_{x \in \mathbb{R}} u'_0(x).$$

Even though this approach seems to suggest that the life span of  $u$  is precisely  $\tau_c$  and  $u_x$  blows up, however this does not follow directly from the proof of the above claim. This is, of course, due to the fact that certain quantity associated to  $u(t, x)$  or  $u(t, x)$  itself may blow up first. The only valid conclusion based on the characteristic approach is that smooth solution to the Hopf equation exists in the interval  $0 \leq \tau < \tau_c$  for smooth initial data  $u_0(x)$ .

---

Several methods exist that can be used to show that the solution stays bounded at the point of gradient catastrophe, see section 9.4. of [49] where inequalities impose contradiction if smooth solutions are assumed to exist for all times.

## Appendix B

# Taylor coefficients of analytic functions: Numerical Computation

Recall that DS system consists of hyperbolic and elliptic equations. In order to solve the entire system, we have to solve for DS II equations a Poisson equation in 2D for a non-zero right-hand-side. Since it is known that the DS II lump solution has an algebraic decrease towards infinity, it is convenient to work on the sphere instead of  $\mathbb{R}^2$ . The former can be covered by two charts,  $r \in [0, 1]$  and  $s = 1/r \in [0, 1]$ . The points in and outside the unit discs are respectively mapped to the points in the south and north hemispheres. The respective end points 0 and 1 are mapped to  $0, \infty$  and 1. The solutions on the sphere are then obtained by gluing together the pair of discs on the boundaries.

A problem in this context is that the solution to the 2D Poisson equation will contain logarithms for generic right hand sides. In the DS II case, the logarithms reappear in the solutions, and numerical errors might lead to the powers in the source term leading to such terms. However such terms are only badly approximate by the polynomial approaches we want to apply which will have excellent approximation properties for smooth functions. In order to filter these terms, we need to identify certain powers in these source terms. Such terms are identifiable via the Taylor series expansion of the solution approximant or interpolant. Nevertheless, we observed in chapter 3 that the classical numerical differentiation schemes such as finite difference method and the polynomial series expansion for computing higher derivatives of a function (equivalently the Taylor coefficients) on the real line  $\mathbb{R}$  are in general badly-conditioned. High accuracy is difficult to reach in finite precision approaches. One of the first few algorithms that existed to compute numerically the derivatives of a function is by Abate and Dubner [1] via the inverse Laplace transform. Lyness and Sande [135] developed an algorithm computing the Taylor coefficients of analytic functions using Möbius numbers from number theory. An algorithm by Fornberg [62] utilizes the fast Fourier Transform (FFT) algorithm to obtain a large number of derivatives (up to 50) of analytic functions defined on the complex plane via contour integrals.

Stability of the numerical differentiation rules is of a great concern. Rivlin [190] and Berman [15], provided an explicit formula for the condition number, estimating the accuracy in the polynomial interpolation for a given set of nodes. Miel and Mooney ([157], pg. 241-251) described, using Lagrangian interpolation, the error-growth in higher derivatives of analytic functions in the interval  $[-1, 1]$ . In Lyness and Sande [135] and Abate and Dubner [1], it is demonstrated that the numerical differentiation of analytic functions evaluable on the complex plane is well-conditioned.

In this part of the appendix we present the Fornberg approach to the numerical computation of Taylor's coefficients of analytic functions via Cauchy integral formula. We apply this approach by interpolating the analytic function  $u(x)$  and its interpolant  $p_N(x)$  on a circle in the complex plane. We use interpolating polynomial functions such as Chebyshev and barycentric polynomial interpolants.

## B.1 Cauchy Integral via fast Fourier transform (FFT)

### B.1.1 Taylor series of analytic functions

An analytic function  $u(x)$  defined on  $[a, b] \subset \mathbb{R}$  can take the form of power series

$$u(x) = \sum_{k=0}^{\infty} a_k (x - x_0)^k, \quad \text{with } |x - x_0| = R < R_c \quad (\text{B.1.1})$$

where  $R_c$  is the radius of convergence. Our concern is to compute the entire Taylor (power) series coefficients  $a_k$ ,  $k = 0, 1, \dots$ , such that for any  $x_0 \in ]a, b[$  the series (B.1.1) converges,<sup>1</sup>. The coefficients  $a_k$ , correspond to the derivatives of  $u(x)$  at a point  $x_0$ .

Consider  $u(z)$  an analytic or entire function represented in the power series form (B.1.1) which converges in some neighbourhood  $D \subset \mathbb{C}$  of the complex plane. In either case, the Taylor coefficients can be computed via the Cauchy integral formula (3.3.24) on a circle  $C_r : |z - z_0| = r < R_c$ , for  $k = 0, 1, \dots$ ,

$$a_k = \frac{u^{(k)}(z_0)}{k!} = \frac{1}{2\pi i} \int_{C_r} \frac{u(z)}{(z - z_0)^{k+1}} dz = \frac{1}{2\pi r^k} \int_0^1 e^{-2\pi i k t} u(z_0 + r e^{2\pi i t}) dt, \quad (\text{B.1.2})$$

where  $R_c = \infty$  when  $u(z)$  is entire and  $0 < R_c < \infty$  if  $u(z)$  is analytic.

Any of the rectangular or trapezoidal quadratures of the integral (B.1.2) of periodic-analytic functions converges geometrically (Davis [42]),<sup>2</sup>. An  $m$ -trapezoidal

<sup>1</sup>We throughout assume, that the interval  $[a, b]$  can be scaled to  $[-1, 1]$  via the transformation, for  $x \in [a, b]$ , that  $y = [2x - (b + a)] / (b - a) = [-1, 1]$ . Without loss of generality we will often use the interval  $[-1, 1]$ .

<sup>2</sup>In fact for periodic analytic functions the trapezoidal and rectangular sums are the same and Clenshaw

quadrature yields, with  $a_k^{(m)} = a_k(r, m)$ ,

$$a_k^{(m)} = \begin{cases} \frac{1}{mr^k} \sum_{j=0}^{m-1} e^{-(2\pi i/m)kj} u(z_0 + re^{(2\pi i/m)j}), & k = 0, 1, \dots, m-1 \\ 0, & k = m, m+1, \dots \end{cases} \quad (\text{B.1.3})$$

One establishes the correspondence (Lyness [135]) induced by (B.1.3) that

$$u(z_0 + re^{-(2\pi i/m)j}) \longleftrightarrow r^k \tilde{a}_k, \quad \text{for } j, k = 0, 1, \dots, m-1. \quad (\text{B.1.4})$$

The approximation (B.1.3) is, precisely, a discrete Fourier Transform (DFT) computable with high accuracy and efficiency via the FFT algorithm, (see Cooley and Tukey [38], Cooley et al. [37]).

According to Cauchy's integral theorem, all the radii  $0 < r < R_c$  should give analytically equal results but not so numerically. As  $r \rightarrow 0$ , the convergence rate of the representation (B.1.3) ameliorates remarkably (especially for  $r$  small), however, results in large amount of cancellation in (B.1.2) leading to blow-up of the relative errors (Lyness [131], pg. 130). When  $r \rightarrow R_c$ , there are stability issues in Cauchy's integral (see Bornemann [19] section 3.1). Thus, finding an optimal radius  $r_*$  is of great concern, since the proper balancing of the overall approximation errors with rounding errors may be attained thereby minimizing the former.

Lyness and Sande [135], in their algorithm considered the absolute error of the normalised Taylor coefficients  $r^k \tilde{a}_k$  by varying  $r$  until the absolute error

$$\epsilon_a^{(m,k)}(r) = r^k |a_k - a_k^{(m)}| \quad (\text{B.1.5})$$

is minimized. This specific choice of error provides some sort of uniform accuracy which is convenient for their algorithm. It is cautioned there as well, accuracy is not guaranteed in computing a large number of coefficients. Fornberg [61],[62] extended the method through searching an optimal  $r$  by fixing a number  $m$  of points on the circle  $C_r$ , which we explain as follows.

### B.1.2 Fornberg algorithm

**Step I:** suppose  $u(z)$  is defined on a circle  $C_r : |z - z_0| = r$ , with  $z = z_0 + re^{2\pi it}$  for  $t \in [0, 1)$ . Applying the expansion of  $u(z)$  in (B.1.1), an equivalent form of (B.1.3) using

Curtis quadrature is the better approximation of the two.

FFT becomes

$$\hat{f}_k := r^k a_k^{(m)} = \frac{1}{m} \sum_{j=0}^{m-1} \sum_{n=0}^{\infty} e^{-(2\pi i/m)kj} a_n r^n e^{(2\pi i/m)jn} = \frac{1}{m} \sum_{n=0}^{\infty} a_n r^n \sum_{j=0}^{m-1} e^{(2\pi ij/m)(k-n)} \quad (\text{B.1.6})$$

However,

$$\sum_{j=0}^{m-1} e^{(2\pi ij/m)(k-n)} = \begin{cases} m, & \frac{k-n}{m} = \ell \in \mathbb{Z} \\ 0, & \text{otherwise.} \end{cases}$$

Thus,  $r^k a_k^{(m)} = \sum_{\ell=0}^{\infty} r^{k+m\ell} a_{k+m\ell} = r^k a_k + r^{k+m} a_{k+m} + r^{k+2m} a_{k+2m} + r^{k+3m} a_{k+3m} + \dots$  yields, for  $m \geq 1$  (since  $k = n + m\ell$ , then  $n$  is swapped by  $k$  because both  $n, k = 0, 1, \dots$ ),

$$a_k^{(m)} = a_k + r^m a_{k+m} + r^{2m} a_{k+2m} + r^{3m} a_{k+3m} + \dots \quad (\text{B.1.7})$$

the terms in the summation  $\sum_{\ell=1}^{\infty} r^{k+m\ell} a_{k+m\ell}$  are aliases that appear due to function evaluation on discrete points (they are a consequence of the fact that higher modes  $k + \ell m$  results are not distinguishable from the  $k$  modes).

**Step II:** based on two tests say  $a_k^{(m,0)}$  and  $a_k^{(m,1)}$ , for the choices of radii  $r_0$  and  $r_1$  respectively, one tries to get rid of the aliasing terms. The Richardson extrapolation (the truncation error elimination) reads

$$A_k^{(m,0)} := a_k^{(m,1)} - \frac{(a_k^{(m,1)} - a_k^{(m,0)})}{1 - \left(\frac{r_0}{r_1}\right)^m} = a_k - (r_0 r_1)^m a_{k+2m} - (r_0^{2m} r_1^m + r_0^m r_1^{2m}) a_{k+3m} + \dots \quad (\text{B.1.8})$$

To eliminate the next truncation error term  $a_{k+2m}$  a third radius  $r_2$  is chosen, the elimination process now involves  $r_1$  and  $r_2$ :

$$A_k^{(m,1)} := a_k^{(m,2)} - \frac{(a_k^{(m,2)} - a_k^{(m,1)})}{1 - \left(\frac{r_1}{r_2}\right)^m} = a_k - (r_1 r_2)^m a_{k+2m} - (r_1^{2m} r_2^m + r_1^m r_2^{2m}) a_{k+3m} + \dots \quad (\text{B.1.9})$$

and the use of Richardson's extrapolation on these two equations (B.1.8) and (B.1.9) gives

$$\begin{aligned} B_k^{(m,0)} &:= A_k^{(m,1)} - \frac{(A_k^{(m,1)} - A_k^{(m,0)})}{1 - \left(\frac{r_0}{r_2}\right)^m} \\ &= a_k + (r_0 r_1 r_2)^m a_{k+3m} + (r_0^{2m} r_1^m r_2^m + r_0^m r_1^{2m} r_2^m + r_0^m r_1^m r_2^{2m}) a_{k+4m} + \dots \end{aligned} \quad (\text{B.1.10})$$

**Step III:** the process is repeated by choosing the next radii and elimination of truncation errors until a required accuracy is attained.

Analogously, assume there are second order approximations in (B.1.7) such that for  $r_j^m = q_j$

for each  $j$ , then for three radii we get

$$\begin{aligned} A_0 &= a_k + a_{k+m}q_0 + a_{k+2m}q_0^2 + \cdots \\ A_1 &= a_k + a_{k+m}q_1 + a_{k+2m}q_1^2 + \cdots \\ A_2 &= a_k + a_{k+m}q_2 + a_{k+2m}q_2^2 + \cdots \end{aligned}$$

The Richardson extrapolation can be obtained by finding  $\alpha, \beta, \gamma$  for which

$$\alpha A_0 + \beta A_1 + \gamma A_3 = a_k + O(q^3) \quad (\text{B.1.11})$$

for arbitrary  $q$  depending on  $q_0, q_1, q_3$ . This is equivalent to solving the Vandermonde system

$$\begin{pmatrix} 1 & q_0 & q_0^2 \\ 1 & q_1 & q_1^2 \\ 1 & q_2 & q_2^2 \end{pmatrix} \begin{pmatrix} a_k \\ a_{k+m} \\ a_{k+2m} \end{pmatrix} = \begin{pmatrix} 1 \\ 0 \\ 0 \end{pmatrix}$$

which has the solution  $(a_k, a_{k+m}, a_{k+2m}) = \left( \frac{q_1 q_2}{(q_0 - q_1)(q_0 - q_2)}, \frac{-(q_1 + q_2)}{(q_0 - q_1)(q_0 - q_2)}, \frac{1}{(q_0 - q_1)(q_0 - q_2)} \right)$ .

**Optimizing the radius of the contour integral (Fornberg [61]):** while we choose the initial radius at random, with  $m$  fixed, two comparison tests are conducted on  $\hat{f}_k$  in (B.1.6) and the computed  $a_k^{(m)}$  to determine the next choice of radius:

**test I:** Letting  $c_k = \hat{f}_k/b_k$ , with  $b_0 = 1$  and  $b_k = 10^{-4/(1-1/k)}$  for  $1 \leq k \leq m-2$  and  $b_{m-1} = 10^{-4}$ , compute

$$C = \max_{0 \leq k \leq m-1} |c_k|, \quad (\text{B.1.12})$$

where  $b_k$  comes from the accuracy required in the algorithm and a power of  $-4$  is used to detect (or trace) the convergence of the FFT. Next we check

$$\begin{cases} \text{if } C \in \{c_0, \dots, c_{k/2-1}\}, & r \text{ increases} \\ \text{otherwise,} & r \text{ decreases} \end{cases} \quad (\text{B.1.13})$$

**test II:** If according to **test I**  $r$  should increase, another comparison test is carried out.

Let  $V = \{z_0 + z_j \in \mathbb{C}\}_{j=1}^3$  be a set of three complex numbers with each  $z_j$  randomly chosen and check if

$$\max_{z \in V} \left( \frac{|u(z) - u_T(z)|}{|u(z)|} \right) < 10^{-3}, \quad z = z_0 + rz_j \quad (\text{B.1.14})$$

where  $u_T(z)$  is an  $m$ -degree Taylor polynomial of  $u(z)$  obtained using the computed coefficients  $a_k^{(m)}$ , for  $k = 0, 1, \dots, m-1$  w.r.t the chosen circle of radius  $r$  centred at  $z_0$ . If  $u(z)$  and  $u_T(z)$  satisfy (B.1.14) then  $r$  should be increased and decreased otherwise. (see

footnote <sup>3</sup>). The second radius is given by  $r_1 = cr_0$  where  $r_0$  is changed by taking either  $c = 2$  or  $c = 1/2$ . Subsequently, the radius is successively changed by a factor taken to be either square root of the preceding one or reciprocal of square root.

It is noteworthy that when  $r$  is too large, i.e.  $r \geq R_c$  radius of convergence, a singularity is included inside the circle and therefore we will deal with Laurent series, and this converges to a different value but not the integral (B.1.2). Thus, in that case  $r$  is always decreased.

### B.1.3 Fornberg error estimates

For  $k = 0, 1, \dots, m - 1$ , let  $a_k^{(m)}$  be an approximation to the  $a_k$ . Suppose using the Richardson extrapolation we get

$$a_k^{(m)}(r) = a_k + R_T(r), \tag{B.1.15}$$

where  $R_T(r)$  is a Richardson extrapolation correction term. If  $\epsilon_M$  is the machine accuracy of precision  $p$ , constant  $\times 10^{-p}$ , the truncation and round-off errors are estimated (Fornberg [61, 62]) as

$$\epsilon_T^{(m)}(r) = \epsilon_M^{3/p} \times R_T(r); \quad \epsilon_{\text{round}}^{(m)}(r) = \frac{C}{r^k} \cdot \epsilon_M \tag{B.1.16}$$

with  $C$  the same constant defined in the equation (B.1.12). The number  $\epsilon_M^{3/p}$ , is a scaling factor for better accuracy of the estimate used, moreover related to  $b_k$  and the choice of our radius  $r$  in the algorithm <sup>4</sup>.

Finally, since all inputs are close to machine precision a good accuracy is attained if the overall error is close to the machine epsilon  $\epsilon_M$ . Therefore it makes sense that the stopping criterion could be attained whenever

$$\max_k |\epsilon_T^{(m)}(r) - \epsilon_{\text{round}}^{(m)}(r)| \leq \epsilon_M. \tag{B.1.17}$$

In other words, the algorithm stops when the quantities in the equation (B.1.16) agreed.

#### Additional Estimates

One observes that if  $R < R_c$ , for  $R$  the lower bound of the radius of convergence, with

<sup>3</sup>Fornberg [61] suggested that any initial radius  $r_0$  chosen producing an error  $\not\leq 3 \times 10^4$  renders the algorithm unreliable. This means the algorithm doesn't work if the initial guess is too far away from the optimal value.

<sup>4</sup>The factor  $\epsilon_M^{4/p}$  is to be used but for safety reason  $\epsilon_M^{1/p}$  is saved.

$|z - z_0| = r < R$ , then an upper bound for  $a_k$  is derived as follows <sup>5</sup>

$$\begin{aligned}
 |r^k a_k|^2 &= \left| r^k \frac{u^{(k)}(z_0)}{k!} \right|^2 = \left| \frac{1}{2\pi i} \int_{C_R} \frac{r^k u(z)}{(z - z_0)^{k+1}} dz \right|^2 \\
 &= \left| \int_0^1 u(z_0 + Re^{2\pi i t}) \left( \frac{r}{R} \right)^k e^{-2\pi i k t} dt \right|^2 \leq \left( \frac{r}{R} \right)^{2k} \int_0^1 |u(z_0 + Re^{2\pi i t})|^2 dt \\
 &\leq \left( \frac{r}{R} \right)^{2k} \|u\|_2^2 = \rho^{2k} \|u\|_2^2, \quad k = 0, 1, 2, \dots \\
 \therefore |r^k a_k| &\leq \rho^k \|u\|_2 \quad \text{or} \quad |a_k| \leq R^{-k} \|u\|_2;
 \end{aligned} \tag{B.1.18}$$

where  $\rho = r/R$  and the weighted  $L^2$ -norm, for  $r < R$ ,

$$\|u\|_2^2 = \frac{1}{2\pi i} \int_{C_R} |u(z)|^2 \frac{dz}{(z - z_0)} = \int_0^1 |u(z_0 + Re^{2\pi i t})|^2 dt, \tag{B.1.19}$$

and Schwartz's inequality is used in obtaining the estimate (B.1.18).

### B.1.4 Implementing the Fornberg algorithm

Suppose an analytic function  $u(x)$  defined on  $[a, b]$  has an  $N$ -degree interpolating polynomial  $p_N(x)$ . If in addition  $u(x)$  and  $p_N(x)$  can be extended analytically onto the complex plane as  $u(z)$  and  $p_N(z)$  respectively, then we are interested in a relation

$$u(z) \simeq p_N(z) = \sum_{n=0}^N c_n \phi_n(z) \tag{B.1.20}$$

$$\text{so that } u(z) \equiv \sum_{n=0}^N a_n (z - z_0)^n, \quad p_N(z) \equiv \sum_{k=0}^N \tilde{a}_k (z - z_0)^k \tag{B.1.21}$$

and  $u(z)|_U = u(x) \equiv p_N(z)|_U$  for some subset  $U \subset \mathbb{R}$ . The  $c_k$  are the spectral expansion coefficients of the interpolant  $p_N(z)$  with their extended basis  $\phi_k(z)$ . Our concern here is how efficiently the coefficients  $a_k$  and  $\tilde{a}_k$  can be computed using Fornberg's algorithm.

### B.1.5 Interpolation and the Fornberg Algorithm

**Analytic function:** a function of interest is  $u(z) = 2/(3 + z)$  on the interval  $[-1, 1]$  and we assume  $u$  extends to the complex plane with Taylor expansion

$$u(z) = \sum_{n=0}^{\infty} \frac{(-1)^n}{2^{n+1}} (z + 1)^n = 1 - \frac{1}{2}(z + 1) + \frac{1}{4}(z + 1)^2 - \frac{1}{8}(z + 1)^3 + \dots \tag{B.1.22}$$

---

<sup>5</sup>The  $R$  is the lower bound of the radius of convergence  $R_c$ , which is the minimum distance from  $z_0$  to  $R_c$  in which the power series doesn't only converge but also agrees with the function  $u(z)$  in the particular neighbourhood.

where  $z_0 = -1$ . The first 10 Taylor coefficients of  $u(z)$  using Fornberg algorithm are given in table B.1.

**Chebyshev Interpolant:** we will call the interpolant (B.1.20) a *Chebyshev Interpolant* whenever  $\phi_k(z) = T_k(z) = \cos(kz)$  such that

$$p_N^C(z) = \sum_{k=0}^N c_k T_k(z) = \sum_{k=0}^N a_k^C (z - z_0)^k \quad (\text{B.1.23})$$

where  $a_k^C$  are the Taylor coefficients of the Chebyshev interpolant  $p_N^C(z)$ .

**Barycentric Interpolant:** we will consider (B.1.20) a barycentric if the interpolant is given by

$$p_N^B(z) = \left( \sum_{k=0}^N \frac{w_k}{(z - x_k)} u_k \right) / \left( \sum_{k=0}^N \frac{w_k}{(z - x_k)} \right), \quad w(z) \sim (1 - z^2)^{-1/2} \pi \quad (\text{B.1.24})$$

where  $x_k$  are the interpolation points  $x_k \in [-1, 1]$  possessing the weights  $w(z)$  with asymptotic form described in (B.1.24). We shall take  $a_k^B$  as the Taylor coefficients of the barycentric interpolant (B.1.24) expressed as in equation (B.1.23).

We shall use these interpolants in order to obtain approximations of the Taylor coefficients  $a_k$  by implementing the Fornberg algorithm, utilizing the Cauchy integral formula on a circle containing  $m$  equispaced points, on both the  $u(z)$  and  $p_N^C(z)$ .

With the function  $2/(3 + x)$ , let  $x_0 = -1$  be the centre of the circle and with the starting radius  $r_0 = 0.89687655$ . The Fornberg algorithm produces approximations of the first 16 and 32 Taylor coefficients (for which the first 10 are shown in the Table B.1, and B.2) having optimal radius  $r_* = 0.634187$ .

The first 10 coefficients $a_k^C$ and $\tilde{a}_k^C$ and $k = 0, 1, \dots, 9$ for $u(z) = 2/(3 + z)$ on $[-1, 1]$				
$k$	$a_k$	$\tilde{a}_k, m = 16$	$a_k^C, N = 26$	$\tilde{a}_k^C, N = 26; m = 16$
0	1.000000e+00	1.0000000000000000e+00	1.0000000000000000e+00	1.0000000000000000e+00
1	-5.000000e-01	-5.0000000000000000e-01	-5.000000000000800e-01	-5.000000000000800e-01
2	2.500000e-01	2.5000000000000000e-01	2.500000000089916e-01	2.500000000089916e-01
3	-1.250000e-01	-1.2500000000000000e-01	-1.250000003886469e-01	-1.250000003886466e-01
4	6.250000e-02	6.24999999999956e-02	6.250000894605472e-02	6.250000894606088e-02
5	-3.125000e-02	-3.12500000000030e-02	-3.125012749347657e-02	-3.125012749348698e-02
6	1.562500e-02	1.56250000000069e-02	1.562622642765359e-02	1.562622642766682e-02
7	-7.812500e-03	-7.81250000000189e-03	-7.820927102209612e-03	-7.820927102308015e-03
8	3.906250e-03	3.90624999999474e-03	3.949300071788153e-03	3.949300071498432e-03
9	-1.953125e-03	-1.95312500000955e-03	-2.121522355966273e-03	-2.121522357154145e-03
	$\max_k  a_k - \tilde{a}_k $	9.545315926562381e-16	1.683973559662732e-04	1.683973571541455e-04
	$\min_k  a_k - \tilde{a}_k $	0.00000000000000e+00	0.00000000000000e+00	0.00000000000000e+00

Table B.1: The first 10 Taylor coefficients computed via Fornberg algorithm.

As one may have noticed in Figure B.1 also in Table B.2, an increase in the degree  $N$

of the Chebyshev  $p_N(x)$  will increase the errors. This is as a result of larger  $N$  than needed will allow rounding errors to pollute the computation process. The best degree in this case is  $N = 26$ . The  $a_k^C$  are the Taylor coefficients of the actual Chebyshev interpolant  $p_N^C(x)$ .

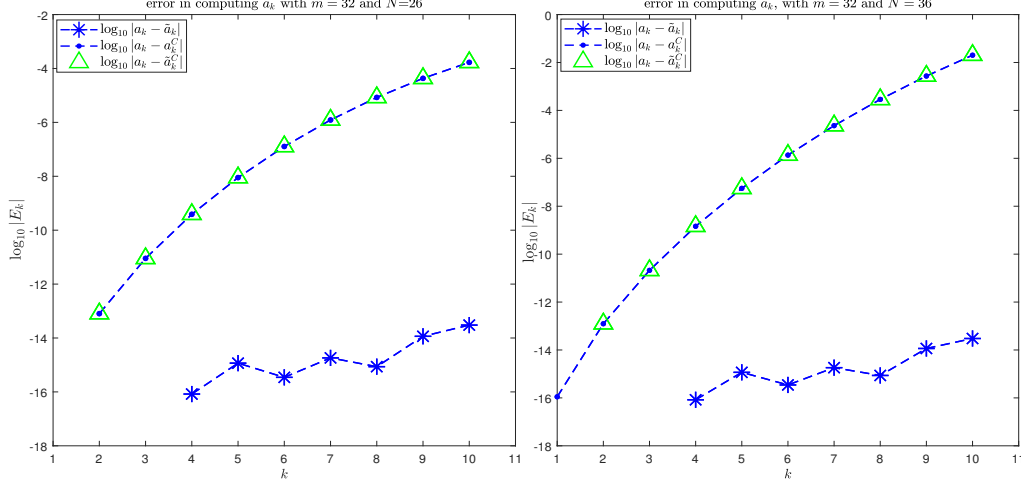


Figure B.1: Close up plots of the errors  $E_k = a_k - \tilde{a}_k$  in the first 10 Taylor coefficients of analytic function  $u(x) = 2/(3+x)$  on  $[-1, 1]$  obtained from Fornberg algorithm on  $u(x)$  having  $m = 32$  points on a circle and its  $N$  degree Chebyshev interpolant  $p_N^C(x)$ . Left: Errors in the Fornberg-Taylor coefficients of the  $u(x)$  (shown in blue starred-dotted lines  $-*$ -) and Taylor-coefficients of the interpolant with  $N = 26$  (in green triangles  $\triangle$ ) and that of the exact interpolant (in blue dotted-broken lines  $-•-$ ). Right: Same as in the left with  $m = 32$  but  $N = 36$  is used.

The first 10 coefficients $a_k^C$ and $\tilde{a}_k^C$ and $k = 0, 1, \dots, 9$ for $f(z) = 2/(3+z)$ on $[-1, 1]$				
$k$	$a_k^C, N = 36$	$\tilde{a}_k^C, N = 36, m = 32$	$a_k^C, N = 64$	$\tilde{a}_k^C, N = 64; m = 32$
0	9.9999999999999999e-01	1.0000000000000000e+00	1.0000000000000000e+00	1.0000000000000000e+00
1	-5.0000000000001243e-01	-5.0000000000001241e-01	-5.0000000000004183e-01	-5.0000000000000000e-01
2	2.500000000210293e-01	2.500000000210293e-01	2.500000003111467e-01	2.5000000000000000e-01
3	-1.250000014549353e-01	-1.250000014549358e-01	-1.250000904830220e-01	-1.2500000000000000e-01
4	6.250005568788995e-02	6.250005568789006e-02	6.251389425622879e-02	6.2500000000000000e-02
5	-3.125136126077135e-02	-3.125136126078187e-02	-3.256366584188703e-02	-3.247070312500000e-02
6	1.564809736115597e-02	1.564809736115719e-02	9.959046509770061e-02	9.936523437500000e-02
7	-8.099694964408190e-03	-8.099694964162652e-03	-3.871350887586098e+00	-3.871337890625000e+00
8	6.624569638114104e-03	6.624569637524690e-03	1.338865986808244e+02	1.338867187500000e+02
9	-2.209657410772823e-02	-2.209657410879337e-02	-3.614385123890202e+03	-3.614385131835938e+03
$\max_k  a_k - \tilde{a}_k $	2.014344910772823e-02	2.014344910771141e-02	3.614383170765202e+03	3.614383178710938e+03
$\min_k  a_k - \tilde{a}_k $	1.110223024625157e-16	2.220446049250313e-16	0.000000000000000e+00	0.000000000000000e+00

Table B.2: The first 10 Fornberg-Taylor coefficients (Chebyshev interpolant).

Note that in the stopping criterion, a tolerance of  $10^{-14}$  in the maximum absolute difference between the truncation errors and the rounding errors is used throughout the computation for the function  $u(x)$  and its Chebyshev interpolant.

**Barycentric interpolation:** for comparison purpose, let us apply the Fornberg algorithm on the barycentric-interpolant  $p_N^B(z)$  to seek for approximations to  $a_k$ . With

The first 10 coefficients $\tilde{a}_k^B$ for various $N$ and $k = 0, 1, \dots, 9$ for $f(z) = 2/(3+z)$ on $[-1, 1]$				
$k$	$\tilde{a}_k^B, N = 26, m = 16$	$\tilde{a}_k^B, N = 36, m = 16$	$\tilde{a}_k^B, N = 64, m = 32$	$\tilde{a}_k^C, N = 72, m = 32$
0	9.999999999999999e-01	1.000000000000000e+00	1.000000000000004e+00	1.000000000000020e+00
1	-5.000000000000008e-01	-5.000000000000835e-01	-5.000000000004312e-01	-5.00000000008707e-01
2	2.500000000003201e-01	2.500000000140346e-01	2.49999998822331e-01	2.49999998762437e-01
3	-1.250000000180554e-01	-1.250000008792693e-01	-1.249999556712778e-01	-1.249999476291039e-01
4	6.250000138940551e-02	6.250002049618965e-02	6.249334909297012e-02	6.249144680252552e-02
5	-3.125006968430450e-02	-3.124982350664076e-02	-3.065616874499411e-02	-3.042164209840790e-02
6	1.562663292829900e-02	1.559945106124037e-02	-1.974962886475518e-02	-3.548288926877079e-02
7	-7.841430138717593e-03	-7.321792487423968e-03	1.386182701637702e+00	1.621115635064802e+00
8	4.143919944432887e-03	2.779022778973802e-02	-1.840058522184746e+01	4.377683456778311e+01
9	-8.922426052348262e-02	-2.122550101573508e+00	-2.797451543100497e+03	-7.559579171530603e+03
$\max_k  a_k - \tilde{a}_k $	8.727113552348262e-02	2.120596976573508e+00	2.797449589975497e+03	7.559577218405603e+03
$\min_k  a_k - \tilde{a}_k $	1.110223024625157e-16	4.440892098500626e-16	3.996802888650564e-15	2.042810365310288e-14

Table B.3: The first 10 Fornberg-Taylor coefficients (barycentric-interpolant).

the different degrees  $N$  and different number of points  $m$  on circle, we plotted the absolute errors shown in Figure B.2.

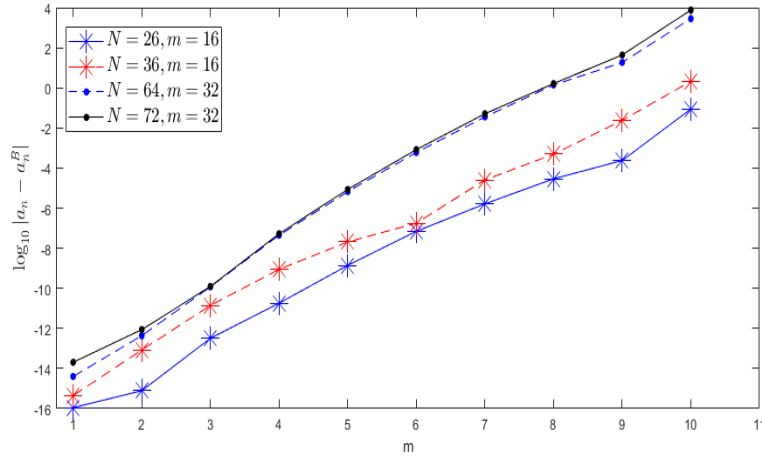


Figure B.2: Close-up view of the absolute error  $|a_n - \tilde{a}_n^B|$  in the Taylor coefficients of an  $N$  degree barycentric polynomial interpolant with  $m$  points on the circle. For  $m = 16$ ,  $N = 26, 32$  (the blue starred-solid line  $-*$  and the red starred-broken-line  $-*$ ) while  $m = 32$  then  $N = 64, 72$  are used (broken lines with blue dots  $\bullet$  and solid line with dots (black)  $\bullet$  resp.).

Using  $r_0 = 8.9687655e-3$ , with the respective optimized radii in all the cases considered in the Table B.3, the final Fornberg-Taylor coefficients are presented in the Table B.3 for various degrees barycentric-interpolant, with  $N = 26, 36, 64, 72$ , for  $m = 16$  or 32 points on the circle. The  $\tilde{a}_N^B$  are the Fornberg computed Taylor's coefficients of the barycentric interpolant. It has just been shown that the barycentric interpolant does not do better than the Chebyshev interpolant with a reasonable degree  $N$ . A very small radius is used due to the reason of the stability of barycentric method as a result of extrapolation outside of the

interval  $[-1, 1]$  when the Chebyshev nodes are used (see details in Trefethen [208], ch. 5 and the references therein).

### B.1.6 More Examples

Examples of the Chebyshev interpolants of the functions:  $1/(a+x^2)$ ,  $\sin(\pi x)$ ,  $e^{-1/(x-2)}$  for  $x \in [-1, 1]$ . Specifically on the interval  $[-1, 1]$  around 0,

$$\begin{aligned} 1/(1+x^2) &= \sum_{k=0}^{\infty} (-1)^k x^{2k} = 1 - x^2 + x^4 - x^6 + x^8 - \dots \\ \sin(\pi x) &= \sum_{k=0}^{\infty} (-1)^k x^{2k+1}/(2k+1)! = \pi x - \pi^3 x^3/3! + \pi^5 x^5/5! - \dots \end{aligned}$$

Again, we use Fornberg algorithm on the Chebyshev interpolants of these functions. The function  $\exp(-1/(x-2))$  with the expansion around the point  $x_0 = 0 \in [-1, 1]$ :

$$e^{-1/(x-2)} = \sqrt{e} \left[ 1 + \frac{1}{4}x + \frac{5}{32}x^2 + \frac{37}{384}x^3 + \frac{361}{6144}x^4 + \frac{4361}{122880}x^5 + \frac{62701}{2949120}x^6 + \dots \right].$$

We present the results of the Fornberg computed Taylor's coefficients in the Table B.4 for the functions concerned along with the absolute errors associated to each of them in Figure B.3 and Figure B.4. Firstly, the errors in the first 16 Fornberg-Taylor coefficients  $\tilde{a}_k$  of the given function  $u(x)$  are depicted together with that of its Chebyshev interpolant  $\tilde{a}_k^C$ . For the function  $1/(1+x^2)$  we found, as Fornberg algorithm is applied, a 42 Chebyshev interpolant has the best approximations compared to higher or lower degree ones. Yet, a better accuracy is attained when applied to the function  $u(x)$ . This is also applied to the other function's interpolant with their corresponding degrees shown in the figures and the table. We expanded the periodic function  $\sin(\pi x)$  about the point  $x = 0$  and exponential function  $\exp(-1/(x-2))$  around  $x = 1$ .

It turns out, what one gets in the bottom figure of Figure B.4 can be part of the warning hinted by the Fornberg that full accuracy is not guaranteed even for some entire functions like  $\exp(z)$ .

Another example worth considering is  $\exp(-1/(1+x^2))$  expanded around  $x_0 = 0$ :

$$\begin{aligned} e^{-1/(1+x^2)} &= \sum_{k=0}^{\infty} \frac{\left(-\frac{1}{x^2+1}\right)^k}{k!} = \left[ 1 + x^2 - \frac{x^4}{2} + \frac{x^6}{6} + \frac{x^8}{24} - \frac{19x^{10}}{120} \right. \\ &\quad \left. + \frac{151x^{12}}{720} - \frac{1091x^{14}}{5040} + \frac{7841x^{16}}{40320} - \dots \right] e^{-1} \end{aligned} \tag{B.1.25}$$

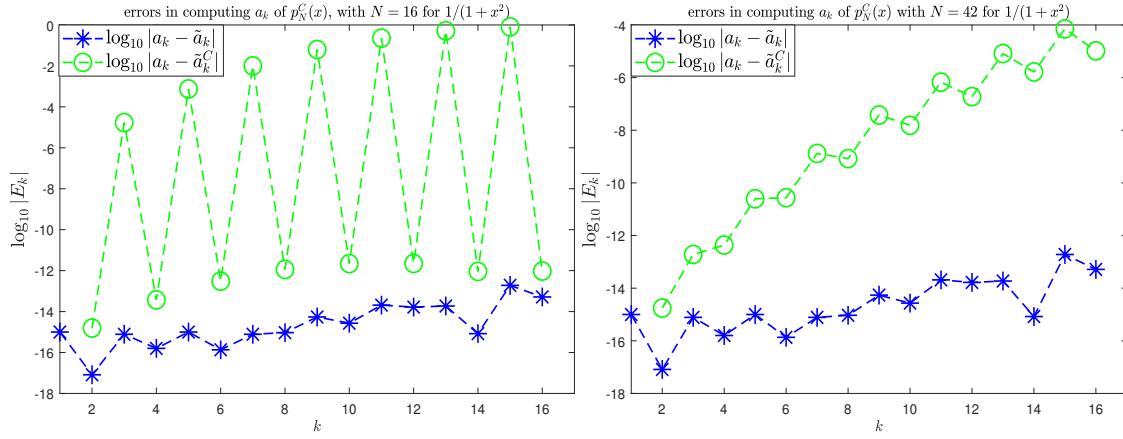


Figure B.3: Absolute errors  $|a_k - \tilde{a}_k^C|$  in the Taylor coefficients of an  $N$  degree Chebyshev polynomial interpolant of  $1/(1+x^2)$  with 32 points on the circle.

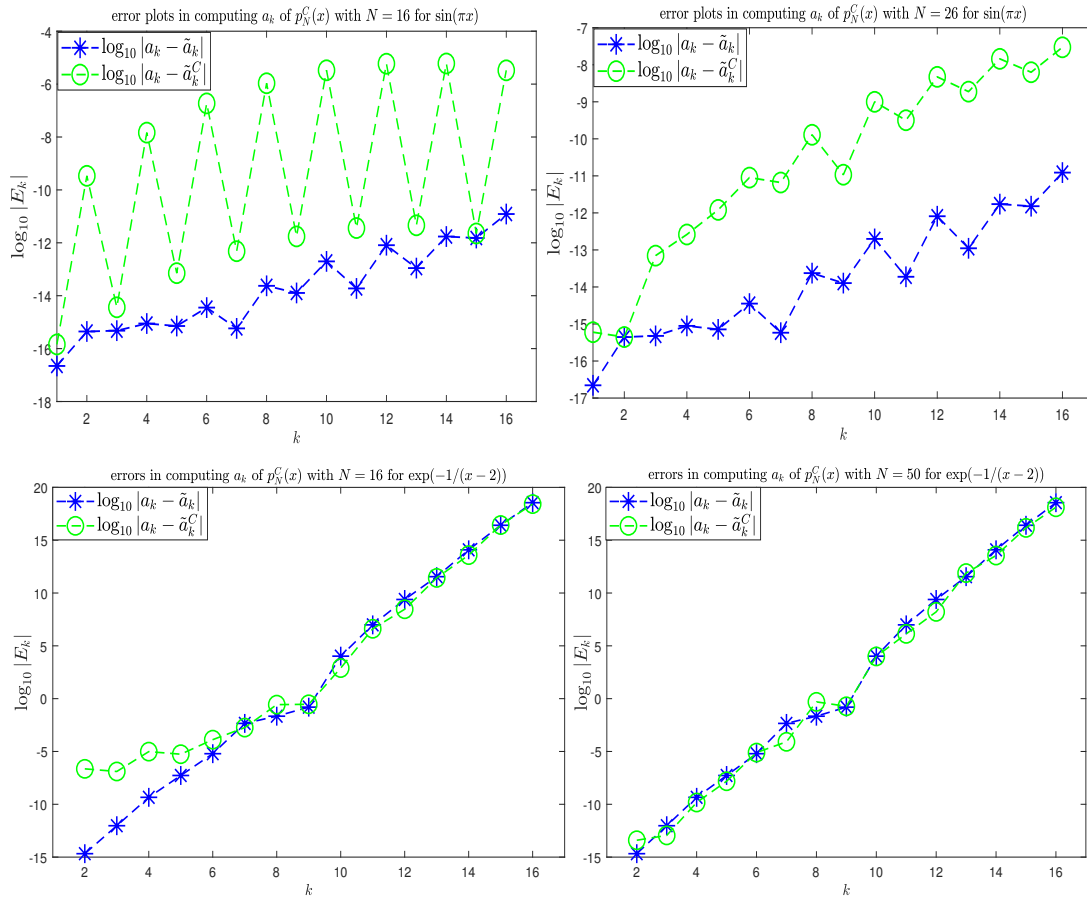


Figure B.4: Absolute errors  $|a_k - \tilde{a}_k^C|$  in the Fornberg Taylor coefficients of degree  $N$  Chebyshev polynomial interpolants of  $\sin(\pi x)$  and  $e^{-1/(x-2)}$  with 32 points on the circle around  $x_0 = 0$ . **Top:** the errors in computing the Fornberg-Taylor coefficients of the function  $\sin(\pi x)$  (blue starred-broken lines  $-*$  and that of its Chebyshev interpolant (in green circled-broken lines  $-o-$ ) are shown. **Bottom:** same for the function  $\exp(-1/(x-2))$ .

The first 16 coefficients $\tilde{a}_k^C$ for various $N$ and $k = 0, 1, \dots, 9$ for $u(x)$ on $[-1, 1]$			
$k$	$\tilde{a}_k^C, N = 48, 1/(1+x^2)$	$\tilde{a}_k^C, N = 26, \sin(\pi x)$	$\tilde{a}_k^C, N = 50, e^{-1/(x-2)}$
0	1.000000000000000e+00	-5.999690314728152e-16	1.648721270700128e+00
1	-4.850569910951675e-16	3.141592653589794e+00	4.121803176750716e-01
2	-1.000000000000514e+00	7.015059858882657e-14	2.576126985470080e-01
3	1.801240971173670e-13	-5.167712780050230e+00	1.588611642512140e-01
4	1.000000000094553e+00	-1.205827581828523e-12	9.687309330045955e-02
5	-1.521423274157593e-11	2.550164039886327e+00	5.852082514033915e-02
6	-1.000000006827656e+00	6.612456995920963e-12	3.513547189987509e-02
7	5.030933494069426e-10	-5.992645294495469e-01	-4.762415038782888e-01
8	1.000000260128113e+00	1.074610737480268e-11	-1.761018329157959e-01
9	-8.682225352144296e-09	8.214588761006840e-02	9.914550130207108e+03
10	-1.000006071255086e+00	-3.180725820103482e-10	1.357481391895635e+06
11	8.977461391004392e-08	-7.370435665466852e-03	-1.636948143124325e+08
12	1.000094879712246e+00	1.882010894933157e-09	-7.729441167910748e+11
13	-6.197549180731891e-07	4.663172636980721e-04	3.528748067427020e+13
14	-1.001052440995684e+00	-6.288960751626695e-09	-1.460326286936149e+16
15	3.445946974576630e-06	-2.194500467339762e-05	-1.308908407129285e+18

Table B.4: The computed Fornberg-Taylor coefficients of Chebyshev interpolants.

The absolute error plot is shown in the figure below.

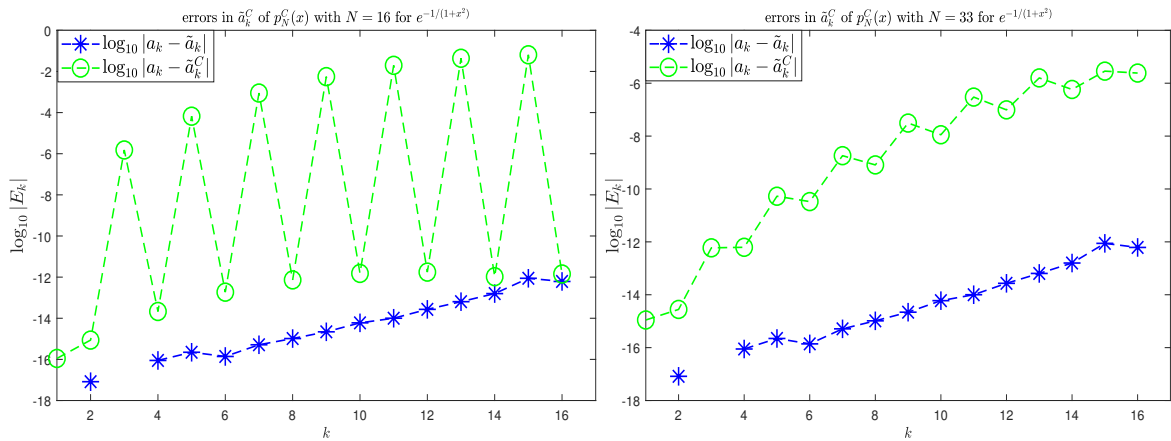


Figure B.5: Absolute errors  $|a_k - \tilde{a}_k^C|$  in the Fornberg Taylor coefficients of degree  $N$  Chebyshev polynomial interpolants of  $e^{-1/(x^2+1)}$  with 32 points on the circle around  $x_0 = 0$ . Same description as in the Figure B.4.

A tolerance in the disparity between the truncation errors and rounding errors estimates is throughout taken to be  $1e-14$ . This is part of the stopping criterion. In order to avoid an infinite loop of the algorithm, as this tolerance may not always be achieved due to accumulation of rounding errors, we impose a condition on the maximum absolute value of the estimated rounding errors that should not go lower than  $1e-12$ . Therefore we adopted any of these two conditions as our stopping criteria.

### B.1.7 Conditioning of the Cauchy Integral for Interpolants

Since classical formulas for differentiation are generally ill-conditioned, we have to investigate when the Cauchy formula can be well-behaved for Forneberg's algorithm implementation. The conditioning of the Cauchy integral of the analytic function  $u(x)$  can be denoted by the number  $\kappa(n, r)$ .

Let us prepare the problem for numerical approximation. The condition number  $\kappa(n, r)$  of the Cauchy integral as defined in (Bornemann [19]) and references therein, is given by

$$\kappa(n, r) := \frac{\int_0^1 |u(z_0 + re^{2\pi it})| dt}{\left| \int_0^1 e^{-2\pi int} u(z_0 + re^{2\pi it}) dt \right|} = \frac{\|u\|_{H^1(C_r)}}{|r^n a_n|} \geq 1. \quad (\text{B.1.26})$$

By definition,  $\kappa(n, r)$  computes the amount of cancellation occurring in the integral (B.1.26), where we have large cancellation when  $\kappa(n, r) \gg 1$ , and virtually zero cancellation whenever  $\kappa(n, r) \approx 1$ . It is independent on how the integral is computed.

Associated to  $\kappa$  are the possible absolute and relative errors  $\epsilon_a$  and  $\epsilon_r$  respectively, when numerical quadratures are involved in the approximation of the Cauchy integral. Since the integrals involved in (B.1.26) are of a periodic function of period 1, it can be evaluated with remarkable efficiency using  $m$ -point Trapezoidal rule (Lyod & Weidmann 2014). If  $\tilde{a}_n(m; r)$  is the approximation of  $a_n$  by the  $m$ -points trapezoidal sum, then

$$r^n \tilde{a}_n := \frac{1}{m} \sum_{j=0}^{m-1} e^{-(2\pi i/m)jn} u(z_0 + re^{(2\pi i/m)j}). \quad (\text{B.1.27})$$

The absolute and relative errors are given by

$$\epsilon_a(m, r) = r^n |a_n - \tilde{a}_n|, \quad \epsilon_r(m, r) = \frac{r^n |a_n - \tilde{a}_n|}{|a_n|}.$$

If in addition,  $\tilde{u}(z)$  is the perturbation of  $u(z)$  with corresponding perturbed data  $\tilde{a}_n, \tilde{\tilde{a}}_n$  of  $a_n$  and  $\tilde{a}_n$  respectively, then

$$\|u(z) - \tilde{u}(z)\| \leq \epsilon, \quad r^n |a_n - \tilde{a}_n| \leq 2\epsilon, \quad r^n |\tilde{a}_n - \tilde{\tilde{a}}_n| \leq 2\epsilon \quad (\text{B.1.28})$$

indicating the presence of small absolute errors  $\epsilon$  in the function  $u(z)$  and the normalised Taylor coefficients  $a_n$  and  $\tilde{a}_n$ . This proves the stability of the trapezoidal sums for the Taylor coefficients of  $u(z)$  with respect to the absolute error of the normalised coefficients. Equivalently, these coefficients are computable effectively using FFT for good choice of  $r$ .

The corresponding condition number evaluated using the  $m$ -point trapezoidal sums is

$$\tilde{\kappa}(n, r) = \frac{\sum_{j=0}^{m-1} |u(z_0 + re^{(2\pi i/m)j})|}{\left| \sum_{j=0}^{m-1} e^{(2\pi i/m)nj} u(z_0 + re^{(2\pi i/m)j}) \right|} \geq 1. \quad (\text{B.1.29})$$

Using the relative error  $\epsilon_r$  with perturbation  $\tilde{u}(z)$ , we have  $\tilde{u}(z) = u(z)(1 + \epsilon_r(z))$ , for  $\|\epsilon_r(z)\|_{C_r} \leq \epsilon$ . The upper bound of the normalised Taylor coefficients of  $u(z)$  is determined as follows

$$r^n |a_n - \tilde{a}_n| = \left| \int_0^1 e^{-2\pi i n t} u(z_0 + re^{2\pi i n t}) \epsilon_r(z_0 + re^{2\pi i n t}) dt \right| \leq \epsilon \int_0^1 |u(z_0 + re^{2\pi i n t})| dt. \quad (\text{B.1.30})$$

Consequently, one gets

$$\frac{|a_n - \tilde{a}_n|}{|a_n|} \leq \kappa(n, r) \cdot \epsilon. \quad (\text{B.1.31})$$

Thus, this establishes the relation between the relative and absolute errors. A similar relation is obtained for  $\tilde{\tilde{a}}_n$ . Now, it is left to obtain the best  $r$  such that the required accuracy is achieved for the computed coefficients.

**Optimal radius:** As mentioned earlier, the problem of finding the best radius becomes an optimization one. The task is to find such  $r_*(n)$  and  $\tilde{r}(n, m)$  for which

$$\begin{aligned} r_*(n) &= \arg \min_{0 < r < R_c} \kappa(n, r), & \kappa_*(n) &= \min_{0 < r < R_c} \kappa(n, r) \\ r_*(n, m) &= \arg \min_{0 < r < R_c} \tilde{\kappa}(n, r), & \tilde{\kappa}_*(n, m) &= \min_{0 < r < R_c} \tilde{\kappa}(n, r). \end{aligned} \quad (\text{B.1.32})$$

Consider a function  $u(z) = 1/(z_0 + z)$ , where  $z_0$  is a complex number. The real version of the function  $u(z)$  is  $u(x) = 1/(x_0 + x)$  restricted to the interval  $[0, 1]$  in particular when  $x_0 = 1$ . Let  $\zeta \in [-1, 1]$  and make the change of variables  $\zeta = 2x - 1$ . Then  $f(x)$  has Chebyshev coefficients given by

$$\begin{aligned} c_k &= \frac{2}{\pi} \int_{-1}^1 \frac{f(x) T_k(x) dx}{\sqrt{1-x^2}} = \frac{2}{\pi} \int_{-1}^1 \frac{f(x) T_k^*(x) dx}{\sqrt{x(1-x)}} = \frac{2}{\pi} \int_{-1}^1 \frac{f(\frac{\zeta+1}{2}) T_k(\zeta)}{\sqrt{1-\zeta^2}} d\zeta \\ &= \begin{cases} \sqrt{2}/2, & k = 0 \\ (-1)^k \sqrt{2}(3 - 2\sqrt{2})^k, & k \geq 1. \end{cases} \end{aligned} \quad (\text{B.1.33})$$

See (Snyder 1974 pg.40 and Mason and Handscomb 2003 eq. 5.21) for details of how  $c_k$  is computed by a tau method. Note that  $T_n^*(x) = T_n(2x - 1)$  is the shifted Chebyshev polynomial when  $x \in [0, 1]$ .

The pole at  $z = z_0 = -1$  associated to the  $u(z)$  verifies that  $0 < r < |z_0 + \sqrt{z_0^2 - 1}| = 1$  the region  $C_r$  of analyticity of  $u(z)$  is contained in the largest ellipse of foci  $\pm 1$ .

Next, the condition number  $\kappa(n, r)$  associated to the Chebyshev series is

$$\frac{\|f\|_{H^1(C_r)}}{r^n a_n^C} = \frac{1}{r^n a_n^C} \int_0^1 |u(z_0 + re^{2\pi it})| dt = \frac{1}{r^n a_n^C} \sum_{k=0}^{\infty} |c_k| \int_0^1 |T_k(z_0 + re^{2\pi it})| dt. \quad (\text{B.1.34})$$

Viewing the Chebyshev polynomial  $T_k(z)$  on the complex plane is equivalent to representing it on an ellipse of foci  $\pm 1$ , i.e.  $T_k(z) = \frac{1}{2}(z^k + z^{-k})$  is a Chebyshev polynomial defined on  $\mathbb{C}^*$  where  $z = e^{i\theta}$  is a unit circle,  $0 \leq \theta \leq 2\pi$ . Restricting the function  $u(z)$  to a circle  $C_r$  contained in the ellipse we have a Chebyshev polynomial

$$T_k(z), \quad \text{for } z = z_0 + re^{i\theta}, \quad 0 \leq \theta \leq 2\pi. \quad (\text{B.1.35})$$

Therefore, with  $u(z_0 + re^{2\pi it}) = \sum_{k=0}^{\infty} c_k z^k = c_0 + c_1 z + c_2 z^2 + \dots$ , the equation (B.1.34) takes the form

$$\kappa^C(n, r) = \frac{1}{a_n^C r^n} \sum_{k=0}^{\infty} |c_k| \int_0^1 (r^2 + z_0^2 + 2rz_0 \cos(2\pi t))^{k/2} dt. \quad (\text{B.1.36})$$

We compute the Taylor coefficients as follows

$$\begin{aligned} a_n^C &= \frac{1}{2\pi i} \int_{C_r} \frac{\sum_{k=0}^{\infty} c_k (z^k + z^{-k})/2}{(z - z_0)^{n+1}} dz \\ &= \sum_{k=0}^{\infty} \frac{c_k}{r^n} \int_0^1 e^{-2\pi nit} (z_0 + re^{2\pi it})^k dt + \sum_{k=0}^{\infty} \frac{c_k}{r^n} \int_0^1 e^{-2\pi nit} (z_0 + re^{2\pi it})^{-k} dt \\ &= \sum_{k=0}^{\infty} \frac{c_k}{r^n} \int_0^1 e^{-2\pi int} \sum_{j=0}^k \binom{k}{j} z_0^{k-j} r^j e^{2\pi ijt} + \sum_{k=0}^{\infty} \frac{c_k}{r^n} \int_0^1 e^{-2\pi int} \sum_{j=0}^{\infty} \binom{-k}{j} z_0^{-k-j} r^j e^{2\pi ijt} \\ &= \sum_{k=0}^{\infty} \frac{c_k}{r^n} \left[ \sum_{j=0}^k \binom{k}{j} C_j z^{k-j} r^j \int_0^1 e^{2\pi i(j-n)t} dt + \sum_{j=0}^{\infty} \binom{k}{j} C_j z^{-k-j} r^j \int_0^1 e^{2\pi i(j-n)t} dt \right] \end{aligned} \quad (\text{B.1.37})$$

where  $\binom{k}{j} = \frac{(-k)(-k-1)\dots(-k-j+1)}{j!} = \frac{(-k)!}{j!(-k-j)!}$ . We therefore have, for  $j = n$

$$r^n a_n^C = \sum_{k=0}^{\infty} c_k \left[ \sum_{n=0}^k \binom{k}{n} C_n z^{k-n} r^n + \sum_{n=0}^{\infty} \binom{k}{n} C_n z^{-k-n} r^n \right]. \quad (\text{B.1.38})$$

We can compute this using a fast Fourier transform of the truncated Chebyshev series with  $N$  sample points. The associated condition number to the interpolant  $u_N$  of  $u(x)$  from (B.1.26) and (B.1.29) is

$$\kappa^C(n, r) \sim \tilde{\kappa}^C(n, r) = \frac{\sum_{j=0}^{m-1} |u_N(z_0 + re^{(2\pi i/m)j})|}{\left| \sum_{j=0}^{m-1} e^{(2\pi i/m)nj} u_N(z_0 + re^{(2\pi i/m)j}) \right|} \geq 1. \quad (\text{B.1.39})$$

**Example B.1.1.** Another particular analytic function  $f(x) = 1/(a + x^2)$ , where  $a = 1$ , has

Chebyshev coefficients given by  $c_0 = \frac{\sqrt{2}}{2}$ ,  $c_k = (-1)^k \frac{(3-2\sqrt{2})^k}{(2k+1)}$ ,  $k \geq 1$ , computed using a tau method, see (Snyder, eq. (4.8) in [198]). However, based on the previous results of Fornberg's approach on interpolants, a satisfactory accuracy cannot be guaranteed.

### B.1.8 Discussion

Fornberg's method is (can be) used to approximate the Taylor coefficients of a given analytic function as accurate as possible. Thus, Fornberg's algorithm on an interpolant approximates the coefficients  $a_k$  (equivalently the derivatives of  $p_N(z)$ ) as shown in the various tables for various degrees of the Chebyshev interpolant. As the analysis suggests, the Fornberg algorithm is preferably applied to the function (analytic), if known, in order to compute numerically the approximate derivative of the function  $u(x)$ . It produces better accuracy for about half the number of the points  $m$  on the circle used on the function itself but about  $m/4$  terms are accurate if the polynomial interpolant  $p_N(x)$  replaces  $u(x)$ . Nevertheless, for some entire functions such as  $\exp(z)$  the computed errors using the algorithm on  $u(x)$  behave just like its interpolant  $p_N^C(x)$ . Larger  $m$  is not required if a smaller one yields the number of coefficients needed for the interpolant as it holds in for known analytic functions ( see Fornberg [61]). In other words, if the maximum error attained approaches machine precision  $\epsilon_M$  for smaller  $m < m'$  there is no need for larger  $m$ .

# Appendix C

## The NLS equation

Consider the NLS equation in  $\mathbb{R}^+ \times \mathbb{R}^d$  with general power non-linearity:

$$\begin{aligned} iu_t + \Delta u &= f(|u|^2)u, & u &= u(t, \mathbf{x}) : [0, \infty) \times \mathbb{R}^d \rightarrow \mathbb{C} \\ u(\mathbf{x}, 0) &= u_0(\mathbf{x}) & u_0 &: \mathbb{R}^d \rightarrow \mathbb{C} \end{aligned} \quad (\text{C.0.1})$$

Assume the solution  $u = u(\mathbf{x}, t)$  is smooth and decays rapidly along with its derivatives, as  $|\mathbf{x}| \rightarrow \infty$ , i.e. assume  $u \in S(\mathbb{R}^d \times \mathbb{R})$  a Schwartz space.

The Lagrangian density of the power nonlinearity NLS (C.0.1) can be derived to take the form ( taking  $\bar{u}$  as a complex conjugate of  $u$ ):

$$\mathcal{L}(u, \bar{u}, \nabla u, \nabla \bar{u}) = \frac{i}{2}(\bar{u}u_t - uu_t) - |\nabla u|^2 - F(|u|^2) \quad (\text{C.0.2})$$

and the energy (Hamiltonian) density can be written in the form

$$\begin{aligned} \mathcal{E}(u, \bar{u}, \nabla u, \nabla \bar{u}) &= \sum_{k=1}^n \dot{q}_k \frac{\partial \mathcal{L}}{\partial \dot{q}_k} - \mathcal{L} = \frac{i}{2}(\bar{u}u_t - uu_t) - \mathcal{L} \\ &= |\nabla u|^2 + F(|u|^2). \end{aligned} \quad (\text{C.0.3})$$

The energy functional  $E[u]$  will be the integral

$$E[u] = \int_{\mathbb{R}^d} \mathcal{E}(u, \bar{u}, \nabla u, \nabla \bar{u}) \mathbf{d}\mathbf{x} = \int_{\mathbb{R}^d} \left( |\nabla u|^2 + F(|u|^2) \right) \mathbf{d}\mathbf{x}. \quad (\text{C.0.4})$$

The variational structure of the equation, due to the Noether theorem for dynamical systems, leads to the corresponding conserved quantities associated to the invariances. Few among the most important invariances include: *mass* or *wave energy*  $M[u]$  due to phase-shift (also called gauge invariance), *energy* or *Hamiltonian*  $E[u]$  due to time translation and *momentum*  $P[u]$  as a result of space translation. These associated quantities of the equation (C.0.1) defined below can be proven to be conserved: with  $F' = f$

$$M[u] = \|u\|_2^2 = \int_{\mathbb{R}^d} |u(\mathbf{x}, t)|^2 \mathbf{d}\mathbf{x}; \quad (\text{C.0.5})$$

$$E[u] = \int_{\mathbb{R}^d} \left( |\nabla u(\mathbf{x}, t)|^2 + F(|u(\mathbf{x}, t)|^2) \right) \mathbf{d}\mathbf{x}; \quad (\text{C.0.6})$$

$$P[u] = \frac{1}{2i} \int_{\mathbb{R}^d} (u \nabla \bar{u} - \bar{u} \nabla u) \mathbf{d}\mathbf{x} = \Im \int_{\mathbb{R}^d} u \nabla \bar{u} \mathbf{d}\mathbf{x}; \quad (\text{C.0.7})$$

These quantities, respectively, describe the conservation of mass, energy and momentum.

**Proposition C.0.1.** *The quantities (C.0.5)-(C.0.7) are conserved.*

*Proof.* Let's use the complex conjugate of the given equation

$$\begin{cases} iu_t + \Delta u = f(|u|^2)u \\ -i\bar{u}_t + \Delta \bar{u} = f(|u|^2)\bar{u} \end{cases} \quad (\text{C.0.8})$$

We first show conservation of mass, therefore we need to verify that  $\frac{d}{dt} \int_{\mathbb{R}^d} |u(\mathbf{x}, t)|^2 d\mathbf{x} = 0$ .

$$\begin{aligned} \frac{d}{dt} \int_{\mathbb{R}^d} |u(\mathbf{x}, t)|^2 d\mathbf{x} &= \frac{d}{dt} \int_{\mathbb{R}^d} u\bar{u} d\mathbf{x} = \int_{\mathbb{R}^d} (u_t\bar{u} + u\bar{u}_t) d\mathbf{x} = \frac{1}{i} \int_{\mathbb{R}^d} (iu_t\bar{u} + u(i\bar{u}_t)) d\mathbf{x} \\ &= \frac{1}{i} \int_{\mathbb{R}^d} \left( (f(|u|^2)u - \Delta u)\bar{u} + u(\Delta\bar{u} - f(|u|^2)\bar{u}) \right) d\mathbf{x} \\ &= \frac{1}{i} \int_{\mathbb{R}^d} \left( -(\Delta u)\bar{u} + u\Delta\bar{u} \right) d\mathbf{x}, \quad \text{use } \Delta u = \nabla \cdot \nabla(u) \\ &= -i \int_{\mathbb{R}^d} \left( \nabla \cdot [u\nabla\bar{u} - (\nabla u)\bar{u}] \right) d\mathbf{x} = 0. \end{aligned}$$

The last integral vanishes due to the divergence theorem. The expression there is obtained by using  $\nabla \cdot (\phi\nabla\psi) = \phi\nabla^2\psi + \nabla\phi \cdot \nabla\psi$  for scalar functions  $\phi, \psi$ , such that

$$\begin{aligned} \nabla \cdot \left( (-\nabla u)\bar{u} \right) &= \nabla \cdot (-\nabla u)\bar{u} + (-\nabla u) \cdot (\nabla\bar{u}) = -(\nabla u)\bar{u} - (\nabla u) \cdot (\nabla\bar{u}); \\ \nabla \cdot (u\nabla\bar{u}) &= u\nabla^2\bar{u} + (\nabla u) \cdot (\nabla\bar{u}) = u\Delta\bar{u} + (\nabla u) \cdot (\nabla\bar{u}). \end{aligned}$$

For the energy, we need the time derivative of the quantity (C.0.6) to vanish. We therefore use similar approach. First we multiply the first equation in (C.0.8) by  $\bar{u}_t$ , the second one by  $u_t$  and taking the sum will give us the equation

$$(\Delta u)\bar{u}_t + (\Delta\bar{u})u_t = f(|u|^2)u\bar{u}_t + f(|u|^2)\bar{u}u_t.$$

Using the divergence identities, this equation is equivalent to

$$\nabla \cdot \left( (\nabla u)\bar{u}_t \right) - (\nabla u) \cdot (\nabla\bar{u}_t) + \nabla \cdot \left( (\nabla\bar{u})u_t \right) - (\nabla\bar{u}) \cdot (\nabla u_t) = f(|u|^2)(|u|^2)_t;$$

and therefore, with  $F' = f$ , we get

$$\nabla \cdot \left[ \nabla(u)\bar{u}_t + \nabla(\bar{u})u_t \right] = (F(|u|^2))_t + (|\nabla u|^2)_t = \frac{d}{dt} \left[ |\nabla u|^2 + F(|u|^2) \right].$$

Consequently,

$$\frac{d}{dt} \int_{\mathbb{R}^d} \left( |\nabla u|^2 + F(|u|^2) \right) d\mathbf{x} = \int_{\mathbb{R}^d} \nabla \cdot \left[ \nabla(u)\bar{u}_t + \nabla(\bar{u})u_t \right] d\mathbf{x} = 0,$$

by divergence theorem. It is left to prove the conservation of the momentum.

We compute the time derivative of the momentum as follows

$$\begin{aligned} \frac{d}{dt} \left[ \frac{1}{2i} \int_{\mathbb{R}^d} (\bar{u}\nabla u - u\nabla\bar{u}) d\mathbf{x} \right] &= \frac{1}{2i} \int_{\mathbb{R}^d} (\bar{u}_t\nabla u + \bar{u}\nabla u_t - u_t\nabla\bar{u} - u\nabla\bar{u}_t) d\mathbf{x} \\ &= \frac{1}{2} \int_{\mathbb{R}^d} \left[ (-i\bar{u}_t)\nabla u - \bar{u}\nabla(iu_t) + (iu_t)\nabla\bar{u} - u\nabla(-i\bar{u}_t) \right] d\mathbf{x} \end{aligned} \quad (\text{C.0.9})$$

Let  $W := (-i\bar{u}_t)\nabla u - \bar{u}\nabla(iu_t) + (iu_t)\nabla\bar{u} - u\nabla(-i\bar{u}_t)$ . Simplifying the integrand to have

$$\begin{aligned} W &= (-\Delta\bar{u} + f(|u|^2)\bar{u})\nabla u - \bar{u}\nabla(-\Delta u + f(|u|^2)u) + (f(|u|^2)u - \Delta u)\nabla\bar{u} - u\nabla(f(|u|^2)\bar{u} - \Delta\bar{u}) \\ &= (-\Delta\bar{u})\nabla u + f(|u|^2)\bar{u}\nabla u + \bar{u}\nabla(\Delta u) - \bar{u}\nabla(f(|u|^2)u) + f(|u|^2)u\nabla\bar{u} - (\Delta u)(\nabla\bar{u}) - \\ &\quad u\nabla(f(|u|^2)\bar{u}) + u\nabla(\Delta\bar{u}) \\ &= (-\Delta\bar{u})\nabla u + f(|u|^2) \cdot \nabla(|u|^2) + \nabla(\bar{u}\Delta u) - (\nabla\bar{u})(\Delta u) - \nabla(\bar{u}f(|u|^2)u) + (\nabla\bar{u})f(|u|^2)u - (\Delta u)(\nabla\bar{u}) \\ &\quad - \nabla(uf(|u|^2)\bar{u}) + (\nabla u)f(|u|^2)\bar{u} + \nabla(u\Delta\bar{u}) - (\nabla u)(\Delta\bar{u}) \\ &= -2(\Delta\bar{u})\nabla u - 2(\Delta u)(\nabla\bar{u}) + \nabla[2F(|u|^2)] + \nabla[\bar{u}\Delta u - \bar{u}f(|u|^2)u - uf(|u|^2) + u\Delta\bar{u}] \\ &= \nabla \cdot \left[ (\nabla\bar{u})(\nabla u) + 2F(|u|^2) + \bar{u}\Delta u - 2f(|u|^2)|u|^2 + u\Delta\bar{u} \right]. \end{aligned}$$

The last equality is found by divergence identity. Then, this proves that

$$\frac{d}{dt} \left[ \frac{1}{2i} \int_{\mathbb{R}^d} (\bar{u}\nabla u - u\nabla\bar{u}) d\mathbf{x} \right] = \frac{d}{dt} \left[ \Im \int_{\mathbb{R}^d} \bar{u}\nabla u d\mathbf{x} \right] = 0.$$

□

### C.0.1 Virial identity

**Proposition C.0.2.** *By the hypothesis of proposition C.0.1, the following identity*

$$\frac{d^2}{dt^2} \int_{\mathbb{R}^d} |\mathbf{x}|^2 |u|^2 dx = \int_{\mathbb{R}^d} \left[ 8|\nabla u|^2 + 4d(f(|u|^2)|u|^2) - F(|u|^2) \right] d\mathbf{x} \quad (\text{C.0.10})$$

holds from equation (C.0.6) and that there doesn't exist a solution of the (super)critical (cubic) NLS equation  $iu_t + \Delta u + |u|^2 u = 0$  in  $\mathbb{R}^d \times (0, \infty)$  for all  $t \geq 0$  if  $d \geq 2$  and

$$E[u(0)] = \int_{\mathbb{R}^d} \left[ |\nabla u(\cdot, 0)|^2 - \frac{|u(\cdot, 0)|^4}{2} \right] d\mathbf{x} < 0. \quad (\text{C.0.11})$$

The identity (C.0.10) is known as variance identity or virial theorem.

*Proof.* Taking the first derivative w.r.t.  $t$

$$\begin{aligned}
\frac{d}{dt} \int_{\mathbb{R}^d} |\mathbf{x}|^2 |u|^2 d\mathbf{x} &= \int_{\mathbb{R}^d} |\mathbf{x}|^2 (u_t \bar{u} + u \bar{u}_t) d\mathbf{x} = \frac{1}{i} \int_{\mathbb{R}^d} |\mathbf{x}|^2 \left[ -(\Delta u) \bar{u} + u (\nabla \bar{u}) \right] d\mathbf{x} \\
&= \frac{1}{i} \int_{\mathbb{R}^d} |\mathbf{x}|^2 \left[ -(\nabla u) \bar{u} + u \nabla \bar{u} \right] d\mathbf{x} \\
&= -i \int_{\mathbb{R}^d} \left\{ \nabla \cdot \left[ |\mathbf{x}|^2 \left( -(\nabla u) \bar{u} + u \nabla \bar{u} \right) \right] - 2\mathbf{x} \cdot \left( -(\nabla u) \bar{u} + u \nabla \bar{u} \right) \right\} d\mathbf{x} \\
&= 2i \int_{\mathbb{R}^d} \mathbf{x} \cdot \left( -(\nabla u) \bar{u} + u \nabla \bar{u} \right) d\mathbf{x}.
\end{aligned}$$

Taking the second derivative w.r.t  $t$

$$\begin{aligned}
\frac{d^2}{dt^2} \int_{\mathbb{R}^d} |\mathbf{x}|^2 |u|^2 d\mathbf{x} &= \frac{d}{dt} \left[ 2i \int_{\mathbb{R}^d} \mathbf{x} \cdot \left( -(\nabla u) \bar{u} + u \nabla \bar{u} \right) d\mathbf{x} \right] \\
&= 2 \int_{\mathbb{R}^d} \mathbf{x} \cdot \left[ -(\nabla(iu_t))(\bar{u}) - (\nabla u)(i\bar{u}_t) + iu_t(\nabla \bar{u}) + u(\nabla i\bar{u}_t) \right] d\mathbf{x} \\
&= 2 \int_{\mathbb{R}^d} \mathbf{x} \cdot \left[ -(\nabla(f(|u|^2))u - \Delta u) \bar{u} + (\nabla u)(f(|u|^2) \bar{u} - \nabla \bar{u}) \right. \\
&\quad \left. + (f(|u|^2)u - \Delta u)(\nabla \bar{u}) + u \left( \nabla(\Delta \bar{u} - f(|u|^2) \bar{u}) \right) \right] d\mathbf{x} \\
&= 2 \int_{\mathbb{R}^d} \mathbf{x} \cdot \left[ -\nabla(f(|u|^2)u \bar{u}) + f(|u|^2)u \nabla \bar{u} + \nabla((\Delta u) \bar{u}) - (\Delta u)(\nabla \bar{u}) \right. \\
&\quad \left. + (\nabla u)(f(|u|^2) \bar{u}) - (\nabla u)(\Delta \bar{u}) + f(|u|^2) \bar{u}(\Delta \bar{u}) - (\Delta u)(\nabla \bar{u}) \right. \\
&\quad \left. + \nabla(u \nabla \bar{u} - f(|u|^2) \bar{u}) - (\nabla u)(\Delta \bar{u} - f(|u|^2) \bar{u}) \right] d\mathbf{x}
\end{aligned}$$

The integrand simplifies to

$$\mathbf{x} \cdot \left( -2(\Delta u)(\nabla \bar{u}) - 2(\Delta \bar{u})(\nabla u) \right) = -2\mathbf{x} \cdot (\Delta u)(\nabla \bar{u}) - 2\mathbf{x} \cdot (\Delta \bar{u})(\nabla u)$$

Using the identity that

$$\begin{aligned}
\mathbf{x} \cdot (\Delta u)(\nabla \bar{u}) &= \left( \sum_{j=1}^d x_j \frac{\partial \bar{u}}{\partial x_j} \right) \left( \sum_{k=0}^d \frac{\partial^2 u}{\partial x_k^2} \right) = \sum_{k=1}^d \left[ \sum_{j=1}^d x_j \frac{\partial \bar{u}}{\partial x_j} \right] \frac{\partial^2 u}{\partial x_k^2} \\
&= \sum_{k=1}^d \frac{\partial}{\partial x_k} \left[ \left( \sum_{j=1}^d x_j \frac{\partial \bar{u}}{\partial x_j} \right) \frac{\partial u}{\partial x_k} \right] - \sum_{k=1}^d \frac{\partial \bar{u}}{\partial x_k} \frac{\partial u}{\partial x_k} - \sum_{k=1}^d \left[ \sum_{j=1}^d x_j \frac{\partial^2 \bar{u}}{\partial x_k \partial x_j} \right] \frac{\partial u}{\partial x_k} \\
&= \nabla \cdot \left( (\mathbf{x} \cdot \nabla \bar{u}) \nabla u \right) - |\nabla u|^2 - \sum_{k=1}^d \left[ \sum_{j=1}^d x_j \frac{\partial^2 \bar{u}}{\partial x_k \partial x_j} \right] \frac{\partial u}{\partial x_k}
\end{aligned}$$

similarly,

$$\mathbf{x} \cdot (\Delta \bar{u})(\nabla u) = \nabla \cdot \left( (\mathbf{x} \cdot \nabla u) \nabla \bar{u} \right) - |\nabla u|^2 - \sum_{k=1}^d \left[ \sum_{j=1}^d x_j \frac{\partial^2 u}{\partial x_k \partial x_j} \right] \frac{\partial \bar{u}}{\partial x_k}.$$

then

$$\begin{aligned}
 -2\mathbf{x} \cdot (\Delta u)(\nabla \bar{u}) - 2\mathbf{x} \cdot (\Delta \bar{u})(\nabla u) &= \nabla \cdot \left[ -2\mathbf{x} \cdot (\Delta u)(\nabla \bar{u}) - 2\mathbf{x} \cdot (\Delta \bar{u})(\nabla u) \right] + 4|\nabla u|^2 \\
 &\quad + 2 \sum_{k=1}^d \left[ \sum_{j=1}^d x_j \frac{\partial^2 u}{\partial x_k \partial x_j} \right] \frac{\partial \bar{u}}{\partial x_k} + 2 \sum_{k=1}^d \left[ \sum_{j=1}^d x_j \frac{\partial^2 \bar{u}}{\partial x_k \partial x_j} \right] \frac{\partial u}{\partial x_k} \\
 &= \nabla \cdot \left[ -2\mathbf{x} \cdot (\Delta u)(\nabla \bar{u}) - 2\mathbf{x} \cdot (\Delta \bar{u})(\nabla u) \right] + 4|\nabla u|^2 \\
 &\quad + 2 \sum_{j=1}^d x_j (|\nabla u|^2)_{x_j} \\
 &= \nabla \cdot \left[ -2\mathbf{x} \cdot (\Delta u)(\nabla \bar{u}) - 2\mathbf{x} \cdot (\Delta \bar{u})(\nabla u) \right] + 4|\nabla u|^2 \\
 &\quad + 2 \sum_{j=1}^d (x_j |\nabla u|^2)_{x_j} - 2 \sum_{j=1}^d |\nabla u|^2 \\
 &= \nabla \cdot \left[ -2(\mathbf{x} \cdot \nabla \bar{u}) \nabla u - 2(\mathbf{x} \cdot \nabla u) \nabla \bar{u} + 2\mathbf{x} |\nabla u|^2 \right] + (4 - 2d) |\nabla u|^2
 \end{aligned} \tag{C.0.12}$$

Substituting back into the main integral we get

$$\begin{aligned}
 \frac{d^2}{dt^2} \int_{\mathbb{R}^d} |\mathbf{x}|^2 |u|^2 \mathbf{d}\mathbf{x} &= 2 \int_{\mathbb{R}^d} \left\{ \mathbf{x} \cdot \nabla \left[ -f(|u|^2)|u|^2 + 2F(|u|^2) + (\nabla u)\bar{u} + u\nabla \bar{u} - f(|u|^2)|u|^2 \right] \right. \\
 &\quad \left. - 2\nabla \cdot [(\nabla u)(\mathbf{x} \cdot (\nabla \bar{u}) + (\nabla \bar{u})(\mathbf{x} \cdot \nabla u) + 2\mathbf{x} |\nabla u|^2)] + (4 - 2d) |\nabla u|^2 \right\} \mathbf{d}\mathbf{x} \\
 &= 2 \int_{\mathbb{R}^d} \left\{ \nabla \cdot \left[ \mathbf{x} \cdot (-2f(|u|^2)|u|^2 + 2F(|u|^2)) + (\nabla u)\bar{u} + u(\Delta \bar{u}) \right] \right. \\
 &\quad \left. + 2df(|u|^2)|u|^2 - 2dF(|u|^2) - d(\Delta u)\bar{u} - du(\Delta \bar{u}) + (4 - 2d) |\nabla u|^2 \right\} \mathbf{d}\mathbf{x} \\
 &= 2 \int_{\mathbb{R}^d} \left\{ 2df(|u|^2)|u|^2 - 2dF(|u|^2) + 2d|\nabla u|^2 + 2d|\nabla u|^2 \right\} \mathbf{d}\mathbf{x} \\
 &= 8 \int_{\mathbb{R}^d} |\nabla u|^2 \mathbf{d}\mathbf{x} + 4d \int_{\mathbb{R}^d} (f(|u|^2)|u|^2 - F(|u|^2)) \mathbf{d}\mathbf{x} \\
 &= 8 \int_{\mathbb{R}^d} (|\nabla u|^2 + |F(|u|^2)|) \mathbf{d}\mathbf{x} + 4 \int_{\mathbb{R}^d} (f(|u|^2)|u|^2 - (d+2)F(|u|^2)) \mathbf{d}\mathbf{x} \\
 &= 8E[u] + 4 \int_{\mathbb{R}^d} \left[ (|u|^2)|u|^2 f d - (d+2)F(|u|^2) \right] \mathbf{d}\mathbf{x}.
 \end{aligned} \tag{C.0.13}$$

This proves the virial formula. In the case of power non-linearity  $f(|u|^2) = \gamma|u|^{2\sigma}$ , for  $\gamma = \pm 1$ , then  $F(|u|^2) = \frac{\gamma}{\sigma+1}|u|^{2\sigma+2}$  and  $f(|u|^2)|u|^2 - F(|u|^2) = \gamma \frac{\sigma}{\sigma+1}|u|^{2\sigma+2}$ . Thus the integral (C.0.13) becomes

$$\begin{aligned}
 \frac{d^2}{dt^2} \int_{\mathbb{R}^d} |\mathbf{x}|^2 |u|^2 \mathbf{d}\mathbf{x} &= 8E[u] + 4\gamma \frac{(\sigma d - 2)}{(\sigma + 1)} \int_{\mathbb{R}^d} |u|^{2\sigma+2} \mathbf{d}\mathbf{x} \\
 &= 8E[u] + 4\gamma \frac{(\sigma d - 2)}{(\sigma + 1)} \|u\|_{2\sigma+2}^{2\sigma+1}.
 \end{aligned} \tag{C.0.14}$$

Next, we check the existence of solution when  $E[u(0)] < 0$  for  $d \geq 2$ . If  $\gamma = -1$  and  $E[u(0)] < 0$ , then we get at the critical dimension  $\sigma d = 2$  with  $\sigma = 1$  the energy function

$$\begin{aligned} E[u(t)] &= \int_{\mathbb{R}^d} (|\nabla u|^2 + F(|u|^2)) \mathbf{d}\mathbf{x} = \int_{\mathbb{R}^d} \left( |\nabla u|^2 + \gamma \frac{1}{\sigma+1} |u|^{2\sigma+2} \right) \mathbf{d}\mathbf{x} \\ &= \int_{\mathbb{R}^d} (|\nabla u|^2 - \frac{1}{2} |u|^4) \mathbf{d}\mathbf{x} = E[u(0)] < 0. \end{aligned}$$

Therefore, on integrating the terms

$$\frac{d^2}{dt^2} \int_{\mathbb{R}^d} |\mathbf{x}|^2 |u|^2 \mathbf{d}\mathbf{x} = 4 \left[ \int_{\mathbb{R}^d} |\nabla u|^2 - \frac{d}{2} |u|^4 \right] \mathbf{d}\mathbf{x} = 4E[u(0)] < 4E[u(0)] \quad (\text{C.0.15})$$

twice w.r.t.  $t$  we get

$$\frac{d^2}{dt^2} \int_{\mathbb{R}^d} |\mathbf{x}|^2 |u|^2 \mathbf{d}\mathbf{x} < \int (4E(0)t + c_0) dt = 2E(0)t^2 + c_0t + c_1.$$

However, the RHS will be negative if  $t$  is large enough. But the LHS is non-negative. This is a contradiction. Thus,  $u$  cannot exist for all  $t \geq 0$ . Hence, QED.  $\square$

## C.0.2 Proof of Pohozaev Identities

Assume  $Q > 0$ . Using the profile equation (4.3.4), we multiply by  $Q$  and integrate by part the term  $\int_{\mathbb{R}^d} Q \Delta Q$  to get  $-\int_{\mathbb{R}^d} |\nabla Q|^2 + \int_{\mathbb{R}^d} |Q|^{2\sigma+2} - \omega \int_{\mathbb{R}^d} |Q|^2 = 0$ . This is equivalent to

$$\|\nabla Q\|_2^2 + \omega \|Q\|_2^2 = \|Q\|_{2\sigma+2}^{2\sigma+2}. \quad (\text{C.0.16})$$

Similarly, multiplying (4.3.4) by  $\mathbf{x} \cdot \nabla Q$  and integrate by part for the first integral

$$\begin{aligned} 0 &= \int_{\mathbb{R}^d} (\mathbf{x} \cdot \nabla Q) \Delta Q + \int_{\mathbb{R}^d} (\mathbf{x} \cdot \nabla Q) (|Q|^{2\sigma} Q - \omega Q) \\ &= - \int_{\mathbb{R}^d} \nabla(\mathbf{x} \cdot \nabla Q) \cdot \nabla Q + \int_{\mathbb{R}^d} \mathbf{x} \cdot \left[ \frac{1}{2\sigma+2} \nabla(|Q|^{2\sigma+2}) - \frac{\omega}{2} \nabla Q^2 \right] \end{aligned}$$

where the  $(\mathbf{x} \cdot \nabla u)f = x_1 \frac{\partial u}{\partial x_1} u + \dots + x_d \frac{\partial u}{\partial x_d} u = \mathbf{x} \cdot \nabla(u^2/2)$  is used for the second integral. Since  $\partial_{x_j}(\mathbf{x} \cdot \nabla Q) = \partial_{x_j} Q + \mathbf{x} \cdot \nabla \partial_{x_j} Q$  then  $\nabla(\mathbf{x} \cdot \nabla Q) = \nabla Q + (\mathbf{x} \cdot \nabla) \nabla Q$ . We proceed as follows

$$\begin{aligned} 0 &= - \int_{\mathbb{R}^d} (\nabla Q + (\mathbf{x} \cdot \nabla) \nabla Q) \cdot \nabla Q - \int_{\mathbb{R}^d} \left( \frac{1}{2\sigma+2} |Q|^{2\sigma+2} - \frac{\omega}{2} Q^2 \right) \nabla \mathbf{x} \\ &= - \int_{\mathbb{R}^d} |\nabla Q|^2 - \frac{1}{2} \int_{\mathbb{R}^d} \mathbf{x} \cdot \nabla (|\nabla Q|^2) - d \int_{\mathbb{R}^d} \left( \frac{1}{2\sigma+2} |Q|^{2\sigma+2} - \frac{\omega}{2} Q^2 \right) \\ &= \left( -1 + \frac{d}{2} \right) \int_{\mathbb{R}^d} |\nabla Q|^2 - \frac{d}{2\sigma+2} \int_{\mathbb{R}^d} |Q|^{2\sigma+2} + \frac{\omega d}{2} \int_{\mathbb{R}^d} |Q|^2. \end{aligned}$$

Therefore, we have

$$(d-2) \|\nabla Q\|_2^2 + \omega d \|Q\|_2^2 = \frac{d}{\sigma+1} \|Q\|_{2\sigma+2}^{2\sigma+2}. \quad (\text{C.0.17})$$

Putting together the equations (C.0.16) and (C.0.16) will lead to the two identities. The first one is obtained by eliminating  $\|Q\|_2^2$  and second one by eliminating  $\|\nabla Q^2\|_2$ . Hence, proved.

### C.1 Asymptotic profile of the ground state $Q$ for NLS

Some of the asymptotic behaviour of  $Q$  for  $r \gg 1$  and  $0 \leq r \ll 1$  are as follows. If we take  $Q \in H^1(\mathbb{R}^d)$  and  $r \gg 1$  and

$$\lim_{r \rightarrow \infty} Q(r) = 0, \quad \text{and} \quad \lim_{r \rightarrow \infty} Q'(r) = 0$$

then a nontrivial solution  $Q$  behaves like

$$Q(r) \sim C e^{(1-d)/2} e^{-r}, \quad r \gg 1, \quad \text{where } C = \text{constant}. \quad (\text{C.1.1})$$

This is proved to hold based on the assumption that  $\lim_{r \rightarrow \infty} |Q|^{2\sigma} Q = 0$  and the solution to the linear problem, at infinity, will lead to the asymptotic result (C.1.1).

If, moreover,  $0 \leq r \ll 1$ , applying l'Hopital rule gives the asymptotic result for  $Q(r)$ . Provided  $Q(0)$  is positive and since  $|Q(0)|^{2\sigma} > \sigma + 1 > 1$  then  $Q''(0) < 0$ . This goes with the results found in the Lemma C.1.0.1 about the global maximum of  $|Q|$  is attained at the origin. The l'hopital rule on the main equation (4.5.3) yields

$$Q''(0) = \frac{1}{d} \lim_{r \rightarrow 0} \Delta Q(r) = \frac{1}{d} \left[ Q(0) - |Q(0)|^{2\sigma+1} \right]. \quad (\text{C.1.2})$$

Using the Taylor series expansion of  $Q(r)$  about the origin and the equation (C.1.2) we have that asymptotically  $Q$  behaves like

$$Q(r) = Q(0) + \frac{1}{2d} \left[ Q(0) - |Q(0)|^{2\sigma+1} \right] r^2 + O(r^4). \quad (\text{C.1.3})$$

**Lemma C.1.0.1** (Fibich [54]). *If  $Q^{(n)}(r)$  is a nontrivial solution of the problem (4.5.3) in  $H^1(\mathbb{R}^d)$  and  $d > 1$ , then for any two extremum points  $0 \leq r_{min} < r_{max}$  satisfying  $dQ^{(n)}(r_{min})/dr = dQ^{(n)}(r_{max})/dr = 0$ , we have  $|Q^{(n)}(r_{max})| < |Q^{(n)}(r_{min})|$ . In particular, this implies that the global maximum of the  $Q^{(n)}(r)$  is reached at the origin  $r = 0$ .*

The  $Q^{(n)}(r)$  are the excited states for  $n > 1$ , with the ground state given by  $n = 0$ . See the proof of this lemma in Fibich ([51], pg. 144).

**Proposition C.1.1** (The Asymptotic profile for  $Q$ ). *The asymptotic solution of (4.6.17) as  $\rho \rightarrow \infty$  decomposes to*

$$Q \sim c_1 Q_1 + c_2 Q_2 = c_1 |\rho|^{-\frac{i}{\alpha} - \frac{1}{\sigma}} + c_2 |\rho|^{\frac{i}{\alpha} + \frac{1}{\sigma} - d} e^{-i\alpha \rho^2/2}, \quad a, b \in \mathbb{C}. \quad (\text{C.1.4})$$

*Proof.* Let us write  $Q(\rho) = X(\rho)Y(\rho)$ . Next, we choose  $X$  in such away that  $Y_\rho$  disappeared from the obtained equation. Therefore, we get

$$X_{\rho\rho}Y + 2X_\rho Y_\rho + XY_{\rho\rho} + \frac{(d-1)}{\rho}(X_\rho Y + XY_\rho) + i\alpha \left( \frac{XY}{\sigma} + \rho X_\rho Y + \rho XY_\rho \right) + |XY|^{2\sigma} XY = 0. \quad (\text{C.1.5})$$

This is equivalent to requiring

$$\left( 2X_\rho + \frac{(d-1)}{\rho}X + i\alpha X_\rho \right) Y = 0, \quad (\text{C.1.6})$$

which has the solution

$$X(\rho) = \rho^{-\frac{(d-1)}{2}} e^{-i\alpha \frac{\rho^2}{4}}. \quad (\text{C.1.7})$$

Therefore, equation (C.1.5) becomes

$$Y'' + \left( \frac{1}{4}\rho^2\alpha^2 + i\alpha \left( \frac{d}{2} - \frac{1}{\sigma} \right) - 1 + \rho^{\sigma(1-d)}|Y|^{2\sigma} - \frac{1}{4\rho^2}(d-1)(d-3) \right) Y = 0. \quad (\text{C.1.8})$$

Again, letting  $Y(\rho) = e^{Z(\rho)}$  transformed (C.1.8) to

$$Z'' + Z'^2 + \frac{1}{4}\rho^2\alpha^2 + i\alpha \left( \frac{\sigma d - 2}{2\sigma} \right) - 1 - \frac{1}{4\rho^2}(d-1)(d-3) = o(\rho^{\sigma(1-d)}e^{2w\sigma}). \quad (\text{C.1.9})$$

As  $\rho \rightarrow \infty$ , solution to the equation (C.1.9) becomes

$$Z_{1,2} \approx \pm i\alpha \frac{\rho^2}{4} \mp \left( \frac{i}{\alpha} \pm \frac{(\sigma \mp (\sigma d - 2))}{2\sigma} \right) \ln |\rho|. \quad (\text{C.1.10})$$

Combining the results of (C.1.7) and (C.1.10), the solution as proposed reads

$$\begin{aligned} Q &\approx c_1 \rho^{-\frac{(d-1)}{2}} |\rho|^{-\frac{i}{\alpha} - \frac{(\sigma - (\sigma d - 2))}{2\sigma}} + c_2 \rho^{-\frac{(d-1)}{2}} e^{-i\alpha \frac{\rho^2}{2}} |\rho|^{\frac{i}{\alpha} - \frac{(\sigma + (\sigma d - 2))}{2\sigma}} \\ &\approx \rho^{-\frac{(d-1)}{2}} |\rho|^{\frac{(d-1)}{2}} \left( c_1 |\rho|^{-\frac{i}{\alpha} - \frac{1}{\sigma}} + c_2 e^{-i\alpha \frac{\rho^2}{4}} |\rho|^{\frac{i}{\alpha} - \frac{1}{\sigma} - d} \right) \\ &\approx c_1 |\rho|^{-\frac{i}{\alpha} - \frac{1}{\sigma}} + c_2 e^{-i\alpha \frac{\rho^2}{4}} |\rho|^{\frac{i}{\alpha} - \frac{1}{\sigma} - d}, \quad \rho > 0. \end{aligned}$$

Note however, that for the components  $Q^{(k)}(\rho) = X(\rho)e^{Z_k}$ , the  $Q^{(1)}, Q_\rho^{(2)} \notin L^2(\mathbb{R}^d)$  but  $Q^{(2)}, Q_\rho^{(1)} \in L^2(\mathbb{R}^d)$ .  $\square$

**Proposition C.1.2** ([202]). *Suppose  $Q$  solves (4.6.17),*

(i) *with  $Q_\rho \in L^2(\mathbb{R}^d)$  and  $Q \in L^{2\sigma+2}(\mathbb{R}^d)$  and  $d \neq 2 + 2/\sigma$ , then the Hamiltonian*

$$\int_{\mathbb{R}} (|Q_\rho|^2 - \frac{1}{\sigma+1}|Q|^{2\sigma+2})\rho^{d-1}d\rho = 0, \quad (\text{C.1.11})$$

*moreover, if  $Q(\rho) = e^{-i\alpha\frac{\rho^2}{4}}S(\rho)$ , i.e. a correction term is involved,*

$$\int_{\mathbb{R}} \left( |S_\rho|^2 - \frac{1}{\sigma+1}|S|^{2\sigma+2} + \alpha\Im(\rho S S_\rho^*) + \frac{\alpha^2\rho^2}{4}|S|^2 \right) \rho^{d-1}d\rho = 0. \quad (\text{C.1.12})$$

(ii) *with  $Q \in H^1(\mathbb{R}^d) \cap L^{2\sigma+2}(\mathbb{R}^d)$  and provided  $\sigma d > 2$ , then  $Q \equiv 0$ .*

*Proof.* (i) Multiplying the equation (4.6.17) with  $\Delta Q^*$  and integrate the imaginary part to get

$$\alpha\Re \int_{\mathbb{R}} \left( \frac{Q}{\sigma} + \rho Q_\rho \right) \Delta Q^* \rho^{d-1}d\rho + \Im \int_{\mathbb{R}} |Q|^{2\sigma} Q \Delta Q^* \rho^{d-1}d\rho = 0. \quad (\text{C.1.13})$$

The first integral yields

$$\begin{aligned} \alpha\Re \int_{\mathbb{R}} \left( \frac{Q}{\sigma} + \rho Q_\rho \right) \Delta Q^* \rho^{d-1}d\rho &= -\left( \frac{1}{\sigma} + 1 \right) \alpha\Re \int_{\mathbb{R}} (|Q_\rho|^2 - \rho Q_\rho) \rho^{d-1}d\rho, \\ &= -\alpha \left( \frac{1}{\sigma} + 1 - \frac{d}{2} \right) \int_{\mathbb{R}} |Q_\rho|^2 \rho^{d-1}d\rho. \end{aligned} \quad (\text{C.1.14})$$

Similarly, the second integral becomes

$$\begin{aligned} \Im \int_{\mathbb{R}} |Q|^{2\sigma} Q \Delta Q^* \rho^{d-1}d\rho &= \Im \int_{\mathbb{R}} Q^{\sigma+1} (Q^*)^\sigma \Delta Q^* \rho^{d-1}d\rho, \\ &= \frac{\alpha}{\sigma+1} \left( \frac{1}{\sigma} + 1 - \frac{d}{2} \right) \int_{\mathbb{R}} |Q_\rho|^{2\sigma+2} \rho^{d-1}d\rho. \end{aligned} \quad (\text{C.1.15})$$

Combining these results lead to the result (C.1.11) since  $d \neq 2 + \sigma/2$ . The equivalent form (C.1.12) is equally obtainable.

(ii) Multiply (4.6.17) by  $Q^*$  and integrate over  $\mathbb{R}^d$  the imaginary part to have

$$\int_{\mathbb{R}} \Im \left[ Q^* \Delta Q + i\alpha \left( \frac{Q}{\sigma} + \rho Q_\rho \right) Q^* + |Q|^{2\sigma} Q Q^* \right] \rho^{d-1}d\rho = 0$$

simplified to, where with  $\partial_\rho(|Q|^2) = Q_\rho Q^* + Q Q_\rho^* = 2\Re(Q_\rho Q^*)$ ,

$$\begin{aligned} \alpha \int_{\mathbb{R}} \left( \frac{|Q|^2}{\sigma} + \rho Q_\rho Q^* \right) \rho^{d-1} d\rho &= \alpha \left[ \frac{1}{\sigma} \int_{\mathbb{R}} |Q|^2 \rho^{d-1} d\rho + \Re \int_{\mathbb{R}} \frac{1}{2} \partial_\rho(|Q|^2) \rho^d d\rho \right] \\ &= \alpha \left[ \frac{1}{\sigma} \int_{\mathbb{R}} |Q|^2 \rho^{d-1} d\rho + \frac{1}{2} \rho^d |Q|^2 \Big|_{\mathbb{R}} - \int_{\mathbb{R}} |Q|^2 \cdot \frac{d}{2} \cdot \rho^{d-1} d\rho \right] \\ &= \alpha \left( \frac{1}{\sigma} - \frac{d}{2} \right) \int_{\mathbb{R}} |Q|^2 \rho^{d-1} d\rho. \end{aligned}$$

Unless  $\sigma d = 2$ , but  $Q$  is identically zero when  $\sigma d > 2$  and  $\alpha > 0$ .  $\square$

**Proposition C.1.3.** *Assume  $\alpha \rightarrow 0^+$ ,  $d(\alpha) \downarrow 2/\sigma$ , then an admissible  $Q$  satisfies the following.*

(i) *If  $\alpha \ll \rho^{-1}$ , then  $Q(\rho) \approx R(\rho)e^{-i\alpha\rho^2/4}$ . Or equivalently, if  $Q(\rho) = P(\rho)e^{-i\alpha\rho^2/4}$ , the function  $P$ , satisfying*

$$P_{\rho\rho} + \frac{(d-1)}{\rho} P_\rho - P + \frac{\alpha^2 \rho^2}{4} P - i\alpha \frac{(\sigma d - 2)}{2\sigma} P + |P|^{2\sigma} P = 0, \quad \rho \in \mathbb{R}^+, \quad (\text{C.1.16})$$

$$\text{subject to } P_\rho(0) = 0, P \rightarrow 0 \text{ as } \rho \rightarrow \infty, \text{ with } P(0) \text{ real,} \quad (\text{C.1.17})$$

*approaches the ground state  $R(\rho)$ .*

(ii) *If  $\alpha \gg \rho^{-1}$ , then  $Q \approx \rho^{-i/\alpha-1/\sigma}$  with  $\sigma\mu^2 = (\sigma d - 2)M_c$*

(iii) *The asymptotic behaviour of  $d(\alpha)$  is determined by*

$$\nu(\alpha) := \frac{\alpha(\sigma d - 2)}{2\sigma} \approx \frac{\nu_0^2}{M_c} e^{-\pi/\alpha}, \quad (\text{C.1.18})$$

*where  $M_c := \int_{\mathbb{R}^+} R^2 \rho^{d-1} d\rho$  defines the critical mass and  $\nu_0 := \lim_{\rho \rightarrow \infty} \rho^{(d-1)/2} R(\rho)$ .*

*Proof.* For the purpose of the second part of the proof (ii) and the rest, it is useful to obtain equation of  $Q$  in terms of amplitude  $R$  and phase  $\theta$ . This is achieved by integrating (4.7.3) over  $[0, \rho]$  to have

$$\theta_\rho + \frac{\alpha}{2}\rho = -\frac{(\sigma d - 2)}{\sigma\rho^{\sigma d - 1}R^2} \int_0^\rho \theta_\rho R^2 \tilde{\rho}^{2/\sigma - 2} d\tilde{\rho}. \quad (\text{C.1.19})$$

(i) With  $\rho$  fixed,  $\alpha \ll \rho^{-1}$ , in the equation (C.1.19), as  $d \rightarrow 2/\sigma$  while  $\alpha \rightarrow 0$ , and  $R$  tends to a real positive solution of the ground state equation

$$R_{\rho\rho} + \frac{(d-1)}{\rho} R_\rho - R + R^{2\sigma+1} = 0 \quad (\text{C.1.20})$$

then we have  $\theta_\rho + \alpha\rho/2 \approx 0$  leading to the solution  $\theta \approx -\alpha\rho^2/4$ . Thus,  $Q(\rho) \approx R(\rho)e^{-i\alpha\rho^2/4}$ .

The results of the alternate form (C.1.16) will directly follows.

(ii) Fixing  $\rho$  and  $\alpha \gg \rho^{-1}$ , for large  $\rho$ , the right-hand-side of the equation (C.1.19) is not negligible. Recall that the asymptotic behaviour of  $Q$  reads, for  $c_1, c_2 \in \mathbb{C}$

$$Q(\rho) \approx e^{-i\alpha\rho^2/4} \rho^{(1-d)/2} \left[ c_1 e^{i\alpha\rho^2/4} \rho^{-\frac{i}{\alpha} - \frac{(\sigma - (\sigma d - 2))}{2\sigma}} + c_2 e^{-i\alpha\rho^2/4} \rho^{\frac{i}{\alpha} - \frac{(\sigma + (\sigma d - 2))}{2\sigma}} \right] \quad (\text{C.1.21})$$

$$\stackrel{\sigma d = 2}{\approx} \rho^{-\frac{1}{\sigma}} \left[ c_1 \rho^{-\frac{i}{\alpha}} + c_2 e^{-i\alpha\rho^2/2} \rho^{\frac{i}{\alpha}} \right].$$

As  $\rho \rightarrow \infty$ , asymptotically  $Q(\rho) \approx e^{i\tilde{\theta}} R(\rho) \approx \mu \rho^{-\frac{1}{\sigma} - \frac{i}{\sigma}} = \mu \rho^{-\frac{1}{\sigma}} e^{-i\frac{1}{\alpha} \ln |\rho|}$  where  $\mu = c_1$ . By comparison, one has  $\tilde{\theta}(\rho) = -\frac{1}{\alpha} \ln |\rho|$  and

$$R(\rho) \approx \mu \rho^{-\frac{1}{\sigma}} \quad \text{and} \quad \tilde{\theta}_\rho \approx -\frac{1}{\alpha \rho}. \quad (\text{C.1.22})$$

This equation (C.1.22) indicates the convergence of the integral in the right-hand-side of (C.1.19). However, the main contribution to this integral comes from  $\alpha \ll \tilde{\rho}^{-1}$ , therefore this results to

$$\int_0^\rho \theta_{\tilde{\rho}} R^2 \tilde{\rho}^{2/\sigma - 2} d\tilde{\rho} \approx -\frac{\alpha}{2} \int_0^\rho R^2 \tilde{\rho}^{2/\sigma - 1} d\tilde{\rho} = -\frac{\alpha}{2} M_c. \quad (\text{C.1.23})$$

Using  $\theta_\rho \approx -1/(\alpha\rho)$  for  $\alpha \gg \rho^{-1}$  in the equation (C.1.19), as  $\rho \rightarrow \infty$ , equate the unbounded terms  $\alpha\rho/2$  and  $\frac{\alpha\rho(\sigma d - 2)}{2\sigma\mu^2} M_c$  will lead to the required result.

(iii) This is proved via WKB approximation, by matching the solution for  $\rho\alpha \gg 2$  to the ground state  $R$  which for sufficiently large  $\rho$ , behaves like  $R(\rho) \approx \nu_0 \rho^{(1-d)/2} e^{-\rho}$ .

Defining  $Y(\rho)$  so that  $Q(\rho) = e^{-i\alpha\rho^2/4} \rho^{-(d-1)/2} Y(\rho)$  satisfies the equation (C.1.8). As seen earlier in (i), the form  $Q(\rho) \approx R(\rho) e^{-i\alpha\rho^2/4} = \rho^{(d-1)/2} e^{-i\alpha\rho^2/4}$  is valid for moderately small  $\rho$  when  $d \approx 2/\sigma$ . However, the assumption  $\rho \gg 1$  reduces (C.1.8) to the equation

$$Y'' - \left( 1 - \frac{\alpha^2 \rho^2}{4} \right) Y = 0. \quad (\text{C.1.24})$$

Noting that, the effect of nonlinearity of  $Q$  in (4.6.17) is only relevant for  $\rho \ll 1$ , up to the quadratic phase factor  $e^{-i\alpha\rho^2/4}$  when the  $Q$  is approximated by the ground-state  $R$ . That is, at large  $\rho$  the equation for  $Q$  is considered as linear one.

The equation (C.1.24) is solvable via WKB approximation [202]. Letting  $x = \alpha\rho^2/2$  and  $p(x) = 1 - x^2$ , the equation (C.1.24) becomes

$$Y_{xx} = \frac{4}{\alpha^2} p(x) Y \quad (\text{C.1.25})$$

Details on the WKB approximation to this equation is discussed in [203] for  $x \ll 1$  and  $x \gg 1$ . Moreover, exact solution can be obtained as a superposition of Weber parabolic

functions [107]. For the completion of this proof see [202] Section 8.1.3.  $\square$

**Proposition C.1.4.** *The asymptotic form of the collapsing solution to the focusing NLS equation at the critical dimensions  $\sigma d = 2$  near singularity is*

$$\psi(t, \mathbf{x}) \approx \frac{1}{\lambda(t)} e^{i\left(\tau(t) - \alpha(t) \frac{|\mathbf{x}|^2}{4\lambda^2(t)}\right)} P\left(\beta(t), \frac{\mathbf{x}}{\lambda(t)}\right) \quad (\text{C.1.26})$$

where  $\tau_t = \lambda^{-2}$ ,  $\alpha = -\lambda_t \lambda$ ,  $\beta = -\lambda^3 \lambda_{tt}$  and  $\beta = \alpha^2 + \alpha_\tau \approx \alpha^2$ . The  $\beta$  obeys

$$\beta_\tau(\tau) = -\frac{2M_c}{M} \nu(\beta) \approx -\frac{2\nu_0^2}{M} e^{-\pi/\sqrt{\beta}}, \quad (\text{C.1.27})$$

where  $M = \frac{1}{4} \int_0^\infty R^2 \rho^2 \rho^{2/\sigma-1} d\rho$  and  $M_c = \int_0^\infty R^2 \rho^{2/\sigma-1} d\rho$ .

*Proof.* One plugs  $V(\tau, \rho) = P(\beta, \rho) + W(\tau, \rho)$  into (4.7.6). Following the simplification of the nonlinear term

$$\begin{aligned} |V|^{2\sigma} V &= |(P+W)|^{2\sigma} (P+W) = (P^* + W^*)^\sigma (P+W)^{\sigma+1} \\ &= P^{*\sigma} (1 + P^{*-1} W^*)^\sigma P^{\sigma+1} (1 + P^{-1} W)^{\sigma+1} \\ &= P^{*\sigma} P^{\sigma+1} (1 + \sigma P^{*-1} W^* + o(W)) (1 + (\sigma+1) P^{-1} W + o(W)) \\ &= P^{*\sigma} P^{\sigma+1} (1 + (\sigma+1) P^{-1} W + \sigma P^{*-1} W^* + \sigma(\sigma+1) P^{*-1} P^{-1} |W|^2 + o(W^3)) \\ &= |P|^{2\sigma} P + (\sigma+1) |P|^{2\sigma} W + \sigma P^{*\sigma-1} P^{\sigma+1} W + o(W) \end{aligned}$$

to get

$$\begin{aligned} i\left(P_\beta \frac{\partial \beta}{\partial \tau} + W_\tau\right) + P_{\rho\rho} + W_{\rho\rho} + \frac{d-1}{\rho} (P_\rho + W_\rho) - W - P + \frac{1}{4} \beta(\tau) \rho^2 (P+W) \\ + |P|^{2\sigma} P + (\sigma+1) |P|^{2\sigma} W + \sigma P^{*\sigma-1} P^{\sigma+1} W + o(W) = 0. \end{aligned}$$

Applying the condition (4.7.9) on  $P$ , the above equation reduces to

$$\begin{aligned} W_{\rho\rho} + \frac{(d-1)}{\rho} W_\rho - W + \frac{1}{4} \beta(\tau) \rho^2 W - i\nu(\sqrt{\beta}) W + (\sigma+1) |P|^{2\sigma} W + \sigma P^{*\sigma-1} P^{\sigma+1} \\ = -i\left(\frac{\partial P}{\partial \beta} \beta_\tau + \nu(\sqrt{\beta}) P\right) + \frac{\nu(\sqrt{\beta})}{2\sqrt{\beta}} \frac{1}{\rho} (P_\rho + W_\rho) - i\nu(\sqrt{\beta}) (P+W) + o(W) \\ \underset{\beta(\tau) \rightarrow 0}{\approx} -i\left(\frac{\partial P}{\partial \beta} \beta_\tau + \nu(\sqrt{\beta}) P\right) + \frac{\nu(\sqrt{\beta})}{2\sqrt{\beta}} \frac{1}{\rho} P_\rho. \end{aligned}$$

Furthermore,  $\partial P / \partial \beta|_{\beta=0} = \zeta$ , where  $\zeta$  satisfies

$$\zeta_{\rho\rho} + \frac{(d-1)}{\rho} \zeta_\rho - \zeta + (2\sigma+1) R^{2\sigma} \zeta - \frac{\rho^2}{4} R = 0 \quad (\text{C.1.28})$$

for ground state solution  $R$ . Letting  $W = S + iT$  and separating the real and imaginary parts yield

$$S_{\rho\rho} + \frac{(d-1)}{\rho}S_{\rho} - S + (2\sigma+1)R^{2\sigma}S = \frac{\nu(\sqrt{\beta})}{2\sqrt{\beta}}\frac{1}{\rho}R_{\rho}, \quad (\text{C.1.29})$$

$$T_{\rho\rho} + \frac{(d-1)}{\rho}T_{\rho} - T + R^{2\sigma}T = -\beta_{\tau}\zeta - \nu(\sqrt{\beta})R. \quad (\text{C.1.30})$$

The equation (C.1.29) is solved [45] by neglecting the right-hand-side. On the other hand, solution to the equation (C.1.30) needs the solvability condition

$$\int_0^{\infty} (\beta_{\tau}\zeta + \nu(\sqrt{\beta})R)R\rho^{d-1}d\rho = 0, \quad (\text{C.1.31})$$

because  $R$  is in the null space of the operator in the left-hand-side of (C.1.30) acting on  $T$ . This leads to

$$\beta_{\tau} = -\frac{2M_c}{M}\nu(\sqrt{\beta}) \quad (\text{C.1.32})$$

where  $M_c$  and  $M$  are as defined in the equation (C.1.27). However, a little bit of work is needed to get  $M$ . Using the equations (C.1.28), (C.1.20) together with

$$\int_0^{\infty} \left( |R_{\rho}|^2 - \frac{1}{1+\sigma}|R|^{2\sigma+1} \right) \rho^{d-1}d\rho = 0, \quad (\text{C.1.33})$$

we get

$$M = 2 \int_0^{\infty} R\zeta\rho^{d-1}d\rho = \frac{1}{4} \int_0^{\infty} \rho^2 R^2 \rho^{d-1}d\rho.$$

Therefore, as  $\tau \rightarrow \infty$ , the asymptotic solution  $V$  takes the form

$$V(\tau, \rho) = P(\beta(\tau), \rho) - \frac{\nu(\sqrt{\beta})}{2\sqrt{\beta}} \left( g(\rho) - 2i\sqrt{\beta}h(\rho) \right), \quad (\text{C.1.34})$$

where  $g$  and  $h$  respectively satisfy

$$\Delta g - g + (2\sigma+1)R^{2\sigma}g = -\frac{R_{\rho}}{\rho}, \quad (\text{C.1.35})$$

$$h_{\rho\rho} + \frac{(d-1)}{\rho}h_{\rho} - h + R^{2\sigma}h = \frac{2M_c}{M}\zeta(\rho) - R. \quad (\text{C.1.36})$$

□

**Proposition C.1.5.** *At leading order, as  $\tau \rightarrow \infty$ ,*

$$\alpha(t) \approx \sqrt{\beta} \approx \pi / \ln(\tau) \quad (\text{C.1.37})$$

and the corresponding scale factor  $\lambda(t)$  in terms of  $t$  has the asymptotic form

$$\lambda(t) \approx \sqrt{\left(\frac{2\pi(T_* - t)}{\ln \ln(1/(T_* - t))}\right)}. \quad (\text{C.1.38})$$

Moreover,

$$\tau(t) \approx \frac{1}{2\pi} \ln\left(\frac{1}{T_* - t}\right) \ln\left[\ln\left(\frac{1}{T_* - t}\right)\right] \quad (\text{C.1.39})$$

and  $R$  is the ground state satisfying (C.1.20).

*Proof.* Assuming  $\beta = \alpha^2$  and the relation (C.1.18) holds. In the limit  $\alpha(\tau) \rightarrow 0$  as  $\tau \rightarrow \infty$ , one gets

$$\alpha_\tau \approx -\frac{\nu_0^2}{M} \frac{1}{\alpha} e^{-1/\alpha}. \quad (\text{C.1.40})$$

Taking  $\tau \rightarrow \infty$ , at the leading order the equation (C.1.40) is solved as

$$\alpha(\tau) \approx \pi / \ln(\tau). \quad (\text{C.1.41})$$

This equation (C.1.41) clearly confirms the assumption that  $\alpha_\tau \ll \alpha^2$ . Moreover, retaining the correction terms will lead an equivalent equation to (C.1.40) to have the solution

$$\alpha(\tau) \approx \pi / (\ln(\tau) + 3 \ln \ln(\tau)). \quad (\text{C.1.42})$$

The scaling factor  $\lambda$  in the limit  $t \rightarrow T_*$  is estimated by choosing a slowly varying function  $q(t)$ , a correction factor, such that  $\lambda(t) = (\sqrt{T_* - t})q(t)$ . Using the relation  $\tau_t = \lambda^{-2}$ . to leading order, we obtain

$$\tau(t) \approx \frac{1}{q^2(\tau)} \ln\left(\frac{1}{T_* - t}\right)$$

provided that compared to  $\ln\left(\frac{1}{T_* - t}\right)$  the  $q(t)$  varies more slowly. Using the equation (C.1.41) will yield  $\alpha(\tau) \approx \pi / \ln \ln(1/(T_* - t))$ . Furthermore, with  $\alpha = -\lambda\lambda_t$  and maintaining the leading order the factor  $q(t)$  is asymptotically written as

$$q(t) \approx \left(\frac{2\pi}{\ln \ln(1/(T_* - t))}\right)^{1/2}. \quad (\text{C.1.43})$$

This leads to the required result. Moreover, if the next order term is included [7], the asymptotic form of  $\tau$  is

$$\tau(t) \approx \frac{1}{2\pi} |\ln(T_* - t)| (|\ln | \ln(T_* - t) | + 4 \ln \ln | \ln(T_* - t) |). \quad (\text{C.1.44})$$

□

# Appendix D

## Algorithms

Here, we provide few of the main algorithms used in the chapter 3. See [185] for more details and some of the relevant algorithms.

### D.1 Function evaluation and differentiation algorithms

Given a truncated Chebyshev series  $p_N(x) = \sum_{n=0}^N c_n T_n(x)$  that approximates certain function, the derivative of the  $p_N(x)$  is computed by the Clenshaw algorithm as:

---

**Clenshaw-Curtis integration:** `chebeval(N,c,x,d)`

---

Given the Chebyshev interpolant  $p_N(x)$ ;  
 $\mathbf{c} : (c_0, c_1, \dots, c_N)$  vector of coefficients of the Chebyshev series on  $[-1, 1]$ ;  
 $x : (x_0, \dots, x_N)$  the evaluation points;  
 $d : (d_1, \dots, d_{N+1})$  initialized vector with  $d_{N+1} = 0, d_N = 0$ , then  
 $d_n = c_n - d_{n+2} + 2xd_{n+1}$  for  $n = N-1, N-2, \dots, 1$  ;  
 $p_N(x) \equiv d_0 = c_0/2 - d_2 + xd_1$  the required evaluated function.

---

**Chebyshev differentiation matrices:** `chebderiv(N,c,a,b)`

---

Given the Chebyshev interpolant  $p_N(x)$ ;  
 $\mathbf{c} : (c_0, c_1, \dots, c_N)$  vector of coefficients of the Chebyshev series;  
 $\mathbf{c}' : (c'_1, \dots, c'_{N+1})$  initialized vector with  $c'_N = 0, c'_{N-1} = 0, c'_{N-2} = 2(N-1)c_{N-1}$   
 $c'_{n-1} = 2nc_n + c'_{n+1}$  for  $n = N-1, N-2, \dots, 1$  .  
 $c'_n = \frac{2}{(b-a)} \cdot c'_n, \quad n = 0, 1, \dots, n$  normalization;  
 $p'_N(x) := \text{chebeval}(N, c, x, d)$  is the required derivative.

---

**Chebfft algorithm for differentiation:** `chebfft(v)`

---

Given the Chebyshev interpolant  $p_N(x)$ ;  
 $d : (d_n)_{n=0}^N$  initial the vector of the derivatives with  $v : (u_n = u(x_n))_{n=0}^N$ .  
Let  $m = N-1$ ; for  $N > 0$  else stop and return  $d = 0$ .  
 $x = \cos(\pi n/m), \quad n = 0, 1, \dots, m$  the Chebyshev nodes.  
 $w = (u_j)_{j=1}^m$  with  $u_j = u_{-m+j}$  to transform  $x$  to  $\theta \in [0, 2\pi)$  for an FFT  $\mathcal{F}$ .  
 $V = \mathcal{F}(w)$  for real  $v$  replace  $V$  with real part of FFT( $w$ ).  
 $W = \text{in}\mathcal{F}^{-1}(V), \quad k = 0, \dots, m-1$  where  $\mathcal{F}^{-1}$  is an iFFT;  
Then  $p'_N(x)$  is then given by the equation (3.3.23).

The `chebfft` approximates the derivative of  $u(x)$  as  $p'_N(x)$ .

### D.2 Numerical stability of algorithm

A numerical method of solving a mathematical problem is considered stable if the sensitivity of the numerical answer to the data is not greater than in the original problem.

Given a problem  $p$  with exact solution  $u$ . If the perturbed problem  $\tilde{p}$  has a solution  $\tilde{u}$  by an algorithm, the algorithm is said to be backward (resp. backward) stable provided there exist some constant  $\alpha$  (resp.  $\beta$ ) not too large such that, respectively,  $\|p - \tilde{p}\| / \|p\| \leq \alpha\epsilon_M$  and  $\|u - \tilde{u}\| / \|u\| \leq \beta\epsilon_M$ , with machine epsilon  $\epsilon_M$ . The constants  $\alpha, \beta$ , known as condition numbers, are expected to be sufficiently small enough so that the computed solution  $\tilde{u}$  is near the exact one  $u$ , and then call the algorithm (or the method) stable.

# Bibliography

- [1] J. Abate, H. Dubner (1968), "*A new method for generating power series expansion of functions*", SIAM, Journal of Numerical Analysis V. 5, pp. 102-112.
- [2] M.J. Ablowitz, S.V. Manakov and C.L. Schultz, On the boundary conditions of the Davey-Stewartson equation, Phys. Lett. A 148 (1990) 50-52.
- [3] M.J. Ablowitz and H. Segur, On the evolution of packets of water waves, J. Fluid Mech. 92 (1979), 691-715.
- [4] Ablowitz M.J., Segur H. (1981) "*Solitons and the Inverse scattering transform*", SIAM Philadelphia, studies in Applied Mathematics.
- [5] Ablowitz M.J., Clarkson P.A., (1991), "*Solitons Nonlinear evolution equations and Inverse Scattering*", program in applied mathematics, Cambridge University press. First published 1991, reprinted 1992.
- [6] S.A. Akhmanov, A. P. Sukharukov, and R. V. Kokhlov (1966), "*Development of an optical waveguide in the propagation of light in a nonlinear medium*" Journal of experimental physics (U.S.S.R) 51, 296-300.
- [7] Akrivis, G.D., Dougalis, V.A., Karakashian, O.A., and McKinney, W.R., 1997 "*Numerical approximation of blow-up of radially symmetric solutions of the nonlinear Schrödinger equation*", submitted to SIAM J. Scient. Comput.
- [8] J. Arbunich, C. Klein, C. Sparber, On a class of derivative Nonlinear Schrödinger-type equations in two spatial dimensions, M2AN 53(5), 1477 - 1505 (2019).
- [9] K.E. Atkinson (1989), *An introduction to numerical analysis*. Second edition. John Wiley & Sons.
- [10] R. Beals and R. R. Coifman, Linear spectral problems, nonlinear equations and the  $\tau$ -method, Inverse Problems 5 no 2 (1989), 87-130.
- [11] Benney, D.J. and Newell, A.C., (1967) "*The propagation of nonlinear wave envelopes*", J. Math. Phys. 46, 133-139.
- [12] D.J. Benney and G.J. Roskes, "*Waves instabilities*", Stud. Appl. Math. 48 (1969), 377-385.

- 
- [13] J.P. Berrut, H. Mittelmann (1997), "*Lebesgue constant minimising linear rational interpolation of continuous functions over the interval*", Computational Maths. Application, 33, pp. 77-86.
- [14] C. Besse, C.H. Bruneau, Numerical study of elliptic-hyperbolic Davey-Stewartson system: dromions simulation and blow-up, Math. Mod. and Meth. in Appl. Sciences 8, No. 8 (1998), 1363-1386.
- [15] D. Berman., "*The solution of extremal problem in in the theory of interpolation*", Izv. Vyssh. Uchebn. Zaved. Mat. 43:10-14 (1968).
- [16] C. Besse, N. Mauser, and H. Stimming, Numerical Study of the Davey-Stewartson System, Math. Model. Numer. Anal., 38 (2004), pp. 1035-1054.
- [17] Boiti, M., Leon, J. J-P., Martina, L. and Pempinelli, F. (1988) Scattering of localized solitons in the plane, Phys. Lett. A 132 (8-9), 432-439.
- [18] M. Boiti, L. Martina, F. Pempinelli, "*Multidimensional localized solitons*", Chaos, Solitons & Fractals, Volume 5, Issue 12, 1995, Pages 2377-2417, ISSN 0960-0779, [https://doi.org/10.1016/0960-0779\(94\)E0106-Y](https://doi.org/10.1016/0960-0779(94)E0106-Y). (<https://www.sciencedirect.com/science/article/pii/0960077994E0106Y>).
- [19] F. Bornemann (2010). "*Accuracy and Stability of computing higher-order derivatives of analytic functions by Cauchy integrals.*" Found of comput. Maths 11,1-63 (2011). Mathematics Subject of classification (2000), 65E05.
- [20] J.P. Boyd (2000). "*Chebyshev and Fourier Spectral Methods*", 2nd ed. University of Michigan. Dover Pub., Inc. 31 East second street mineola, New York 11501.
- [21] Breuer an Everson (1992), "*On the errors incurred calculating derivatives using Chebyshev polynomials*". DOI:10.1016/0021-9991(92)90274-3 Corpus ID: 119417075.
- [22] L. Brutman (1997), "*Lebesgue functions for polynomial interpolation-a survey*", Ann. Numerical Maths., 4, pp. 111-127.
- [23] C. Budd, S. Chen and R. Russell. New self-similar solutions of the nonlinear Schrödinger equation with moving mesh computations. J. of Computational Phy. V. 152, issue 2, (1999), pg. 756-789.
- [24] Cajori, F. (1961), *A History of Mathematics*, MacMillan.

- 
- [25] Cazenave T. and Weissler, F., 1998 Asymptotically self-similar global solutions of the nonlinear Schrödinger and heat equations, *Math. Z.* 228, 83–120.
- [26] Cazenave T. and Weissler, F., (1998) More self-similar solutions of the nonlinear Schrödinger equation, *Nonlinear Diff. Equ. Appl.* 5, 355–365.
- [27] T. Cazenave and F.B. Weissler, "*Some remarks on the nonlinear Schrödinger equation in critical case*". In "nonlinear semigroups, Partial Differential equations and Attractors". *Lecture notes in Math.* **1394** (1989), 18-29, MR1021011.
- [28] T. Cazenave and F.B. Weissler, "*The Cauchy problem for the critical nonlinear Schrödinger equation in  $H^s$* ". *Nonlinear Anal.* **14** (1990), 807-836. MR1055532.
- [29] Cazenave, T., 1989 An introduction to nonlinear Schrödinger equation, *Textos de Métodos Matemáticos* 26, Instituto de Matemática, UFRJ, Rio de Janeiro.
- [30] Cazenave, T., 1994 Blow up and scattering in the nonlinear Schrödinger equation, *Textos de Métodos Matemáticos* 30, Instituto de Matemática, UFRJ, Rio de Janeiro.
- [31] T. Cazenave, F.B. Weissler, The Cauchy problem for the critical nonlinear Schrödinger equation in  $H^s$ . *Nonlin. Anal.* 14, 807–836 (1990)
- [32] T. Cazenave, "*Semilinear Schrödinger Equations, volume 10 of Courant Lecture Notes in Mathematics*". (New York University, Courant Institute of Mathematical Sciences, New York, 2003)
- [33] R.Y. Chiao, E. Garmire, and C.H. Townes (1964), "*Self-trapping of optical beams*". *Phys. Rev. Lett.* 13,479.
- [34] H. Chihara, The initial value problem for the elliptic-hyperbolic Davey-Stewartson equation, *J.Math.Kyoto Univ.* 39 no 1 (1999), 41-66.
- [35] C.W. Clenshaw, "*A note on the summation of Chebyshev series*" *MTAC*, v.9,1955,p. 118-120. MR 17, 194.
- [36] C. Clenshaw (1962), "*Chebyshev series for mathematical functions:Mathematical Tables, V.5,*", London, 1962.
- [37] J. W. Cooley, P. A. W. Lewis, and P. D. Welch (1969). "*The Fast Fourier Transform and Its Application.*" *IEEE Transactions On Education*, Vol.12, No. 1, March 1969.

- [38] J. W. Cooley and J. W. Tukey. "An Algorithm for the Machine Calculation of Complex Fourier Series". IBM Watson Research Center Yorktown Heights, New York.
- [39] Craik, A.D.D., 1985 "Wave interaction and fluid flows", Cambridge Monographs on Mechanics and Applied Mathematics, Cambridge University Press.
- [40] Clarke S.R. and Miller P.D. (2001), "On the semi-classical limit for the focusing nonlinear Schrödinger equation: sensitivity to analytic properties of the initial data". 10.1098/rspa.2001.0862.
- [41] Davey, A., & Stewartson, K. (1974). On Three-Dimensional Packets of Surface Waves. Proceedings of the Royal Society of London. Series A, Mathematical and Physical Sciences, 338(1613), 101–110. <http://www.jstor.org/stable/78429>
- [42] P.J. Davis (1959). "On the numerical integration of the analytic periodic function." Proceedings of a Symposium, Madison, Apr.21-23, 1958. Univ. Of Wisconsin Press, Madison pg. 45-59.
- [43] V.D. Djordjevic and L.G. Redekopp, On two-dimensional packets of capillary-gravity waves, J. Fluid Mech. 79 (1977), 703-714.
- [44] T. Driscoll, A composite Runge-Kutta Method for the spectral Solution of semilinear PDEs, Journal of Computational Physics, 182 (2002), pp. 357-367.
- [45] Dyachenko, S., Newell, A.C., Pushkarev, A., and Zakharov, V.E., 1992 "Optical turbulence: weak turbulence, condensates and collapsing filaments in the nonlinear Schrödinger equation", Physica D 57, 96–160.
- [46] Dysthe K, Krogstad H.E, Müller P, (2008). "Oceanic rogue waves". Annual Review of fluid Mechanics. 40 (1): 287-310.
- [47] C.J. Elliot and B.R. Suydam, (1975). "Self-focusing phenomena in air-glass laser structures". IEEE J. Quantum Electron. QE-11, 863.
- [48] K. J. Engel, N. Rainer. "One-parameter semigroups for linear evolution equations". Springer (2000).
- [49] L.C. Evans, "Partial differential equations". Graduate Studies in Mathematics, V 19 American Mathematical Society.
- [50] Farlow, S. J. (1993), *Partial Differential Equations for Scientists and Engineers*, Chapter 17, Dover Publications, New York.

- [51] G. Fibich, "*The nonlinear Schrödinger equation and, singular solutions and optical collapse.*" J. Applied Mathematical science, V. 192. Springer.
- [52] G. Fibich, "*Singular solutions of the subcritical nonlinear Schrödinger equation.*" Physica D 240, 1119–1122 (2011)
- [53] G. Fibich, F. Merle, P. Raphaël, Proof of a spectral property related to the singularity formation for the  $L^2$  critical nonlinear Schrödinger equation, Physica D, 220: 2006, 1-13.
- [54] G. Fibich, N. Gavish, X.P. Wang, "*Singular ring solutions of critical and supercritical nonlinear Schrödinger equations.*" Physica D 231, 55–86 (2007).
- [55] Fokas AS. 1983 On the inverse scattering of first order systems in the plane related to nonlinear multidimensional equations. Phys. Rev. Lett. 51, 3-6. (doi:10.1103/PhysRevLett.51.3) 47.
- [56] Fokas, A.S. and Ablowitz, M.J. (1983) Phys. Rev. Lett. 51 pp. 7-10.
- [57] Fokas AS, Ablowitz MJ. 1983 On a method of solution for a class of multi-dimensional nonlinear evolution equations. Phys. Rev. Lett. 51, 7-10. (doi:10.1103/PhysRevLett.51.7)
- [58] A.S. Fokas and P.M. Santini, Dromions and a boundary value problem of the Davey-Stewartson I equation, Physica D 44 (1990) 99-130.
- [59] Fokas, A.S. and Sung, L.Y., 1992 "*On the solvability of the  $n$ -wave, Davey-Stewartson and Kadomtsev-Petviashvili equations.*", Inverse Problems, 8, 673–708.
- [60] Forest, M.G., & McLaughlin, K.T.-R (1998), "*Onset of oscillations in nonsolitons pulses in nonlinear dispersive fibers.*" J. Nonlin. Sci. 7, 43-62.
- [61] B. Fornberg, *Numerical differentiation of analytic functions*, ACM Trans. Math. Softw. 7, 512–526 (1981).
- [62] B. Fornberg, *Algorithm 579: CPSC: Complex power series coefficients*, ACM Trans. Math. Softw. 7, 542- 547 (1981).
- [63] G. M. Fraiman, Sov. Phys. JETP-USSR 61, 228 (1985);
- [64] J. S. Francis (1965), *An algorithm for summing orthogonal polynomial series and their derivatives with Applications to Curve-Fitting and Interpolation.*

- [65] B. Franchi, E. Lanconelli, J. Serrin, "*Existence and uniqueness of non-negative solutions of quasilinear equations in  $\mathbb{R}^n$* ". Adv. Math. 118, 177–243 (1996).
- [66] H. Fujita (1966), "*On the blowing up solutions of the Cauchy problem  $u_t = \Delta u + u^{\alpha+1}$* ". J. Fac. Sci. Univ. Tokyo Sect. Maths., 16 (1966), 105-113.
- [67] E. Gagliardo, Proprieta di alcune classi di funzioni in piu varibili. Ricerche di Math. 7, 102–137 (1958)
- [68] E. Gagliardo, Ulteriora proprieta di alcune classi di funzioni in piu varibili. Ricerche di Math. 8, 24–51 (1959).
- [69] Gardner, C. S. 1971. "*The Korteweg–de Vries equation and generalizations. IV. The Korteweg–de Vries equation as a Hamiltonian system*". Journal of mathematical physics, 12: 1548-1551.
- [70] W. Gautschi (1997). "*Numerical Analysis*", Birkhäuser, Boston.
- [71] J.-M. Ghidaglia and J.-C. Saut, On the initial value problem for the Davey-Stewartson systems, Nonlinearity, 3, (1990), 475-506.
- [72] Ginibre, J. and Velo, G., 1979 "*On a class of Schrödinger equations. I: The Cauchy problem, a general case*", J. Funct. Anal. 32, 1–32.
- [73] Ginibre, J., 1998 "*Introduction aux equations de Schrödinger non linéaires*," Cours de DEA 1994-1995, Paris Onze Edition.
- [74] M. V. Goldman, "*Strong turbulence of plasma waves*". Rev. Mod. Phys. 56, 709 (1984).
- [75] D. Gottlieb and L. Lustman, "*The Dufort-Frankel Chebyshev method for parabolic initial boundary value problems*", Comput. Fluids 11 (1983), 107-120.
- [76] Graham W Griffiths and William E. Schiesser (2009), [Scholarpedia](#), 4(7):4308.
- [77] Gross(1963). Hydrodynamics of superfluid condensate. Journal of Mathematical Physics 4, 195 (1963); <https://doi.org/10.1063/1.1703944>.
- [78] J. Hadamard, "*Sur les problèmes aux dérivés partielles et leur signification physiques*". Princeton University Bulletin, 13:49:-52, 1902.
- [79] Halmos P. R. (1974). *A Hilbert Space Problem Book*, Springer 2nd edition.

- 
- [80] N. Hayashi, Local existence in time of solutions to the elliptic-hyperbolic Davey-Stewartson system without smallness condition on the data, *J. Analyse Mathématique* 73, (1997), 133-164.
- [81] N. Hayashi and H. Hirota, Global existence and asymptotic behaviour in time of small solutions to the elliptic-hyperbolic Davey-Stewartson system, *Nonlinearity* 9 (1996), 1387-1409.
- [82] N. Hayashi and J.-C. Saut, Global existence of small solutions to the Davey-Stewartson and the Ishimori systems, *Diff. Int. Equations* 8 (7) (1995), 1657-1675.
- [83] W. Heinrichs (1989), "*Improved condition number for spectral methods*", *Journal of Math. Comp.* 53 (1989), 103-119.
- [84] W Heinrichs, "strong convergence estimates for Pseudo-spectral methods", *Applied Maths.*, 37 (1992), pp. 401-417.
- [85] N. Higham (2002). "*Accuracy and Stability of Numerical Algorithms (2nd ed)*". SIAM. p. 5.
- [86] Hirota, R., Exact solution of the Korteweg-de Vries equation for multiple collisions of solitons. *Phys. Rev. Lett.* v27. 1192-1194.
- [87] G. Huang, L. Deng, C. Hang. "Davey-Stewartson description of 2 dimensional nonlinear excitations in Bose-Einstein Condensates." American Physical Society. (2005).
- [88] John K. Hunter. "Nonlinear Evolution Equations". 1996.
- [89] Kadomtsev, B.B. and Karpman V.I., 1971 "*Nonlinear waves*", *Sov. Phys. Uspekhi* 14, 40-60.
- [90] Kadomtsev, B.B., 1979 "*Phénomènes collectifs dans les plasmas*", MIR (Moscow), translated from Russian (original edition 1976).
- [91] Kato, Trotter's product formula for an arbitrary pair of self-adjoint contraction semigroups, vol. 3, Academic Press, Boston, 1978, pp. 185-195.
- [92] C. Klein, Fourth order time-stepping for low dispersion Korteweg-de Vries and nonlinear Schrödinger equation, *ETNA* Vol. 29 116-135 (2008).

- 
- [93] C. Klein and K. McLaughlin, Spectral approach to D-bar problems, *Comm. Pure Appl. Math.*, DOI: 10.1002/cpa.21684 (2017).
- [94] C. Klein, K. McLaughlin, N. Stoilov, High precision numerical approach for Davey-Stewartson II type equations for Schwartz class initial data, *Proc. Royal Soc. A* 476, <https://doi.org/10.1098/rspa.2019.0864>.
- [95] C. Klein, K. McLaughlin, N. Stoilov, Spectral approach to the scattering map for the semi-classical defocusing Davey-Stewartson II equation, *Physica D*, [doi.org/10.1016/j.physd.2019.05.006](https://doi.org/10.1016/j.physd.2019.05.006)
- [96] C. Klein and J-C. Saut, "Nonlinear dispersive equations: Inverse Scattering". To appear.
- [97] C. Klein, B. Muite, K. Roidot (2011), "Numerical study of Blow-up in The Davey-Stewartson System (DS)". AMS subject Classifications. Primary, 65M70; Secondary, 65L05, 65M20.
- [98] C. Klein and J.-C. Saut, *IST versus PDE, a comparative study*, in *Hamiltonian Partial Differential Equations and Applications* ed. by P. Guyenne, D. Nicholls, C. Sulem, *Fields Inst. Commun.* 75, 338-449 (2015), DOI: 10.1007/978-1-4939-2950-4.
- [99] C. Klein and J.-C. Saut, *A numerical approach to Blow-up issues for Davey-Stewartson II type systems*, *Comm. Pure Appl. Anal.* 14:4, 1443–14674 (2015)
- [100] C. Klein and R. Peter, *Numerical study of blow-up in solutions to generalized Korteweg-de Vries equations*, 2014.
- [101] C. Klein and K. Roidot, Fourth order time-stepping for Kadomtsev-Petviashvili and Davey-Stewartson equations, *SIAM J. Sci. Comput.*, 33(6), 3333-3356. DOI: 10.1137/100816663 (2011).
- [102] C. Klein, C. Sparber and P. Markowich, *Numerical study of oscillatory regimes in the Kadomtsev-Petviashvili equation*, *J. Nonl. Sci.* Vol. 17(5), 429-470 (2007).
- [103] C. Klein and N. Stoilov, A numerical study of blow-up mechanisms for Davey-Stewartson II systems, *Stud. Appl. Math.*, DOI : 10.1111/sapm.12214 (2018).

- 
- [104] C. Klein, N. Stoilov, Multi-domain spectral approach for the Hilbert transform on the real line, SN Partial Differential Equations and Applications (2:36) (2021) <https://doi.org/10.1007/s42985-021-00094-8>.
- [105] C. Klein, N. Stoilov, Numerical study of the transverse stability of the Peregrine solution, Stud Appl Math. 2020; 1-16. <https://doi.org/10.1111/sapm.12306>.
- [106] Kiristine Embree, "*Blowup equation with  $u^p$  nonlinearity*". 28 Feb. 2021.
- [107] Koppel, N. and Landman, M., (1995) "*Spatial structure of the focusing singularity of the nonlinear Schrödinger equation: a geometrical analysis*", SIAM J. Appl. Math. 55, 1297–1323.
- [108] N.E. Kosmatov, V.F. Shvets, V.E. Zakharov, Computer simulation of wave collapses in the nonlinear Schrödinger equation. Physica D 52, 16–35 (1991).
- [109] Konopelchenko, B.G. (1993) Solitons in Multidimensions, World Scientific, Singapore.
- [110] Kreyszig, E. (1993), *Advanced Engineering Mathematics - Seventh Edition*, Wiley.
- [111] J. Kuntzmann (1959). "*Méthode Numériques: Interpolation-Dérivées*". Dunod, Paris, 1959.
- [112] E.A. Kuznetsov, J.J. Rasmussen, K. Rypdal, S.K. Turitsyn, Sharper criteria for the wave collapse. Physica D 87, 273–284 (1995).
- [113] E. A. Kuznetsov (1974), "*The collapse of electromagnetic waves in a plasma*".Zh. Eksp. Teor. Fiz. 66, 2037 (1974) [Sov. Phys.—JETP 39, 1003 (1974)].
- [114] Lagarias, J. C., J. A. Reeds, M. H. Wright, and P. E. Wright. Convergence Properties of the Nelder-Mead Simplex Method in Low Dimensions. SIAM Journal of Optimization. Vol. 9, Number 1, 1998, pp. 112-147.
- [115] Lamb M.A., Hydrodynamics. Cambridge Mathematical Library, 6th edition.
- [116] J. D. Lambert. "*Numerical Methods for ordinary differential Systems*", John-Wiley & Sons Ltd., Chichester, 1991. IVP.
- [117] C. Lanczos (1956), *Applied analysis*, Prentice-Hall Mathematics series. pg. 371-378.
- [118] Landman, M.J., LeMesurier, B.J, Papanicolaou, G.C., Sulem, C., and Sulem, P.L., 1989 Singular solutions of the cubic Schrödinger equation, "Integrable systems and

- Application”, (M. Balabane, P. Lochak, and C. Sulem, eds.), 207–217, Lecture Notes in Physics, 342, Springer-Verlag.
- [119] Landman, M.J., Papanicolaou, G.C., Sulem, C., and Sulem, P.L., 1988 Rate of blowup for solutions of the Nonlinear Schrödinger equation at critical dimension, *Phys. Rev. A* 38, 3837–3843.
- [120] Landman, M.J., Papanicolaou, G.C., Sulem, C., Sulem, P.L., and Wang, X.P., 1991 Stability of isotropic singularities for the nonlinear Schrödinger equation, *Physica D* 47, 393–415.
- [121] Landman, M.J., Papanicolaou, G.C., Sulem, C., Sulem, P.L., and Wang, X.P., 1992 Stability of isotropic self-similar dynamics for scalar-wave collapse, *Phys. Rev. A* 46, 7869–7876.
- [122] D. Lannes, *Water waves: mathematical theory and asymptotics*, Mathematical Surveys and Monographs, vol 188 (2013), AMS, Providence.
- [123] H. Leblond, Electromagnetic waves in ferromagnets, *J. Phys. A* 32 (45) (1999), 7907-7932.
- [124] H. Leblond, "The Davey-Stewartson Model in Quadratic Media: A way to control Pulses", page 1-2. UMR CNRS 6136, Université d'Angers, 2 Bd Lavoisier 49045 Dedexl, France.
- [125] B.J. LeMesurier, G.C. Papanicolaou, C.Sulem, P.L. Sulem (1988), "*Local structure of the self-focusing singularity of the nonlinear Schrödinger equation*". *Physica D* 32, pg. 210-226, North-Holland, Amsterdam.
- [126] B.J. LeMesurier, G. Papanicolaou, C. Sulem and P.L. Sulem (1988) "*Focusing and Multi-focusing solutions of the non-linear Schrödinger equation*". *Physica D* 31 (1988) 78-102 North-Holland, Amsterdam.
- [127] H.A. Levine (1990), "*The role of critical exponents in blowup theorems*". SIAM, Vol. 32, No. 2, pp. 262-288, June 1990.
- [128] Lin, J.E. and Strauss, W., 1978 "*Decay and scattering of solutions of a nonlinear Schrödinger equation*", *J. Funct. Anal.* 30, 245–263.
- [129] F. Linares and G. Ponce, *On the Davey-Stewartson Systems*, *Ann. Inst. Henri Poincaré, Anal. nonlinéair* 10 (1993), 523-548.

- 
- [130] F. Linares and G. Ponce, *Introduction to Nonlinear Dispersive Equations*, Springer, Universitex, 2nd edition.
- [131] J.N. Lyness (1967). "Numerical algorithms based on the theory of the complex variable." Proceedings of the 1967 22nd national conference, pg. 125-133.
- [132] J.N. Lyness (1968), "Differentiation formulas for analytic functions" Computational Maths., 22 (1968), pp. 352-362.
- [133] J. N. Lyness, "Differentiation formulas for analytic functions," Math. Comp.
- [134] J.N. Lyness, C.B. Moler, "Numerical Differentiation of the Analytic functions" SIAM Journal of Numerical Analysis V.4., pp. 202-210.
- [135] J.N. Lyness and G. Sande (1971). "Evaluation of normalised taylor coefficients of an analytic function." Algorithm 413: ENTCAF and ENTCRE. Communication in ACM 14, pg. 669-675.
- [136] G. Maess, "Vorlesungen ueber Numerische Mathematik II, Analysis", Berlin, Akademie-Verlag, 1984-1988,
- [137] Malomed, Boris (2005), "Nonlinear Schrödinger Equations", in Scott, Alwyn (ed.), Encyclopedia of Nonlinear Science, New York: Routledge, pp. 639-643.
- [138] Y. Martel, F. Merle, Stability of the blow-up profile and lower bounds for blow-up rate for the critical generalized KdV equation. Arxiv:math/0405229v1 [Math.Ap] 12 May, 2004.
- [139] Y. Martel, F. Merle, P. Raphaël, Blow up for the critical gKdV equation I: Dynamics near the soliton, Preprint available at: arXiv:1204.4625.
- [140] Y. Martel, F. Merle, P. Raphaël, Blow up for the critical gKdV equation II: Minimal mass dynamics, Preprint available at: arXiv:1204.4624.
- [141] Y. Martel, F. Merle, P. Raphaël, Blow up for the critical gKdV equation III: Exotic regimes, Preprint available at: arXiv:1209.2510.
- [142] J. Marzuola, G. Simpson, Spectral Analysis for Matrix Hamiltonian Operators, Nonlinearity, vol. 24 (2011), 389-429.
- [143] M. McConnell, A.S. Fokas, B. Pelloni, Localised coherent solutions of the DSI and DSII equations—a numerical study, Math. Comp. Sim. 69 (2005) 424–438

- 
- [144] D.W. McLaughlin, G.C. Papanicolaou, C.Sulem, P.L. Sulem (1986), "*Focusing singularity of the cubic nonlinear Schrödinger equation*". Physical Review A, Vol. 34, No. 2.
- [145] F. Merle, Nonexistence of minimal blow-up solutions of equations  $iu_t = -\delta u - k(x)|u|^{4/N}u$  in  $\mathbb{R}^N$ . Ann. Inst. Henri Poincaré 64, 33–85 (1996).
- [146] F. Merle, Existence of blow-up solutions in the energy space for the critical generalized KdV equation, J. Amer. Math. Soc. 14 (3) (2001) 555–578.
- [147] F. Merle, P. Raphael, Blow-up dynamics and upper bound on the blow-up rate for the critical nonlinear Schrödinger equation. Ann. Math. 161, 157–222 (2005).
- [148] F. Merle, P. Raphael, Profiles and quantization of the blow-up mass for critical nonlinear Schrödinger equation. Commun. Math. Phys. 253, 675–704 (2005).
- [149] F. Merle, P. Raphael, On a sharp lower bound on the blow-up rate for the  $L^2$  critical nonlinear Schrödinger equation. J. Amer. Math. Soc. 19, 37–90 (2006).
- [150] F. Merle, P. Raphael, On one blow up point solutions to the critical nonlinear Schrödinger equation. J. Hyperbolic Diff. Equat. 2,919–962 (2006).
- [151] F. Merle, P. Raphael, Sharp upper bound on the blow-up rate for the critical nonlinear Schrödinger equation. Geom. Funct. Anal. 13, 591–642 (2003).
- [152] F. Merle, P Raphael, On universality of blow-up profile for  $L^2$  critical nonlinear Schrödinger equation, Invent. math. **156**, 565–672 (2004).
- [153] F. Merle and P. Raphael, J. Am. Math Soc. 19, 37 (2006).
- [154] F. Merle, P. Raphael, J. Szeftel, The instability of Bourgain-Wang solutions for the  $L^2$  critical NLS. Amer. J. Math. 135, 967–1017 (2013).
- [155] F. Merle, Y. Tsutsumi (1990), " *$L^2$  concentration of blow-up solutions for the nonlinear Schrödinger equation with critical power nonlinearity*". J. Diff. Equat. 84, 205–214.
- [156] Merryfield and Shizgal (1993), "*Properties of the collocation third-derivative operator*", Journal of computational physics, 105:182-5.
- [157] G. Miel and R. Mooney (1985). "*On the condition number of Lagrangian Numerical differentiation*". Elsevier Science Publishing Co. Inc., NY 10017.

- [158] S.L. Musher, A.M. Rubenchik and V.E. Zakharov, Hamiltonian approach to the description of nonlinear plasma phenomena, *Phys. Rep.* 129 (5) (1985), 285-366.
- [159] H. Nawa, Asymptotic profiles of blow-up solutions of the nonlinear Schrödinger equation with critical power nonlinearity. *J. Math. Soc. Jpn.* 46, 557–586 (1994)
- [160] H. Nawa, M. Tsutsumi, " *On blow-up for the pseudo-conformally invariant nonlinear Schrödinger equation*". *Funkcial. Ekvac.* 32, 417–428 (1989)
- [161] H. Nawa, M. Tsutsumi, " *On blow-up for the pseudo-conformally invariant nonlinear Schrödinger equation II*". *Comm. Pure Appl. Math.* 51, 373–383 (1998)
- [162] A. Newell and J.V. Moloney, *Nonlinear Optics*, Addison-Wesley (1992).
- [163] Newell, A.C., 1974 " *Envelope equations*", *Lectures in Applied Mathematics* 15, 157–163.
- [164] L. Nirenberg, On elliptic partial differential equations. *Ann. Scuola Norm. Sup. Pisa* 13, 115–162 (1959).
- [165] K. Nishinari, K. J. Abe, J. Satsuma, "A new type of soliton behaviour of the Davey-Stewartson Equations in plasma System." *Teoret. Mat. Fiz.*, pp. 487-498., 99 (1994).
- [166] K. Nishinari and J. Satsuma, " *Multi-dimensional localised Behaviour of electrostatics Ion wave in magnetized Plasma*", *Surikaisekikenkyusho Kokyuroku*, (1994), pp. 191-202. *The mathematics of wave motion phenomena in fluids and its applications* (Japanese) (Kyoto, 1993).
- [167] K. Nishinari, T. Yajima, Numerical analyses of the collision of localised structures in the Davey-Stewartson equations, *Phys. Rev. E* 51 (1995) 4986–4993.
- [168] K. Nishinari, T. Yajima, T. Nakao, Time Evolution of Gaussian Type Initial Conditions Associated With The Davey- Stewartson Equations, *J. Phys. A: Math. Gen.* 29 (1996) 4237–4245.
- [169] S. P. Novikov, S. V. Manakov, L. P. Pitaevskii, V. E. Zakharov, *Theory of Solitons: The Inverse Scattering Method*, Springer-Verlag (1984), ISBN 0-306-10977-8.
- [170] Ogawa, T. and Tsutsumi, Y., 1991 Blow-up of  $H^1$  solution for the one dimensional nonlinear Schrödinger equation with critical power nonlinearity, *Proc. Amer. Math. Soc.* 111, 487–496.

- [171] Ogawa, T. and Tsutsumi, Y., 1991 Blow-up of  $H^1$  solution for the nonlinear Schrödinger equation, J. Diff. Eq. 92, 317–330.
- [172] Onorato M, Proment D, Clauss G, Klein, M (2013), "Rogue waves: From Nonlinear Schrödinger Breather solutions to sea-Keeping Test". PloS ONE 8(2): e54629. doi:10.1371/journal.pone.0054629.
- [173] T. Ozawa, Exact Blow-Up Solutions to the Cauchy Problem for the Davey-Stewartson Systems, Proc. R. Soc. Lond. A., 436 (1992), pp. 345–349.
- [174] G. Papanicolaou and G. Fibich (2000), "Self-focusing in a perturbed and unperturbed nonlinear Schrödinger equation in critical dimensions", SIAM J. of Applied Math 60, 183-240.
- [175] G.C. Papanicolaou, C. Sulem, P.L. Sulem and X.P. Wang, Focusing singularities of Davey-Stewartson equations for gravity-capillary waves, preprint.
- [176] Papanicolaou, C.G., McLaughlin, D., and Weinstein, M. 1982 "Focusing singularity for the nonlinear Schrödinger equation", Lecture Notes in Num. Appl. Anal. 5, 253–257.
- [177] Papanicolaou, G.C., Sulem, C., Sulem, P.L., and Wang, X.P., 1991 "Singular solutions of the Zakharov equations for Langmuir turbulence", Phys. Fluids B 3, 969–980.
- [178] Papanicolaou, G.C., Sulem, C., Sulem, P.L., and Wang, X.P., 1994 "The focusing singularity of the Davey–Stewartson equations for gravity–capillary surface waves", Physica D 72, 61–8.
- [179] J. Paul, L. N. Trefethen. "Barycentric Lagrange Interpolation". Society for Industrial and Applied Maths., SIAM REVIEW Vol. 46, No. 3, pp.501-517.
- [180] D. H., Peregrine, "water waves", J. Aust. Math. Soc. Ser. B 25 (1983) 16.
- [181] R. Peyret, *Introduction to Spectral Methods*, Von Karman Institute, 1986.
- [182] Poisson, S. D. 1809. "Mémoire sur la variation des constantes arbitraires dans les questions de mécanique [Memoir on the variation of arbitrary constants in mechanics]". Journal de l'École polytechnique, cahier XV: 266-298.
- [183] S. Pohozaev, Eigenfunctions of the equation  $\Delta u + \lambda f(u) = 0$ . Soviet Math. Dokl. 6, 1408–1411 (1965).

- 
- [184] M. J. Powell (1981), "Approximation theory and Methods", Cambridge University press, Cambridge UK.
- [185] W. H. Press, S.A. Teukolsky, W.T. Vetterling, B. P. Flannery (1997), *Numerical recipe in C*, The Art of Scientific computing. Second edition, Cambridge Univ. Press.
- [186] P. Raphael, Stability of the log-log bound for blow up solutions to the critical non linear Schrödinger equation. *Math. Ann.* 331, 577–609 (2005).
- [187] P. Raphael, "On the blow up phenomenon for the  $L^2$  critical nonlinear Schrödinger Equation".
- [188] J. Rasmussen and K. Rypdal. Blow-up in nonlinear Schrödinger equations-I a general review. *Physica Script a* 33 481-497 (1986).
- [189] F. Riesz; Nagy B., "Functional analysis". Books on Advanced Mathematics (1995), Dover, ISBN 0-486-66289-6.
- [190] T.J. Rivlin(1975). "Optimally Stable Lagrangian Numerical Differentiation". *SIAM J. Numerical Analysis* V12, No.5, Oct. 1975.
- [191] T.J. Rivlin(1974). "The Chebyshev Interpolation polynomials". Pure and Applied Mathematics. Wiley-Interscience [John Wiley & Sons], New York-London-Sydney, 1974. pp. 9-18, 56–123.
- [192] T.J. Rivlin (1969), "An introduction to approximation of functions". Blaisdell Book in Numerical Analysis and Computer Science.
- [193] S. Russell, J. (1845). Report on Waves: "Made to the Meetings of the British Association in 1842-43". Boussinesq, J. (1871). "
- [194] Y. Saad and M. Schultz, GMRES: a generalized minimal residual algorithm for solving non- symmetric linear systems, *SIAM J. Sci. Comput.* 7 (1986), 856-869.
- [195] J. Satsuma, J. Ablowitz, *Mathematical Journal* (1989), "2-dimensional Journal Lumps in nonlinear dispersive syetems" *Journal of Mathematical Physics* 20(7), pg. 1496.
- [196] E.I. Schulman, On the integrability of equations of Davey-Stewartson type, *Theor. Math. Phys.* 56 (1983), 131-136.

- 
- [197] A. Smoktunowicz (2002), "*Backward Stability of Clenshaw's Algorithm*". BIT Numerical Mathematics 42, 600–610 (2002).
- [198] Snyder, M.A. (1966) *Chebyshev Methods in Numerical Approximation*. Prentice-Hall, Inc., Englewood Cliffs.
- [199] O. Staffans. "*Wellposed Linear-Systems*". Cambridge University Press (2005).
- [200] Strang, Gilbert. On the construction and comparison of difference schemes. SIAM Journal on Numerical Analysis 5.3 (1968): 506-517. doi:10.1137/0705041.
- [201] Strauss, W. A. (1992), *Partial Differential Equations: An Introduction*, Wiley.
- [202] C. Sulem, P. L. Sulem (1999), "*The Nonlinear Schrödinger equation: Self-focusing and wave collapse*". Springer 1999.
- [203] C. Sulem, P. L. Sulem (1997), "*Focusing nonlinear Schrödinger equation and wave-packet collapse*". Nonlinear Analysis, Theory, Methods, and Applications. V.30, pg. 833–844.
- [204] R. Suydam, IEEEJ (1975). "*Effect of Refractive-Index nonlinearity on the Optical Quality of High-Power Laser Beams*". Quantum Electron. QE-11, 225.
- [205] J. Szabados and P. Vértesi (1990), *interpolation of functions*. World Scientific Publishing Co.
- [206] O. Tadahiro (2015), "*Global existence for the defocusing nonlinear schrödinger equations with limit periodic initial data*". Analysis of PDEs (Math.AP), arXiv:1502.02258.
- [207] V.I. Talanov (1964), "*On Self-focusing of Electromagnetic Waves in nonlinear-media*", Izv. Vuzov, Radiophysica, 7, 564–565 (1964) –First time translation from Russian.
- [208] L. N. Trefethen, *Spectral Methods in Matlab*, SIAM, Philadelphia, PA, 2000. <https://www.comlab.ox.ac.uk/ouc1/work/nick.trefethen>.
- [209] L. N. Trefethen, "*Approximation theory and approximation practice*", Society for industrial and applied Maths., Philadelphia 2013.
- [210] H. Trotter, On the Product of Semi-Groups of Operators, Proceedings of the American Math-ematical Society, 10 (1959), pp. 545551.

- 
- [211] Tsutsumi, Y., 1987 " $L^2$  solutions for the nonlinear Schrödinger equation and nonlinear groups", Funkcial. Ekvac. 30, 115–125.
- [212] Tsutsumi, M., 1978 "*Nonexistence and instability of solutions of nonlinear Schrödinger equations*", Unpublished.
- [213] Totz, N. Global Well-posedness of 2D Non-focusing Schrödinger equation via rigorous modulation approximation.
- [214] S.K. Turitsyn, Nonstable solitons and sharp criteria for wave collapse. Phys. Rev. E 47, R13–R16 (1993).
- [215] S.N. Vlasov, V.A. Petrishchev, V.I. Talanov, Averaged description of wave beams in linear and nonlinear media. Radiophys. Quant. Electron. 14, 1062–1070 (1971)
- [216] H. Wang, D. Huybrechs (2016), "Fast and Accurate computation of Chebyshev Coefficients in Complex plane". Revised 2016., Oxford University Press.
- [217] Weideman, J.A.C. and Reddy, S.C., A Matlab differentiation matrix suite, ACM TOMS, 26 (2000), 465–519.
- [218] M.I. Weinstein, "*Nonlinear Schrödinger equations and sharp interpolation estimates*". Comm. Math. Phys. 87, 567–576 (1983)
- [219] F. B. Weissler, "*Existence and nonexistence of global solutions for a semilinear heat equation*", Israel J. Math., 38 (1981), 292-295.
- [220] B. D. Welfert, *Generation of pseudo-spectral differentiation matrices I*, SIAM J. Numer. Anal. 34 (1997), 1640-1657.
- [221] P. White and J. Weideman, Numerical Simulation of Solitons and Dromions in the Davey-Stewartson System, Math. Comput. Simul., 37 (1994), pp. 469-479.
- [222] G.B. Whitham. *Linear and Non-linear waves*. 1974, A Wiley-Inter-science publication. pp. 601–606 & 489–491. ISBN 0-471-94090-9.
- [223] Whitham, G.B.(1999). *Linear and Nonlinear Waves*, Wiley, New Jersey. Reprinted.
- [224] *Numerical Solution of the KdV* [Wikiwaves](#).
- [225] Graham W Griffiths and William E, *Linear and nonlinear wave equations*, [Nonlinear waves](#).

- [226] J.F. Williams (1998), "*The Optical Parametric Oscillator: Saturating Blow-Up in the large detuning Limit.*",
- [227] Wolfgang P. Schleich, Daniel M.G, et al. "Schrödinger equation revisited". pg.1, February 2013.
- [228] K. Yang, S. Roudenko and Y. Zhao (2018), "*Blow-up dynamics and spectral property in the  $L^2$ -critical non-linear Schrödinger equation in higher dimensions*", Non-linearity No. 9, Vol. 31, pg. 4354-4392.
- [229] E. J. Yarmchuk, M. J. V. Gordon, and R. E. Packard. Observation of stationary vortex arrays in rotating superfluid helium, Phys. Rev. Lett.43, pg. 214–217.
- [230] H. Yoshida, Construction of higher Order symplectic Integrators, Physics Letters A, 150(1990), pp. 262–268.
- [231] Zakharov, V.E., 1984 Collapse and self-focusing of Langmuir waves, Handbook of plasma physics, (M.N. Rosenbluth and R.Z. Sagdeev, eds.), vol. 2, (A.A. Galeev and R.N. Sudan, eds.), 81–121, Elsevier.
- [232] V. E. Zakharov (1972), "*Collapse of Langmuir Waves*". Journal of theoretical physics 62, 1745 (1972 [Sov. Phys.—JETP 35, 908 (1972)]).
- [233] V. E. Zakharov (1984), "*Collapse of Self Focusing of Langmuir Waves, Vol. 2 of Handbook of Plasma Physics*", edited by M. N. Rosenbluth and R. Z. Sagdeev (Elsevier, Nnv York, 1984).
- [234] Zakharov, V. E. and Faddeev, L. D. 1971. Korteweg–de Vries equation: a completely integrable Hamiltonian system. Functional analysis and its applications, 5: 280-287.
- [235] Zakharov, V.E., Musher, S.L., and Rubenchik, A.M., 1985 "*Hamiltonian approach to the description of non-linear plasma phenomena*", Phys. Reports 129, 285–366.
- [236] V. E. Zakharov and A. M. Rubenchik, Nonlinear interaction of high-frequency and low frequency waves, Prikl. Mat. Techn. Phys.,5 (1972), 84-98.
- [237] V. E. Zakharov and, E. I. Schulman, Degenerate dispersion laws, motion invariants and kinetic equations, Physica 1D (1980), 192-202.
- [238] V. E. Zakharov and, E. I. Schulman, Integrability of nonlinear systems and perturbation theory, in What is integrability? (V.E. Zakharov, ed.), (1991), 185-250, Springer Series on Nonlinear Dynamics, Springer-Verlag.

- [239] V. E. Zakharov and A. B. Shabat, Zh. Eksp. Teor. Fiz. 61, 118(1971)[Sov. Phys.—JETP 34, 62 (1972)].
- [240] Zhen-jiang Zhou, Jing-zhi Fu, Zhi-bin Li "*Maple packages for computing Hirota's bilinear equation and multisoliton solutions of nonlinear evolution equations*", Applied Maths. and Computation 2010, 217, 1, 92-104.